5-12-2024

Development and application of small-molecule probes targeting ghrelin O-acyltransferase

Jacob Moose
Syracuse University

Recommended Citation

Abstract

Ghrelin is a 28-amino acid peptide hormone that has wide-ranging physiological effects, including on metabolism, adipogenesis, insulin regulation, and addiction. Ghrelin offers an intriguing option for treatment of pathophysiologies related to these effects, as it requires a unique post-translational octanoyl modification to bind and activate its cognate receptor, growth hormone secretagogue 1a (GHSR). The enzyme responsible for this modification, ghrelin *O*-acyltransferase (GOAT) therefore offers the ability to modulate ghrelin signaling through inhibition of the maturation pathway. Due to a lack of structural or mechanistic information about GOAT, pharmaceutical development of molecules capable of GOAT inhibition has been desired, but few molecules have been reported. To aid in the development of small-molecule inhibitors capable of GOAT inhibition, we have altered an existing GOAT activity assay for high-throughput screening capabilities. Utilization of this modified assay in conjunction with computational modeling has led to the development of novel molecules capable of GOAT inhibition. In addition, new classes of GOAT inhibitors have led to insights on the potential catalytic mechanism of GOAT.

Development and application of small-molecule probes targeting ghrelin *O*-acyltransferase

Jacob E. Moose

B.S., Nazareth College, 2016

M.Phil., Syracuse University, 2018

Dissertation

Submitted in partial fulfillment of the requirements for the degree of

Doctor of Philosophy in Chemistry

Syracuse University

June 2024

© Jacob E. Moose, 2024

Acknowledgements

I would first like to acknowledge my advisor, Dr. James Hougland, who has supported my cross-disciplinary interest from the beginning. I have valued his scientific acumen and rigor over the years and appreciated his mentorship to become the scientist I am today. I would also like to thank him for his patience and support that have allowed me to explore my interest in not just performing chemistry, but also teaching it. I would like to thank Dr. John Chisholm for allowing me to take his time, patience, resources, and lab space to explore interesting avenues that would not have been possible without his assistance. I would also like to thank my committee members, Dr. Robert Doyle, Dr. Rachel Steinhardt, Dr. Xiaoran Hu, and Dr. Era Jain for their consideration and comments.

I would like to thank the people that have made the Hougland lab a joy to work in. Thank you to Michelle Sieburg for being a fantastic lab manager/mom, as well as a welcoming, caring presence. Thank you to Dr. Kayleigh McGovern-Gooch for being my first graduate mentor, and someone whose advice I still think back to often. Thanks to Dr. Elizabeth Cleverdon, Dr. Melanie Blanden, Dr. Maria Campana, Dr. Sudhat Ashok, and Tasha Davis for welcoming me to the lab and fostering an amazing lab community. Thanks to Dr. Mariah Pierce, Sadie Novak, Amber Ford, Andrea Sprague-Getsy, and Kate Brand for being the best colleagues and friends that I could have hoped for. Thank you to the undergraduate students who worked with me on many of the projects contained within this dissertation: Rebecca Walker, Jackson Calhoun, Zachary Spada, Daniera Gomez-Sotomayor, and Nicholas Burgado. I would also like to thank

the members of the Chisholm lab for their guidance and friendship: Dr. Rowan Meador, Dr. Nilamber Mate, Dr. Katelyn Leets, Dr. Shea Meyer, Dr. Shawn Dormann, Robert Anderson, and Dr. Angela Pacherille, thank you!

Finally, I would like to thank my family. To my parents, Richard and Maureen, to whom I owe the start and continuation of my interest in the sciences, as well as their willingness to listen when things were tough. To my wife, Jess, this work would not have been completed without your love and understanding throughout my years as a graduate student. I owe more to your support and love than I think I can adequately express. And finally, to my daughter Vivienne, should you ever read this, know that I am so excited to see you grow up and meet the person you'll become!

Table of Contents

1. **Chapter 1: Introduction**

4.   **Chapter 4: Privileged electrophile inhibition of GOAT supports involvement of an activated serine/threonine in GOAT catalysis**

6.   Chapter 6: Conclusions and Future Directions

List of Figures

List of Tables:

List of Schemes

List of Abbreviations

ABP	Activity-based probe
ACAT	Acetyl-coenzyme A acetyltransferase
AcDan	acrylodan
AGRP	Agouti-related protein
AMPK	5' adenosine monophosphate-activated protein kinase
AUD	Alcohol use disorder
BChE	butyrylcholine esterase
BF$_3$OEt	boron trifluoride etherate
BMI	body mass index
cat-ELCCA	catalytic assay using enzyme-linked click-chemistry
cLPCAT3	chicken lysophophatidylcholine acyltransferase 3
CoA	Coenzyme-A
CPP	conditioned place preference
cryo-EM	cryogenic electron microscopy
Dap	2,3-diaminoproprionic acid
DCI	3,4-dichloroisocoumarin
DCM	dichloromethane
DGAT	Diacylglycerol O-acyltransferase
Dhh	Desert Hedgehog
DIBAL	diisobutylaluminum hydride
DlTB	D-alanyl transfer protein
DMAP	4-dimethylaminopyridine

DMF	dimethyl formamide
DMSO	dimethyl sulfoxide
ELISA	enzyme-linked immunsorbent assay
EMS	ethyl methyl sulfone
EtOAc	ethyl acetate
fMRI	functional magnetic resonance imaging
FRET	fluorescence resonance energy transfer
GH	growth hormone
GHSR	growth hormone secretagogue receptor 1a
GOAT	ghrelin O-acyltransferase
HEPES	4-(2-hydroxyethyl)-1-piperazineethanesulfonic acid
hGOAT	human ghrelin O-acyltransferase
HH	Hedgehog
HHAT	Hedgehog acyltransferase
HMTS	hexyl methane thiosulfonate
HPLC	high performance liquid chromatography
HRMS	high-resolution mass spectrometry
HRP	horseradish peroxidase
HRTF	homogenous time-resolved fluorescence
HTS	high-throughput screening
IC_{50}	half-maximal inhibitory concentration
Ihh	Indian Hedgehog
IV	intravenous

MAFP	methl arachidonyl fluorophosphonate
MBOAT	membrane bound acyltransferase
mCPBA	meta-chloroperoxybenzoic acid
MD	molecular dynamics
MF	membrane fraction
mGOAT	mouse ghrelin O-acyltransferase
MMTS	methyl methane thiosulfonate
mRNA	messenger ribonucleic acid
MTS	methane thiosulfonate
NEM	N-ethyl malemide
NMR	Nuclear Magnetic Resonance
NPY	Neuropeptide Y
oct-CoA	octanoyl-Coenzyme A
PCC	pyridinium chlorochromate
PORCN	Porcupine
ppm	parts per million
PTCH1	Patched
PVDF	polyvinylidene fluoride
PWS	Prader-Willi syndrome
RFU	relative fluorescence units
RP-HPLC	reverse-phase high performance liquid chromatography
SAR	structure-activity relationship
SF	sulfonyl fluoride

Shh   Sonic Hedgehog

T2DM   Type II Diabetes Mellitus

Tat   transactivator of transcription

TBAB   tetrabutylammonium bromide

TCA   trichloroacetic acid

TCAN   trichloroacetonitrile

TEA   triethylamine

TEBAC   triethylbenzylammonium chloride

TFA   trifluoroacetic acid

THF   tetrahydrofuran

TSA   p-toluenesulfonic acid

VTA   ventral tegmental area

Wnt   wingless-related integration site

YASARA   Yet Another Scientific Artificial Reality Application

Appendices

Chapter 1: Introduction

1.1 Ghrelin signaling

1.1.1 The discovery of ghrelin

Ghrelin was initially discovered during the search for the endogenous ligand for the orphan receptor growth hormone secretagogue receptor 1a (GHSR). [1, 23] When a synthetic ghrelin peptide failed to exhibit the same retention time on reverse-phase HPLC (RP-HPLC) as ghrelin extracted from rats, the shorter retention time of the natural ghrelin indicated a hydrophobic modification not present in the synthetic peptide. This modification was identified as an octanoyl moiety by mass spectrometry. Synthetic ghrelin octanoylated on serine-3 coeluted with natural ghrelin by RP-HPLC, verifying the modification as an *n*-octanoyl acylation of the serine-3 residue of ghrelin and establishing a unique post-translational modification. [1] *O*-acylation is a relatively uncommon modification in the proteome, perhaps being most well-known in acylation of a serine residue in Wnt. [4]

1.1.2 Physiological effects of ghrelin

Ghrelin is a secreted peptide hormone that is produced throughout the digestive tract. [1, 5-10] During the identification of ghrelin, an octanoyl moiety was found to be modifying serine-3 of the peptide due to retention time shifts between naturally-produced and synthetic forms of ghrelin. This octanoylation was found to be required for activity at GHSR, the endogenous receptor for ghrelin. [1] Through binding GHSR, ghrelin causes a release of growth hormone (GH), followed by stimulation of the AMPK pathway and feeding response. [11, 12] While most well-known for its orexigenic effects, ghrelin also exerts other metabolic effects. Adiposity increases in neuropeptide Y deficient mice lacking the ability for GH to activate feeding response indicates

an additional role for ghrelin in caloric distribution and storage. [13, 14] Mice lacking critical

enzymes for the synthesis and release of ghrelin succumb to fatal hypoglycemia when exposed to

starvation conditions, exhibiting reduced GH secretion.[15, 16] The effects of starvation on ghrelin-

lacking mice can also be attributed to the role of ghrelin in insulin secretion and sensitivity,

where ghrelin decreases insulin production and increases blood glucose levels. [17-20] This suggests

that ghrelin is protective in low-calorie environments through increasing blood glycemia, and

that lacking this protective benefit exacerbates hypoglycemia through insulin-regulated uptake of

glucose.

Ghrelin is also implicated in aspects of memory and reward systems. Ghrelin crosses the

blood-brain barrier independent from its relationship with GHSR, and binds to hippocampal

neurons, with ghrelin administration increasing recall of avoidance behavior in mice. [21, 22]

Knockouts of ghrelin and GHSR impair the memory of mice as well, further implicating the

hormone in the formation of memories. [22-24] Perhaps related, chronic exposure to ghrelin

increases fear memory and fear memory response. [25, 26] Ghrelin serves as a biomarker for chronic

stress while having protective effects against stress-induced depressive behavior in mice. [27, 28]

1.1.3 Ghrelin processing and maturation

Ghrelin undergoes multiple processing steps before secretion as a mature peptide

hormone. Initially translated as the 117 amino acid preproghrelin, the peptide is cleaved by

signal peptidase to the prohormone proghrelin. [29] Proghrelin is then converted to the familiar

octanoylated form by ghrelin *O*-acyltransferase, (GOAT), and octanoylated ghrelin is secreted

after cleavage of C-terminal regions of proghrelin to yield the mature 28 amino acid hormone. [29-

[34] Ghrelin can be cleaved by serum esterases to desacyl-ghrelin, removing the ester-linked octanoyl chain and the ability to activate GHSR. [32-34] While the full nature of the esterases affecting ghrelin deacylation is not yet characterized, butyrylcholine esterase (BChE) has been shown to be capable of this activity while also decreasing adiposity in mice treated with BChE. [35, 36] Although desacyl-ghrelin does not activate GHSR, evidence suggests biologically activity through alternative pathways, with desacyl-ghrelin playing a role in insulin secretion. [17, 37-39] This may be a result of a complex acylation-deacylation pathway for ghrelin, as acylation of exogenous desacyl-ghrelin in bone marrow and the hippocampus has been shown to be a result of GOAT expression on the plasma membrane. [40, 41] This has been supported by the cellular uptake of fluorescent ligands in HEK 293 and prostate cancer cells, indicating that extracellular GOAT interacts with extracellular peptides, providing a pathway for localized acylation of plasma desacyl-ghrelin. [42]

1.2   Disorders with potential ghrelin modulation pathophysiologies

1.2.1   Diabetes

One of the areas drawing the most pharmaceutical interest for modulation of GOAT is Type II Diabetes Mellitus (T2DM). T2DM is a disease closely linked with obesity and is classified by dysregulation of the insulin signaling system. Due to inability of islet β-cells to secrete enough insulin to counteract resistance, patients exhibit clinical hyperglycemia due to lack of glucose uptake. [43-45] Ghrelin has been linked to glucose regulation and energy balance through effects on insulin signaling. [46-49] The treatment of human subjects with acyl ghrelin injection has been found to increase blood glucose levels and decrease insulin levels, consistent with rodent studies. [17, 50-52] Acylated ghrelin has been detected in the pancreatic islets, reducing Ca^{2+} signaling resulting in the inhibition of glucose-dependent insulin secretion. [18] Exogenous acyl ghrelin reduces the insulin response to glucose and indicates that endogenous ghrelin may play a role in physiologic insulin secretion. A combination of ghrelin and desacyl-ghrelin strongly improves insulin sensitivity in humans. [39] Desacyl-ghrelin correlates with lower insulin resistance in humans, and lowering the ratio of ghrelin to desacyl-ghrlelin may be important in increasing insulin functionality. [53, 54] Injections of desacyl-ghrelin and desacyl-ghrelin analogues suppress the development of insulin intolerance in murine models of diabetes. [55] Ghrelin antagonists may be able to improve β-cell function by altering this ratio, providing a potential route towards treatment of T2DM. [20] The acylation of ghrelin then provides a potentially useful target in the efforts to modulate the ghrelin/desacyl-ghrelin ratio, which could lead to new treatments for diabetes.

1.2.2 Obesity/eating disorders

Ghrelin signaling has been linked to appetite control and stimulation, consistent with its role as the "hunger hormone". [1, 13, 56, 57] Ghrelin binding to GHSR in the arcuate nucleus of the hypothalamus stimulates neuropeptide Y- (NPY) and Agouti-related protein- (AGRP) containing neurons, increasing food consumption and decreasing energy spending. [11] While increasing food consumption logically increases weight through increased caloric intake, ghrelin has been shown to independently increase weight gain through the upregulation of adipogenesis regardless of caloric load. [40, 58] Despite the ability of ghrelin to influence weight gain, obese patients exhibit lower plasma ghrelin levels than controls. [59, 60] Interestingly, ghrelin levels do not fall after a meal in obese humans when compared to lean controls, indicating abnormal ghrelin signaling may be part of the pathophysiology of obesity. [61] Mice subjected to diet-induced obesity do not respond to exogenous ghrelin, failing to stimulate food intake, GH release, or NPY/AGRP signaling. Peptide-based inhibitors targeting the biosynthesis of acyl ghrelin have shown some promise in abating weight gain in mice, validating the potential therapeutic value of targeting ghrelin signaling in treating obesity. [62] However, a desacyl-ghrelin mimetic also increased weight gain and rebound feeding following fasting in mice without directly impacting ghrelin acylation. [63] This suggests additional complexity in the role and impact of ghrelin on these aspects of metabolic control that remains to be fully defined, and further exploration of the chemical space controlling ghrelin acylation may lead to breakthroughs on this front.

Perturbations in ghrelin signaling have also been investigated in eating disorders including anorexia nervosa and bulimia. Adolescents with anorexia nervosa have been shown to exhibit higher levels of ghrelin than controls, with a return to normal serum ghrelin concentrations after weight recovery. [64, 65] Higher ghrelin concentrations have been generally

observed in patients with anorexia, while ghrelin measurements in bulimic patients have shown more variability between studies. [66-68] In these disorders, the impact of ghrelin upon behavior has been proposed to occur through the reward centers within the brain leading to reinforcement of restrictive behaviors regarding food intake and purging. [69-71] Treatment with exogenous ghrelin or GHSR agonists has been shown to increase hunger and food intake in patients with anorexia nervosa and cancer-induced cachexia. [72-76] A parallel study of peptide-based GHSR receptor agonists and antagonists demonstrated treatment with both types of agents stimulated appetite in a rodent model, underscoring the necessity to develop a more refined molecular understanding of ghrelin signaling. [77]

1.2.3   Addiction

Ghrelin has been shown to have neurological effects beyond the canonical orexigenic effects, including stimulation of motion when anticipating food. [78] Stimulation of the mesolimbic dopaminergic system, located in the ventral tegmental area (VTA) of the brain, results in dopamine release in local neurons. This release is associated with the reward pathways triggered through pleasurable behaviors like feeding or drugs of abuse. [79-83] Ghrelin injections into the VTA have been shown to release dopamine in a manner consistent with the activation of this reward pathway. [78] This ability for ghrelin to alter the brain response to pleasurable stimuli led to the examination of ghrelin in the context of altered seeking behaviors, including drug addiction.

A study performed with patients in hospital treatment for alcohol addiction reported that ghrelin levels were significantly increased in this cohort, even when corrected for BMI. [84, 85] Over the course of patient withdrawal plasma ghrelin levels continued to increase, but could not

be correlated to craving experienced by the subjects. [84] Other studies have positively correlated ghrelin levels to alcohol cravings. [86-89] Furthermore, recent fMRI studies have indicated that increased acyl ghrelin levels are significantly associated with alcohol cue-induced brain response, while an increase in total ghrelin level does not induce the same response. [90, 91]

Pretreatment with synthetic ghrelin lowered the apparent threshold for cocaine to induce conditioned place preference (CPP) and locomotion in rats. [92-94] Ghrelin also has been shown to modulate the drug-seeking behavior of rats exposed to cocaine, increasing the response of the animals to cocaine-associated cues. [95] Locomotion and CPP have been shown to be reduced by the introduction of a GHSR antagonist, indicating that the receptor plays a role in the exhibition of addictive behaviors. [96] Ghrelin has also been shown to have effects on the addiction pathway of nicotine and methamphetamine, as inhibition of GHSR similarly reduces locomotion and CPP under treatment with these substances. [96-99]

The ghrelin signaling pathway may also play a role in the addiction to opioids. GHSR antagonist pretreatment has been shown to reduce morphine-induced behavior in rats. [100] Measurement of endocannabinoids released under morphine challenge showed significant alteration following the introduction of a GHSR antagonist, implicating ghrelin as an actor in opioid reinforcing mechanisms. [101] GHSR antagonism has also been shown to reduce heroin seeking behaviors, as well as reduce fentanyl-induced dopamine release in rats. [102, 103]

1.2.4 Prader-Willi Syndrome

Patients with Prader-Willi syndrome (PWS) exhibit multiple symptoms, including mild mental retardation, growth hormone deficiency, short stature, and behavioral issues. Obesity and

excessive weight gain are common for those affected by PWS, as one of the features of the disorder is an insatiable appetite leading to chronic overeating. [104, 105] While the mechanism for many of PWS symptoms are as yet unknown, initial studies of PWS indicated that the hallmark hyperphagia was likely due to lack of satiation rather than an increased hunger. [105] The discovery of ghrelin in 1999 offered a possibility that the hyperphagia and adiposity associated with PWS might be a result of dysfunctional ghrelin signaling. [1, 106] Examining the levels of serum ghrelin associated with PWS revealed elevated ghrelin levels in both adults and children. [106-108] Complicating the connection between ghrelin and PWS symptoms, elevated ghrelin levels are detected prior to the onset of hyperphagia. [109, 110] As assays for ghrelin have improved, increased ratios of ghrelin to desacyl-ghrelin have been detected in patients exhibiting hyperphagia or weight gain, while patients prior to the onset of these symptoms exhibit abnormally low ghrelin to desacyl-ghrelin ratios. [111, 112] These studies reconcile the anorexia shown by infants with the hyperphagia displayed by adults by demonstrating a reversal in the ghrelin/desacyl-ghrelin ratio, but the mechanism for this switch has yet to be deciphered.

Previous attempts to reduce ghrelin levels with somatostatin and its long-acting analogue octreotide have not led to reduction in the symptoms of PWS patients. [113, 114] A PWS mouse model, *Snord116del* has also exhibited lower sensitivity to GHSR receptor targeted anorexic agents. [115] The inability of these molecules to affect cessation of PWS symptoms emphasize the need to develop alternative routes for targeting the ghrelin signaling pathway that do not depend on GHSR, and the need to be able to change the grelin/desacyl-ghrelin ratio. Targeting the biosynthetic pathway of ghrelin, particularly the acylation catalyzed by GOAT could theoretically have provided such a measure. Clinical studies involving ghrelin-modulating compounds have provided mixed results in reducing hyperphagia in PWS patients. Phase 2a

clinical trials involving cylic desacyl-ghrelin analogue AZP-531 found that the molecule was well-tolerated and reduced hunger as measured by the Hyperphagia Questionnaire and patient-reported appetite, as well as reducing fat mass and waist-circumference. In contrast, no change in ghrelin levels or the ghrelin/desacyl-ghrelin ratio was found. [116] Based on the reported findings, it seems likely that the findings are a result of increasing insulin sensitivity similar to previous trials involving treatment with desacyl-ghrelin. [53-55] Extended Phase 2b clinical trials utilizing AZP-531 (livoletide) did not find statistically significant reduction of hyperphagia in PWS patients, and the development of livoletide for treatment of PWS has been halted as of 2020. [117] A 2022 Phase 2 clinical trial involving the GOAT inhibitor GLWL-01 reported no reduction in hyperphagia based on the Hyperphagia Questionnaire, while confirming a reduction in ghrelin levels, indicating that direct reduction of ghrelin via inhibition of GOAT does not seem to be a viable treatment option for PWS. [118]

1.3 Ghrelin *O*-acyltransferase

1.3.1   The discovery of GOAT as the ghrelin acyltransferase

The identity of the acyltransferase responsible for the ghrelin octanoylation modification was unknown for close to a decade following the discovery of ghrelin itself. In 2008, two independent labs reported the identity of the enzyme responsible for ghrelin acylation. Previously identified as MBOAT4, this enzyme was renamed ghrelin *O*-acyltransferase in reference to its now-identified substrate. [30, 31] The acylation of ghrelin by GOAT is unique, both in that serine octanoylation is not represented otherwise in the proteome, and in that ghrelin is the only predicted substrate for GOAT. [119] The combination of these two factors make GOAT an appealing target for modulation of pathophysiologies linked to ghrelin signaling, as the specificity of the substrate-enzyme interaction provides limits on undesired interactions *in vivo*. GOAT has been found to be highly expressed in areas where ghrelin is located, including in the stomach and gastrointestinal tract, as well as in the hypothalamus and pituitary. [30, 31, 120]

1.3.2   Mechanistic questions about GOAT

The catalytic mechanism of GOAT is currently unknown, although recent insights from the structures of several MBOATS, including protein-modifying Hedgehog acyltransferase (HHAT) and Porcupine (PORCN), has provided some points of comparison for potential catalytic mechanisms. As with other members of the MBOAT family, GOAT activity is found to depend on two highly conserved, functionally essential residues, N307 and H338. Functional and topological studies of GOAT have shown that mutation of either of these residues prevents GOAT activity, and that H338 is placed in the lumen while N307 is located on the cytosolic face

of the membrane. [30, 31, 121] The conserved histidine in other MBOATS has been located within the transmembrane channel, positioned near the middle of the transmembrane region, consistent with a role as a general base to catalyze the acyl transfer. [122-124] H338 has also been implicated in the binding of the ghrelin peptide to GOAT, which has been supported by a recent paper indicating that ghrelin-analogue peptides are not internalized by GOAT producing cells when H338A mutants are expressed. [42]

The major mechanistic question surrounding GOAT asks whether the enzyme utilizes a direct transfer mechanism or an acyl-enzyme intermediate. In a direct transfer reaction, the reaction takes place in one step as enzyme catalyzes the substrate to act directly as a nucleophile and attacking the thioether. Resolving this intermediate results in the transfer of the acyl group to the substrate as a result of the loss of the CoA. Alternatively, in forming an acyl-enzyme intermediate the enzyme will catalyze the transfer of the acyl group to the enzyme through a nucleophilic attack. This is then followed by the secondary transfer of the acyl group from the enzyme to the substrate through the attack of the substrate at the enzyme-thioester bond, resulting in the loss of the enzyme. These two possibilities will be discussed further below, as well as in relation to experimental evidence in Chapters 3 and 4.

1.4 Transmembrane catalysis

1.4.1   GOAT computational model insights

The recent publication of the first computational model of GOAT has allowed a closer examination of the three-dimensional architecture of the enzyme. This model was developed through co-evolutionary contact analysis to evaluate how residues in close proximity in the structure will respond as the residues continue to change between evolving species. The computational model is consistent with previous reports that indicated GOAT consists of 11 transmembrane domains, with a reentrant loop between the 5th and 6th transmembrane domains. [121] Novel from the model was that the transmembrane domains organize to form an internal transmembrane channel. Whereas H338 was previously identified as lumen-facing, the organization of the model places H338 in the internal channel, consistent with the potential for the residue to act as a general base in a catalytic mechanism. The octanoyl-CoA binding site was also established through mutation of residues implicated in acyl-donor binding, finding that the conserved N307 likely plays a role in this binding. [125] The culmination of these findings indicate that GOAT likely exhibits transmembrane catalysis through the combination of the substrates binding to opposite faces of the enzyme, although more experiments are required to identify the exact residues and mechanisms involved.

1.4.2   Comparison to HHAT/PORCN

Some comparison can be made between three members of the MBOAT family due to their shared acylation of proteins: Hedgehog acyltransferase (HHHAT), Porcupine (PORCN), and GOAT (**Figure 1.1**). HHAT palmitoylates the N-terminal cysteine of three mammalian
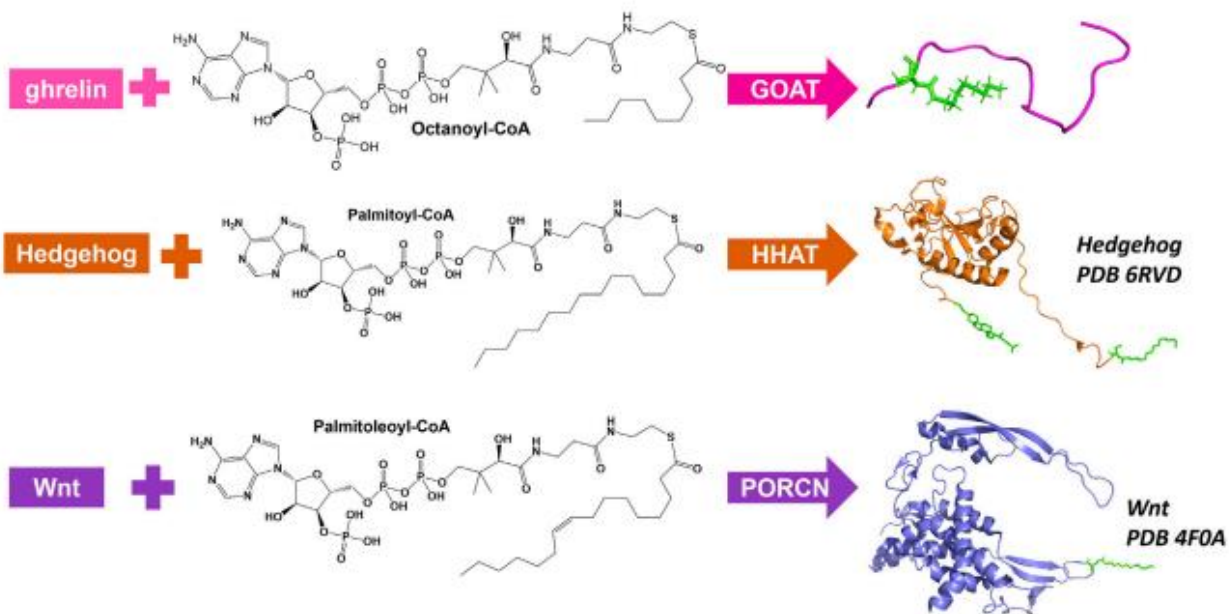
Figure 1.1: Acylation of proteins in the mammalian proteome. Representations of the lipidations performed by the three mammalian peptide/protein modifying MBOATS. Figure created by Mariah Pierce and James Hougland and utilized under the terms of the Creative Commons Attribution License. [130]

proteins, Sonic Hedgehog (Shh), Indian Hedgehog (Ihh), and Desert Hedgehog (Dhh). [126, 127] Palmitoylation of SHH is not essential for binding with the cognate receptor Patched (PTCH1), but is required to lead to significant upregulation of Hedgehog (HH) signaling. [128] Recent studies have implicated a heme-bound cysteine in HHAT as essential for catalysis, as activity is lost when this cysteine is mutated, although this residue is likely not catalytic due to distance to the canonical active site of D339 and H379. [129] The same study draws a comparison between the conserved D339, corresponding to the conserved N307 in GOAT, and a potential role in stabilizing peptidic residues for acylation in a transmembrane channel similar to that of GOAT. H379 (analogous to H338 in GOAT) is also implicated in catalysis due to the location near the bound inhibitor site and previous studies identifying the residue as important for catalysis. [123, 131, 132] The culmination of these studies involved the mechanistic hypothesis that D339 activates the N-terminal cysteine to attack the palmitoyl-CoA thioether bond in a direct-transfer mechanism. [123] HHAT has also been proposed to be involved in transportation of palmitoyl-CoA, for which the mechanism is not fully understood. [133] This draws an interesting comparison to the recently-identified ability for GOAT to play a role in the internalization of ghrelin peptides. [42]

PORCN is similar to HHAT and GOAT in that it acylates the secreted protein Wnt with palmitoleate (Figure 1.1). [4, 134, 135] Additionally, catalysis by PORCN places the acylation on a serine in Wnt similar to the *O*-acylation of ghrelin by GOAT, and is similarly required for activation of the cognate receptor, Frizzled. [136, 137] Two computational models of PORCN were published in 2021, both of which indicated a transmembrane channel through the center of the enzyme, with the conserved H341 located in the center of the channel in both. [138, 139] Shortly afterward, PORCN was able to be purified and the structure determined by cryo-EM. This structure was consistent with the previously-published computational models, and identified 11

transmembrane domains surrounding a transmembrane channel that contained the catalytic core of the enzyme, including H336. [122] Docking of the palmitoleoyl-CoA into the structure of PORCN revealed the S209 hydroxyl group of Wnt directed at the thioester bond, and in close proximity to H336, leading to the hypothesized mechanism being direct transfer of the palmitoleoyl to Wnt after activation of S209 by H336. However, the authors do note that this structure does not rule out an acyl-enzyme intermediate. [122]

1.5 Progress on GOAT inhibitors

1.5.1   Peptidomimetic Compounds

The initial molecules capable of GOAT inhibition were related to the peptidic nature of the GOAT substrate and the acylated product. Acylated octanoyl ghrelin has been shown to inhibit GOAT with a moderate potency of 7 μM (**Compound 1.1, Figure 1.2**).[140] Protecting this molecule from hydrolysis of the ester bond by replacing the serine-3 with 2,3-diaminoproprionic acid (Dap) to yield an N-acylated side chain increased the potency of the peptide mimetic **1.2** to 0.2 μM. [140] N-terminal truncations of the ghrelin peptide inhibit GOAT as long as the C-terminus is amidated and inhibition of GOAT by the peptide GS*A*FL-NH$_2$ lacking the acylation site indicated that these peptides did not inhibit through providing competitive octanoylation sites, but rather by competing for the peptide binding site. [140] Further optimization of the inhibitory sequence required from ghrelin allowed the truncation of the peptide sequence to the first five amino acids (GSSFL) and demonstrated the preference for an octanoyl acyl modification for maximal inhibitory efficacy, with the initial reported IC$_{50}$ for the octanoyl-[Dap^3]-ghrelin (1-5)-NH$_2$ (**1.3**) pentapeptide reported as 1 μM. [140] More recent methods indicate that the potency was originally underestimated, with the most recent reports placing the IC$_{50}$ at 15 nM. [141] Similar Dap-containing peptides have recently been utilized as fluorescent probes (**1.4**) to study the uptake of extracellular ghrelin into cells that contain GOAT on the exterior of the lipid bilayer, finding that GOAT functions to transport internalization of ghrelin. [42] As part of this study, it was found that hGOAT H338A mutants did not bind to the fluorescent Dap-ghrelin analogue, indicating an essential interaction between the ligand and H338. It is proposed that this altered behavior occurs due to a loss of a hydrogen bond between the side-chain Dap amine and the imidazole ring of
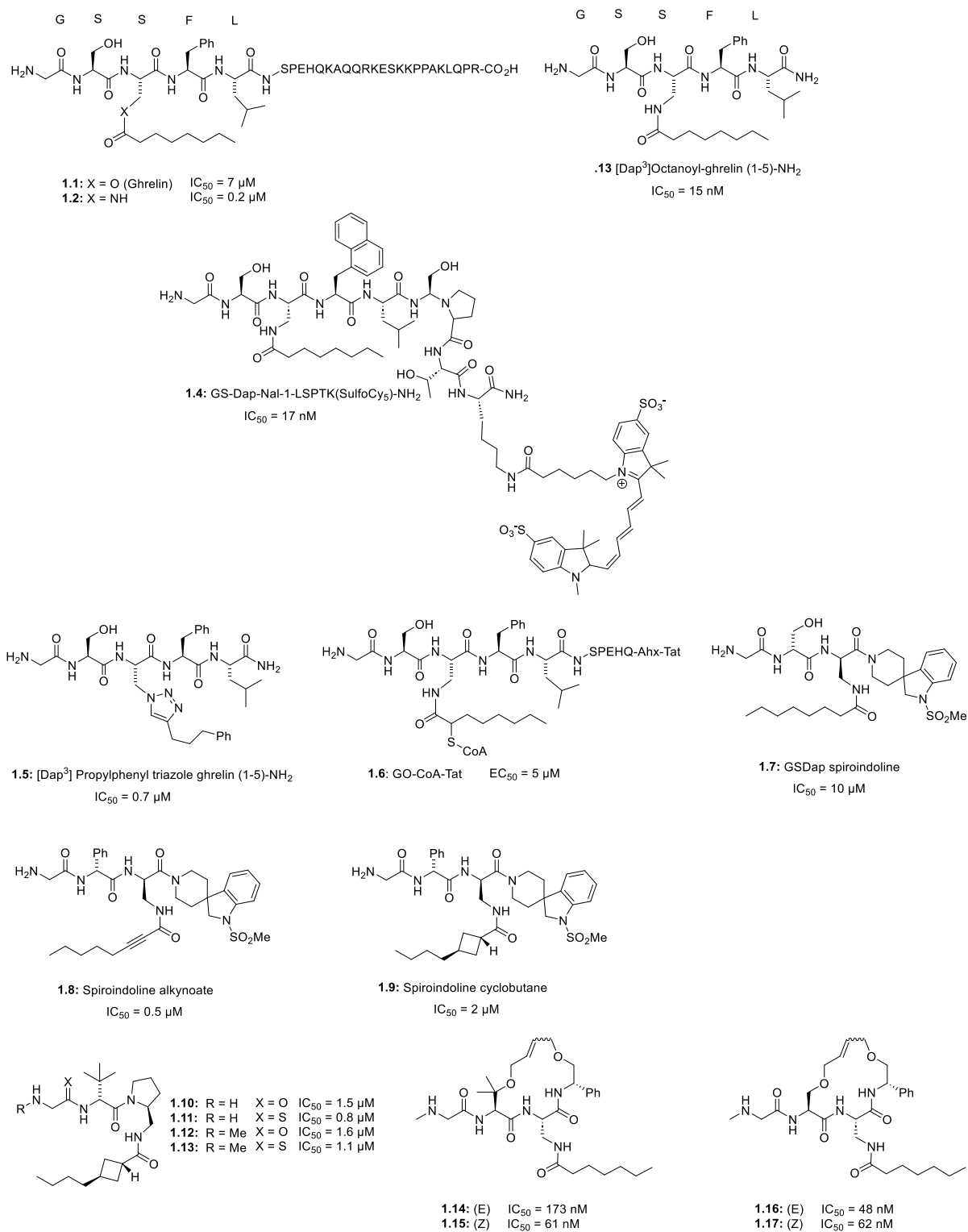
Figure 1.2: Peptidomimetic inhibitors of GOAT. Adapted from Moose et Al. (2020). [142]

the aforementioned histidine, giving more physiological context to the increased potency exhibited by Dap-containing peptides.

Alternate modifications to the ester bond have been explored to further enhance the resistance to hydrolysis. Replacement of the sidechain ester or amide bond of previous peptidomimetic compounds with the isosteric non-hydrolysable triazole led to the development of highly customizable Dap-containing alkyltriazole inhibitors. These alkyltriazoles were used to explore modifications of the alkyl sidechain, including the addition of a phenyl group that led to the sub-micromolar potency ($IC_{50} = 0.7 \mu M$) of **Compound 1.5**.[143] Further exploration of this chemical space may be possible to lead to additional compounds capable of GOAT inhibition but have not been characterized at this time.

A bisubstrate approach resulted in the development of GO-CoA-Tat, an inhibitory compound that combined both the peptide and octanoyl CoA substrates of GOAT with the cell-penetrating peptide sequence Tat to create a molecule capable of inhibiting cellular production of ghrelin with an EC_{50} around 5 μM (**1.6**). This molecule was integral in substantiating GOAT inhibition as a pharmaceutical target for obesity, as injections of mice with GO-CoA-Tat resulted in lowered ghrelin levels, prevented weight gain on a high-fat diet, and a reduction of fat mass, while showing none of these effects in ghrelin knock-out mice. Mice treated with GO-CoA-Tat also showed increased insulin response, validating the potential for GOAT inhibitors to play a role in the treatment of Type 2 Diabetes.[62]

Similar in approach to the previous bisubstrate peptidomimetic compound, altering a previous GHSR agonist also yielded a molecule capable of inhibiting GOAT. This approach found that combining an octanoylated three-peptide sequence of GSDap with a spiroindoline **7** created a smaller molecule than previous peptide-reliant compounds while retaining an IC_{50} of

10 μM. Optimization of potency led to the rigidification of the alkyl chain with an alkynoate (**8**), which was inactive in cell studies, potentially due to the ability of the alkynoate to act as a Michael acceptor, raising concerns about cross-reactivity with readily available biological thiols such as glutathione. [144] This alkynoate was replaced by the biologically stable cyclobutene (**9**) while retaining similar potency ($IC_{50} = 2$ μM), and this structure was ultimately reduced in molecular mass by replacing the spiroindoline with a pyrrolidine and the side chain phenyl group with a *tert*-butyl moiety without altering potency (**1.10**). [144, 145] Alternative molecules retaining the pyrrolidine replaced the N-terminal glycine with a thioamide, retaining GOAT inhibitory activity with an IC_{50} of 0.8 μM (**Compounds 1.11-1.13**). These molecules were found to be poorly orally available but to retain the ability to inhibit GOAT *in vivo*. [144] This same lab has recently explored creating macrocyclic peptide-containing molecules in combination with some of the chemical space explored in previous inhibitor iterations in order to increase cell permeability. The initial 4-mer peptide sequence explored contained a mono methylation of the N-terminal glycine, replacement of the Ser-2 sidechain with the previously-identified *tert*-butyl chain, octanoylated Dap-3, and amidation of the C-terminal phenylalanine (**1.14** and **1.15**). Cyclization was achieved by utilizing an alkene linker connecting a modified version of the *tert*-butyl side or the original serine sidechain to Phe-4 (**1.16** and **1.17**). These molecules were found to compete for the GOAT peptide binding site, with sub micromolar IC_{50}s. While potent, these molecules were found to still suffer from low oral bioavailability. [146]

1.5.2 Small-molecule inhibitors

In the transition away from peptidomimetic inhibitors, the first small-molecule inhibitors of GOAT contained some features analogous to previous molecules, presenting with alkyl chains

that may mimic the octanoate of ghrelin (**Figure 1.3**).[147, 148] While representing an exciting new avenue for development, the potency of these compounds is not exceptional (**1.18** = 7.5 μM and **1.19** = 13.1 μM IC$_{50}$), and the screening done in this study was undertaken exclusively with naphthalene-based molecules generated by the Ugi reaction as part of the development of their cat-ELCCA assay, limiting the scope of this development. Further publications on this compound have not materialized, and the physiological effects of this molecule are unknown.

Another series of small-molecule inhibitors based on triterpenoid scaffolds has also been published. Resulting from a screening of the Diversity Set IV library from the NCI, this screen relied on detecting acylation of a fluorescent ghrelin peptide truncation, allowing direct measurement of GOAT acylation activity. [149, 150] This screen found synthetic triterpenoid **1.20**, 1-[2-cyano-3,12-dioxooleana-1,9(11)-dien-28-oyl]imidazole (CDDO-Im). [151] Investigation into similar triterpenoid revealed the efficacy of the triterpenoid scaffold, finding compounds **1.21**-**1.23**, all compounds with <50 μM IC$_{50}$s. A structure-activity-relationship study revealed that truncating the scaffold to move to a steroid scaffold did not negatively affect potency (compounds **25-27**). Altering the α-cyano warhead revealed that the α,β unsaturated ketone was essential for potency, and that lessening or removing the polarity, as in **1.26** and **1.27** respectively, of the α moiety worsened the potency of the molecules by greater than 10-fold. As α-cyano enones are capable Michael acceptors, the mechanism of inhibition was investigated and found to be consistent with reversible covalent inhibition, suggesting that the molecules may be interacting with a nucleophile capable of Michael additions, such as a cysteine. This led to the hypothesis that GOAT catalyzed ghrelin acylation through use of a cysteine nucleophile, although the identity and location of such a residue was unknown. [151]

1.18: n = 0 IC_{50} = 13.1 µM
1.19: n = 2 IC_{50} = 7.5 µM

1.20: X = IC_{50} = 38 µM

1.21: X = $NHCH_2CH_3$ IC_{50} = 8 µM
1.22: X = $NHCH_2CF_3$ IC_{50} = 44 µM
1.23: X = OMe IC_{50} = 6 µM
1.24: X = OH IC_{50} = > 100 µM

1.25: X = CN IC_{50} = 8 µM
1.26: X = Br IC_{50} = 83 µM
1.27: X = H IC_{50} = 170 µM
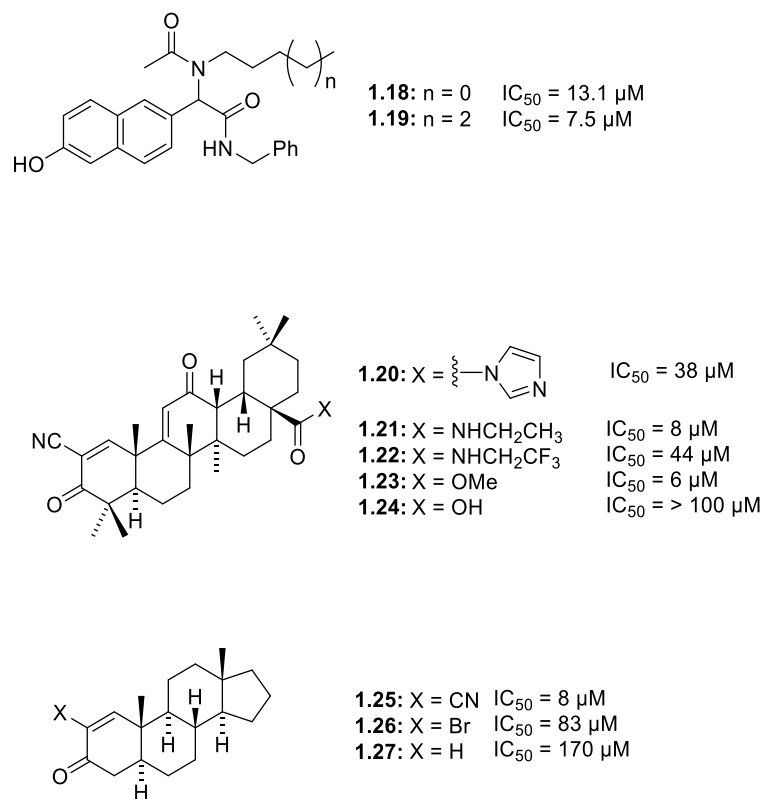
Figure 1.3: Selected small-molecule inhibitors of GOAT developed in academic research labs. Adapted from Moose et Al. (2020). [142]

1.5.3 Molecules of clinical interest

Several GOAT inhibitors have made it to various stages of clinical trials. One such clinical trial evaluated the ability of compound **1.32**, identified as LY3073084, now called GLWL-01, to treat Type II Diabetes. Originally found through a high-throughput screen by researchers at Eli Lilly, furanopyridines such as **1.28** and **1.29** inhibited GOAT with sub-micromolar IC_{50}s. Structure-activity relationship studies from the lead compound found in the initial screen found that altering the methyl to larger groups (**1.30, 1.31**) lowered potency. Optimization of initial pharmacokinetic properties led to removal of a biologically active furan and replacement with chlorine (**1.32**) while replacing the carboxylic acid with a piperidine-substituted amide. Similar aminopyridine-containing molecules were found to be similarly potent (**1.33, 1.34**). The final optimization to create GLWL-01 led to a reported IC_{50} of 69 nM, indicating enough potential to be selected for clinical trials. [152-155] Clinical trial NCT02377362 found no significant effect of GLWL-01 on ghrelin, insulin, weight, or waist circumference in treated patients. [156] As mentioned previously, GLWL-01 was also the subject of a clinical trial attempting to treat hyperphagia in PWS patients, and was similarly ineffective in that trial. [118] Two other clinical trials have also been begun investigating the possibility of utilizing GLWL-01 to reduce alcohol use disorder symptoms and to assist in weight loss in conjunction with bariatric surgery, although data is not currently available for these studies. [157, 158] While clinical trials involving GLWL-01 were found lacking, GLWL-01 was also shown to be competitive with octanoyl-CoA, marking the first molecule shown to be competitive with the lipid substrate rather than the peptide substrate of GOAT.

Takeda Pharmaceutical utilized a high-throughput screen of a large small-molecule library to discover two lead molecules capable of inhibiting ghrelin acylation. Optimization of

A. Eli Lilly

1.28: R = Me IC$_{50}$ = 0.17 μM
1.29: R = H IC$_{50}$ = 4 μM
1.30: R = Et IC$_{50}$ = >100 μM
1.31: R = i-Pr IC$_{50}$ = >100 μM

1.32: GLWL-01
IC$_{50}$ = 69 nM

1.33:
IC$_{50}$ = 70 nM

1.34:
IC$_{50}$ = 56 nM
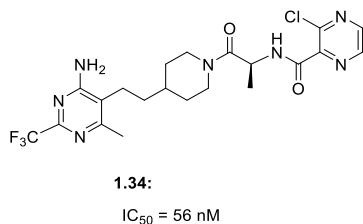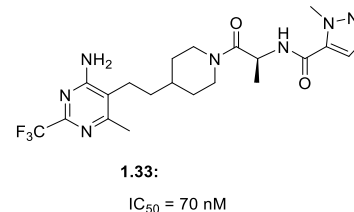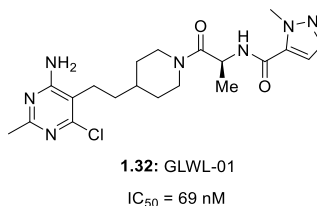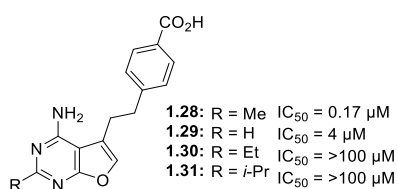
B. Takeda and GlaxoSmithKline

1.35: Takeda A
IC$_{50}$ = 8.6 nM

1.36: Takeda B
IC$_{50}$ = 1.7 nM

1.37a,b: R$_1$ = CF$_3$ R$_2$ = Cl R$_3$ = Cl X = CH$_2$ IC$_{50}$ <50 nM
1.38a,b: R$_1$ = Cl R$_2$ = Cl R$_3$ = H X = CH$_2$ IC$_{50}$ <50 nM
1.39a,b: R$_1$ = CF$_3$ R$_2$ = Cl R$_3$ = F X = CH$_2$ IC$_{50}$ <50 nM
1.40a,b: R$_1$ = H R$_2$ = Cl R$_3$ = H X = O IC$_{50}$ <50 nM

1.41:
95.2% inhibition at 10 μM

1.42:
93.7% inhibition at 10 μM

C. Boehringer Ingelheim

1.43:
IC$_{50}$ = 0.25 nM

1.44:
IC$_{50}$ = 0.25 nM

1.45:
IC$_{50}$ = 28 pM

1.46:
IC$_{50}$ = 35 pM
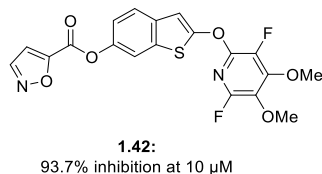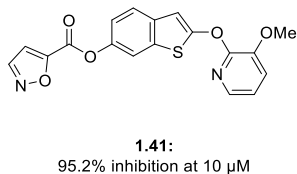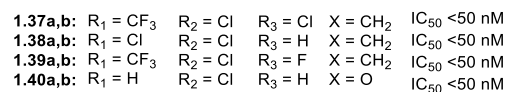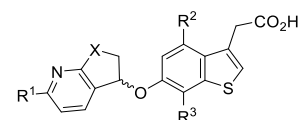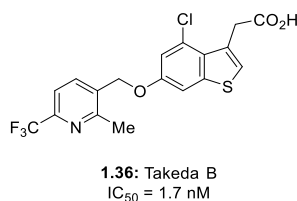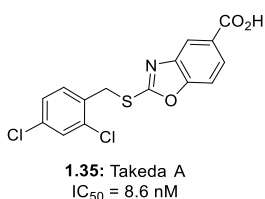
1.47:
IC$_{50}$ = 34 pM

Figure 1.4: Pharmaceutical compounds of interest for the inhibition of GOAT. From **a.)** Eli Lilly, **b.)** Takeda Pharmaceutical and GlaxoSmithKline, **c.)** Boehringer Ingelheim Adapted from Moose et Al. (2020). [142]

hit compound **1.35** involved altering the benzene ring to a pyridine, and the replacement of the 2-thiobenzoxazole with a combination of an ether linkage and altering the heterocycle to a benzothiophene to molecule **1.36**. [141, 159] **Compound 1.36** was found to have higher activity and bioavailability after oral administration, and has been reported to have been licensed to Rhythm Pharmaceuticals although no clinical trials have been started currently. Both compounds were shown to be octanoyl-CoA competitive, similar to the Eli Lilly compounds previously described, and were the first published, widely-known compounds to inhibit GOAT in such a manner. [141]

A set of benzothiophene-incorporating molecules similar to those reported by Takeda were also published by GlaxoSmithKline. With similar molecules being patented by GlaxoSmithKline in 2015 as agonists of the transmembrane receptor GTP-binding protein coupling receptor 40 (GPR40) for treatment of Type II Diabetes, the molecules include a benzothiophene core attached to another heterocycle through an ether linkage. [160] The stereochemistry of this ether does not seem to significantly affect potency, as both molecules **1.39a** and **1.39b** exhibited IC_{50} values below 50 nM. Preclinical work in mice, rats, and monkeys at found a significant reduction in ghrelin concentration at does from 1 to 10 mg/kg. [161, 162] Alternate molecules based on the benzothiophene core have also been reported, utilizing a substituted pyridine addition to substituting the ether linkage for an ester (**1.41, 1.42**). [163]

Currently the most potent reported GOAT inhibitors have been published by Boehringer Ingelheim. These molecules utilize a 7-amino-[-[1,2,4]triazolo[1,5,-a]pyrimidine scaffold, with the most potent containing a methyl substitution at the 5-position of the pyrimidine as well as a benzylic pyridyl addition at the 6-position and addition of a fluorinated ether or amine at the 2-position, as exemplified by compounds **1.43** and **1.44**. These compounds were found to have sub-nanomolar potency, and alteration of the triazole heterocycle to a 7-amino-

[1,2,5]oxadiazolo[3,4,-b]pyridines reduced the IC$_{50}$ even further, resulting in compounds with ~20 pm IC$_{50}$s (**1.45**-**1.47**). [164-167] Clinical trials with the molecule BI 1356225 have recently been published, and while the molecule was capable of reducing ghrelin levels by ~80%, no corresponding weight loss or lessened hunger cues were identified, bringing into question whether GOAT inhibition is a clinically relevant treatment for obesity. [168]

1.6 Assays for GOAT activity

Assays for the determination of inhibitor binding have heavily relied on the production of the acylated product of the reaction. The discovery of GOAT as part of the ghrelin maturation pathway relied on several processes for this purpose, including immunoblotting, mass spectrometry, and HPLC separation of peptides. [30, 31] The identification of GOAT by Yang and coworkers involved cotransfection of rat insulinoma cells with 16 MBOATs and preproghrelin, which allowed a visible shift in the acylated product on SDS-PAGE gel when visualized with anti-ghrelin antibodies following separation by reverse-phase chromatography. [30] At the same time, Gutierrez and coworkers developed a similar approach, cotransfecting candidate enzymes and preproghrelin into HEK-293 cells, but resolved the resulting peptides through immunoprecipitation and analysis by mass spectrometry to prove acylation. [31] Both approaches allowed identification of MBOAT4 as the putative ghrelin *O*-acyltransferase, but both require significant preparation of samples that would make analysis of GOAT inhibitors difficult.

1.6.1 Radioligand assays for GOAT activity

As mentioned previously, the first published inhibitors of GOAT consisted of an octanoylated pentapeptide. These inhibitors were discovered by Yang and coworkers who modified their approach to a radioligand assay used to support their previous discovery of GOAT, transfecting Sf9 insect cells to produce a GOAT-containing microsomal fraction. [^{3}H]octanoyl-CoA was used as a lipid donor, which transferred a tritium-labeled octanoyl moiety to proghrelin when incubated with the membrane fraction. Quantification of GOAT activity was calculated by separation via transfer of proteins to a PVDF membrane post electrophoresis, then

scintillation counting slices of the PVDF membrane to determine radioactivity of the section. [140] While effective, this methodology relied on radioactive tritium, while also require incubation of the autoradiology film for 5 days, making the process inconvenient for large-scale detection of GOAT activity.

Discovery of the bisubstrate-mimetic GO-CoA-Tat also relied on a version of this radioligand assay. Unlike the previous studies, this work expressed GOAT and proghrelin in human cell lines (HeLa and HEK-293T). Using a biotin-containing ghrelin peptide, this assay utilized a streptavidin column to isolate the radioactive acylated ghrelin before scintillation counting. [62] The same group eventually adopted producing microsomal fraction from insectoid Sf9 cells, following Yang et al, using GOAT activity to evaluate constructs in support the of the first topological model of GOAT and ability to utilize alternate ghrelin substrates. [121, 169]

An alternate take utilizing radiolabeling was used to determine acyl donor preference for GOAT. In this assay, Chinese hamster ovary cells expressing GOAT were used to create membrane fraction which was then reacted with the CoAs of various fatty acids. These reactions were analyzed using radiolabeled antibodies that either nonspecifically recognized both the acyl- and des-acyl forms of ghrelin, or specifically bound only the acylated ghrelin. [170]

1.6.2 Antibody based assays for GOAT activity

The most widely reported assay for GOAT activity utilizes an enzyme-linked immunsorbent assay (ELISA) to measure ghrelin and/or desacyl-ghrelin levels in reactions. Originally designed to detect ghrelin levels in studies elucidating the physiological effects of ghrelin, a two-site sandwich assay was originally reported in 2008. [171] This study designed a

ghrelin-specific 384-well plate assay utilizing an acyl-specific antibody, followed by treatment with biotinylated antibody recognizing the ghrelin C-terminus, and reported using streptavidin-HRP and a fluorescent substrate to amplify signal. This approach was simultaneously utilized to detect desacyl-ghrelin through the use of a C-terminal recognizing antibody and a biotinylated N-terminal antibody as the reporter.

Takeda Pharmaceutical used a combined homogeneous time-resolved fluorescence (HTRF) and ELISA-based approach to find their reported benzothiophene-based inhibitor. To screen the large number of samples required for high-throughput screening, the HTRF assay utilized ghrelin-selective antibody to detect acyl ghrelin, then signal amplification by FRET from a streptavidin-containing fluorophore to a europium-conjugated secondary antibody that was detected via multiplate fluorescence reader. For the confirmation via ELISA, synthetic HRP-labeled ghrelin was used to compete with acyl ghrelin produced over the course of reaction, and amplification of the fluorescent signal was achieved through commercially available ELISA substrate. [141] GOAT activity assays used in the discovery of similar benzothiophene-containing inhibitors by GlaxoSmithKline have also utilized a FRET-based assay that utilized a streptavidin-europium energy transfer in a multiplate reader format. [161, 162]

Patents from Boehringer Ingelheim and Eli Lilly reporting on molecules of pharmaceutical interest have also utilized ELISA-based approaches to determining the reduction in GOAT activity based on their molecules. [152, 153, 165, 172] Some academic-based labs have also utilized this approach to effect, notably used by Harran and coworkers in the development of former GHSR agonists to inhibit GOAT. [145, 146, 173]

An alternative enzyme-linked approach was utilized in the finding of the first small-molecule inhibitor of GOAT by Garner and Janda. [148] Called cat-ELCCA (catalytic assay using

enzyme-linked click-chemistry), this approach relied on an immobilized biotinylated ghrelin peptide and an alkyne-containing octanoyl-CoA. When transferred to ghrelin, the alkyne could then be reacted via copper-catalyzed Huisgen cycloaddition to an azide-containing HRP to form the triazole, covalently linking HRP directly to the product of the reaction. The ghrelin-HRP conjugate was then exposed to the fluorogenic substrate amplex red, providing signal amplification and detection in a multiplate reader system.

1.6.3 Fluorescence-based GOAT activity Assays

To facilitate direct measurement of GOAT activity, our research lab developed a fluorescence-based approach of ghrelin detection. Utilizing the discovery that ghrelin C-terminus based pentapeptides can function as GOAT substrates, the first five amino acids of ghrelin (GSSFL) were altered to include an acrylodan fluorophore through conjugation to a terminal cysteine. [119, 140, 149] This fluorescent peptide, GSSFLC$_{AcDan}$, acts as a substrate for GOAT and once acylated exhibits a retention-time shift on reverse-phase HPLC due to the increased hydrophobicity after addition of the octanoyl modification, while the acrylodan fluorophore allows for analysis via fluorescence detection. This approach has several advantages to previously described methods, in that the assay can simultaneously detect both the substrate and product of the reaction in the same sample, allowing for calculation of percent activity as a fraction of the converted product to the total. [150] This enabled the identification of the triterpenoid- and steroid-based inhibitors published in 2017. [151] In contrast to the ELISA assays, there is no amplification step, nor a reliance on antibody binding to detect the product, allowing direct readout of the product not possible since the original radiology assay, but without the requirement for a specialized radioactive acyl donor.

1.7 Aims of this work

The main goal of this work is to expand our current hGOAT inhibitory capabilities and work towards a pharmaceutically relevant hGOAT inhibitor. To this effect, we first developed a continuous fluorescence plate-reader assay capable of high-throughputs screening. We utilized this screen in conjunction with the recently-developed computational model of hGOAT to identify targets of interest, with this combined methodology producing three novel hGOAT inhibitors with low micromolar potency. The predicted binding sites of these molecules was validated, and also assisted our identification of a common inhibitor binding site within the transmembrane channel of hGOAT.

Development of small-molecule probes explored the mechanistic hypothesis proposed by McGovern-Gooch et al, that the functionally essential cysteine identified through an inhibitor screen was involved in the catalytic mechanism of ghrelin acylation. [151] Utilizing cysteine-reactive molecules, we found that these inhibitors potencies exhibited chain-length dependence and a reversible binding mechanism. These studies supported work indicating the previous cysteine-catalyzed mechanistic hypothesis to be unlikely.

Identification of privileged electrophile inhibition of hGOAT supported a revised mechanistic hypothesis, indicating the presence of an activated residue to act as the nucleophile in the acylation of ghrelin. The irreversible nature of these molecules provides a pathway towards the identification of the catalytic residues within hGOAT through future labeling studies.

We examined the effects of ethanol and alcohol use disorder treatments on hGOAT activity in conjunction with collaborators to develop an enzyme-to-patient level understanding of the effects of these molecules on patients. Although GOAT was not found to be affected by the

tested molecules, our collaborative efforts have led towards a better understanding of the mechanism of action of these molecules and reinforced the importance of understanding the effects of GHSR-targeting molecules on GOAT.

The studies shown in this work have broadened the inhibitory potential for GOAT-targeting small molecules. These investigations have narrowed the mechanistic possibilities of ghrelin acylation, providing the first clues towards the GOAT catalytic residues outside of the MBOAT-family conserved H338 and N307, as well as the first rationally acyl-donor competitive hGOAT inhibitors. These studies have provided the framework for the identification of the specific hGOAT catalytic residues through taking advantage reactions with mechanism-based small molecule inhibitors.

Appendix I: Reference Reprint permission for Reference 130, Chapter 1

Appendix II: Reprint permission for Reference 142, Chapter 1

1.8 References

1.   Kojima, M.; Hosoda, H.; Date, Y.; Nakazato, M.; Matsuo, H.; Kangawa, K. Ghrelin is a growth-hormone-releasing acylated peptide from stomach. *Nature* **1999**, *402* (6762), 656-660, Article. DOI: 10.1038/45230.

2.   Howard, A. D.; Feighner, S. D.; Cully, D. F.; Arena, J. P.; Liberator, P. A.; Rosenblum, C. I.; Hamelin, M.; Hreniuk, D. L.; Palyha, O. C.; Anderson, J.; et al. A receptor in pituitary and hypothalamus that functions in growth hormone release. *Science* **1996**, *273* (5277), 974-977. DOI: 10.1126/science.273.5277.974.

3.   Perello, M.; Dickson, S. L.; Zigman, J. M.; Leggio, L.; Ghrelin Nomenclature Consensus, G. Toward a consensus nomenclature for ghrelin, its non-acylated form, liver expressed antimicrobial peptide 2 and growth hormone secretagogue receptor. *J Neuroendocrinol* **2023**, *35* (1), e13224. DOI: 10.1111/jne.13224

4.   Hofmann, K. A superfamily of membrane-bound O-acyltransferases with implications for wnt signaling. *Trends Biochem Sci* **2000**, *25* (3), 111-112. DOI: 10.1016/s0968-0004(99)01539-x.

5.   Date, Y.; Kojima, M.; Hosoda, H.; Sawaguchi, A.; Mondal, M. S.; Suganuma, T.; Matsukura, S.; Kangawa, K.; Nakazato, M. Ghrelin, a novel growth hormone-releasing acylated peptide, is synthesized in a distinct endocrine cell type in the gastrointestinal tracts of rats and humans. *Endocrinology* **2000**, *141* (11), 4255-4261. DOI: 10.1210/en.141.11.4255.

6.   Hosoda, H.; Kojima, M.; Matsuo, H.; Kangawa, K. Ghrelin and des-acyl ghrelin: two major forms of rat ghrelin peptide in gastrointestinal tissue. *Biochem Biophys Res Commun* **2000**, *279* (3), 909-913. DOI: 10.1006/bbrc.2000.4039.

7.   Sakata, I.; Yang, J.; Lee, C. E.; Osborne-Lawrence, S.; Rovinsky, S. A.; Elmquist, J. K.; Zigman, J. M. Colocalization of ghrelin O-acyltransferase and ghrelin in gastric mucosal cells. *American Journal of Physiology - Endocrinology and Metabolism* **2009**, *297* (1), E134-E141, Article. DOI: 10.1152/ajpendo.90859.2008 Scopus.

8.   Korbonits, M.; Bustin, S. A.; Kojima, M.; Jordan, S.; Adams, E. F.; Lowe, D. G.; Kangawa, K.; Grossman, A. B. The expression of the growth hormone secretagogue receptor ligand ghrelin in normal and abnormal human pituitary and other neuroendocrine tumors. *J Clin Endocrinol Metab* **2001**, *86* (2), 881-887. DOI: 10.1210/jcem.86.2.7190.

9.   Gnanapavan, S.; Kola, B.; Bustin, S. A.; Morris, D. G.; McGee, P.; Fairclough, P.; Bhattacharya, S.; Carpenter, R.; Grossman, A. B.; Korbonits, M. The tissue distribution of the mRNA of ghrelin and subtypes of its receptor, GHS-R, in humans. *J Clin Endocrinol Metab* **2002**, *87* (6), 2988. DOI: 10.1210/jcem.87.6.8739.

10.   Ghelardoni, S.; Carnicelli, V.; Frascarelli, S.; Ronca-Testoni, S.; Zucchi, R. Ghrelin tissue distribution: comparison between gene and protein expression. *J Endocrinol Invest* **2006**, *29* (2), 115-121. DOI: 10.1007/BF03344083.

11.   Cowley, M. A.; Smith, R. G.; Diano, S.; Tschop, M.; Pronchuk, N.; Grove, K. L.; Strasburger, C. J.; Bidlingmaier, M.; Esterman, M.; Heiman, M. L.; et al. The distribution and mechanism of action of ghrelin in the CNS demonstrates a novel hypothalamic circuit regulating energy homeostasis. *Neuron* **2003**, *37* (4), 649-661. DOI: 10.1016/s0896-6273(03)00063-1.

12.   Chen, H. Y.; Trumbauer, M. E.; Chen, A. S.; Weingarth, D. T.; Adams, J. R.; Frazier, E. G.; Shen, Z.; Marsh, D. J.; Feighner, S. D.; Guan, X. M.; et al. Orexigenic action of peripheral ghrelin is mediated by neuropeptide Y and agouti-related protein. *Endocrinology* **2004**, *145* (6), 2607-2612. DOI: 10.1210/en.2003-1596.

13.   Tschop, M.; Smiley, D. L.; Heiman, M. L. Ghrelin induces adiposity in rodents. *Nature* **2000**, *407* (6806), 908-913. DOI: 10.1038/35038090.

14.   Tschop, M.; Statnick, M. A.; Suter, T. M.; Heiman, M. L. GH-releasing peptide-2 increases fat mass in mice lacking NPY: indication for a crucial mediating role of hypothalamic agouti-related protein. *Endocrinology* **2002**, *143* (2), 558-568. DOI: 10.1210/endo.143.2.8633.

15.   Zhao, T.-J.; Liang, G.; Li, R. L.; Xie, X.; Sleeman, M. W.; Murphy, A. J.; Valenzuela, D. M.; Yancopoulos, G. D.; Goldstein, J. L.; Brown, M. S. Ghrelin O-acyltransferase (GOAT) is essential for growth hormone-mediated survival of calorie-restricted mice. *Proceedings of the National Academy of Sciences* **2010**, *107* (16), 7467-7472. DOI: 10.1073/pnas.1002271107.

16.   Xie, T. Y.; Ngo, S. T.; Veldhuis, J. D.; Jeffery, P. L.; Chopin, L. K.; Tschop, M.; Waters, M. J.; Tolle, V.; Epelbaum, J.; Chen, C.; Steyn, F. J. Effect of Deletion of Ghrelin-O-Acyltransferase on the Pulsatile Release of Growth Hormone in Mice. *J Neuroendocrinol* **2015**, *27* (12), 872-886. DOI: 10.1111/jne.12327.

17.   Broglio, F.; Arvat, E.; Benso, A.; Gottero, C.; Muccioli, G.; Papotti, M.; van der Lely, A. J.; Deghenghi, R.; Ghigo, E. Ghrelin, a natural GH secretagogue produced by the stomach, induces hyperglycemia and reduces insulin secretion in humans. *J Clin Endocrinol Metab* **2001**, *86* (10), 5083-5086. DOI: 10.1210/jcem.86.10.8098.

18.   Dezaki, K.; Hosoda, H.; Kakei, M.; Hashiguchi, S.; Watanabe, M.; Kangawa, K.; Yada, T. Endogenous ghrelin in pancreatic islets restricts insulin release by attenuating Ca2+ signaling in beta-cells: implication in the glycemic control in rodents. *Diabetes* **2004**, *53* (12), 3142-3151. DOI: 10.2337/diabetes.53.12.3142.

19.   Lindqvist, A.; Shcherbina, L.; Prasad, R. B.; Miskelly, M. G.; Abels, M.; Martinez-Lopez, J. A.; Fred, R. G.; Nergard, B. J.; Hedenbro, J.; Groop, L.; et al. Ghrelin suppresses insulin

secretion in human islets and type 2 diabetes patients have diminished islet ghrelin cell number and lower plasma ghrelin levels. *Mol Cell Endocrinol* **2020**, *511*, 110835. DOI: 10.1016/j.mce.2020.110835

20. Tong, J.; Prigeon, R. L.; Davis, H. W.; Bidlingmaier, M.; Kahn, S. E.; Cummings, D. E.; Tschop, M. H.; D'Alessio, D. Ghrelin suppresses glucose-stimulated insulin secretion and deteriorates glucose tolerance in healthy humans. *Diabetes* **2010**, *59* (9), 2145-2151. DOI: 10.2337/db10-0504.

21. Rhea, E. M.; Salameh, T. S.; Gray, S.; Niu, J.; Banks, W. A.; Tong, J. Ghrelin transport across the blood-brain barrier can occur independently of the growth hormone secretagogue receptor. *Mol Metab* **2018**, *18*, 88-96. DOI: 10.1016/j.molmet.2018.09.007.

22. Diano, S.; Farr, S. A.; Benoit, S. C.; McNay, E. C.; da Silva, I.; Horvath, B.; Gaskin, F. S.; Nonaka, N.; Jaeger, L. B.; Banks, W. A.; et al. Ghrelin controls hippocampal spine synapse density and memory performance. *Nat Neurosci* **2006**, *9* (3), 381-388. DOI: 10.1038/nn1656.

23. Davis, J. F.; Choi, D. L.; Clegg, D. J.; Benoit, S. C. Signaling through the ghrelin receptor modulates hippocampal function and meal anticipation in mice. *Physiol Behav* **2011**, *103* (1), 39-43. DOI: 10.1016/j.physbeh.2010.10.017.

24. Albarran-Zeckler, R. G.; Brantley, A. F.; Smith, R. G. Growth hormone secretagogue receptor (GHS-R1a) knockout mice exhibit improved spatial memory and deficits in contextual memory. *Behavioural Brain Research* **2012**, *232* (1), 13-19. DOI: 10.1016/j.bbr.2012.03.012.

25. Meyer, R. M.; Burgos-Robles, A.; Liu, E.; Correia, S. S.; Goosens, K. A. A ghrelin-growth hormone axis drives stress-induced vulnerability to enhanced fear. *Mol Psychiatry* **2014**, *19* (12), 1284-1294. DOI: 10.1038/mp.2013.135.

26.   Harmatz, E. S.; Stone, L.; Lim, S. H.; Lee, G.; McGrath, A.; Gisabella, B.; Peng, X.; Kosoy, E.; Yao, J.; Liu, E.; et al. Central Ghrelin Resistance Permits the Overconsolidation of Fear Memory. *Biol Psychiatry* **2017**, *81* (12), 1003-1013. DOI: 10.1016/j.biopsych.2016.11.009.

27.   Lutter, M.; Sakata, I.; Osborne-Lawrence, S.; Rovinsky, S. A.; Anderson, J. G.; Jung, S.; Birnbaum, S.; Yanagisawa, M.; Elmquist, J. K.; Nestler, E. J.; Zigman, J. M. The orexigenic hormone ghrelin defends against depressive symptoms of chronic stress. *Nat Neurosci* **2008**, *11* (7), 752-753. DOI: 10.1038/nn.2139.

28.   Yousufzai, M.; Harmatz, E. S.; Shah, M.; Malik, M. O.; Goosens, K. A. Ghrelin is a persistent biomarker for chronic stress exposure in adolescent rats and humans. *Transl Psychiatry* **2018**, *8* (1), 74. DOI: 10.1038/s41398-018-0135-5.

29.   Zhu, X.; Cao, Y.; Voogd, K.; Steiner, D. F. On the processing of proghrelin to ghrelin. *J Biol Chem* **2006**, *281* (50), 38867-38870. DOI: 10.1074/jbc.M607955200.

30.   Yang, J.; Brown, M. S.; Liang, G.; Grishin, N. V.; Goldstein, J. L. Identification of the acyltransferase that octanoylates ghrelin, an appetite-stimulating peptide hormone. *Cell* **2008**, *132* (3), 387-396. DOI: 10.1016/j.cell.2008.01.017.

31.   Gutierrez, J. A.; Solenberg, P. J.; Perkins, D. R.; Willency, J. A.; Knierman, M. D.; Jin, Z.; Witcher, D. R.; Luo, S.; Onyia, J. E.; Hale, J. E. Ghrelin octanoylation mediated by an orphan lipid transferase. *Proc Natl Acad Sci U S A* **2008**, *105* (17), 6320-6325. DOI: 10.1073/pnas.0800708105.

32.   Delhanty, P. J.; Huisman, M.; Julien, M.; Mouchain, K.; Brune, P.; Themmen, A. P.; Abribat, T.; van der Lely, A. J. The acylated (AG) to unacylated (UAG) ghrelin ratio in esterase inhibitor-treated blood is higher than previously described. *Clin Endocrinol (Oxf)* **2015**, *82* (1), 142-146. DOI: 10.1111/cen.12489.

33.   De Vriese, C.; Gregoire, F.; Lema-Kisoka, R.; Waelbroeck, M.; Robberecht, P.; Delporte, C. Ghrelin degradation by serum and tissue homogenates: identification of the cleavage sites. *Endocrinology* **2004**, *145* (11), 4997-5005. DOI: 10.1210/en.2004-0569.

34.   Satou, M.; Sugimoto, H. The study of ghrelin deacylation enzymes. *Methods Enzymol* **2012**, *514*, 165-179. DOI: 10.1016/B978-0-12-381272-8.00011-8.

35.   Chen, V. P.; Gao, Y.; Geng, L.; Brimijoin, S. Butyrylcholinesterase regulates central ghrelin signaling and has an impact on food intake and glucose homeostasis. *Int J Obes (Lond)* **2017**, *41* (9), 1413-1419. DOI: 10.1038/ijo.2017.123.

36.   Brimijoin, S.; Chen, V. P.; Pang, Y. P.; Geng, L.; Gao, Y. Physiological roles for butyrylcholinesterase: A BChE-ghrelin axis. *Chem Biol Interact* **2016**, *259* (Pt B), 271-275. DOI: 10.1016/j.cbi.2016.02.013.

37.   Broglio, F.; Gottero, C.; Prodam, F.; Gauna, C.; Muccioli, G.; Papotti, M.; Abribat, T.; Van Der Lely, A. J.; Ghigo, E. Non-acylated ghrelin counteracts the metabolic but not the neuroendocrine response to acylated ghrelin in humans. *J Clin Endocrinol Metab* **2004**, *89* (6), 3062-3065. DOI: 10.1210/jc.2003-031964.

38.   Gauna, C.; Kiewiet, R. M.; Janssen, J. A. M. J. L.; De Zande, B. V.; Delhanty, P. J. D.; Ghigo, E.; Hofland, L. J.; Themmen, A. P. N.; Van der Lely, A. J. Unacylated ghrelin acts as a potent insulin secretagogue in glucose-stimulated conditions. *Am J Physiol-Endoc M* **2007**, *293* (3), E697-E704. DOI: DOI 10.1152/ajpendo.00219.2007.

39.   Gauna, C.; Meyler, F. M.; Janssen, J. A.; Delhanty, P. J.; Abribat, T.; van Koetsveld, P.; Hofland, L. J.; Broglio, F.; Ghigo, E.; van der Lely, A. J. Administration of acylated ghrelin reduces insulin sensitivity, whereas the combination of acylated plus unacylated ghrelin strongly

improves insulin sensitivity. *J Clin Endocrinol Metab* **2004**, *89* (10), 5035-5042. DOI: 10.1210/jc.2004-0363.

40.	Hopkins, A. L.; Nelson, T. A.; Guschina, I. A.; Parsons, L. C.; Lewis, C. L.; Brown, R. C.; Christian, H. C.; Davies, J. S.; Wells, T. Unacylated ghrelin promotes adipogenesis in rodent bone marrow via ghrelin O-acyl transferase and GHS-R(1a) activity: evidence for target cell-induced acylation. *Sci Rep* **2017**, *7*, 45541. DOI: 10.1038/srep45541.

41.	Murtuza, M. I.; Isokawa, M. Endogenous ghrelin-O-acyltransferase (GOAT) acylates local ghrelin in the hippocampus. *J. Neurochem.* **2018**, *144* (1), 58-67, 10.1111/jnc.14244. DOI: 10.1111/jnc.14244.

42.	Campana, M. B.; Davis, T. R.; Novak, S. X.; Cleverdon, E. R.; Bates, M.; Krishnan, N.; Curtis, E. R.; Childs, M. D.; Pierce, M. R.; Morales-Rodriguez, Y.; et al. Cellular Uptake of a Fluorescent Ligand Reveals Ghrelin O-Acyltransferase Interacts with Extracellular Peptides and Exhibits Unexpected Localization for a Secretory Pathway Enzyme. *ACS Chem Biol* **2023**, *18* (8), 1880-1890. DOI: 10.1021/acschembio.3c00334.

43.	DeFronzo, R. A.; Ferrannini, E.; Groop, L.; Henry, R. R.; Herman, W. H.; Holst, J. J.; Hu, F. B.; Kahn, C. R.; Raz, I.; Shulman, G. I.; et al. Type 2 diabetes mellitus. *Nat Rev Dis Primers* **2015**, *1*, 15019. DOI: 10.1038/nrdp.2015.19.

44.	Kahn, S. E.; Cooper, M. E.; Del Prato, S. Pathophysiology and treatment of type 2 diabetes: perspectives on the past, present, and future. *Lancet* **2014**, *383* (9922), 1068-1083. DOI: 10.1016/S0140-6736(13)62154-6.

45.	Ferrannini, E.; Mari, A. beta-Cell function in type 2 diabetes. *Metabolism* **2014**, *63* (10), 1217-1227. DOI: 10.1016/j.metabol.2014.05.012.

46.   Heppner, K. M.; Tong, J. Mechanisms in endocrinology: regulation of glucose metabolism by the ghrelin system: multiple players and multiple actions. *Eur J Endocrinol* **2014**, *171* (1), R21-32. DOI: 10.1530/EJE-14-0183.

47.   Delhanty, P. J.; van der Lely, A. J. Ghrelin and glucose homeostasis. *Peptides* **2011**, *32* (11), 2309-2318. DOI: 10.1016/j.peptides.2011.03.001.

48.   van der Lely, A. J. Ghrelin and new metabolic frontiers. *Horm Res* **2009**, *71 Suppl 1*, 129-133. DOI: 10.1159/000178055.

49.   van der Lely, A. J.; Tschop, M.; Heiman, M. L.; Ghigo, E. Biological, physiological, pathophysiological, and pharmacological aspects of ghrelin. *Endocr Rev* **2004**, *25* (3), 426-457. DOI: 10.1210/er.2002-0029.

50.   Yada, T.; Damdindorj, B.; Rita, R. S.; Kurashina, T.; Ando, A.; Taguchi, M.; Koizumi, M.; Sone, H.; Nakata, M.; Kakei, M.; Dezaki, K. Ghrelin signalling in beta-cells regulates insulin secretion and blood glucose. *Diabetes Obes Metab* **2014**, *16 Suppl 1*, 111-117. DOI: 10.1111/dom.12344.

51.   Egido, E. M.; Rodriguez-Gallardo, J.; Silvestre, R. A.; Marco, J. Inhibitory effect of ghrelin on insulin and pancreatic somatostatin secretion. *Eur J Endocrinol* **2002**, *146* (2), 241-244. DOI: 10.1530/eje.0.1460241.

52.   Reimer, M. K.; Pacini, G.; Ahren, B. Dose-dependent inhibition by ghrelin of insulin secretion in the mouse. *Endocrinology* **2003**, *144* (3), 916-921. DOI: 10.1210/en.2002-220819.

53.   Barazzoni, R.; Zanetti, M.; Ferreira, C.; Vinci, P.; Pirulli, A.; Mucci, M.; Dore, F.; Fonda, M.; Ciocchi, B.; Cattin, L.; Guarnieri, G. Relationships between desacylated and acylated ghrelin and insulin sensitivity in the metabolic syndrome. *J Clin Endocrinol Metab* **2007**, *92* (10), 3935-3940. DOI: 10.1210/jc.2006-2527.

54.   Granata, R.; Settanni, F.; Julien, M.; Nano, R.; Togliatto, G.; Trombetta, A.; Gallo, D.; Piemonti, L.; Brizzi, M. F.; Abribat, T.; et al. Des-acyl ghrelin fragments and analogues promote survival of pancreatic beta-cells and human pancreatic islets and prevent diabetes in streptozotocin-treated rats. *J Med Chem* **2012**, *55* (6), 2585-2596. DOI: 10.1021/jm201223m.

55.   Delhanty, P. J.; Huisman, M.; Baldeon-Rojas, L. Y.; van den Berge, I.; Grefhorst, A.; Abribat, T.; Leenen, P. J.; Themmen, A. P.; van der Lely, A. J. Des-acyl ghrelin analogs prevent high-fat-diet-induced dysregulation of glucose homeostasis. *FASEB J* **2013**, *27* (4), 1690-1700. DOI: 10.1096/fj.12-221143.

56.   Wren, A. M.; Small, C. J.; Abbott, C. R.; Dhillo, W. S.; Seal, L. J.; Cohen, M. A.; Batterham, R. L.; Taheri, S.; Stanley, S. A.; Ghatei, M. A.; Bloom, S. R. Ghrelin causes hyperphagia and obesity in rats. *Diabetes* **2001**, *50* (11), 2540-2547. DOI: 10.2337/diabetes.50.11.2540.

57.   Kojima, M.; Kangawa, K. Ghrelin: structure and function. *Physiol Rev* **2005**, *85* (2), 495-522. DOI: 10.1152/physrev.00012.2004.

58.   Perez-Tilve, D.; Heppner, K.; Kirchner, H.; Lockie, S. H.; Woods, S. C.; Smiley, D. L.; Tschop, M.; Pfluger, P. Ghrelin-induced adiposity is independent of orexigenic effects. *FASEB J* **2011**, *25* (8), 2814-2822. DOI: 10.1096/fj.11-183632.

59.   Shiiya, T.; Nakazato, M.; Mizuta, M.; Date, Y.; Mondal, M. S.; Tanaka, M.; Nozoe, S.; Hosoda, H.; Kangawa, K.; Matsukura, S. Plasma ghrelin levels in lean and obese humans and the effect of glucose on ghrelin secretion. *J Clin Endocrinol Metab* **2002**, *87* (1), 240-244. DOI: 10.1210/jcem.87.1.8129.

60.   Tschop, M.; Weyer, C.; Tataranni, P. A.; Devanarayan, V.; Ravussin, E.; Heiman, M. L. Circulating ghrelin levels are decreased in human obesity. *Diabetes* **2001**, *50* (4), 707-709. DOI: 10.2337/diabetes.50.4.707.

61.   English, P. J.; Ghatei, M. A.; Malik, I. A.; Bloom, S. R.; Wilding, J. P. Food fails to suppress ghrelin levels in obese humans. *J Clin Endocrinol Metab* **2002**, *87* (6), 2984. DOI: 10.1210/jcem.87.6.8738.

62.   Barnett, B. P.; Hwang, Y.; Taylor, M. S.; Kirchner, H.; Pfluger, P. T.; Bernard, V.; Lin, Y. Y.; Bowers, E. M.; Mukherjee, C.; Song, W. J.; et al. Glucose and weight control in mice with a designed ghrelin O-acyltransferase inhibitor. *Science* **2010**, *330* (6011), 1689-1692. DOI: 10.1126/science.1196154.

63.   Wellman, M. K.; Patterson, Z. R.; MacKay, H.; Darling, J. E.; Mani, B. K.; Zigman, J. M.; Hougland, J. L.; Abizaid, A. Novel Regulator of Acylated Ghrelin, CF801, Reduces Weight Gain, Rebound Feeding after a Fast, and Adiposity in Mice. *Front Endocrinol (Lausanne)* **2015**, *6*, 144. DOI: 10.3389/fendo.2015.00144.

64.   Soriano-Guillen, L.; Barrios, V.; Campos-Barros, A.; Argente, J. Ghrelin levels in obesity and anorexia nervosa: effect of weight reduction or recuperation. *J Pediatr* **2004**, *144* (1), 36-42. DOI: 10.1016/j.jpeds.2003.10.036.

65.   Misra, M.; Miller, K. K.; Herzog, D. B.; Ramaswamy, K.; Aggarwal, A.; Almazan, C.; Neubauer, G.; Breu, J.; Klibanski, A. Growth hormone and ghrelin responses to an oral glucose load in adolescent girls with anorexia nervosa and controls. *J Clin Endocrinol Metab* **2004**, *89* (4), 1605-1612. DOI: 10.1210/jc.2003-031861.

66.   Misra, M.; Klibanski, A. Endocrine consequences of anorexia nervosa. *Lancet Diabetes Endocrinol* **2014**, *2* (7), 581-592. DOI: 10.1016/S2213-8587(13)70180-3.

67.   Fabbri, A. D.; Deram, S.; Kerr, D. S.; Cordás, T. A. Ghrelin and eating disorders. *Archives of Clinical Psychiatry (São Paulo)* **2015**, *42* (2), 52-62. DOI: 10.1590/0101-60830000000048.

68.   Schorr, M.; Miller, K. K. The endocrine manifestations of anorexia nervosa: mechanisms and management. *Nat Rev Endocrinol* **2017**, *13* (3), 174-186. DOI: 10.1038/nrendo.2016.175.

69.   Smitka, K.; Papezova, H.; Vondra, K.; Hill, M.; Hainer, V.; Nedvidkova, J. The role of "mixed" orexigenic and anorexigenic signals and autoantibodies reacting with appetite-regulating neuropeptides and peptides of the adipose tissue-gut-brain axis: relevance to food intake and nutritional status in patients with anorexia nervosa and bulimia nervosa. *Int J Endocrinol* **2013**, *2013*, 483145. DOI: 10.1155/2013/483145.

70.   Berner, L. A.; Brown, T. A.; Lavender, J. M.; Lopez, E.; Wierenga, C. E.; Kaye, W. H. Neuroendocrinology of reward in anorexia nervosa and bulimia nervosa: Beyond leptin and ghrelin. *Mol Cell Endocrinol* **2019**, *497*, 110320. DOI: 10.1016/j.mce.2018.10.018.

71.   Monteleone, A. M.; Castellini, G.; Volpe, U.; Ricca, V.; Lelli, L.; Monteleone, P.; Maj, M. Neuroendocrinology and brain imaging of reward in eating disorders: A possible key to the treatment of anorexia nervosa and bulimia nervosa. *Prog Neuropsychopharmacol Biol Psychiatry* **2018**, *80* (Pt B), 132-142. DOI: 10.1016/j.pnpbp.2017.02.020.

72.   Collden, G.; Tschop, M. H.; Muller, T. D. Therapeutic Potential of Targeting the Ghrelin Pathway. *Int J Mol Sci* **2017**, *18* (4). DOI: 10.3390/ijms18040798.

73.   Hotta, M.; Ohwada, R.; Akamizu, T.; Shibasaki, T.; Takano, K.; Kangawa, K. Ghrelin increases hunger and food intake in patients with restricting-type anorexia nervosa: a pilot study. *Endocr J* **2009**, *56* (9), 1119-1128. DOI: 10.1507/endocrj.k09e-168.

74.   Neary, N. M.; Small, C. J.; Wren, A. M.; Lee, J. L.; Druce, M. R.; Palmieri, C.; Frost, G. S.; Ghatei, M. A.; Coombes, R. C.; Bloom, S. R. Ghrelin increases energy intake in cancer

patients with impaired appetite: acute, randomized, placebo-controlled trial. *J Clin Endocrinol Metab* **2004**, *89* (6), 2832-2836. DOI: 10.1210/jc.2003-031768.

75.   Haruta, I.; Fuku, Y.; Kinoshita, K.; Yoneda, K.; Morinaga, A.; Amitani, M.; Amitani, H.; Asakawa, A.; Sugawara, H.; Takeda, Y.; et al. One-year intranasal application of growth hormone releasing peptide-2 improves body weight and hypoglycemia in a severely emaciated anorexia nervosa patient. *J Cachexia Sarcopenia Muscle* **2015**, *6* (3), 237-241. DOI: 10.1002/jcsm.12028.

76.   Strasser, F.; Lutz, T. A.; Maeder, M. T.; Thuerlimann, B.; Bueche, D.; Tschop, M.; Kaufmann, K.; Holst, B.; Brandle, M.; von Moos, R.; et al. Safety, tolerability and pharmacokinetics of intravenous ghrelin for cancer-related anorexia/cachexia: a randomised, placebo-controlled, double-blind, double-crossover study. *Br J Cancer* **2008**, *98* (2), 300-308. DOI: 10.1038/sj.bjc.6604148.

77.   Hassouna, R.; Labarthe, A.; Zizzari, P.; Videau, C.; Culler, M.; Epelbaum, J.; Tolle, V. Actions of agonists and antagonists of the ghrelin/GHS-R pathway on GH secretion, appetite, and cFos activity. *Frontiers in Endocrinology* **2013**, *4* (MAR), Article. DOI: 10.3389/fendo.2013.00025 Scopus.

78.   Jerlhag, E.; Egecioglu, E.; Dickson, S. L.; Douhan, A.; Svensson, L.; Engel, J. A. Ghrelin administration into tegmental areas stimulates locomotor activity and increases extracellular concentration of dopamine in the nucleus accumbens. *Addict Biol* **2007**, *12* (1), 6-16. DOI: 10.1111/j.1369-1600.2006.00041.x.

79.   Wise, R. A. Brain reward circuitry: insights from unsensed incentives. *Neuron* **2002**, *36* (2), 229-240. DOI: 10.1016/s0896-6273(02)00965-0.

80.   Martel, P.; Fantino, M. Mesolimbic dopaminergic system activity as a function of food reward: A microdialysis study. *Pharmacol Biochem Be* **1996**, *53* (1), 221-226. DOI: Doi 10.1016/0091-3057(95)00187-5.

81.   Volkow, N. D.; Wang, G. J.; Maynard, L.; Jayne, M.; Fowler, J. S.; Zhu, W.; Logan, J.; Gatley, S. J.; Ding, Y. S.; Wong, C.; Pappas, N. Brain dopamine is associated with eating behaviors in humans. *Int J Eat Disord* **2003**, *33* (2), 136-142. DOI: 10.1002/eat.10118.

82.   Wise, R. A. The role of reward pathways in the development of drug dependence. *Pharmacol Ther* **1987**, *35* (1-2), 227-263. DOI: 10.1016/0163-7258(87)90108-2.

83.   Nestler, E. J. Is there a common molecular pathway for addiction? *Nat Neurosci* **2005**, *8* (11), 1445-1449. DOI: 10.1038/nn1578.

84.   Kraus, T.; Schanze, A.; Groschl, M.; Bayerlein, K.; Hillemacher, T.; Reulbach, U.; Kornhuber, J.; Bleich, S. Ghrelin levels are increased in alcoholism. *Alcohol Clin Exp Res* **2005**, *29* (12), 2154-2157. DOI: 10.1097/01.alc.0000191753.82554.7e.

85.   Kim, D. J.; Yoon, S. J.; Choi, B.; Kim, T. S.; Woo, Y. S.; Kim, W.; Myrick, H.; Peterson, B. S.; Choi, Y. B.; Kim, Y. K.; Jeong, J. Increased fasting plasma ghrelin levels during alcohol abstinence. *Alcohol Alcohol* **2005**, *40* (1), 76-79. DOI: 10.1093/alcalc/agh108.

86.   Leggio, L.; Ferrulli, A.; Cardone, S.; Nesci, A.; Miceli, A.; Malandrino, N.; Capristo, E.; Canestrelli, B.; Monteleone, P.; Kenna, G. A.; et al. Ghrelin system in alcohol-dependent subjects: role of plasma ghrelin levels in alcohol drinking and craving. *Addict Biol* **2012**, *17* (2), 452-464. DOI: 10.1111/j.1369-1600.2010.00308.x.

87.   Akkisi Kumsar, N.; Dilbaz, N. Relationship between craving and ghrelin, adiponectin, and resistin levels in patients with alcoholism. *Alcohol Clin Exp Res* **2015**, *39* (4), 702-709. DOI: 10.1111/acer.12689.

88.   Hillemacher, T.; Kraus, T.; Rauh, J.; Weiss, J.; Schanze, A.; Frieling, H.; Wilhelm, J.; Heberlein, A.; Groschl, M.; Sperling, W.; et al. Role of appetite-regulating peptides in alcohol craving: an analysis in respect to subtypes and different consumption patterns in alcoholism. *Alcohol Clin Exp Res* **2007**, *31* (6), 950-954. DOI: 10.1111/j.1530-0277.2007.00388.x.

89.   Addolorato, G.; Capristo, E.; Leggio, L.; Ferrulli, A.; Abenavoli, L.; Malandrino, N.; Farnetti, S.; Domenicali, M.; D'Angelo, C.; Vonghia, L.; et al. Relationship between ghrelin levels, alcohol craving, and nutritional status in current alcoholic patients. *Alcohol Clin Exp Res* **2006**, *30* (11), 1933-1937. DOI: 10.1111/j.1530-0277.2006.00238.x.

90.   Koopmann, A.; Bach, P.; Schuster, R.; Bumb, J. M.; Vollstadt-Klein, S.; Reinhard, I.; Rietschel, M.; Witt, S. H.; Wiedemann, K.; Kiefer, F. Ghrelin modulates mesolimbic reactivity to alcohol cues in alcohol-addicted subjects: a functional imaging study. *Addict Biol* **2019**, *24* (5), 1066-1076. DOI: 10.1111/adb.12651.

91.   Bach, P.; Bumb, J. M.; Schuster, R.; Vollstadt-Klein, S.; Reinhard, I.; Rietschel, M.; Witt, S. H.; Wiedemann, K.; Kiefer, F.; Koopmann, A. Effects of leptin and ghrelin on neural cue-reactivity in alcohol addiction: Two streams merge to one river? *Psychoneuroendocrinology* **2019**, *100*, 1-9. DOI: 10.1016/j.psyneuen.2018.09.026.

92.   Davis, K. W.; Wellman, P. J.; Clifford, P. S. Augmented cocaine conditioned place preference in rats pretreated with systemic ghrelin. *Regul Pept* **2007**, *140* (3), 148-152. DOI: 10.1016/j.regpep.2006.12.003.

93.   Wellman, P. J.; Hollas, C. N.; Elliott, A. E. Systemic ghrelin sensitizes cocaine-induced hyperlocomotion in rats. *Regul Pept* **2008**, *146* (1-3), 33-37. DOI: 10.1016/j.regpep.2007.07.007.

94.   Jang, J. K.; Kim, W. Y.; Cho, B. R.; Lee, J. W.; Kim, J. H. Microinjection of ghrelin in the nucleus accumbens core enhances locomotor activity induced by cocaine. *Behav Brain Res* **2013**, *248*, 7-11. DOI: 10.1016/j.bbr.2013.03.049.

95.   Tessari, M.; Catalano, A.; Pellitteri, M.; Di Francesco, C.; Marini, F.; Gerrard, P. A.; Heidbreder, C. A.; Melotto, S. Correlation between serum ghrelin levels and cocaine-seeking behaviour triggered by cocaine-associated conditioned stimuli in rats. Addict Biol 2007, 12 (1), 22-29. DOI: 10.1111/j.1369-1600.2007.00052.x.

96.   Jerlhag, E.; Egecioglu, E.; Dickson, S. L.; Engel, J. A. Ghrelin receptor antagonism attenuates cocaine- and amphetamine-induced locomotor stimulation, accumbal dopamine release, and conditioned place preference. *Psychopharmacology (Berl)* **2010**, *211* (4), 415-422. DOI: 10.1007/s00213-010-1907-7.

97.   Jerlhag, E.; Engel, J. A. Ghrelin receptor antagonism attenuates nicotine-induced locomotor stimulation, accumbal dopamine release and conditioned place preference in mice. *Drug Alcohol Depend* **2011**, *117* (2-3), 126-131. DOI: 10.1016/j.drugalcdep.2011.01.010.

98.   Havlickova, T.; Charalambous, C.; Lapka, M.; Puskina, N.; Jerabek, P.; Sustkova-Fiserova, M. Ghrelin Receptor Antagonism of Methamphetamine-Induced Conditioned Place Preference and Intravenous Self-Administration in Rats. *Int J Mol Sci* **2018**, *19* (10). DOI: 10.3390/ijms19102925.

99.   Wellman, P. J.; Clifford, P. S.; Rodriguez, J.; Hughes, S.; Eitan, S.; Brunel, L.; Fehrentz, J. A.; Martinez, J. Pharmacologic antagonism of ghrelin receptors attenuates development of nicotine induced locomotor sensitization in rats. *Regul Pept* **2011**, *172* (1-3), 77-80. DOI: 10.1016/j.regpep.2011.08.014.

100.   Magdalena, S.-F.; Pavel, J.; Tereza, H.; Petr, K.; Miloslav, K. E.15 - Ghrelin Receptor Antagonism Attenuates Morphine-Induced Accumbal Dopamine Release and Behavioral Stimulation in Rats. *Behavioural Pharmacology* **2013**, *24*, e45. DOI: 10.1097/01.fbp.0000434834.85386.4a.

101.   Sustkova-Fiserova, M.; Jerabek, P.; Havlickova, T.; Syslova, K.; Kacer, P. Ghrelin and endocannabinoids participation in morphine-induced effects in the rat nucleus accumbens. *Psychopharmacology (Berl)* **2016**, *233* (3), 469-484. DOI: 10.1007/s00213-015-4119-3.

102.   D'Cunha, T. M.; Chisholm, A.; Hryhorczuk, C.; Fulton, S.; Shalev, U. A role for leptin and ghrelin in the augmentation of heroin seeking induced by chronic food restriction. *Psychopharmacology (Berl)* **2019**. DOI: 10.1007/s00213-019-05415-9.

103.   Sustkova-Fiserova, M.; Puskina, N.; Havlickova, T.; Lapka, M.; Syslova, K.; Pohorala, V.; Charalambous, C. Ghrelin receptor antagonism of fentanyl-induced conditioned place preference, intravenous self-administration, and dopamine release in the nucleus accumbens in rats. *Addict Biol* **2019**, e12845. DOI: 10.1111/adb.12845.

104.   Holm, V. A.; Cassidy, S. B.; Butler, M. G.; Hanchett, J. M.; Greenswag, L. R.; Whitman, B. Y.; Greenberg, F. Prader-Willi syndrome: consensus diagnostic criteria. *Pediatrics* **1993**, *91* (2), 398-402.

105.   Lindgren, A. C.; Barkeling, B.; Hagg, A.; Ritzen, E. M.; Marcus, C.; Rossner, S. Eating behavior in Prader-Willi syndrome, normal weight, and obese control groups. *J Pediatr* **2000**, *137* (1), 50-55. DOI: 10.1067/mpd.2000.106563.

106.   DelParigi, A.; Tschop, M.; Heiman, M. L.; Salbe, A. D.; Vozarova, B.; Sell, S. M.; Bunt, J. C.; Tataranni, P. A. High circulating ghrelin: a potential cause for hyperphagia and obesity in

prader-willi syndrome. *J Clin Endocrinol Metab* **2002**, *87* (12), 5461-5464. DOI: 10.1210/jc.2002-020871.

107.   Haqq, A. M.; Farooqi, I. S.; O'Rahilly, S.; Stadler, D. D.; Rosenfeld, R. G.; Pratt, K. L.; LaFranchi, S. H.; Purnell, J. Q. Serum ghrelin levels are inversely correlated with body mass index, age, and insulin concentrations in normal children and are markedly increased in Prader-Willi syndrome. *J Clin Endocrinol Metab* **2003**, *88* (1), 174-178. DOI: 10.1210/jc.2002-021052.

108.   Cummings, D. E.; Clement, K.; Purnell, J. Q.; Vaisse, C.; Foster, K. E.; Frayo, R. S.; Schwartz, M. W.; Basdevant, A.; Weigle, D. S. Elevated plasma ghrelin levels in Prader Willi syndrome. *Nat Med* **2002**, *8* (7), 643-644. DOI: 10.1038/nm0702-643.

109.   Feigerlova, E.; Diene, G.; Conte-Auriol, F.; Molinas, C.; Gennero, I.; Salles, J. P.; Arnaud, C.; Tauber, M. Hyperghrelinemia precedes obesity in Prader-Willi syndrome. *J Clin Endocrinol Metab* **2008**, *93* (7), 2800-2805. DOI: 10.1210/jc.2007-2138.

110.   Kweh, F. A.; Miller, J. L.; Sulsona, C. R.; Wasserfall, C.; Atkinson, M.; Shuster, J. J.; Goldstone, A. P.; Driscoll, D. J. Hyperghrelinemia in Prader-Willi syndrome begins in early infancy long before the onset of hyperphagia. *Am J Med Genet A* **2015**, *167A* (1), 69-79. DOI: 10.1002/ajmg.a.36810.

111.   Kuppens, R. J.; Diene, G.; Bakker, N. E.; Molinas, C.; Faye, S.; Nicolino, M.; Bernoux, D.; Delhanty, P. J.; van der Lely, A. J.; Allas, S.; et al. Elevated ratio of acylated to unacylated ghrelin in children and young adults with Prader-Willi syndrome. *Endocrine* **2015**, *50* (3), 633-642. DOI: 10.1007/s12020-015-0614-x.

112.   Beauloye, V.; Diene, G.; Kuppens, R.; Zech, F.; Winandy, C.; Molinas, C.; Faye, S.; Kieffer, I.; Beckers, D.; Nergardh, R.; et al. High unacylated ghrelin levels support the concept

of anorexia in infants with prader-willi syndrome. *Orphanet J Rare Dis* **2016**, *11* (1), 56. DOI: 10.1186/s13023-016-0440-0.

113.   Haqq, A. M.; Stadler, D. D.; Rosenfeld, R. G.; Pratt, K. L.; Weigle, D. S.; Frayo, R. S.; LaFranchi, S. H.; Cummings, D. E.; Purnell, J. Q. Circulating ghrelin levels are suppressed by meals and octreotide therapy in children with Prader-Willi syndrome. *J Clin Endocrinol Metab* **2003**, *88* (8), 3573-3576. DOI: 10.1210/jc.2003-030205.

114.   De Waele, K.; Ishkanian, S. L.; Bogarin, R.; Miranda, C. A.; Ghatei, M. A.; Bloom, S. R.; Pacaud, D.; Chanoine, J. P. Long-acting octreotide treatment causes a sustained decrease in ghrelin concentrations but does not affect weight, behaviour and appetite in subjects with Prader-Willi syndrome. *Eur J Endocrinol* **2008**, *159* (4), 381-388. DOI: 10.1530/EJE-08-0462.

115.   Lin, D.; Wang, Q.; Ran, H.; Liu, K.; Wang, Y.; Wang, J.; Liu, Y.; Chen, R.; Sun, Y.; Liu, R.; Ding, F. Abnormal response to the anorexic effect of GHS-R inhibitors and exenatide in male Snord116 deletion mouse model for Prader-Willi syndrome. *Endocrinology* **2014**, *155* (7), 2355-2362. DOI: 10.1210/en.2013-2083.

116.   Allas, S.; Caixas, A.; Poitou, C.; Coupaye, M.; Thuilleaux, D.; Lorenzini, F.; Diene, G.; Crino, A.; Illouz, F.; Grugni, G.; et al. AZP-531, an unacylated ghrelin analog, improves food-related behavior in patients with Prader-Willi syndrome: A randomized placebo-controlled trial. *PLoS One* **2018**, *13* (1), e0190849. DOI: 10.1371/journal.pone.0190849.

117.   Therapeutics, M. *Millendo Therapeutics Announces Topline Results for Pivotal Phase 2b Study of Livoletide in Patients with Prader-Willi Syndrome (PWS)*. 2020. https://www.biospace.com/article/releases/millendo-therapeutics-announces-topline-results-for-pivotal-phase-2b-study-of-livoletide-in-patients-with-prader-willi-syndrome-pws-/ (accessed 2023.

118.   Miller, J. L.; Lacroix, A.; Bird, L. M.; Shoemaker, A. H.; Haqq, A.; Deal, C. L.; Clark, K. A.; Ames, M. H.; Suico, J. G.; de la Pena, A.; Fortier, C. The Efficacy, Safety, and Pharmacology of a Ghrelin O-Acyltransferase Inhibitor for the Treatment of Prader-Willi Syndrome. *J Clin Endocrinol Metab* **2022**, *107* (6), e2373-e2380. DOI: 10.1210/clinem/dgac105.

119.   Darling, J. E.; Zhao, F.; Loftus, R. J.; Patton, L. M.; Gibbs, R. A.; Hougland, J. L. Structure-Activity Analysis of Human Ghrelin O-Acyltransferase Reveals Chemical Determinants of Ghrelin Selectivity and Acyl Group Recognition. *Biochemistry* **2015**, *54* (4), 1100-1110. DOI: 10.1021/bi5010359 From American Chemical Society .

120.   Gahete, M. D.; Cordoba-Chacon, J.; Salvatori, R.; Castano, J. P.; Kineman, R. D.; Luque, R. M. Metabolic regulation of ghrelin O-acyl transferase (GOAT) expression in the mouse hypothalamus, pituitary, and stomach. *Mol Cell Endocrinol* **2010**, *317* (1-2), 154-160. DOI: 10.1016/j.mce.2009.12.023.

121.   Taylor, M. S.; Ruch, T. R.; Hsiao, P. Y.; Hwang, Y.; Zhang, P.; Dai, L.; Huang, C. R.; Berndsen, C. E.; Kim, M. S.; Pandey, A.; et al. Architectural organization of the metabolic regulatory enzyme ghrelin O-acyltransferase. *J Biol Chem* **2013**, *288* (45), 32211-32228. DOI: 10.1074/jbc.M113.510313.

122.   Liu, Y.; Qi, X.; Donnelly, L.; Elghobashi-Meinhardt, N.; Long, T.; Zhou, R. W.; Sun, Y.; Wang, B.; Li, X. Mechanisms and inhibition of Porcupine-mediated Wnt acylation. *Nature* **2022**, *607* (7920), 816-822. DOI: 10.1038/s41586-022-04952-2.

123.   Jiang, Y.; Benz, T. L.; Long, S. B. Substrate and product complexes reveal mechanisms of Hedgehog acylation by HHAT. *Science* **2021**, *372* (6547), 1215-1219. DOI: 10.1126/science.abg4998.

124.   Qian, H.; Zhao, X.; Yan, R.; Yao, X.; Gao, S.; Sun, X.; Du, X.; Yang, H.; Wong, C. C. L.; Yan, N. Structural basis for catalysis and substrate specificity of human ACAT1. *Nature* **2020**, *581* (7808), 333-338. DOI: 10.1038/s41586-020-2290-0

125.   Campaña, M. B.; Irudayanathan, F. J.; Davis, T. R.; McGovern-Gooch, K. R.; Loftus, R.; Ashkar, M.; Escoffery, N.; Navarro, M.; Sieburg, M. A.; nangia, S.; Hougland, J. L. Molecular architecture of a membrane-spanning hormone acyltransferase required for metabolic regulation. *bioRxiv* **2019**, 556233. DOI: 10.1101/556233.

126.   Bitgood, M. J.; McMahon, A. P. Hedgehog and Bmp genes are coexpressed at many diverse sites of cell-cell interaction in the mouse embryo. *Dev Biol* **1995**, *172* (1), 126-138. DOI: 10.1006/dbio.1995.0010.

127.   Echelard, Y.; Epstein, D. J.; St-Jacques, B.; Shen, L.; Mohler, J.; McMahon, J. A.; McMahon, A. P. Sonic hedgehog, a member of a family of putative signaling molecules, is implicated in the regulation of CNS polarity. *Cell* **1993**, *75* (7), 1417-1430. DOI: 10.1016/0092-8674(93)90627-3.

128.   Pepinsky, R. B.; Zeng, C.; Wen, D.; Rayhorn, P.; Baker, D. P.; Williams, K. P.; Bixler, S. A.; Ambrose, C. M.; Garber, E. A.; Miatkowski, K.; et al. Identification of a palmitic acid-modified form of human Sonic hedgehog. *J Biol Chem* **1998**, *273* (22), 14037-14045. DOI: 10.1074/jbc.273.22.14037.

129.   Coupland, C. E.; Andrei, S. A.; Ansell, T. B.; Carrique, L.; Kumar, P.; Sefer, L.; Schwab, R. A.; Byrne, E. F. X.; Pardon, E.; Steyaert, J.; et al. Structure, mechanism, and inhibition of Hedgehog acyltransferase. *Mol Cell* **2021**, *81* (24), 5025-5038 e5010. DOI: 10.1016/j.molcel.2021.11.018.

130.   Pierce, M. R.; Hougland, J. L. A rising tide lifts all MBOATs: recent progress in structural and functional understanding of membrane bound O-acyltransferases. *Front Physiol* **2023**, *14*, 1167873. DOI: 10.3389/fphys.2023.1167873

131.   Buglino, J. A.; Resh, M. D. Identification of conserved regions and residues within Hedgehog acyltransferase critical for palmitoylation of Sonic Hedgehog. *PLoS One* **2010**, *5* (6), e11195. DOI: 10.1371/journal.pone.0011195.

132.   Lanyon-Hogg, T.; Ritzefeld, M.; Zhang, L.; Andrei, S. A.; Pogranyi, B.; Mondal, M.; Sefer, L.; Johnston, C. D.; Coupland, C. E.; Greenfield, J. L.; et al. Photochemical Probe Identification of a Small-Molecule Inhibitor Binding Site in Hedgehog Acyltransferase (HHAT). *Angew Chem Int Ed Engl* **2021**, *60* (24), 13542-13547. DOI: 10.1002/anie.202014457.

133.   Asciolla, J. J.; Resh, M. D. Hedgehog Acyltransferase Promotes Uptake of Palmitoyl-CoA across the Endoplasmic Reticulum Membrane. *Cell Rep* **2019**, *29* (13), 4608-4619 e4604. DOI: 10.1016/j.celrep.2019.11.110.

134.   Zhai, L.; Chaturvedi, D.; Cumberledge, S. Drosophila wnt-1 undergoes a hydrophobic modification and is targeted to lipid rafts, a process that requires porcupine. *J Biol Chem* **2004**, *279* (32), 33220-33227. DOI: 10.1074/jbc.M403407200.

135.   Rios-Esteves, J.; Haugen, B.; Resh, M. D. Identification of key residues and regions important for porcupine-mediated Wnt acylation. *J Biol Chem* **2014**, *289* (24), 17009-17019. DOI: 10.1074/jbc.M114.561209.

136.   Janda, C. Y.; Waghray, D.; Levin, A. M.; Thomas, C.; Garcia, K. C. Structural basis of Wnt recognition by Frizzled. *Science* **2012**, *337* (6090), 59-64. DOI: 10.1126/science.1222879.

137. Takada, R.; Satomi, Y.; Kurata, T.; Ueno, N.; Norioka, S.; Kondoh, H.; Takao, T.; Takada, S. Monounsaturated fatty acid modification of Wnt protein: its role in Wnt secretion. *Dev Cell* **2006**, *11* (6), 791-801. DOI: 10.1016/j.devcel.2006.10.003.

138. Galli, L. M.; Anderson, M. O.; Gabriel Fraley, J.; Sanchez, L.; Bueno, R.; Hernandez, D. N.; Maddox, E. U.; Lingappa, V. R.; Burrus, L. W. Determination of the membrane topology of PORCN, an O-acyl transferase that modifies Wnt signalling proteins. *Open Biol* **2021**, *11* (6), 200400. DOI: 10.1098/rsob.200400.

139. Yu, J.; Liao, P. J.; Xu, W.; Jones, J. R.; Everman, D. B.; Flanagan-Steet, H.; Keller, T. H.; Virshup, D. M. Structural model of human PORCN illuminates disease-associated variants and drug-binding sites. *J Cell Sci* **2021**, *134* (24). DOI: 10.1242/jcs.259383.

140. Yang, J.; Zhao, T. J.; Goldstein, J. L.; Brown, M. S. Inhibition of ghrelin O-acyltransferase (GOAT) by octanoylated pentapeptides. *PNAS* **2008**, *105* (31), 10750-10755, Article. DOI: 10.1073/pnas.0805353105 Scopus.

141. Yoneyama-Hirozane, M.; Deguchi, K.; Hirakawa, T.; Ishii, T.; Odani, T.; Matsui, J.; Nakano, Y.; Imahashi, K.; Takakura, N.; Chisaki, I.; et al. Identification and Characterization of a New Series of Ghrelin O-Acyl Transferase Inhibitors. *SLAS Discovery* **2018**, *23* (2), 154-163, 10.1177/2472555217727097. DOI: 10.1177/2472555217727097.

142. Moose, J. E.; Leets, K. A.; Mate, N. A.; Chisholm, J. D.; Hougland, J. L. An overview of ghrelin O-acyltransferase inhibitors: a literature and patent review for 2010-2019. *Expert Opin Ther Pat* **2020**, *30* (8), 581-593. DOI: 10.1080/13543776.2020.1776263.

143. Zhao, F.; Darling, J. E.; Gibbs, R. A.; Hougland, J. L. A new class of ghrelin O-acyltransferase inhibitors incorporating triazole-linked lipid mimetic groups. *Bioorganic &*

Medicinal Chemistry Letters **2015**, *25* (14), 2800-2803. DOI: 10.1016/j.bmcl.2015.05.009 From American Chemical Society . All Rights Reserved. CAPLUS.

144.   Hollibaugh, R. A. Defining a Minimal Pharmacophore to Selectively Inhibit MBOAT4. UCLA, 2016.

145.   Harran, P. G.; Hollibaugh, R. A.; Liu, H. Small lipopeptidomimetic inhibitors of ghrelin o-acyl transferase. WO2016044467A1, 2016.

146.   Murzinski, E. S.; Saha, I.; Ding, H.; Strugatsky, D.; Hollibaugh, R. A.; Liu, H.; Tontonoz, P.; Harran, P. G. In Search of Small Molecules That Selectively Inhibit MBOAT4. *Molecules* **2021**, *26* (24). DOI: 10.3390/molecules26247599.

147.   Garner, A. L.; Janda, K. D. A small molecule antagonist of ghrelin O-acyltransferase (GOAT). *Chem. Commun.* **2011**, *47* (26), 7512-7514, 10.1039/c1cc11817j. DOI: 10.1039/c1cc11817j.

148.   Garner, A. L.; Janda, K. D. cat-ELCCA: A Robust Method To Monitor the Fatty Acid Acyltransferase Activity of Ghrelin O-Acyltransferase (GOAT). *Angew. Chem., Int. Ed.* **2010**, *49* (50), 9630-9634, 10.1002/anie.201003387. DOI: 10.1002/anie.201003387.

149.   Darling, J. E.; Prybolsky, E. P.; Sieburg, M.; Hougland, J. L. A fluorescent peptide substrate facilitates investigation of ghrelin recognition and acylation by ghrelin O-acyltransferase. *Analytical Biochemistry* **2013**, *437* (1), 68-76. DOI: 10.1016/j.ab.2013.02.013

150.   Hougland, J.; Darling, J. Fluorescence assay for ghrelin o-acyltransferase activity. US20140212904A1, 2014.

151.   McGovern-Gooch, K. R.; Mahajani, N. S.; Garagozzo, A.; Schramm, A. J.; Hannah, L. G.; Sieburg, M. A.; Chisholm, J. D.; Hougland, J. L. Synthetic Triterpenoid Inhibition of Human Ghrelin O-Acyltransferase: The Involvement of a Functionally Required Cysteine Provides

Mechanistic Insight into Ghrelin Acylation. *Biochemistry* **2017**, *56* (7), 919-931. DOI: 10.1021/acs.biochem.6b01008

152.   Galka, C. S.; Hembre, E. J.; Honigschmidt, N. A.; Keding, S. J.; Martinez-Grau, M. A.; Plaza, G. R.; Rubio, A.; Smith, D. L. Preparation of N-acylamino acid derivatives as ghrelin o-acyl transferase inhibitors. WO2016168225A1, 2016.

153.   Galka, C. S.; Hembre, E. J.; Honigschmidt, N. A.; Martinez-Grau, M. A.; Plaza, G. R.; Rubio, A. Preparation of 5-[2-[1-[N-acyl-L-alanyl]piperidin-4-yl]ethyl]-2-(trifluoromethyl)-6-methylpyrimidin-4-amine as ghrelin o-acyl transferase inhibitors. WO2016168222A1, 2016.

154.   Ruano, G.; Galka, C.; Hembre, E.; Honigschmidt, N.; Martinez-Grau, M.; Nevill, C. R.; Rubio, A.; Brier, R.; He, M.; Chen, Y.; et al. Ghrelin O-acyl transferase (GOAT) inhibitors: Optimization of the 6-chloro-2-methyl-5-[2-(4-piperidyl)ethyl]pyrimidin-4-amine scaffold. 2016; American Chemical Society: pp MEDI-385.

155.   Hembre, E.; Brier, R.; Chen, Y.; Dominguez, C.; Galka, C.; He, M.; Honigschmidt, N.; Jesudason, C.; Keding, S.; Martinez-Grau, M.; et al. Discovery of LY3073084, a novel non-peptide small molecule ghrelin-O-acyl transferase (GOAT) inhibitor. 2016; American Chemical Society: pp MEDI-277.

156.   A Study to Assess the Safety, Tolerability, Pharmacokinetics, and Pharmacodynamics of GLWL-01. **2019**. (acccessed 12/27/2023).

157.   Batterham, R. L.; Zakeri, R. Investigating the Role of Ghrelin in Regulating Appetite and Energy Intake in Patients Following Bariatric Surgery. ClinicalTrials.gov Identifier: NCT03641417, 2018-2019.

158.   Manipulating Ghrelin Signaling Via GOAT Inhibition in Alcohol Use Disorder. **2023**.

159.   Takakura, N.; Banno, Y.; Terao, Y.; Ochida, A.; Morimoto, S.; Kitamura, S.; Tomata, Y.; Yasuma, T.; Ikoma, M.; Masuda, K. Preparation of benzothiophenyl- and benzofuranacetic acid derivatives as inhibitors of GOAT for treating obesity. WO2013125732A1, 2013.

160.   Kang, X.; Chen, Z. Carboxylic Acid Compounds in Tretment of Diabetes Mellitus. WO2015/024526, 2015.

161.   Bandyopadhyay, A.; Cheung, M.; Eidam, H. S.; Joshi, H.; Su, D.-S. Preparation of ghrelin O-acyltransferase inhibitors for treatment of metabolic disorders. IN201811004277A, 2019.

162.   Bandyopadhyay, A.; Cheung, M.; Eidam, H. S.; Joshi, H.; Su, D.-S. Ghrelin O-acyltransferase Inhibitors. WO2019/149959A1, 2019.

163.   Wang, L. Preparation of benzo[b]thiophene compounds for treating obesity and diabetes. CN108610337A, 2018.

164.   Trieselmann, T.; Godbout, C.; Hoenke, C.; Vintonyak, V. Preparation of triazolopyrimidine derivatives as ghrelin o-acyl transferase (GOAT) inhibitors. WO2019149660A1, 2019.

165.   Godbout, C.; Trieselmann, T.; Vintonyak, V. Preparation of oxadiazolopyridine derivatives for use as ghrelin o-acyl transferase (GOAT) inhibitors. WO2018024653A1, 2018.

166.   Godbout, C.; Trieselmann, T.; Vintonyak, V. Preparation of heterocyclyl-substituted oxadiazolopyridine derivatives for use as ghrelin o-acyl transferase inhibitors. WO2019149658A1, 2019.

167.   Trieselmann, T.; Godbout, C.; Hoenke, C.; Vintonyak, V. Preparation of benzyl-, (pyridin-3-yl)methyl- or (pyridin-4-yl)methyl-substituted oxadiazolopyridine derivatives as ghrelin o-acyl transferase (GOAT) inhibitors. WO2019149657A1, 2019.

168.   Bianzano, S.; Henrich, A.; Herich, L.; Kalsch, B.; Sarubbi, D.; Seitz, F.; Forst, T.

Efficacy and safety of the ghrelin-O-acyltransferase inhibitor BI 1356225 in overweight/obesity:

Data from two Phase I, randomised, placebo-controlled studies. *Metabolism* **2023**, *143*, 155550.

DOI: 10.1016/j.metabol.2023.155550.

169.   Taylor, M. S.; Dempsey, D. R.; Hwang, Y.; Chen, Z.; Chu, N.; Boeke, J. D.; Cole, P. A.

Mechanistic analysis of ghrelin-O-acyltransferase using substrate analogs. *Bioorg Chem* **2015**,

62, 64-73. DOI: 10.1016/j.bioorg.2015.07.003.

170.   Ohgusu, H.; Shirouzu, K.; Nakamura, Y.; Nakashima, Y.; Ida, T.; Sato, T.; Kojima, M.

Ghrelin O-acyltransferase (GOAT) has a preference for n-hexanoyl-CoA over n-octanoyl-CoA

as an acyl donor. *Biochem Biophys Res Commun* **2009**, *386* (1), 153-158. DOI:

10.1016/j.bbrc.2009.06.001.

171.   Liu, J.; Prudom, C. E.; Nass, R.; Pezzoli, S. S.; Oliveri, M. C.; Johnson, M. L.; Veldhuis,

P.; Gordon, D. A.; Howard, A. D.; Witcher, D. R.; et al. Novel ghrelin assays provide evidence

for independent regulation of ghrelin acylation and secretion in healthy young men. *J Clin

Endocrinol Metab* **2008**, *93* (5), 1980-1987. DOI: 10.1210/jc.2007-2235.

172.   Trieselmann, T.; Godbout, C.; Vintonyak, V. Preparation of heterocyclyl-substituted

oxadiazolopyridine derivatives for use as ghrelin o-acyl transferase inhibitors.

WO2019149659A1, 2019.

173.   Harran, P. G.; Brown, M. S.; Goldstein, J. L.; Yang, J.; Zhao, T.-J. Small molecule

inhibitors of ghrelin o-acyltransferase and therapeutic use thereof. US Patent

US20100086955A1, 2010.

Chapter 2: Inhibitor binding sites within ghrelin O-acyltransferase revealed by structural modeling and high-throughput screening

Initial virtual screen using MTiOpenScreen and generation of LigPlot files (Figures 2.13 and 2.16) were performed by Dr. John Chisholm (Department of Chemistry, Syracuse University). Synthesis of JH101 (Takeda A) was performed by Cassie Grossman and Dr. Katelyn Leets (John Chisholm Laboratory, Department of Chemistry, Syracuse University).

Computational modeling and discussion of inhibitor poses against hGOAT using molecular dynamics and YASARA was performed by Jingjing Ji and Dr. Shikha Nangia (Shikha Nangia Laboratory, Department of Biomedical and Chemical Engineering, Syracuse University).

Dr. Kayleigh McGovern-Gooch (James Hougland Laboratory, Department of Chemistry, Syracuse University) performed initial plate reader experiments to determine viability of GSSC$_{AcDan}$LS and GSSFLC$_{AcDan}$ for assay development. Jackson Calhoun and Zachary Spada (both James Hougland Laboratory, Department of Chemistry, Syracuse University) assisted with initial optimization of the plate-reader assay.

I performed all biochemical assay validation and data collection shown in this chapter, including peptide labeling, inhibitor potency and behavior analysis, hGOAT activity assays via HPLC and plate-reader, continuous fluorescence assay development, inhibitor library generation, mutant hGOAT expression and analysis, and analysis of inhibitor contacts.

2.1 Introduction

Molecules capable of ghrelin modulation have been desired for the treatment of Type II Diabetes, obesity, addiction, and other pathophysiologies. [1-8] As ghrelin O-acyltransferase (GOAT) is responsible for the octanoylation that activates GOAT for its cognate receptor, GOAT is a target of interest for the development of compounds capable of modulating ghrelin signaling. [9, 10] In order to find these molecules, two things are necessary; a set of compounds to test, and an assay capable of detecting changes in GOAT activity.

Identification of ghrelin O-acyltransferase acylation activity has relied on detection of the acylated ghrelin product. Initial detection of GOAT activity and inhibition performed by Yang et al. relied on scintillation counting to detect the transfer of tritium-labeled octanoate from octanoyl-CoA to ghrelin. [11] This assay has been recently utilized to validate oxadiazolopyridine GOAT inhibitors. [12] Developed at the same time as the scintillation assay, Gutierrez et al. utilized mass spectrometry of cells contransfected with ghrelin and GOAT to identify the octanoylated product of the reaction. [9]

As the majority of the initial molecules found for the inhibition of GOAT were rationally-designed peptide-mimetic structures, these inhibitors likely compete with ghrelin to cause inhibition. These inhibitors include [Dap^3]-ghrelin (1-5)-NH$_2$, [Dap^3] propylphenyl triazole ghrelin (1-5)-NH$_2$, as well as similar derivatives. [11, 13] Fused peptidic molecules targeting multiple GOAT or GHSR binding sites represent another class of potential peptide competitive compounds. Combining GHSR agonist MK-0677 and the [Dap^3]-ghrelin (1-5)-NH$_2$ peptide lead to a series of compounds with low micromolar affinities for GOAT. [14] Interestingly, a macrocyclic compound developed from the Dap^3 inhibitor has been shown to compete for the peptide binding site as well. [12] The bisubstrate mimetic molecule GO-CoA-Tat was developed

through the combination of both the ghrelin peptide and octanoyl-CoA, as well as with the cell-penetrating Tat peptide sequence to aid cellular uptake, could theoretically compete with both peptide and lipid substrates of GOAT. [15, 16]

To broaden the potential chemical scaffolds available to inhibit GOAT, assays capable of screening large numbers of small-molecules became necessary. A fluorescence-based screening assay was used to identify the first small-molecule, non-peptide mimetic inhibitor of GOAT. [17] This assay, called catalytic enzyme-linked click chemistry assay or cat-ELCCA, reacted alkynyl octanoyl-CoA and an immobilized ghrelin peptide. Conjugation of the labeled octanoylated ghrelin to azido-HRP through a copper-catalyzed [3+2] cycloaddition and addition of a fluorogenic HRP substrate provided signal amplification. [18, 19] A review of the relevant patent literature indicates that acyl-ghrelin specific enzyme-linked immunosorbent assays (ELISA) are used in pharmaceutical detection of GOAT activity. [20] This approach is exemplified in the 2018 report of octanoyl-CoA competitive inhibitors from Takeda Pharmaceutical resulting from a library screen accomplished through a ghrelin selective antibody primary screen followed by a ghrelin-specific ELISA plate secondary screening. [21]

As mentioned above, previous efforts to discover novel GOAT inhibitors have screened large numbers of small molecules through library screens. The initial small-molecule inhibitors from Garner and Janda were found through a small library screen of 4000 compounds. [17, 18] Takeda Pharmaceutical tested more than 500,000 compounds in their initial screen, resulting in 301 molecules being selected for secondary screening, a reported hit rate of 0.05%. [21] The first report of acyl-donor competitive behavior was the result of this library screen from Takeda Pharmaceutical, with two compounds showing decreased inhibition of GOAT at high concentrations of octanoyl-CoA. [21] While currently unproven, the structural similarities between

the Takeda compounds and compounds developed by Eli Lilly, GlaxoSmithKline and Boehringer-Ingelheim suggest these compounds may also act as acyl-donor competitive inhibitors. [22-25]

Other reported GOAT inhibitors do not currently have suggested specific binding sites within GOAT based on their mode of inhibition. While the Garner and Janda inhibitor was the first small-molecule inhibitor of GOAT, the binding site of this compound is unknown. [17] Triterpenoids and steroid scaffolds have been shown to inhibit GOAT, presumably targeting cysteine residues due to the Michael-accepting enone moieties, but the identity of the targeted cysteine is unknown. [26]

Further understanding the interactions between inhibitors, substrates, and GOAT should be a priority to expand our current pharmacological profile and ability to rationally design relevant drug-like inhibitors. Due to the limited number of molecules with characterized binding classes, current studies of GOAT inhibitors lack the context necessary to design molecules targeting specific substrate interactions with GOAT, leading to limited opportunities for rational design of molecules. In 2019, the Hougland lab published a computational model of GOAT derived through coevolutionary contact modeling coupled with molecular dynamics. [27] The computational model revealed a transmembrane channel spanning the entirety of GOAT, and docking studies indicated the location of the octanoyl-CoA binding site on the cytoplasmic face of the enzyme. This model was further supported by biochemical validation, with GOAT mutations of predicted contacts to octanoyl-CoA altering GOAT preference for lipid donor length. This model also indicates the MBOAT family conserved N307 and H338 are in different locations within the enzyme, with N307 being located in the acyl-donor binding site and H338 positioned within the transmembrane channel. The availability of this model now allows for

identification of new classes of GOAT inhibitors, specific interactions between GOAT and novel inhibitors, as well as rational design of derivatives of hit compounds. This information also allows the discovery of the binding sites of literature inhibitors and comparison to novel compounds.

2.2 Results

2.2.1 Development and validation of the Continuous Fluorescence Assay

In the HPLC-based GOAT acylation assay used in previous inhibitor studies in our research group, a six amino acid ghrelin mimetic peptide is octanoylated in the presence of GOAT and octanoyl-CoA. GOAT catalyzes addition of an the octanoyl group to serine-3 (bold) of the ghrelin "GS**S**F" sequence in both the native protein and peptide mimetics (**Figure 2.1a**). [11, 17, 28-30] The peptide sequence GSSFLC enables peptide labeling with an acrylodan fluorophore at the C-terminal cysteine residue. [29] In addition to reverse-phase HPLC retention time increase due to the addition of the octanoyl moiety, this GSSFLC$_{AcDan}$ substrate exhibits enhanced fluorescence upon octanoylation due to the increased nonpolar environment near the solvatochromatic acrylodan fluorophore. [31, 32] The octanoylation-dependent fluorescence increase for the GSSFLC$_{AcDan}$ peptide is insufficient to support direct reproducible detection of peptide acylation (data not shown), leading us to explore options to maximize the fluorescence enhancement upon peptide acylation.

Inspired by studies indicating hGOAT efficiently binds ghrelin-mimetic peptides with hydrophobic amino acids larger than phenyalanine adjacent to the serine-3 acylation site, a GSSCLS peptide was designed to position the acrylodan fluorophore adjacent to the acylation site (**Figure 2.1a**). [33-35] As acrylodan is environmentally sensitive and increases in fluorescence in response to an increase in hydrophobicity in the environment, moving the fluorophore closer to lipidation site in GSSC$_{AcDan}$LS was anticipated to greatly enhance the fluorescence of the acrylodan moiety above that exhibited by the previously-utilized GSSFLC$_{AcDan}$. [36] Following incubation with hGOAT and octanoyl-CoA under standard HPLC reaction conditions,

octanoylation of the GSSC$_{AcDan}$LS peptide was confirmed by both reverse-phase HPLC and mass spectrometry (**Figure 2.1b**).

Following HPLC verification of serine octanoylation by hGOAT, the GSSC$_{AcDan}$LS peptide was incubated with hGOAT-containing membrane protein fraction in either the presence or absence of octanoyl-CoA in a 96-well plate and peptide fluorescence was monitored (**Figure 2.2a**). Incubation in the absence of octanoyl-CoA resulted in a small time-dependent fluorescence increase, with a much larger time-dependent fluorescence increase in reactions containing the octanoyl-CoA acyl donor. The small increase in the negative control reaction can be attributed to nonspecific peptide interaction with microsomal lipids in the membrane protein fraction and has been similarly observed with the first generation GSSFLC$_{AcDan}$ substrate (data not shown). To account for background non-acylation dependent fluorescence increase, corrected fluorescence values were calculated by subtracting the fluorescence values from a negative control reaction lacking octanoyl-CoA to reveal fluorescence increases attributable to peptide acylation by hGOAT (**Figure 2.2b**).

Octanoylation of the GSSC$_{AcDan}$LS peptide under the plate reader assay conditions was confirmed by reverse phase HPLC analysis of reaction samples taken at various time points (**Figure 2.3**), which showed that the peak at the known retention time for octanoylated GSSC$_{AcDan}$LS increased in conjunction with the lipidation-derived RFU increase. Reaction conditions were explored to determine maximal signal while limiting membrane fraction and peptide consumption. Since hGOAT has not been purified in its active form, the concentration of total protein for each reaction was calculated using a Bradford assay. 32 µg membrane protein proved to provide sufficient corrected RFU values while minimizing the amount of enriched
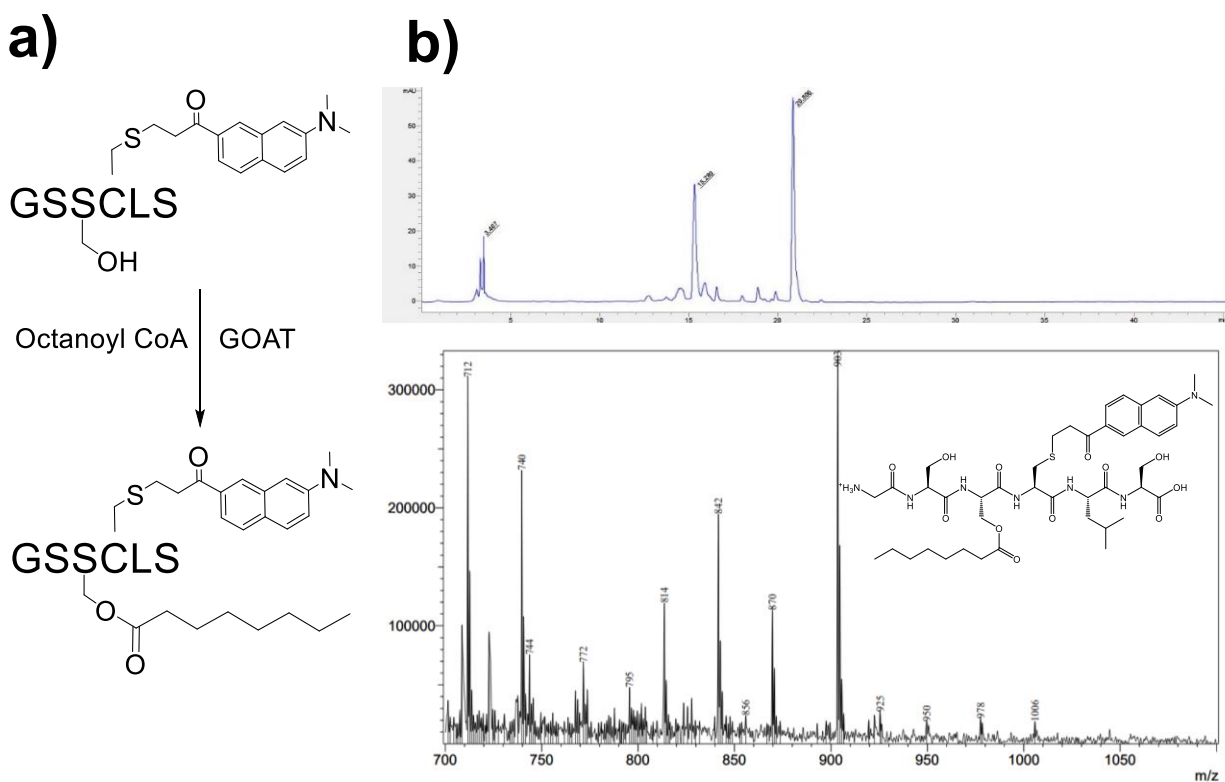
Figure 2.1: Octanoylation of a fluorescent ghrelin peptide. **a.)** Schematic of the octanoylation of acrylodan-labeled GSSC$_{AcDan}$LS by GOAT; **b.)** HPLC chromatogram of the product of the octanoylation reaction of GSSC$_{AcDan}$LS by GOAT. Peak at 15.3 min represents unreacted GSSC$_{AcDan}$LS, while octanoylated peptide elutes at 20.8 min and was collected for mass spectrometry. Expected mass 904, observed mass 903.
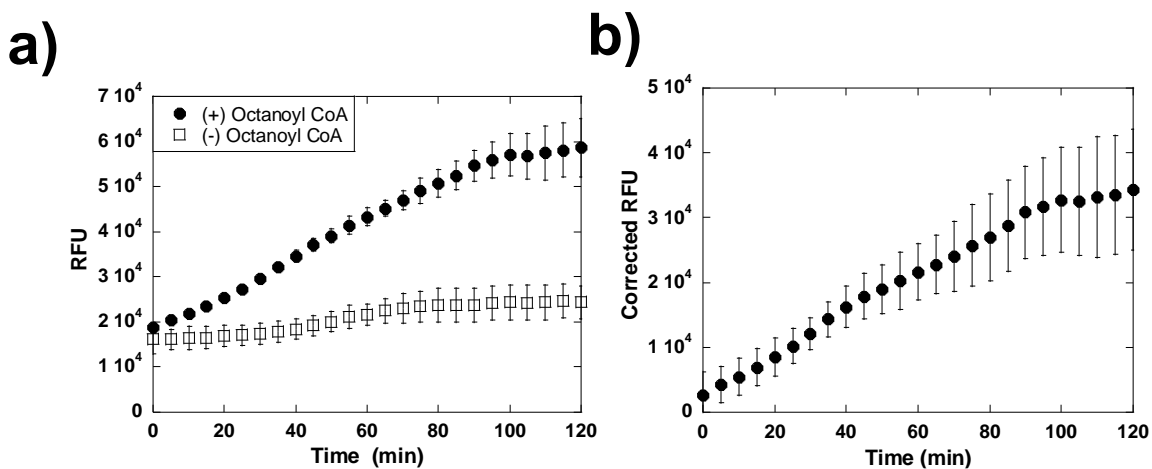
Figure 2.2: Plate reader-based fluorescence detection of hGOAT acylation activity a) Fluorescence values (plotted as RFU) for reactions containing oct-CoA (circles) and (-) oct-CoA (squares) indicating increased fluorescence on octanoylation of peptide. b) Subtraction of (-) oct-CoA RFU from reactions yields background corrected RFU. Error bars represent the standard deviation from three independent trials.
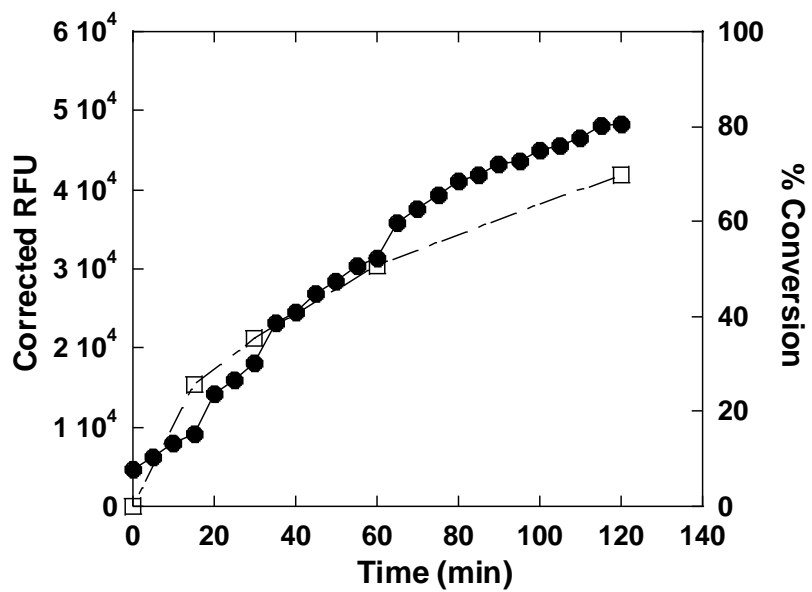
Figure 2.3: Comparison of hGOAT acylation activity by RFU and percent conversion.
Reaction time course with fluorescence (black circles) and percent conversion as calculated by HPLC retention shifts (open squares) overlaid.

membrane fraction required to perform a single assay (**Figure 2.4a**). The amount of peptide required for the assay was also titrated, revealing 1.0 µM GSSC$_{AcDan}$LS to provide the optimal reaction performance (**Figure 2.4b**), minimizing reagent use while simultaneously minimizing non-specific RFU increase. Use of the lower 0.5 µM GSSC$_{AcDan}$LS condition was also considered but was found to be more susceptible to membrane fraction variation in lipid concentration due to lower corrected RFU-to-background ratio. Titration of the acyl donor determined the maximum reaction rate required 50 µM octanoyl-CoA (**Figure 2.5**).

When determining optimized reaction conditions, Z' factor analysis indicated adequate assay performance (Z' = 0.39) at 45 minutes reaction time in the presence of ~30 µg membrane fraction protein and 1 µM peptide substrate (**Figure 2.6**). Z' is a statistical parameter that allows quantitation of the statistical probability of a hit falling within the range of the negative control data.[37] An assay with a score between 0.25 – 0.5 on the Z' scale indicates an acceptable assay in a complex system such as GOAT enriched membrane fraction.[38] The Z' factor of 0.39 indicates this assay is appropriate for initial high-throughput GOAT inhibitor screening, especially in conjunction with an assay such as the current HPLC assay.[37] Lower peptide concentrations were found to have inconsistent results across different membrane fraction due to lower dynamic range, which can be attributed to varying concentrations of membrane lipids in differing preparations providing higher values for the negative controls. As a result, the higher concentrations of 1.0 or 2.0 µL peptide were used to increase the dynamic range of the assay and consistency of the assay across membrane fractions.[38]

The suitability of the plate reader-based fluorescence GOAT activity assay to monitor hGOAT inhibition was validated with **Compound 2.1**, a previously described
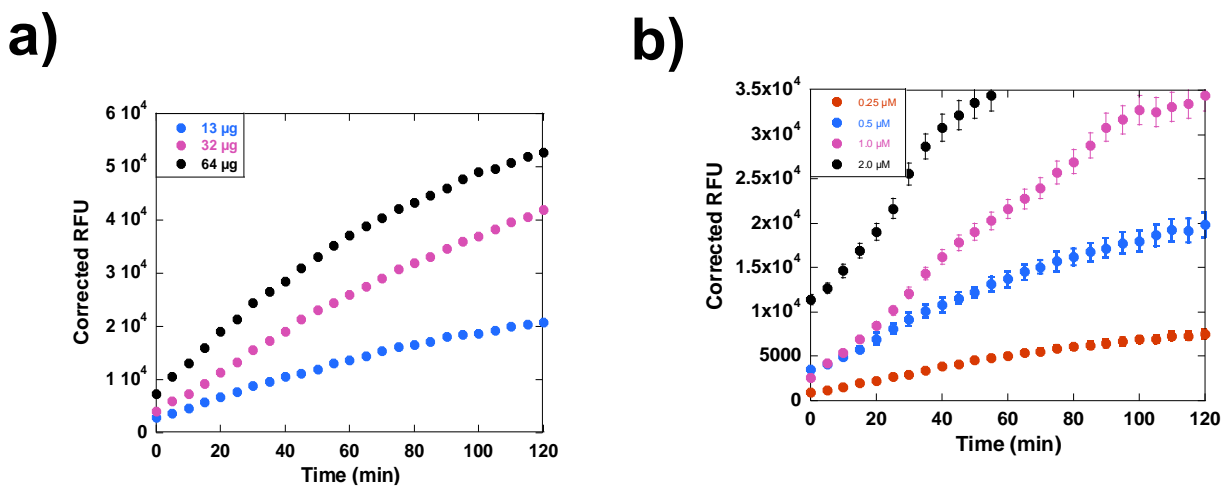
Figure 2.4: Initial optimization of membrane protein and peptide concentrations a) Membrane protein titration, total membrane protein concentration calculated through Bradford assay. b) $GSSC_{AcDan}LS$ peptide titration. Error bars represent the standard deviation of three independent trials.
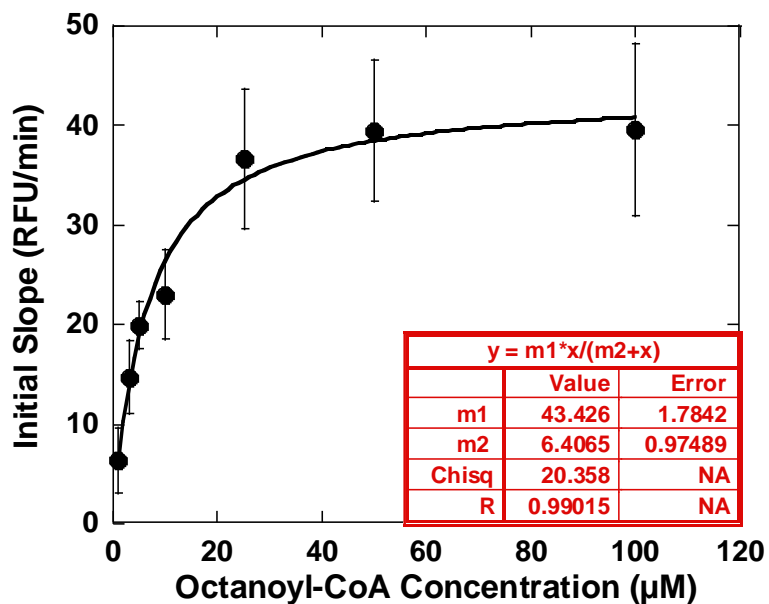
Figure 2.5: Titration of hGOAT activity as a function of acyl donor concentration.

Octanoyl-CoA titration indicating saturation at 30 μM octanoyl-CoA. Error bars represent the standard deviation of three independent trials.
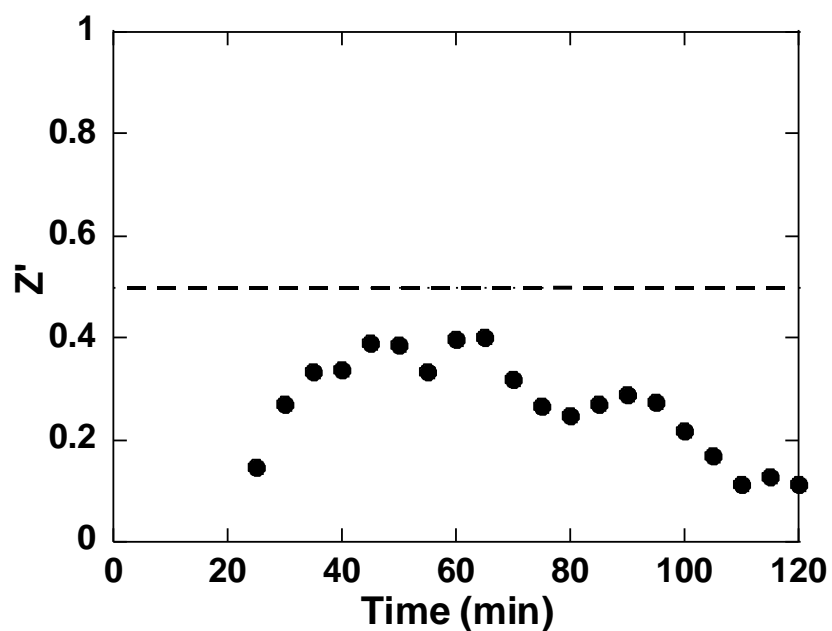
Figure 2.6: Analysis of reaction conditions using Z'. Z' factor analysis plot as a factor of time. Reaction conditions included 50 µM octanoyl-CoA, 1.0 µM GSSC$_{AcDan}$LS, and 30 µg membrane protein. As Z' increases, the less likely a data point is to fall within the range of the negative control. Dotted line represents Z' of 0.5, representing an ideal assay behavior under non-complex conditions.

α-cyanoenone inhibitor of hGOAT, (**Figure 2.7a**), which was given the identifier JH100. As part of the assembly of the screening library, compounds were assigned identifiers based on inhibitor status. Known inhibitors of hGOAT were given identifiers starting with JH1XX, and compounds to be screened were given identifiers starting with JH2XX. JH100 is a covalent reversible inhibitor of hGOAT with an IC_{50} of 8 ± 4 µM as determined previously by reverse-phase HPLC assay. [26] For the continuous fluorescence assay, reactions were stopped at 45 minutes and the corrected fluorescence was normalized to the vehicle control to determine hGOAT activity in each reaction. Fitting **Equation 2.1** to the plot of percent activity against concentration yields an IC_{50} value of 10 ± 6 µM for JH100 in the fluorescence enhancement assay (**Figure 2.7**), in agreement with literature. This consensus validates the utility of the plate reader assay for hGOAT inhibitor screening.

2.2.2 Continuous Fluorescence Assay enables High Throughput Screening for GOAT inhibitors

The initial virtual docking study was performed by Dr. John Chisholm (Department of Chemistry, Syracuse University), utilizing MTiOpenScreen. MTiOpenScreen utilizes a library of pharmaceutical-like molecules generated from PubChem molecules in order to dock these molecules into the provided hGOAT structure. [39] This generated a set of ~1500 drug-like molecules in three poses ranked by predicted binding energies. This set of molecules was then manually examined for purchasable compounds within 100 highest-ranked, building a screening library of 54 compounds that were purchased for testing. This library of hGOAT inhibitor candidates derived from the initial virtual screening (JH200-JH254) were assayed for hGOAT inhibition at two concentrations (10 and 100 µM) in duplicate (**Figure 2.8a,b**). In this initial

screen, compounds were selected for further study based on two criteria: a minimum of 50%

hGOAT inhibition and concentration dependent inhibition. Initial screening identified 13

compounds of interest which were subjected to a second round of validation screening with the

same criteria (concentration dependence and at least 50% hGOAT inhibition), identifying 7

compounds that fell within the criteria for further examination (**Figure 2.9**). Normalized activity

>100% indicates an increase in activity from the positive control, often due to inherent

fluorescent behavior of molecules.

From this validation screening, we selected three compounds based on >50% hGOAT

inhibition in the replication trial and current commercial availability to determine IC_{50} values for

hGOAT inhibition. Reactions containing these compounds were analyzed by the fluorescence

plate reader assay for inhibition of hGOAT activity for one hour, at which point reactions were

stopped and analyzed by RP-HPLC analysis. The IC_{50} values obtained by these two analytical

methods were comparable (**Table 2.1**), confirming the discovery of three novel hGOAT

inhibitors with micromolar potency and further validating the ability of the continuous

fluorescence assay to find viable hGOAT inhibitors (**Figure 2.10**). JH210 was removed from

consideration due to the inability to purchase more of the molecule.
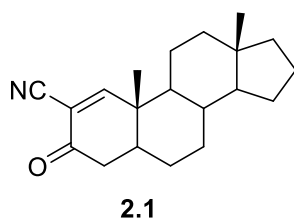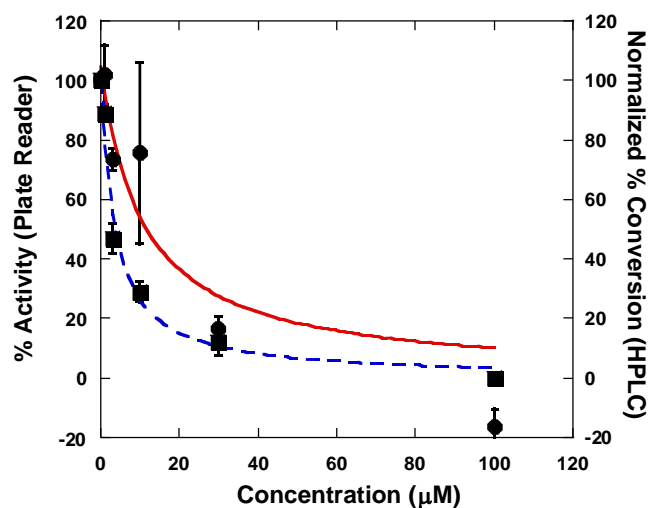
Figure 2.7 Inhibition of hGOAT in plate-reader assay by known inhibitor JH100: a.) JH100, α-cyanoenone inhibitor of GOAT. **b.)** IC_{50} of JH100 utilizing continuous fluorescence assay (red) and HPLC (blue). Reactions containing 1.0 µM $GSSC_{AcDan}LS$, 50 µM octanoyl-CoA, and 32 µg membrane protein were run in 96-well plates before being quenched after 60 minutes and transferred to HPLC vials. Error bars represent the standard deviation of four independent trials.

a)

MTiOpenScreen to analyze 99,288
compounds by *in silico* docking

⬇

Top 1500 compounds ranked by
interaction energy

⬇

54 commercially available compounds
purchased

b)
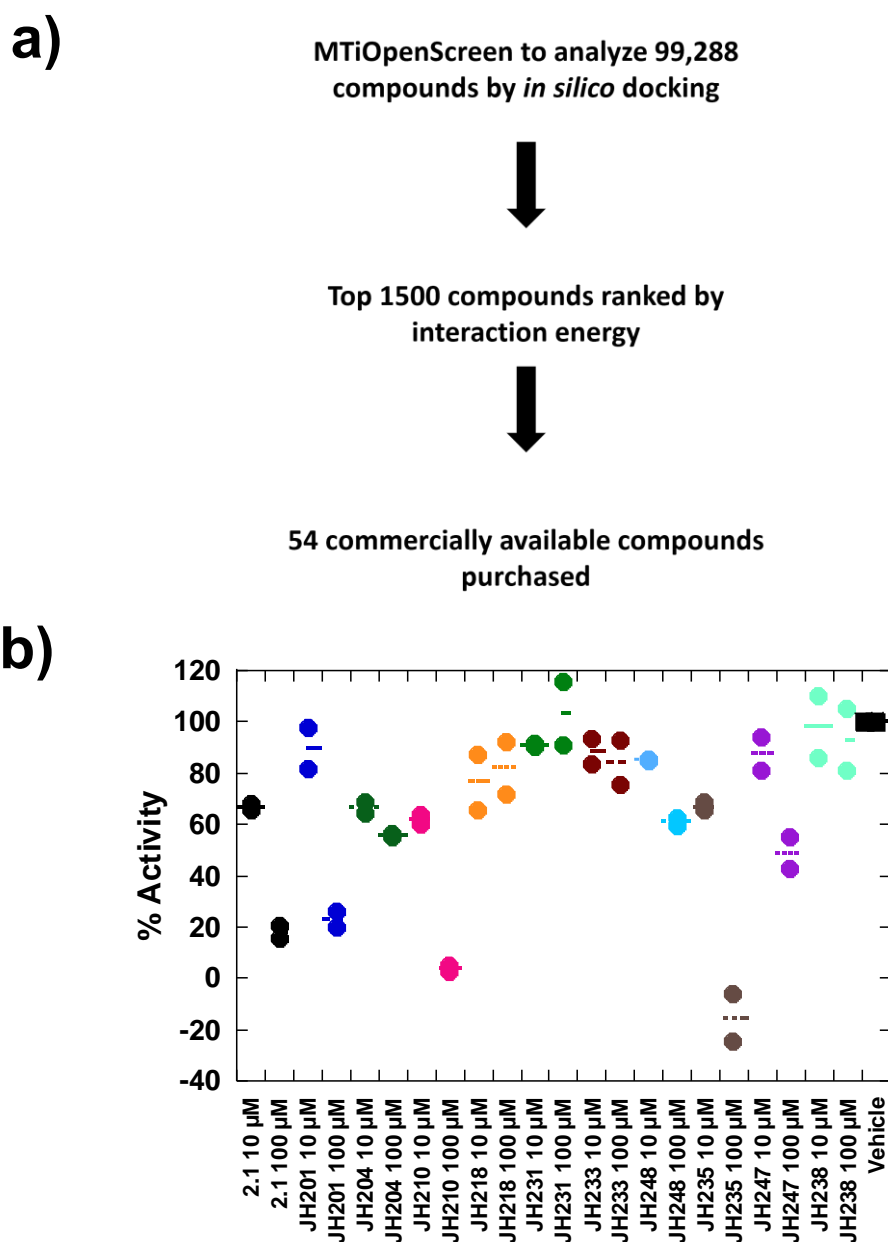
Figure 2.8: Initial screening methodology for a small library of compounds utilizing plate-reader assay, a.) Flowchart detailing methodology utilized to identify potential compounds for initial testing. **b.)** Initial screening of compounds of interest. Molecules were tested at both 10 and 100 µM using the 96-well plate reader format, with duplicate wells of each molecule. Duplicate wells are shown as dots, with the average percent activity of the duplicate wells shown as a line.
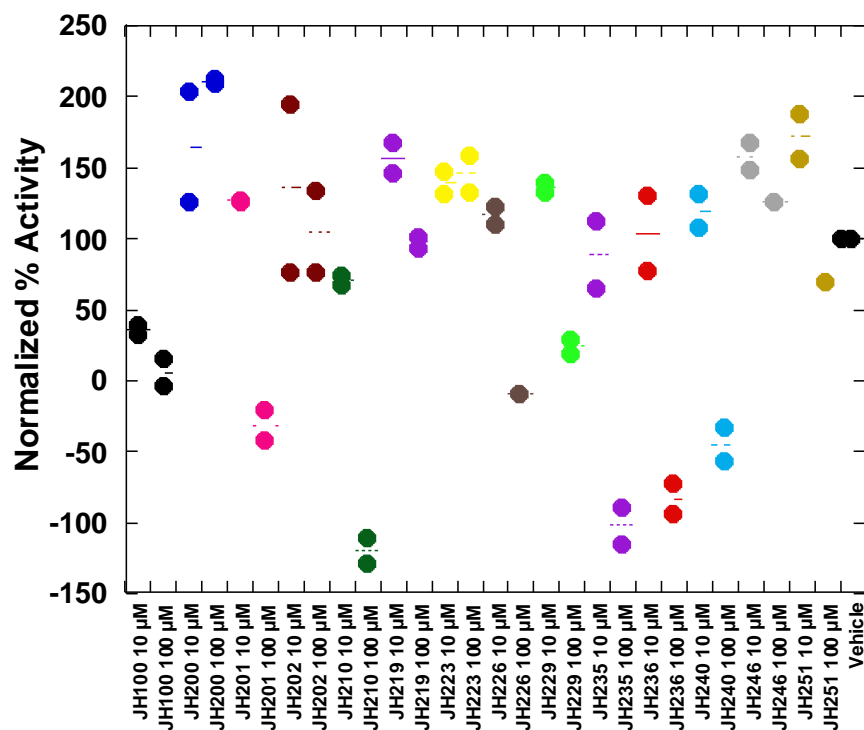
Figure 2.9: Secondary screen of initial hit compounds. Molecules of interest from initial screen were subjected to secondary screening in duplicate. Negative activity is indicative of extremely low hGOAT activity in comparison to the negative control, leading to compartmentalization of non-octanloylated peptide outweighing increased fluorescence as a function of lipidation. Duplicate wells from the same plate are shown as dots, with the average percent activity of the duplicate wells shown as a line.

Compounds JH226, JH229, JH235, and JH101 (a literature inhibitor of hGOAT and mGOAT published by Takeda Pharmaceuticals as compound A) were tested for potency against the mouse isoform of GOAT (mGOAT). [21] JH100 and other cysteine-modifying agents do not inhibit mGOAT with the same efficacy as hGOAT, indicating that these molecules are targeting a non-conserved, potentially non-catalytic site between hGOAT and mGOAT. [26] All four compounds retained potency within twofold of the determined hGOAT IC_{50} (**Table 2.2**), indicating that these compounds may be targeting a conserved region of the enzyme, in contrast to previously identified molecules. The novel compounds inhibiting both isoforms of GOAT increases the likelihood of interacting with an essential, unlikely to diverge through evolution set of residues, potentially a catalytic portion of the enzyme.

2.2.3 Computational docking studies and biochemical assays confirm inhibitor binding sites within hGOAT

As the binding sites of the small-molecule inhibitors are unknown, identification of inhibitor binding sites could allow for the development of novel rationally-designed GOAT inhibitors. With the availability of the hGOAT model, comparison of the novel and published inhibtors of GOAT, allow us insight into the specific binding interactions of these molecules for the first time. To compare the potential binding site or sites of the inhibitors, docking studies were performed with molecular dynamics simulations and docking performed by Jinging Ji (Nangia laboratory, Syracuse University, Department of Biomedical and Chemical Engineering. Comparison of static YASARA docking and molecular dynamics simulations did not markedly improve or alter the predicted binding sites (**Figure 2.11**), indicating that the poses of these molecules to not radically change over time and that the pose within the binding site is unlikely

to change. JH226 was found to bind in the channel central to the hGOAT structure towards the luminal face of the enzyme, with a binding pocket consisting of Q128, Y255, W259, W351, indicating that the compound shares binding contacts with but does not occupy space within the acyl binding pocket. Previous work on the determination of the acyl binding pocket of hGOAT identified W351 as a "gatekeeper" residue in the acyl binding site, with W351A mutation altering the selectivity of hGOAT to allow utilization of the twelve- and fourteen carbon lipids of lauryl- and myristoyl-CoA respectively. [27] JH235 also exhibits contacts to the aforementioned residues, as well as W306. The pose of JH235 indicates that it partially shares a binding site with JH226, but occupies space in the channel further towards the cytosolic, rather than the luminal face. JH229 binds in the transmembrane channel within the acyl donor binding site towards the cytosolic face of hGOAT, extending from Y255 and W351 to N307 and T382. This binding site represents a separate binding pocket from the pose exhibited by JH226, while sharing the common contact W351, representing the end of the canonical acyl-binding site. Docking octanoyl-CoA to the hGOAT model also reveals that the structures of JH235 and JH229 occupy the space predicted for the tail of the acyl chain, indicating the potential for acyl donor competition (**Figure 2.12a,c,e**), (**Figure 2.13.a-d**).
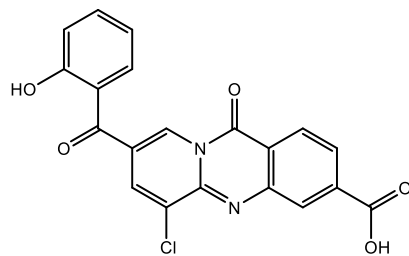
2.2 JH226
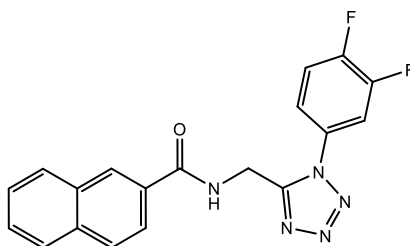
2.3 JH229
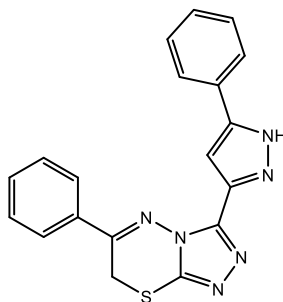
2.4 JH235

Figure 2.10: Structures of novel GOAT inhibitors found through Continuous Fluorescence Assay

Table 2.1: **Same-well IC$_{50}$ values of hit compounds via conventional HPLC assay and Continuous Fluorescence Assay.** Reactions containing 1.0 µM GSSC$_{AcDan}$Ls, 50 µM octanoyl-CoA, and 30 µg membrane protein were tested for fluorescence enhancement before being quenched after an hour and transferred into HPLC vials for chromatography.

Compound	Fluorescence IC$_{50}$ (µM)	HPLC IC$_{50}$ (µM)
JH100	8 ± 4	3.5 ± 0.2
JH210	9 ± 1	11 ± 5
JH226	19 ± 17	23 ± 12
JH229	32 ± 24	12 ± 3
JH235	5 ± 1	12 ± 4

Table 2.2: IC$_{50}$ of compounds against hGOAT and mGOAT. IC$_{50}$ values were determined through HPLC-based hGOAT activity assay. IC$_{50}$ with asterisks indicate values previously published. [26] Reactions containing 2.0 µM GSSC$_{AcDan}$Ls, 50 µM octanoyl-CoA, and 30 µg membrane protein were analyzed by HPLC.

Compound	hGOAT IC$_{50}$	mGOAT IC$_{50}$	Ratio of mGOAT IC$_{50}$/hGOAT IC$_{50}$
JH100	8 ± 4 µM *	60 ± 8 µM *	7.5
JH101	27 ± 8 nM	11 ± 3 nM	0.41
JH226	16 ± 3 µM	33 ± 8 µM	2.1
JH229	19 ± 8 µM	22 ± 6 µM	1.2
JH235	27 ± 8 µM	26 ± 2 µM	0.96

Figure 2.11: Comparison of YASARA docking with molecular dynamics (MD) simulations.
Contacts were determined as residues within 5 Å of the inhibitor. YASARA and MD
calculations performed by Jinging Ji (Shika Nangia Laboratory, Department of Biomedical and
Chemical Engineering, Syracuse University).
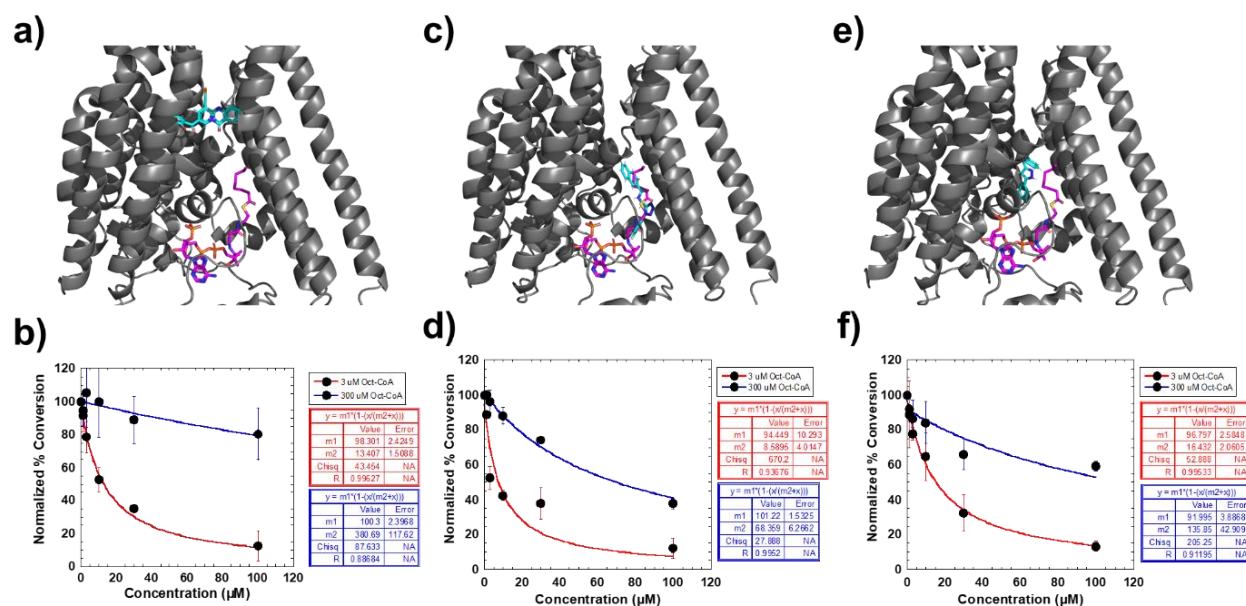
Figure 2.12: Predicted binding sites of novel inhibitors and resulting acyl donor competition. a.) c.) e.) Visualization of the predicted inhibitor binding sites in hGOAT, indicating that JH229 (c) and JH235 (e) occupy space within the octanoyl-coA (magenta) binding site while JH226 shares contacts but occupies a different binding site. Inhibitors represented in cyan. **b.) d.) f.)** IC$_{50}$ curves taken in the presence of 3 µM oct-CoA (low CoA condition) and 300 µM (high CoA condition). Error bars represent the standard deviation of three trials.

Figure 2.13: LigPlot plots of novel inhibitor and octanoyl-CoA binding sites in hGOAT. a.) JH226 and predicted binding contacts. **b.)** JH229 and predicted binding contacts. **c.)** JH235 and predicted binding contacts. **d.)** Octanoyl-CoA and binding contacts. Residues highlighted in blue (Q128), green (Y255), and yellow (W351) were selected for mutation studies. Plots generated by Dr. John Chisholm, Department of Chemistry, Syracuse University.

Table 2.3: Comparison of hGOAT inhibitors at low (3 μM) and high (300 μM) lipid donor conditions.

Compound Identifier	IC_{50} in the presence of 3 μM Oct-CoA (μM)	IC_{50} in the presence of 300 μM Oct-CoA (μM)	Ratio of High Oct-CoA/ Low Oct-CoA
JH100	4 ± 1	9 ± 2	2.25
JH101	0.033 ± .011	.290 ± .122	8.79
JH226	13 ± 2	380 ± 117	29.2
JH229	8 ± 4	68 ± 6	8.50
JH235	16 ± 2	135 ± 43	8.44

To validate the predicted acyl-donor competitive nature of these inhibitors, we performed octanoyl-CoA competition experiments. IC_{50}s were determined in the presence of 3 μM oct-CoA or 300 μM oct-CoA. JH100, a non-acyl donor competitive inhibitor, was found to increase the IC_{50} twofold in the presence of high oct-CoA conditions (**Table 2.3**). Comparatively, the IC_{50} of the inhibitors JH226, JH229, and JH235 were found to increase between eightfold and thirtyfold under high oct-CoA conditions, indicating competition with the acyl donor (**Figures 2.12b,d,f** and **Table 2.3**). JH101, previously published as Compound A by Takeda Pharmaceuticals in 2018 as an octanoyl-CoA competitive inhibitor of hGOAT, was synthesized by Cassie Grossman (Chisholm laboratory, Syracuse University) as a control for competition and exhibited a ninefold increase in potency. These findings support the docking prediction that the JH2XX inhibitors are acyl donor competitive molecules. While the docking studies with JH226 do not support direct occupation of the octanoyl-CoA binding site due to the inhibitor binding towards the luminal face of the enzyme, the competition experiment resulted in a thirtyfold increase in IC_{50}. This may be the result in both binding sites requiring interactions with the residues Y255, W306, and W351, with introduction of octanoyl-CoA altering the inhibitor binding site.

2.2.4 Computational docking studies of previously reported small molecule hGOAT inhibitors consistent with a common inhibitor binding site

After successful prediction of inhibitor competition behavior through docking studies,, YASARA docking was performed on known inhibitors (**Figure 2.14**) published by pharmaceutical companies to determine a potential consensus inhibitor binding site for these molecules. Takeda Compound A, used as our acyl donor competition positive control, was found to contact Q128, Y255, W259, W306, and W351, as did Takeda Compound B (**Figure 2.15a,b**).

The GlaxoSmithKline inhibitor also contacted these residues, indicating a potential consensus inhibitor binding site (**Figure 2.15c**). This hypothesis was further supported by both the Boehringer and Eli Lilly GOAT inhibitors contacting Y255, W259, and W351. The Boehringer inhibitor binds into a similar pocket to the JH229 inhibitor, positioned further towards the octanoyl-CoA binding site and contacting V301 and T382 (**Figure 2.15d**). Finally, the Eli Lilly inhibitor makes similar contacts to the JH226 inhibitor, being located towards the luminal face of hGOAT and making contacts with M124, Q128, Y255, W259, W306, W351, and R400 (**Figure 2.15e**). From the binding interactions predicted by the docking of the JH2XX and previously published inhibitors, we can detail a tripartite binding site. The residues Y255, W259, and W351 form contacts with all inhibitors bound to the hGOAT model, indicating an essential binding pocket that has supplementary interactions to either side of these three residues (**Figures 2.16 and 2.17**). We refer to this binding pocket as the obligate binding domain (O). Supplementary domain 1 (S_1) consists of the residues towards the cytosolic end of the transmembrane channel including the acyl binding pocket. S_1 contains the aforementioned V301 and T382, as well as W306, R315, M354, V355, and D358, and is where JH229, the Boehringer inhibitor, and the Takeda compound form their supplementary contacts.

2.5

2.6

2.7

2.8

2.9
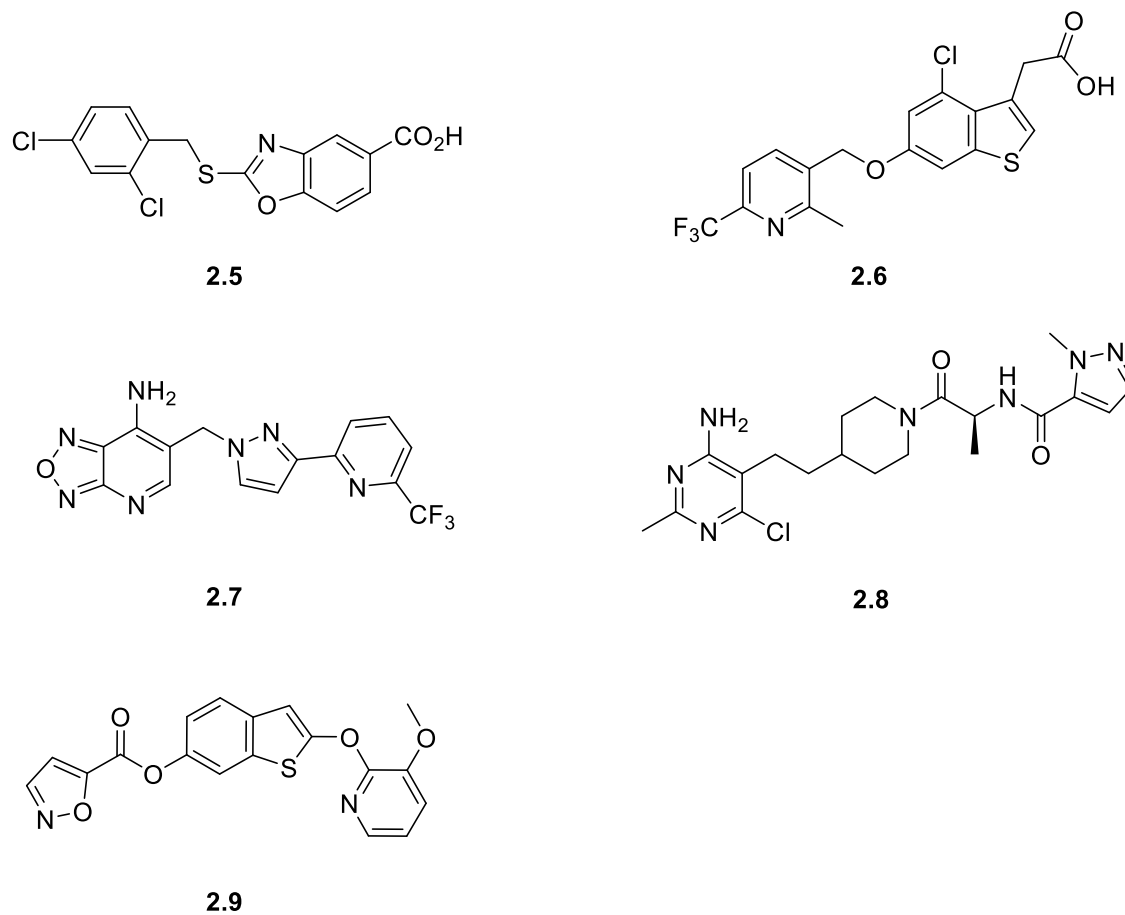
Figure 2.14: Structure of literature inhibitors used in binding site analysis. Compound 2.5:
Takeda A. [21] **Compound 2.6**: Takeda B. [21] **Compound 2.7**: Boehringer. [40] **Compound 2.8**: Eli
Lilly. [41] **Compound 2.9**: GlaxoSmithKline. [42]
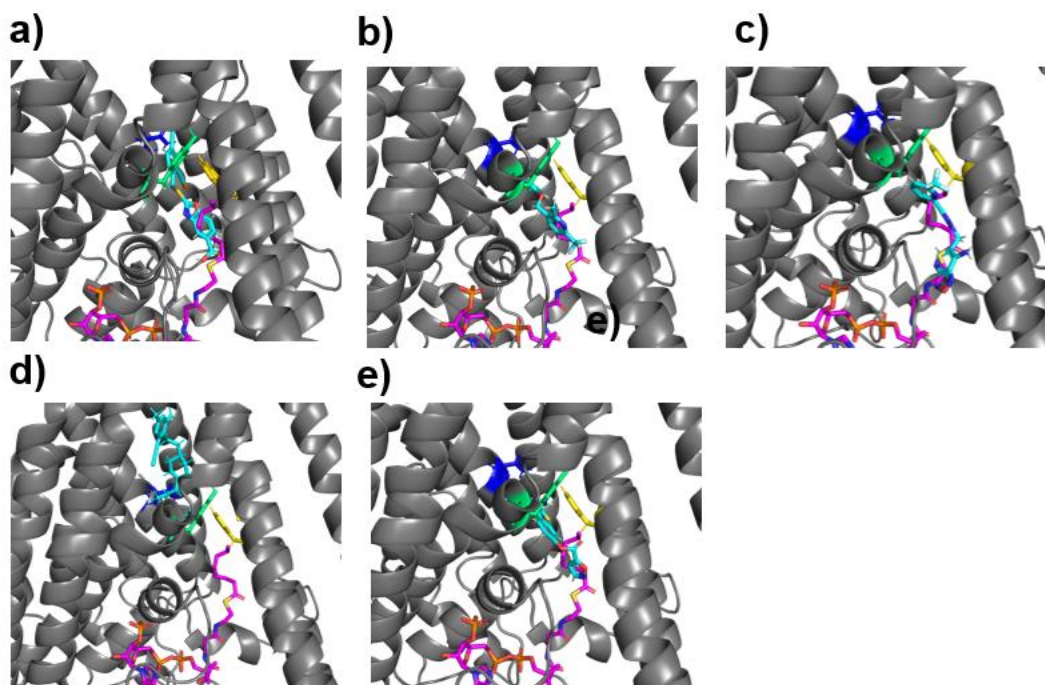
Figure 2.15: Literature GOAT inhibitors bound to hGOAT model. Inhibitors shown in cyan, octanoyl-CoA shown in magenta, and mutation sites highlighted. **a.)** Takeda compound A. [21] **b.)** Takeda compound B. [21] **c.)** Boehringer. [40] **d.)** Eli Lilly. [41] **e.)** GlaxoSmithKline. [42]
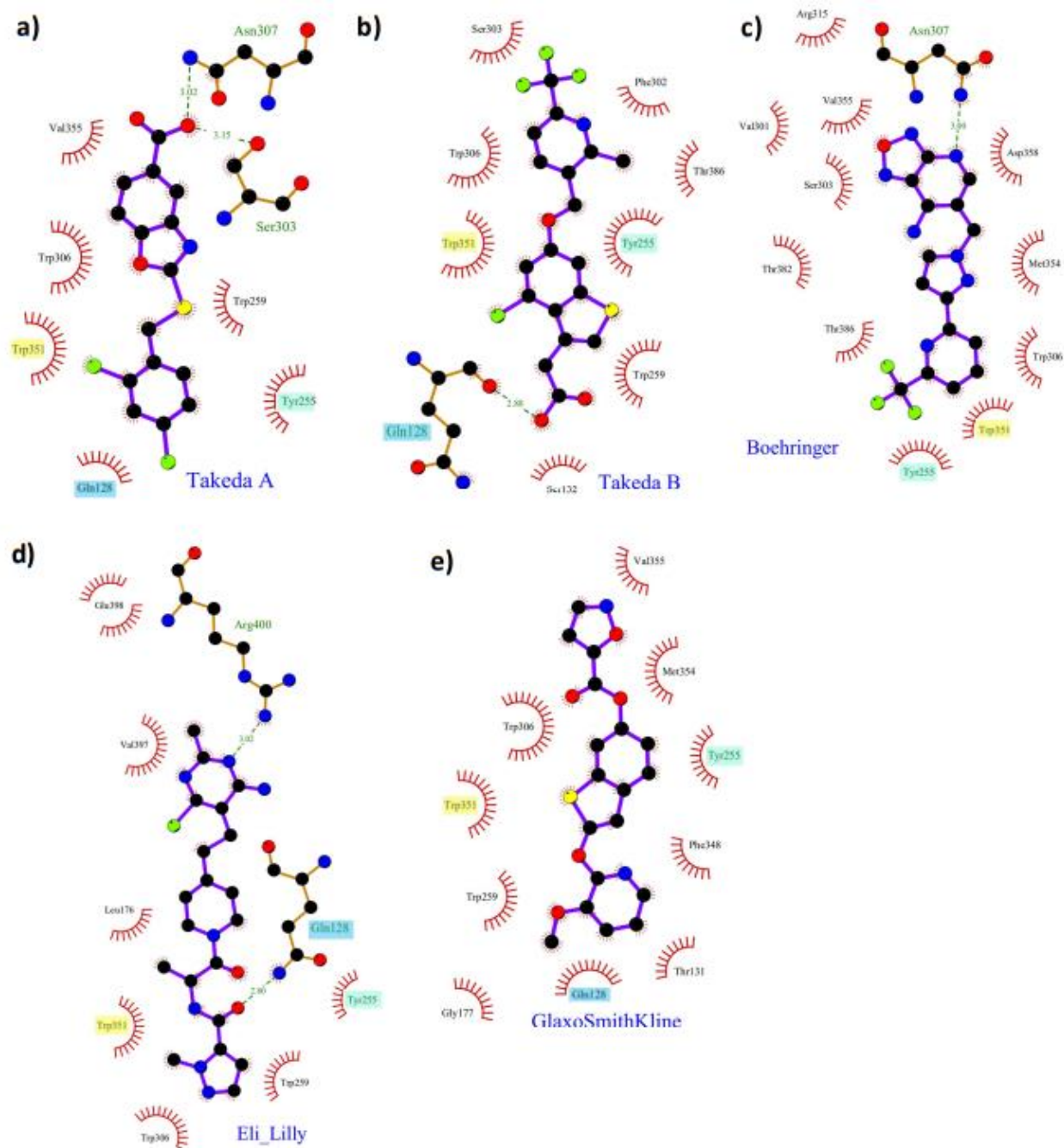
Figure 2.16: LigPlot plot of literature inhibitors showing anticipated binding contacts with hGOAT. a.) Takeda compound A. [21] **b.)** Takeda compound B. [21] **c.)** Boehringer. [40] **d.)** Eli Lilly. [41] **e.)** GlaxoSmithKline. [42] Residues highlighted in blue (Q128), green (Y255), and yellow (W351) were selected for mutation studies. Plots generated by Dr. John Chisholm, Department of Chemistry, Syracuse University
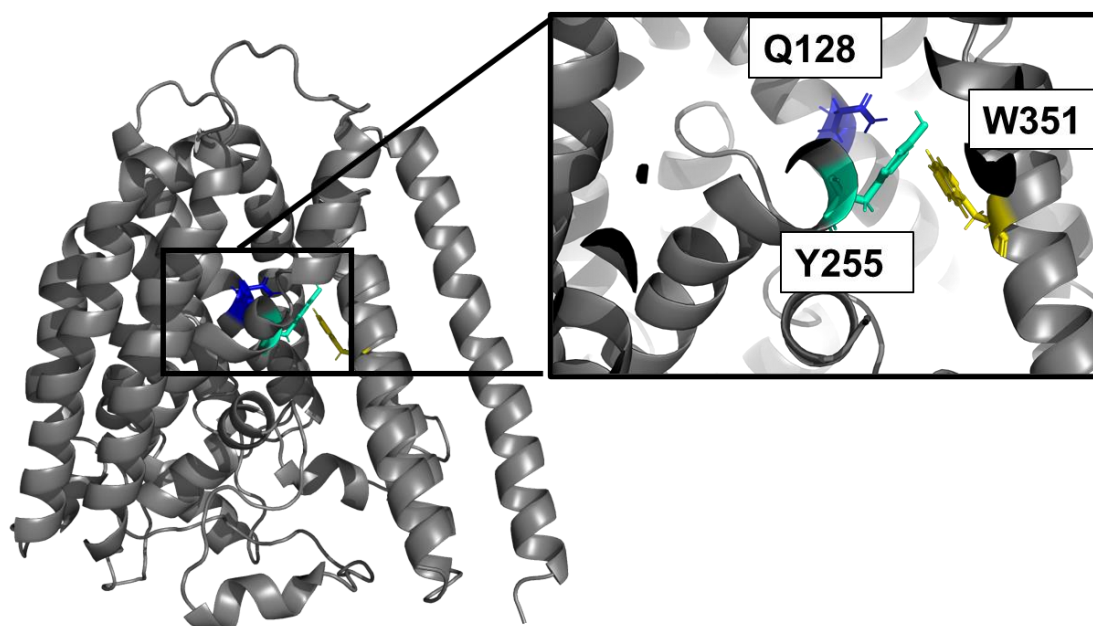
Figure 2.17: **Identification of potential residues commonly implicated in inhibitor binding region.** Alanine mutations of the highlighted residues of Q128 (blue), Y255 (green), and W351 (yellow) were generated.

Supplementary domain 2 (S_2) contains residues located towards the luminal end of the transmembrane channel including M124, Q128, L176, and T254, and is noted by the binding of JH226 and the Eli Lilly inhibitor. The overlap of the binding site of these inhibitors is consistent with the reports of the Takeda compounds being octanoyl-CoA competitive, as they overlap with the acyl donor binding site detailed earlier. [21]

To test the validity of the predicted binding sites, alanine mutants of hGOAT were generated for highly-contacted residues Q128, Y255, and W351. The IC_{50} values for hGOAT inhibitors JH226, JH229, JH235, were determined against mutant hGOAT with the expectation that removal of the predicted binding contacts of these compounds would decrease their potency for the mutants in comparison to wild-type. Mutation of W351 severely reduced the affinity (>10-fold decrease) of all novel inhibitors for the mutant enzyme, as expected due to the loss of a common binding contact in the O domain. (**Table 2.4**). Compounds JH226 and JH235 were both predicted to contact Q128, but alteration of this contact resulted in less than a 2-fold change in affinity for each of these molecules. This result indicates that the binding of JH226 and JH235 do not rely on the contact with Q128 as much as was predicted in the initial proximity analysis. JH229 was not predicted to contact Q128 and saw no change in potency as a result of the mutation. Y255 was predicted to contact JH229 and JH235, and not to contact JH226. JH235 potency decreased by over 5-fold when tested against Y255A, while JH229 decreased 3-fold, indicating that these molecules are likely contacting Y255 as predicted. No corresponding change in potency for JH226 was observed against the mutant Y225A, correlating to the predicted lack of binding interaction. Compound JH100 and GSDapFL were also tested as negative controls for acyl donor competition, with GSDapFL expected to bind to the ghrelin peptide site rather than the acyl donor site due to the peptide-mimetic nature of the inhibitor. [34]

GSDapFL binding was disrupted by all three mutants (>26-fold increase for each), while JH100 was unperturbed other than a 3.5-fold decrease in potency against the Q128A mutant. Alterations in GSDapFL binding to the mutant enzymes follows that the peptidomimetic structure should make interactions in the intermembrane channel that would allow the native peptide to be acylated, likely sharing some interactions with the octanoyl-CoA binding site to facilitate the transfer. The lack of change in JH100 affinity for Y255A and W351A is expected, as JH100 is unaffected by acyl-donor concentration, indicating that it is unlikely to share contacts with the acyl-binding site. As JH101 is predicted to make contacts in all three inhibitor binding domains, JH101 was tested against these hGOAT mutants as a test of whether the literature compounds may bind into their predicted binding sites. This literature inhibitor is predicted to contact Q128, Y255, and W351, exhibiting reduced potency (>3 fold) against Q128A as predicted. However, a less than 2-fold affinity change against Y255A, and only slightly greater than a 2-fold change against W351A is counter to the octanoyl-CoA competitive behavior that this molecule displays. This discrepancy may be due to the type of interactions being disrupted, as the Q128A mutant removes a potential polar contact, while Y255A and W351A removes weaker non-polar interactions.

From this data, it is apparent that W351 is essential to the binding of compounds binding in the hGOAT intramembrane channel, representing an example of the putative O domain. While Y255 is less essential, mutation still results in a mild perturbation of molecules predicted to interact with the S_1 domain. The S_2 domain is currently unsupported by the tested molecules, but this data may also indicate that Q128 may play a role in binding ghrelin and ghrelin-mimetic peptides, with the peptidomimetic GSDapFL exhibiting a large potency loss against Q128A.

Table 2.4: **IC$_{50}$ values generated for inhibitors with mutant hGOAT**. Samples were tested in triplicate, error is representative of standard deviation of three samples.

Compound	WT	Q128A	Ratio mutant IC$_{50}$/WT IC$_{50}$	Y255A	Ratio mutant IC$_{50}$/WT IC$_{50}$	W351A	Ratio mutant IC$_{50}$/WT IC$_{50}$
JH100	4.6 ± 0.8 µM	16 ± 6 µM	3.5	2.0 ± 0.5 µM	0.43	4 ± 1 µM	0.87
JH101	41 ± 16 nM	142 ± 66 nM	3.5	71 ± 14 nM	1.7	100 ± 31 nM	2.4
JH226	27 ± 8 µM	45 ± 25 µM	1.67	52 ± 15 µM	1.9	> 100 µM	N.D
JH229	16 ± 3 µM	12 ± 8 µM	0.75	48 ± 12 µM	3.0	> 100 µM	N.D
JH235	19 ± 8 µM	31 ± 11 µM	1.63	>100 µM	N.D	> 100 µM	N.D
GSDapFL	17 ± 2 nM	961 ± 479 nM	57	>1000 nM	N.D	439 ± 156 nM	26

2.3 Discussions and Conclusions

It is an ongoing challenge to develop small molecules that target proteins in the absence of experimental structural information. Computational modeling has become an increasingly accessible route for developing structural models capable of supporting biochemical studies. Homology modeling is widely used in the generation of 3D structures of proteins for biochemical applications, with a wide range of programs available for the production of models. [43, 44] Homology models have allowed for informed evaluation of compounds in the absence of experimentally-determined structures, like in the case of recent 1,3,4-oxadiazole anticonvulsants. [45, 46] As more information about related protein structures becomes available, homology modeling can be used to model previously unresolved structures such as MBOATs PORCN and HHAT. [47, 48] Coevolutionary contact analysis proposes that amino acids in proteins are linked through evolution, with mutations in some residues leading to a compensatory mutation in others. [49-51] This approach has been used to develop models of membrane-bound proteins, as shown recently in the first published computational model of GOAT. [27] The recently developed AlphaFold utilizes coevolutionary contact methods and a neural network to model long-distance interactions in proteins. [52] The second-generation AlphaFold (dubbed AlphaFold2) has demonstrated increased accuracy and has been applied to the human proteome, covering 98.5% of human proteins. [53, 54] Consequently, the application of machine learning to complex protein folding problems has the potential to address currently unanswered questions in bioinformatics.

We have identified several commercially available compounds as modulators of GOAT. Since the MTiOpenScreen library was generated from a filtered list of PubChem BioAssay Database molecules, we accessed the molecules of interest to identify any known biological activity. JH235 was synthesized in 2001 as part of an antimicrobial screen, and found to have a

MIC of 30 µg/mL against *P. mirabilis.* [55] It was also identified in a class of potential anticancer therapies, inhibiting the STAT3 pathway with an IC_{50} of 27 ± 17 µM. [56] These triazolo-thiadiazines exhibited poor metabolic stability, attributed to oxidation of the thioether, identifying a potential alteration for further development of the compound for biological activity against GOAT. [56] While the exact molecule JH210 was not evaluated, minor modifications of the core scaffold have been reported to exhibit greater antinociceptive activity than aspirin in a 100 mg/kg dose. [57] JH229 and JH226 do not appear to have been tested for biological activity. The repurposing of these scaffolds offers novel avenues for inhibitor development and optimization targeting GOAT.

As the interest in development of GOAT inhibitors other than peptide- and product-mimetic compounds has grown, screening large libraries of compounds has been necessary to generate small-molecule hits. The recent generation of a computational model of hGOAT has allowed us to perform a virtual screen of ~100,000 drug-like molecules and identify new inhibitors. These inhibitors represent new scaffolds for the development of lead compounds for the modulation of ghrelin signaling. This also serves as a validation for the combined approach utilizing our computational model of hGOAT and the continuous fluorescence assay. Furthermore, we were able to predict the acyl-donor competitive nature of the compounds found in our screen by examining the predicted binding sites in the model. By examining known inhibitors of hGOAT and the newly identified compounds in our model, we propose a consensus inhibitor binding site in the transmembrane channel of hGOAT. Understanding the nature of this inhibitor binding site allows for rational design of new inhibitory molecules, while also allowing engineering of derivatives intended to increase pharmacokinetic properties.

2.4 Materials and Methods

2.4.1 General Experimental Details

Methyl arachidonyl fluorophosphonate (MAFP) was diluted in DMSO from a stock in methyl acetate (Cayman Chemical, Ann Arbor, MI). Octanoyl coenzyme A (CoALA Biosciences, Elgin, TX) was solubilized to 5 mM in 10 mM Tris-HCL and stored in low adhesion tubes at -80°C until use. The $GSSFLC_{NH2}$ and $GSSCLS_{NH2}$ peptides were obtained from Sigma-Genosys (The Woodlands, TX) and synthesized in Pepscreen format. Peptides was solubilized in 50 mM HEPES pH 7.0 solution and stored at -80°C. Peptide concentration was determined spectrophotometrically at 412 nm by reaction of the cysteine thiol with 5,5'dithiobis(2-nitrobenzoic acid) using an ϵ_{412} of 14150 M^{-1} cm^{-1}.[58]

2.4.2 Inhibitor candidate purchasing, synthesis, and compound validation

Synthetic method for JH100

JH100 (**2.1**) was synthesized according to an adaptation of previously published method.[26]

5α-androstan-3β-ol (2.10) - To a mixture of potassium hydroxide (103.3 mmol) in 30 mL of diethylene glycol was added epiandrosterone (20.7 mmol) and hydrazine (82.6 mmol). The reaction mixture was stirred at 245°C for 24 hrs, at which point the solution was allowed to cool to room temperature. 150 mL of brine was added, followed by 75 mL of dichloromethane, before transferring the mixture to a separatory funnel. The mixture was worked up by extracting the organic three times with 100 mL of dichloromethane. The organic layer was washed three times with saturated sodium chloride (100 mL) and dried with sodium sulfate and filtered. The organic

layer was then removed under vacuum, leaving the compounds as a white powder with 91%

yield. ^{1}H NMR (400 MHz, CDCl$_3$) δ 3.61-3.55 (m, 1H), 1.81 (q, J = 12 Hz, 1H), 1.74-1.50 (m, 8H), 1.41 (td, J = 6 Hz, 2H), 1.34-1.24 (m, 6H), 1.14-1.09 (m, 4H), 0.98-0.88 (m, 3H), 0.81 (s, 3H), 0.69 (s, 3H), 0.69-0.62 (m, 1H).
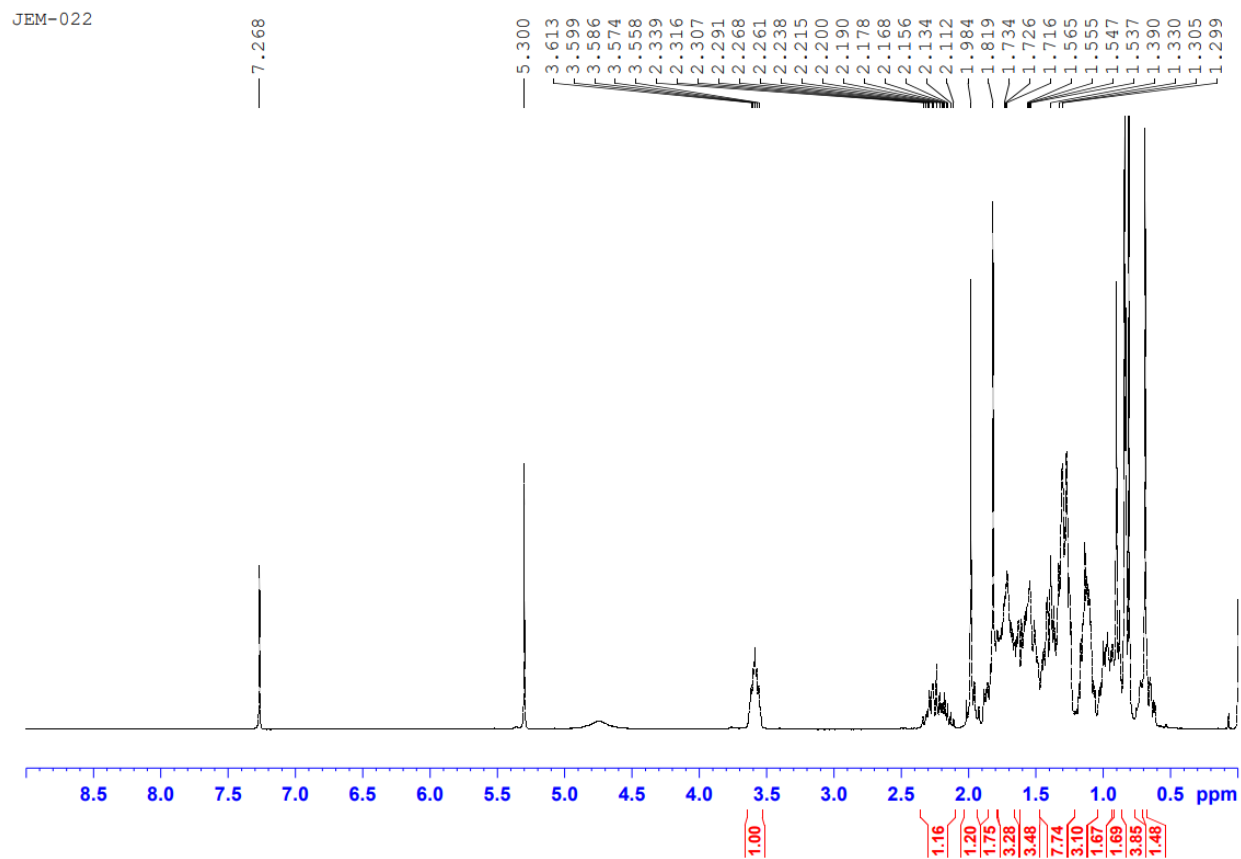
Figure 2.18: ^{1}H NMR of 5α-androstan-3β-ol (2.10)

(2R,5S,8S,9S,10S,13S,14S)–10,13–dimethyl 4,5,6,7,8,9,10,11,12,13,14,15,16,17–

tetradecahydro–3H–cyclopenta[a]phenanthren–3–one (2.11) - To a mixture of 3.5 g (12.6

mmol) of 5α-androstan-3β-ol **(2.10)**, in 200 mL dimethyl sulfoxide at 90°C was added 10 g (35.7

mmol) 2-iodoxybenzoic acid. The mixture was stirred at 90°C for 6 hrs before being returned to

room temperature. The reaction mixture was transferred to a separatory funnel, to which was

added 200 mL ethyl acetate. The mixture was extracted with 100 mL 5% sodium bicarbonate,

then twice washed with 100 mL saturated sodium chloride. The organic layer was concentrated

under vacuum before being purified using silica gel chromatography (10% Ethyl acetate/ 90%

hexanes) to provide the α,β-unsaturated ketone **(2.11)** (1.67 g, 49%). ^{1}H NMR (400 MHz,

CDCl$_3$) δ 7.16 (d, J = 10, 1H) 5.84 (dd, J = 10 Hz, 0.4 Hz, 1H), 2.41-2.36 (m, 1H), 2.15 (dd, J =

14.4 Hz, 3.5 Hz, 1H) 1.89-1.79 (m 1H), 1.74-1.63 (m, 3H) 1.63-1.47 (m, 3H), 1.45-1.29 (m, 5H),

1.18-1.05 (m, 4H,) 0.98-.87 (m, 6H), .67 (s, 3H).
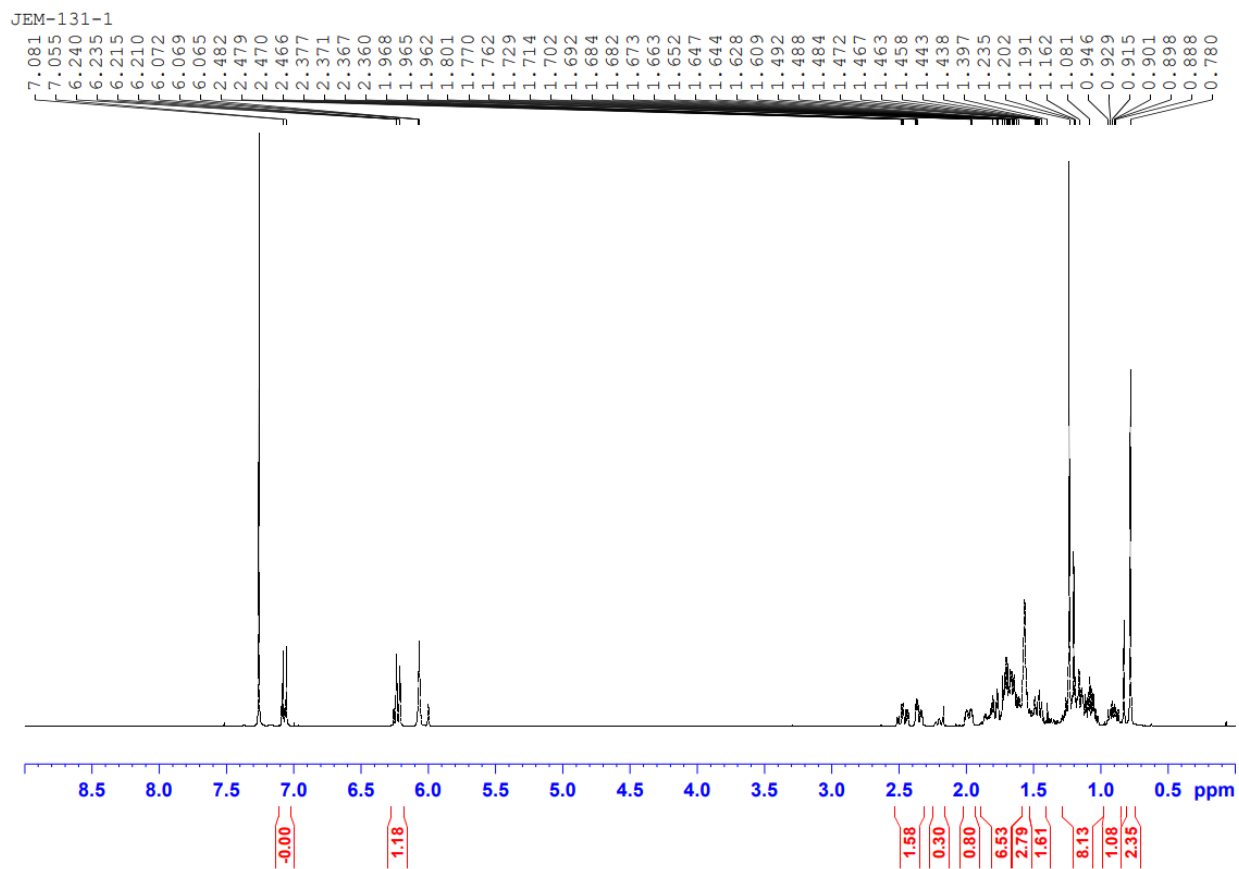
Figure 2.19: ¹H NMR of α-β unsaturated ketone (2.11)

(5S,8S,9S,10S,13S,14S)-10,13-dimethyl-3-oxo-4,5,6,7,8,9,10,11,12,13,14,15,16,17-

tetradecahydro-3H-cyclopenta[a]phenanthrene-2-bromide (2.12) - 400 mg (1.47 mmol) of

α,β-unsaturated ketone (**2.11**) was dissolved in 4 mL dry dichloromethane (DCM) and cooled in

an ice bath. To the reaction mixture was added dropwise a 0° solution of 75 µL (1.47 mmol)

liquid bromine in 4 mL DCM over 30 minutes. 0.41 mL (2.94 mmol) triethylamine, precooled to

0°C, was added slowly and the whole reaction was allowed to warm to room temperature and stir

for 1.5 hours. The reaction was quenched with 1 M HCl and washed with 2 X 8 mL 10% sodium

thiosulfate and 1 X 8 mL brine. The organics were dried with magnesium sulfate before being

removed under reduced pressure. The residue was subjected to column chromatography (10%

EtOAc/hexanes) providing the bromide (**2.12**) in 63% yield (320 mg). ^{1}H NMR (400 MHz,

CDCl$_3$) δ 7.59 (s, 1H), 2.58-2.43 (m, 2H), 2.03-1.94 (m, 1H), 1.85-1.52 (m, 6H), 1.48-1.34 (m,

5H), 1.22-1.12 (m, 3H), 1.05 (s, 3H), 1.02-0.93 (m, 3H), 0.73 (s, 3H)
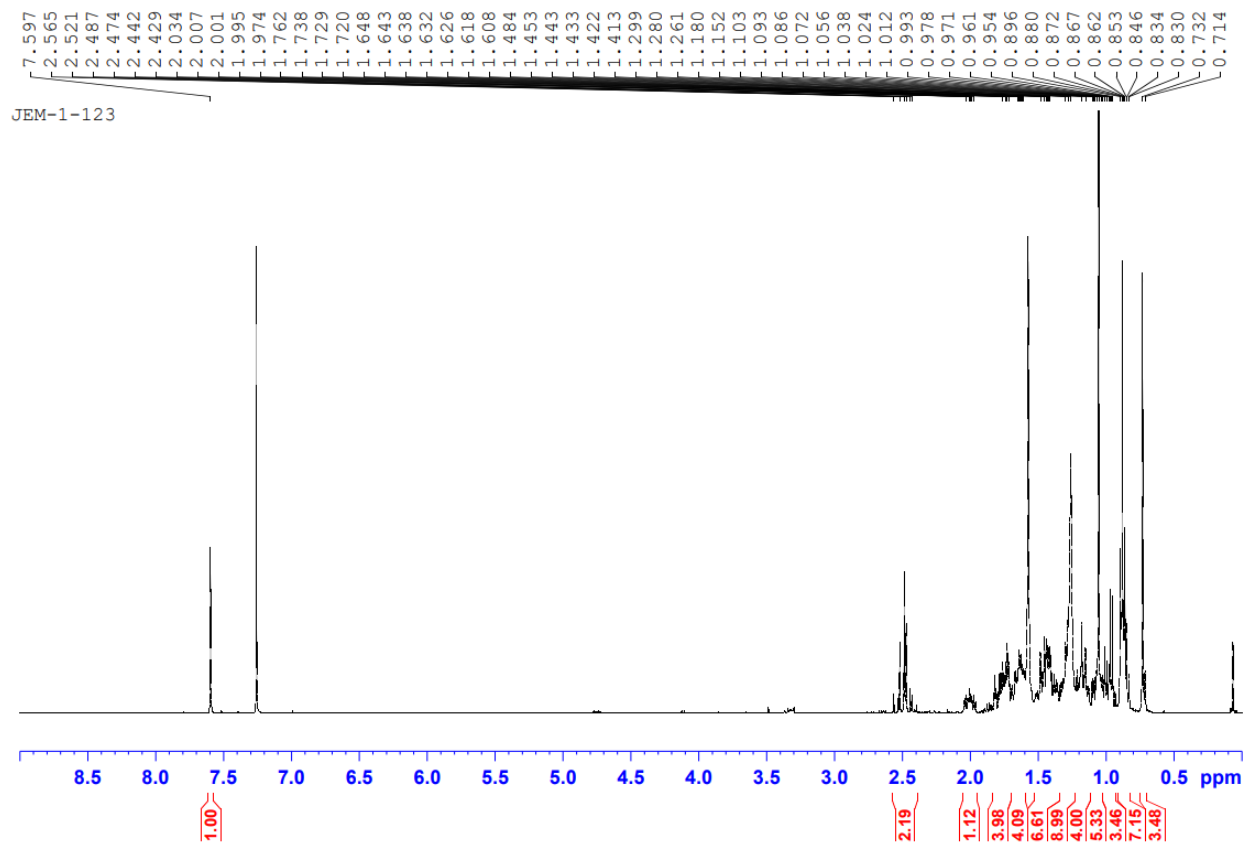
Figure 2.20: ¹H NMR of α-bromo-α,β-unsaturated ketone (2.12)

(5S,8S,9S,10S,13S,14S)-10,13-dimethyl-3-oxo-4,5,6,7,8,9,10,11,12,13,14,15,16,17-

tetradecahydro-3H-cyclopenta[a]phenanthrene-2-carbonitrile (2.13) - To a solution of 200

mg (0.56 mmol) of bromide **(2.12)** in 4 mL of dimethylformamide (DMF) was added 9.2 mg

(0.056 mmol) of potassium iodide and 56 mg (0.62 mmol) copper (I) cyanide. The reaction

mixture was heated to 120°C for 24 hours before being returned to room temperature and

quenched with 10 mL water and diluted with 35 mL EtOAc. The layers were separated and the

organics were washed with 2 X 10 mL saturated sodium bicarbonate and 1 X 10 mL brine before

being dried with magnesium sulfate. Organics were removed under reduced pressure and the

residue was purified via column chromatography (30% EtOAc/hexanes), yielding α-cyanoenone

(2.1) as a light-yellow powder in 12% yield (20 mg). ^{1}H NMR (400 MHz, CDCl$_3$) δ 7.88 (s, 1H),

2.48-2.35 (m, 2H), 2.02-1.93 (m, 1H), 1.87-1.57 (m, 7H), 1.50-1.38 (m, 5H), 1.22- 1.12 (m, 3H),

1.09 (s, 3H), 1.05-0.94 (m, 2H), 0.75 (s, 3H)

JEM-1-145

7.880
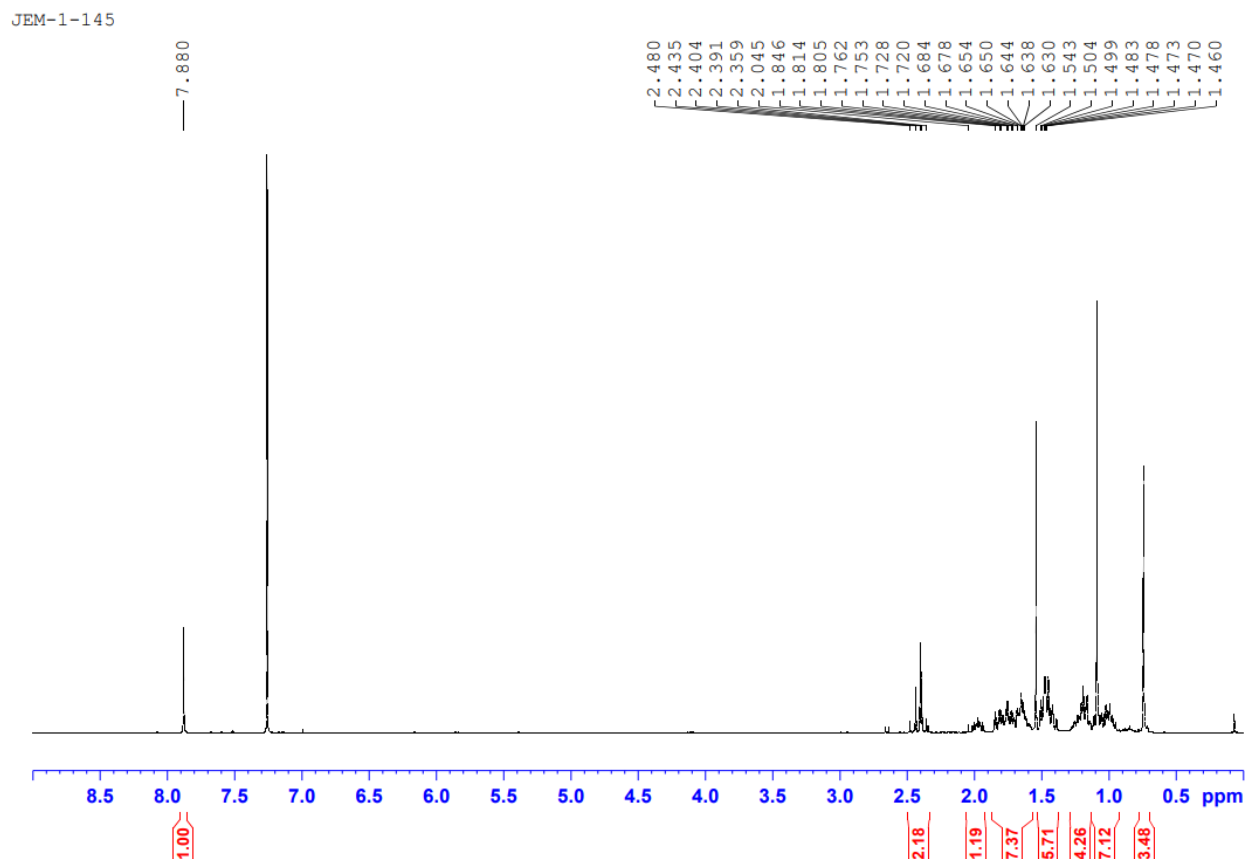
Figure 2.21: ¹H NMR of α-cyano-α,β-unsaturated ketone (2.1)

Synthetic method for JH101

Note: The following procedure for the synthesis of JH101 (Takeda A) was performed by Cassie Grossman, (Chisholm lab, Syracuse University) and developed from G. Mohan, et al. [59]

2-mercapto-5-carbomethoxy benzoxazole (2.14) - To an oven dried round bottom flask under argon, potassium hydroxide (2.53 g, 45.0 mmol, 15 equiv.) was stirred in dry methanol (14 mL, .22 M). 4-carbomethoxy-2-aminophenol (500 mg, 3.0 mmol) was added, followed by carbon disulfide (2.7 mL, 45.0 mmol, 15 equiv.). The reaction mixture was refluxed for 24 hrs. The reaction mixture was cooled to room temperature and acidified with 1M HCl (10 ml). The

organic layer was extracted with ethyl acetate (3x 50 mL). The organic layers were combined and washed with brine, dried over Na_2SO_4, and concentrated *in vacuo*. The crude residue was purified by silica gel flash chromatography (1% methanol/dichloromethane) to give 2-mercapto-5-carbomethoxy benzoxazole (**2.6**) (560 mg, 89%) as a white solid. NMR spectra is consistent with reported spectra.[60] ^{1}H NMR (400 MHz, DMSO-d_6) δ: 7.89 (d, J = 8.8 Hz, 1H), 7.69 (s, 1H), 7.62 (d, J = 8.7 Hz, 1H), 3.87 (s, 3H).

Methyl 2-[(2,4-dichlorobenzyl)sulfanyl]-1,3-benzoxazole-5-carboxylate (2.15) - The same procedure from Sakamoto et al. [21] was followed. To an oven dried round bottom flask under argon, 2-mercapto-5-carbomethoxy benzoxazole (560 mg, 2.68 mmol) was dissolved in dry DMF (7 ml, 2.7 M). 2,4-dichlorobenzylchloride (.44 ml, 2.94 mol, 1.1 equiv.) and potassium carbonate (370 mg, 2.68 mmol, 1.0 equiv.) were added. The reaction mixture was stirred at room temperature for 3 hrs. Water was added to the reaction mixture and the organic layer extracted with ethyl acetate. The organic layer was washed with brine, dried over Na_2SO_4, and concentrated *in vacuo*. The crude residue was purified by silica gel flash chromatography (100% hexanes to 50% ethyl acetate/50% hexanes) to give methyl 2-[(2,4-dichlorobenzyl)sulfanyl]-1,3-benzoxazole-5-carboxylate (760 mg, 77%) as a colorless solid. NMR spectra is consistent with reported spectra[3]. ^{1}H NMR (400 MHz, CDCl$_3$) δ: 8.31 (d, J = 1.1 Hz, 1H), 8.01 (dd, J = 8.5, 1.6 Hz, 1H), 7.62 (d, J = 8.3 Hz, 1H), 7.48-7.42 (m, 2H), 7.21 (dd, J = 8.2, 2.1, 1H), 4.62 (s, 2H), 3.95 (s, 3H).

2-[(2,4-dichlorobenzyl)sulfanyl]-1,3-benzoxazole-5-carboxylic acid (2.16) - The following procedure was developed from Sakamoto et al. [21] To a round bottom flask, methyl 2-[(2,4-dichlorobenzyl)sulfanyl]-1,3-benzoxazole-5-carboxylate (**2.15**) (760 mg, 2.06 mmol) was

dissolved in a 8:1 H_2O:THF (34.2 mL, 4.15 mL) mixture. 1 N NaOH solution (4.15 mL, 4.13 mmol, 2.0 equiv.) was added. The reaction mixture was warmed to 50°C and stirred for 7 hrs. The reaction mixture was cooled to room temperature and concentrated *in vacuo*. H_2O (38 mL) and THF (11 mL) was added to the resulting residue and the mixture was washed with diethyl ether. The water layer was acidified with 1 M HCl (5 mL). The organic layer was extracted with a 1:1 ethyl acetate:THF mixture. The organic layer was washed with H_2O and brine successively, dried over Na_2SO_4, and concentrated *in vacuo*. The crude residue was purified by silica gel flash chromatography (40% ethyl acetate/hexanes to 90% ethyl acetate/hexanes). The fractions were concentrated *in vacuo*, then methanol added to the resulting residue. The remaining white solid was filtered, washed with methanol, and dried to obtain 2-[(2,4-dichlorobenzyl)sulfanyl]-1,3-benzoxazole-5-carboxylic acid (**2.16**) (228 mg, 31%) as a white solid. NMR spectra is consistent with reported spectra. [21] ^{1}H NMR (400 MHz, DMSO-d$_6$) δ: 13.10 (bs, 1H), 8.16 (d, *J* = 1.1 Hz, 1H), 7.95 (dd, *J* = 8.6, 1.6 Hz, 1H), 7.74 (q, *J* = 8.6, 4.7 Hz, 2H), 7.68 (d, *J* = 1.9 Hz, 1H), 7.43 (dd, *J* = 8.4, 2.0 Hz, 1H), 4.71 (s, 2H). ^{13}C NMR (100 MHz, DMSO-d$_6$) δ: 166.80, 164.94, 154.03, 141.25, 134.37, 133.57, 132.94, 132.84, 129.07, 127.72, 127.63, 126.14, 119.44, 110.33, 33.31. Elemental analysis calculated (%) for $C_{15}H_9Cl_2NO_3S$: C 50.87, H 2.56, N 3.91. Found: C 50.85, H 2.67, N 3.91.

Purchasing compounds for library screen

Compounds of interest were purchased utilizing MolPort as a distributor. Identity of hit compounds were verified with HRMS. The HRMS analysis was completed at Old Dominion University using positive-ion mode electrospray ionization with an Apollo II ion source on a Bruker 10 Tesla APEX -Qe FTICR-MS. Expected M/Z of JH210 (417.229), observed M/Z (417.228). Expected M/Z of JH226 (395.043), observed M/Z (395.043). Expected M/Z of JH229 (388.098), observed M/Z (388.098). Expected M/Z of JH235 (359.107), observed (359.107).

2.4.3 Peptide substrate labeling with acrylodan

Peptide substrates GSSFLC and GSSCLS were labeled with acrylodan on either C4 or C6 and purified via HPLC according to literature procedure. [29, 33]

2.4.4 Expression and enrichment of hGOAT-containing membrane protein fraction

hGOAT and mGOAT were expressed in insect cells (Sf9) and enriched in cell membrane fractions using published procedures. [29, 33]

2.4.5 Fluorescence enhancement assay development

For initial development of the continuous fluorescence enhancement assay, membrane fractions from Sf9 cells expressing hGOAT were first thawed on ice, then passed through an 18-gauge needle ten times to homogenize. A master mix was created containing 50 mM HEPES

buffer pH 7.0, 2.5 µM MAFP, and 30 µg membrane protein per reaction, plus water to bring the reaction to 100 µL after the addition of octanoyl CoA, and peptide. The mix was then allowed to preincubate for 30 minutes at room temperature while covered. The master mix was then distributed (44 µL) into black 96 well non-binding plates (Reference number 3650, Corning, ME), and reactions were initiated by the addition of 6.0 µL octanoyl-CoA (833 µM, final concentration 50 µM) or (-) oct-CoA (10 mM Tris-HCl), followed by 50 µL of variable concentrations of acrylodan-labeled GSSC$_{AcDan}$LS peptide, for a total reaction volume of 100 µL. This reaction was monitored by plate reader (BioTek Synergy H1 High Energy Plate Reader) (Excitation: 365 nm, Emission: 485) for 2 hours, taking a timepoint every five minutes. Relative Fluorescence Units (RFU) were plotted in Excel as a function of time to give a timecourse of reaction progress. Correction was achieved by subtracting the RFU of the (-) octanoyl CoA control reaction from the RFU of the reaction of interest at each timepoint.

2.4.6 Library Screening via Continuous Fluorescence Enhancement Assay

The plate reader screen was performed as described above with minor alterations. Membrane fractions were thawed on ice and homogenized through an 18-gauge needle. A master mix was prepared containing 50 mM HEPES, 2.5 µM MAFP, and 30 µg of protein per reaction, with enough water to volume the reaction to 100 µL after addition of inhibitor, octanoyl-CoA, and peptide. This master mix was incubated covered at room temperature for 30 minutes, then distributed (42 µL) into a 96 well plate. To each well was added 2 µL inhibitor or vehicle, then the reactions were incubated for 30 minutes. To initiate reaction, 6 µL of octanoyl-CoA (50 µM final concentration) and 50 µL 2.0 µM GSSC$_{AcDan}$LS (1.0 µM final concentration) were added to solution, then the reactions were monitored for two hours by plate reader as described above.

The RFU and corrected RFU were then calculated as above, and the % activity for each inhibitor dilution was calculated using equation 2.1 below.

$$\% \ activity = \frac{Corrected \ RFU \ of \ inhibited \ sample}{Corrected \ RFU \ of \ vehicle} * 100 \qquad (eq. \ \mathbf{2.1})$$

Plots of plate data were created using Kaleidagraph.

2.4.7 Continuous Fluorescence Inhibition Assay analyzed by HPLC

For inhibition assays, the samples were run as in the previous section. Membrane fractions from Sf9 cells expressing hGOAT were first thawed on ice, then passed through an 18-gauge needle ten times to homogenize. A master mix was created as above, adding water to bring the reaction to 100 µL after the addition of sample, octanoyl CoA, and peptide and incubating for 30 minutes. The reaction was initiated as described above and reacted for one hour before being stopped with 100 µL of 20% acetic acid in isopropanol. 100 µL of the resulting solution was then removed from the wells and transferred into low-adhesion centrifuge tubes (LPS inc.), and excess membrane fraction was then removed via precipitation by the addition of 33.4 µL 20% trichloroacetic acid followed by a 1000g centrifugation for 1 minute. The supernatant was then analyzed via reverse-phase HPLC using published approaches.[30]

2.4.8 Determination of GOAT Activity by HPLC

Membrane fractions containing hGOAT or mGOAT were thawed on ice and homogenized through an 18-gauge needle. A master mix was prepared containing 50 mM HEPES, 2.5 µM MAFP, and 30 µg of protein per reaction, with enough water to volume the reaction to 100 µL after addition of inhibitor, octanoyl-CoA, and peptide. This master mix was

incubated covered at room temperature for 30 minutes, then distributed (42 µL) into low-adhesion microcentrifuge tubes. To each well was added 2 µL inhibitor or vehicle, then the reactions were incubated for 30 minutes. To initiate reaction, 6 µL of octanoyl-CoA (50 µM final concentration), followed by 50 µL 4.0 µM GSSC$_{acdan}$LS (2.0 µM final concentration) were added to solution, then the reactions were reacted for one hour before being stopped with 100 µL of 20% acetic acid in isopropanol. Excess membrane fraction was then removed via precipitation after the addition of 33.4 µL 20% trichloroacetic acid followed by a 1000g centrifugation for 1 minute. The supernatant was then analyzed via reverse-phase HPLC.

2.4.9 Determination of acyl-competition by HPLC

Membrane fractions were thawed on ice and homogenized through an 18-gauge needle. A master mix was prepared containing 50 mM HEPES, 2.5 µM MAFP, and 30 µg of protein per reaction, with enough water to volume the reaction to 100 µL after addition of inhibitor, octanoyl-CoA, and peptide. This master mix was incubated covered at room temperature for 30 minutes, then distributed (42 µL) into low-adhesion microcentrifuge tubes. To each well was added 2 µL inhibitor or vehicle, then the reactions were incubated for one. To initiate reaction, 6 µL of octanoyl-CoA to give a final concentration of 3 µM or 300 µM, followed by 50 µL 2.0 µM GSSC$_{AcDan}$LS were added to solution, then the reactions were reacted for one hour before being stopped with 100 µL of 20% acetic acid in isopropanol. Excess membrane fraction was then removed via precipitation after the addition of 33.4 µL 20% trichloroacetic acid followed by a 1000g centrifugation for 1 minute. The supernatant was then analyzed via reverse-phase HPLC.

2.4.10 HPLC analysis of GOAT Assays

Assays were analyzed on reverse-phase HPLC (Zorbax Eclipse XDB column, 4.6 150 mm) using a solvent gradient from 30% acetonitrile in aqueous 0.05% TFA to 63% acetonitrile in aqueous 0.05% TFA over 5 minutes at a flow rate of 1 mL/min, followed by 100% acetonitrile for 5 minutes. Peptides were detected by the attached acrylodan label with the UV absorbance at 360 nm and fluorescence ($\lambda_{ex} = 360$ nm, $\lambda_{em} = 485$ nm). Octanoylated peptide typically eluted around 8 minutes, with the des-acyl peptide eluting around 4 minutes. Chemstation for LC (Agilent Technologies) was used for peak integration.

2.4.11 Calculation of Z' factor for fluorescence GOAT assay

Z' factor was calculated using the following equation (**2.2**): [37, 61]

$$Z' = 1 - (\frac{3(stdev\ of\ sample + stdev\ of\ negative\ control)}{|average\ of\ sample - average\ of\ negative\ control|}) \qquad (eq.\ \textbf{2.2})$$

2.4.12 Determination of IC$_{50}$ Values

For IC$_{50}$ determination via HPLC, peak integration of the product peak was used to determine inhibition in the presence of either sample or vehicle (DMSO). IC$_{50}$ values were determined by fitting **Equation 2.3** to the plot of peak integration against inhibitor concentration.

$$\text{Peak integration} = \left(1 - \frac{[inhibitor]}{[inhibitor] + IC50}\right) \qquad (eq.\ \textbf{2.3})$$

Plots and data fitting were performed with Kaleidagraph (Synergy Software, Reading, PA)

2.4.13 Virtual screening using the MTiOpenScreen web interface

Note: Virtual screening for new inhibitors was performed by John Chisholm (Syracuse University)

Virtual screening for new inhibitors was performed on the model of hGOAT with the MTI-OpenScreen web server[39] using their diverse chemical compound collection (Diverse-lib) of 99,288 drug-like PubChem molecules. MTI-OpenScreen utilizes AutoDock Vina, [62] which employs a gradient-based conformational search approach and defines the search space by a grid box. The grid box encompassed the Acetyl-CoA binding site. The compounds with the best predicted binding were then retrieved from the PubChem online database (https://pubchem.ncbi.nlm.nih. gov/).[63] More information on MTI-OpenScreen can be found at their website here: https://bioserv.rpbs.univ-paris-diderot.fr/services/MTiOpenScreen/

2.4.14 Computational inhibitor docking and binding site analysis

Note: All molecular docking of inhibitor molecules was performed by Jingjing Ji (Nangia Lab, Syracuse University).

Molecular docking of the inhibitor molecules was performed using VINA (Vina Is Not Autodock) [64] utility available in YASARA (Yet Another Scientific Artificial Reality Application) program. [65] The molecular structures of the inhibitors were generated from CHARMMGUI Ligand Reader & Modeler. [66, 67] The docking procedure involved predicting the noncovalent binding energies (BE) dissociation constants (Kd) of the inhibitor molecule with the hGOAT. For each inhibitor, a rank-ordered list of docking poses was generated **(Table 2.5).** The top three poses for each inhibitor in **Table 2.5** were investigated further for stability using molecular dynamics (MD) simulations.

CHARMM-GUI solution builder[66, 68-70] was used to build the inhibitor-hGOAT system in the all-atom resolution for MD simulations. The CHARMM36m force field[71] parameters were used for inhibitors, hGOAT protein, TIP3P water, and salt (0.15 M). The simulations were performed using GROMACS (version 2019 package).[72] Each inhibitor-hGOAT system was energy minimized, followed by equilibration in isothermal-isochoric (*NVT*) and isothermal-isobaric (*NPT*) for 1 ns each, and production MD run under *NPT* conditions for 300 ns. The heavy atoms of the hGOAT protein and the inhibitor molecule were restrained during *NVT* and *NPT* equilibration. The restraints on the inhibitor heavy atoms were removed during the production MD. The temperature of each system was maintained at 298.15 K using the v-rescale thermostat[73] with τ_t = 1.0 ps. In the pre-production *NPT* run, isotropic pressure of 1 bar was maintained using Berendsen barostat[74] with τ_p = 5.0 ps and compressibility of 4.5×10^{-5} bar^{-1}. In the production MD, we used the Parrinello-Rahman barostat[75] with τ_p = 5.0 ps and compressibility of 4.5×10^{-5} bar^{-1}. Three-dimensional periodic boundary conditions (PBC) were applied to each system. A 2 fs time step was used, and the nonbonded interaction neighbor list was updated every 20 steps. A 1.2 nm cutoff was used for the electrostatic and van der Waals interactions. The long-range electrostatic interactions were calculated using the Particle-Mesh Ewald (PME) method after a 1.2 nm cutoff. The bonds involving hydrogen atoms were constrained using the linear constraint solver (LINCS) algorithm.

Table 2.5. Calculated energies and binding affinities of selected inhibitor poses. The unit of energy of binding E is kcal/mol and the unit of dissociation constant Kd is pM.

Boehringer		Eli		GlaxoSmithKline		JH226		Takeda_A		Takeda_B	
E	Kd	E	Kd	E	Kd	E	Kd	E	Kd	E	Kd
−10.688	1.46×10^4	−8.683	4.32×10^5	−9.099	2.14×10^5	−9.028	2.41×10^5	−8.827	3.39×10^5	−10.349	2.59×10^4
−10.320	2.72×10^4	−8.486	6.02×10^5	−8.965	2.68×10^5	−8.965	2.68×10^5	−8.664	4.46×10^5	−9.841	6.12×10^4
−10.108	3.90×10^4	−8.388	7.10×10^5	−8.337	7.74×10^5	−8.288	8.41×10^5	−8.380	7.20×10^5	−9.627	8.78×10^4
−9.496	1.09×10^5	−8.332	7.81×10^5	−8.047	1.26×10^6	−7.976	1.42×10^6	−7.301	4.45×10^6	−9.245	1.67×10^5
−9.491	1.10×10^5	−7.951	1.49×10^6	−7.125	5.99×10^6					−9.152	1.96×10^5
−9.472	1.14×10^5	−7.915	1.58×10^6	−7.044	6.87×10^6					−8.600	4.97×10^5
−9.405	1.28×10^5	−7.893	1.64×10^6	−6.836	9.75×10^6					−8.516	5.72×10^5
−9.391	1.31×10^5	−7.820	1.85×10^6							−8.217	9.48×10^5
−9.232	1.71×10^5	−7.522	3.06×10^6							−8.096	1.16×10^6
−9.098	2.14×10^5	−7.340	4.17×10^6							−8.040	1.28×10^6
−8.703	4.17×10^5									−7.924	1.55×10^6
−8.400	6.96×10^5										
−8.393	7.04×10^5										
−8.166	1.03×10^6										
−7.996	1.38×10^6										

2.5 References Cited

1.   Barazzoni, R.; Zanetti, M.; Ferreira, C.; Vinci, P.; Pirulli, A.; Mucci, M.; Dore, F.; Fonda, M.; Ciocchi, B.; Cattin, L.; Guarnieri, G. Relationships between desacylated and acylated ghrelin and insulin sensitivity in the metabolic syndrome. *J Clin Endocrinol Metab* **2007**, *92* (10), 3935-3940. DOI: 10.1210/jc.2006-2527.

2.   Delhanty, P. J.; Huisman, M.; Baldeon-Rojas, L. Y.; van den Berge, I.; Grefhorst, A.; Abribat, T.; Leenen, P. J.; Themmen, A. P.; van der Lely, A. J. Des-acyl ghrelin analogs prevent high-fat-diet-induced dysregulation of glucose homeostasis. *FASEB J* **2013**, *27* (4), 1690-1700. DOI: 10.1096/fj.12-221143.

3.   Tong, J.; Prigeon, R. L.; Davis, H. W.; Bidlingmaier, M.; Kahn, S. E.; Cummings, D. E.; Tschop, M. H.; D'Alessio, D. Ghrelin suppresses glucose-stimulated insulin secretion and deteriorates glucose tolerance in healthy humans. *Diabetes* **2010**, *59* (9), 2145-2151. DOI: 10.2337/db10-0504.

4.   Wren, A. M.; Seal, L. J.; Cohen, M. A.; Brynes, A. E.; Frost, G. S.; Murphy, K. G.; Dhillo, W. S.; Ghatei, M. A.; Bloom, S. R. Ghrelin enhances appetite and increases food intake in humans. *Journal of Clinical Endocrinology and Metabolism* **2001**, *86* (12), 5992-5995, Article. DOI: 10.1210/jc.86.12.5992

5.   Wren, A. M.; Small, C. J.; Abbott, C. R.; Dhillo, W. S.; Seal, L. J.; Cohen, M. A.; Batterham, R. L.; Taheri, S.; Stanley, S. A.; Ghatei, M. A.; Bloom, S. R. Ghrelin causes hyperphagia and obesity in rats. *Diabetes* **2001**, *50* (11), 2540-2547. DOI: 10.2337/diabetes.50.11.2540.

6.   Jerlhag, E.; Egecioglu, E.; Dickson, S. L.; Douhan, A.; Svensson, L.; Engel, J. A. Ghrelin administration into tegmental areas stimulates locomotor activity and increases extracellular concentration of dopamine in the nucleus accumbens. *Addict Biol* **2007**, *12* (1), 6-16. DOI: 10.1111/j.1369-1600.2006.00041.x.

7.   Jerlhag, E.; Egecioglu, E.; Dickson, S. L.; Engel, J. A. Ghrelin receptor antagonism attenuates cocaine- and amphetamine-induced locomotor stimulation, accumbal dopamine release, and conditioned place preference. *Psychopharmacology (Berl)* **2010**, *211* (4), 415-422. DOI: 10.1007/s00213-010-1907-7.

8.   Davis, K. W.; Wellman, P. J.; Clifford, P. S. Augmented cocaine conditioned place preference in rats pretreated with systemic ghrelin. *Regul Pept* **2007**, *140* (3), 148-152. DOI: 10.1016/j.regpep.2006.12.003.

9.   Gutierrez, J. A.; Solenberg, P. J.; Perkins, D. R.; Willency, J. A.; Knierman, M. D.; Jin, Z.; Witcher, D. R.; Luo, S.; Onyia, J. E.; Hale, J. E. Ghrelin octanoylation mediated by an orphan lipid transferase. *Proc Natl Acad Sci U S A* **2008**, *105* (17), 6320-6325. DOI: 10.1073/pnas.0800708105.

10.   Yang, J.; Brown, M. S.; Liang, G.; Grishin, N. V.; Goldstein, J. L. Identification of the acyltransferase that octanoylates ghrelin, an appetite-stimulating peptide hormone. *Cell* **2008**, *132* (3), 387-396. DOI: 10.1016/j.cell.2008.01.017.

11.   Yang, J.; Zhao, T. J.; Goldstein, J. L.; Brown, M. S. Inhibition of ghrelin O-acyltransferase (GOAT) by octanoylated pentapeptides. *Proc Natl Acad Sci U S A* **2008**, *105* (31), 10750-10755, Article. DOI: 10.1073/pnas.0805353105.

12.   Murzinski, E. S.; Saha, I.; Ding, H.; Strugatsky, D.; Hollibaugh, R. A.; Liu, H.; Tontonoz, P.; Harran, P. G. In Search of Small Molecules That Selectively Inhibit MBOAT4. *Molecules* **2021**, *26* (24). DOI: 10.3390/molecules26247599.

13.   Zhao, F.; Darling, J. E.; Gibbs, R. A.; Hougland, J. L. A new class of ghrelin O-acyltransferase inhibitors incorporating triazole-linked lipid mimetic groups. *Bioorganic & Medicinal Chemistry Letters* **2015**, *25* (14), 2800-2803. DOI: 10.1016/j.bmcl.2015.05.009

14.   Hollibaugh, R. A. Defining a Minimal Pharmacophore to Selectively Inhibit MBOAT4. UCLA, 2016.

15.   Barnett, B. P.; Hwang, Y.; Taylor, M. S.; Kirchner, H.; Pfluger, P. T.; Bernard, V.; Lin, Y. Y.; Bowers, E. M.; Mukherjee, C.; Song, W. J.; et al. Glucose and weight control in mice with a designed ghrelin O-acyltransferase inhibitor. *Science* **2010**, *330* (6011), 1689-1692. DOI: 10.1126/science.1196154.

16.   Costantino, L. Methods for synthesis and uses of inhibitors of ghrelin O-acyltransferase inhibitors as potential therapeutic agents for obesity and diabetes. *Expert Opin Ther Pat* **2010**, *20* (11), 1603-1607. DOI: 10.1517/13543776.2011.527333.

17.   Garner, A. L.; Janda, K. D. A small molecule antagonist of ghrelin O-acyltransferase (GOAT). *Chem. Commun.* **2011**, *47* (26), 7512-7514, 10.1039/c1cc11817j. DOI: 10.1039/c1cc11817j.

18.   Garner, A. L. cat-ELCCA: catalyzing drug discovery through click chemistry. *Chem Commun (Camb)* **2018**, *54* (50), 6531-6539. DOI: 10.1039/c8cc02332h.

19.   Garner, A. L.; Janda, K. D. cat-ELCCA: A Robust Method To Monitor the Fatty Acid Acyltransferase Activity of Ghrelin O-Acyltransferase (GOAT). *Angew. Chem., Int. Ed.* **2010**, *49* (50), 9630-9634, DOI: 10.1002/anie.201003387.

20.   Moose, J. E.; Leets, K. A.; Mate, N. A.; Chisholm, J. D.; Hougland, J. L. An overview of ghrelin O-acyltransferase inhibitors: a literature and patent review for 2010-2019. *Expert Opin Ther Pat* **2020**, *30* (8), 581-593. DOI: 10.1080/13543776.2020.1776263.

21.   Yoneyama-Hirozane, M.; Deguchi, K.; Hirakawa, T.; Ishii, T.; Odani, T.; Matsui, J.; Nakano, Y.; Imahashi, K.; Takakura, N.; Chisaki, I.; et al. Identification and Characterization of a New Series of Ghrelin O-Acyl Transferase Inhibitors. *SLAS Discovery* **2018**, *23* (2), 154-163,. DOI: 10.1177/2472555217727097.

22.   Galka, C. S.; Hembre, E. J.; Honigschmidt, N. A.; Keding, S. J.; Martinez-Grau, M. A.; Plaza, G. R.; Rubio, A.; Smith, D. L. Preparation of N-acylamino acid derivatives as ghrelin o-acyl transferase inhibitors. WO2016168225A1, 2016.

23.   Bandyopadhyay, A.; Cheung, M.; Eidam, H. S.; Joshi, H.; Su, D.-S. Preparation of ghrelin O-acyltransferase inhibitors for treatment of metabolic disorders. IN201811004277A, 2019.

24.   Trieselmann, T.; Godbout, C.; Hoenke, C.; Vintonyak, V. Preparation of triazolopyrimidine derivatives as ghrelin o-acyl transferase (GOAT) inhibitors. WO2019149660A1, 2019.

25.   Godbout, C.; Trieselmann, T.; Vintonyak, V. Preparation of oxadiazolopyridine derivatives for use as ghrelin o-acyl transferase (GOAT) inhibitors. WO2018024653A1, 2018.

26.   McGovern-Gooch, K. R.; Mahajani, N. S.; Garagozzo, A.; Schramm, A. J.; Hannah, L. G.; Sieburg, M. A.; Chisholm, J. D.; Hougland, J. L. Synthetic Triterpenoid Inhibition of Human Ghrelin O-Acyltransferase: The Involvement of a Functionally Required Cysteine Provides Mechanistic Insight into Ghrelin Acylation. *Biochemistry* **2017**, *56* (7), 919-931. DOI: 10.1021/acs.biochem.6b01008

27.   Campana, M. B.; Irudayanathan, F. J.; Davis, T. R.; McGovern-Gooch, K. R.; Loftus, R.; Ashkar, M.; Escoffery, N.; Navarro, M.; Sieburg, M. A.; Nangia, S.; Hougland, J. L. The ghrelin O-acyltransferase structure reveals a catalytic channel for transmembrane hormone acylation. *J Biol Chem* **2019**, *294* (39), 14166-14174. DOI: 10.1074/jbc.AC119.009749.

28.   Barnett, B. P.; Hwang, Y.; Taylor, M. S.; Kirchner, H.; Pfluger, P. T.; Bernard, V.; Lin, Y.-y.; Bowers, E. M.; Mukherjee, C.; Song, W.-J.; et al. Glucose and Weight Control in Mice with a Designed Ghrelin O-Acyltransferase Inhibitor. *Science* **2010**, *330* (6011), 1689-1692, DOI: 10.1126/science.1196154.

29.   Darling, J. E.; Prybolsky, E. P.; Sieburg, M.; Hougland, J. L. A fluorescent peptide substrate facilitates investigation of ghrelin recognition and acylation by ghrelin O-acyltransferase. *Analytical Biochemistry* **2013**, *437* (1), 68-76. DOI: 10.1016/j.ab.2013.02.013

30.   Sieburg, M. A.; Cleverdon, E. R.; Hougland, J. L. Biochemical Assays for Ghrelin Acylation and Inhibition of Ghrelin O-Acyltransferase. *Methods Mol Biol* **2019**, *2009*, 227-241. DOI: 10.1007/978-1-4939-9532-5_18.

31.   Prendergast, F. G.; Meyer, M.; Carlson, G. L.; Iida, S.; Potter, J. D. Synthesis, Spectral Properties, and Use of 6-Acryloyl-2-Dimethylaminonaphthalene (Acrylodan) - a Thiol-Selective, Polarity-Sensitive Fluorescent-Probe. *Journal of Biological Chemistry* **1983**, *258* (12), 7541-7544.

32.   Tricerri, M. A.; Behling Agree, A. K.; Sanchez, S. A.; Jonas, A. Characterization of apolipoprotein A-I structure using a cysteine-specific fluorescence probe. *Biochemistry* **2000**, *39* (47), 14682-14691. DOI: 10.1021/bi0014251.

33.   Darling, J. E.; Zhao, F.; Loftus, R. J.; Patton, L. M.; Gibbs, R. A.; Hougland, J. L. Structure-Activity Analysis of Human Ghrelin O-Acyltransferase Reveals Chemical

Determinants of Ghrelin Selectivity and Acyl Group Recognition. *Biochemistry* **2015**, *54* (4), 1100-1110. DOI: 10.1021/

34.   Cleverdon, E. R.; Davis, T. R.; Hougland, J. L. Functional group and stereochemical requirements for substrate binding by ghrelin O-acyltransferase revealed by unnatural amino acid incorporation. *Bioorg Chem* **2018**, *79*, 98-106. DOI: 10.1016/j.bioorg.2018.04.009.

35.   Campaña, M. B.; Davis, T. R.; Cleverdon, E. R.; Bates, M.; Krishnan, N.; Curtis, E. R.; Childs, M. D.; Morales-Rodriguez, Y.; Sieburg, M. A.; Hehnly, H.; et al. Ghrelin O-acyltransferase interacts with extracellular peptides and exhibits unexpected cellular localization for a secretory pathway enzyme. *BioRxiv* **2021**. DOI: 10.1101/2021.06.01.446150.

36.   Weber, G.; Farris, F. J. Synthesis and spectral properties of a hydrophobic fluorescent probe: 6-propionyl-2-(dimethylamino)naphthalene. *Biochemistry* **1979**, *18* (14), 3075-3078. DOI: 10.1021/bi00581a025.

37.   Zhang, J. H.; Chung, T. D.; Oldenburg, K. R. A Simple Statistical Parameter for Use in Evaluation and Validation of High Throughput Screening Assays. *J Biomol Screen* **1999**, *4* (2), 67-73. DOI: 10.1177/108705719900400206.

38.   Bar, H.; Zweifach, A. Z' Does Not Need to Be > 0.5. *SLAS Discov* **2020**, *25* (9), 1000-1008. DOI: 10.1177/2472555220942764.

39.   Labbe, C. M.; Rey, J.; Lagorce, D.; Vavrusa, M.; Becot, J.; Sperandio, O.; Villoutreix, B. O.; Tuffery, P.; Miteva, M. A. MTiOpenScreen: a web server for structure-based virtual screening. *Nucleic Acids Res* **2015**, *43* (W1), W448-454. DOI: 10.1093/nar/gkv306.

40.   Trieselmann, T.; Godbout, C.; Vintonyak, V. Preparation of heterocyclyl-substituted oxadiazolopyridine derivatives for use as ghrelin o-acyl transferase inhibitors. WO2019149659A1, 2019.

41.   Takakura, N.; Banno, Y.; Terao, Y.; Ochida, A.; Morimoto, S.; Kitamura, S.; Tomata, Y.; Yasuma, T.; Ikoma, M.; Masuda, K. Preparation of benzothiophenyl- and benzofuranacetic acid derivatives as inhibitors of GOAT for treating obesity. WO2013125732A1, 2013.

42.   Wang, L. Ghrelin O-acyltransferase (GOAT) inhibitor and its applications in obesity and diabetes. CN108516972A, 2018.

43.   Hameduh, T.; Haddad, Y.; Adam, V.; Heger, Z. Homology modeling in the time of collective and artificial intelligence. *Comput Struct Biotechnol J* **2020**, *18*, 3494-3506. DOI: 10.1016/j.csbj.2020.11.007.

44.   Muhammed, M. T.; Aki-Yalcin, E. Homology modeling in drug discovery: Overview, current applications, and future perspectives. *Chem Biol Drug Des* **2019**, *93* (1), 12-20. DOI: 10.1111/cbdd.13388.

45.   Singh, R. B.; Das, N.; Singh, G. K.; Singh, S. K.; Zaman, K. Synthesis and pharmacological evaluation of 3-[5-(aryl-[1,3,4]oxadiazole-2-yl]-piperidine derivatives as anticonvulsant and antidepressant agents. *Arabian Journal of Chemistry* **2020**, *13* (5), 5299-5311. DOI: 10.1016/j.arabjc.2020.03.009.

46.   Wang, S.; Liu, H.; Wang, X.; Lei, K.; Li, G.; Li, J.; Liu, R.; Quan, Z. Synthesis of 1,3,4-oxadiazole derivatives with anticonvulsant activity and their binding to the GABAA receptor. *Eur J Med Chem* **2020**, *206*, 112672. DOI: 10.1016/j.ejmech.2020.112672.

47.   Galli, L. M.; Anderson, M. O.; Gabriel Fraley, J.; Sanchez, L.; Bueno, R.; Hernandez, D. N.; Maddox, E. U.; Lingappa, V. R.; Burrus, L. W. Determination of the membrane topology of PORCN, an O-acyl transferase that modifies Wnt signalling proteins. *Open Biol* **2021**, *11* (6), 200400. DOI: 10.1098/rsob.200400.

48.   Lanyon-Hogg, T.; Ritzefeld, M.; Zhang, L.; Andrei, S. A.; Pogranyi, B.; Mondal, M.; Sefer, L.; Johnston, C. D.; Coupland, C. E.; Greenfield, J. L.; et al. Photochemical Probe Identification of a Small-Molecule Inhibitor Binding Site in Hedgehog Acyltransferase (HHAT). *Angew Chem Int Ed Engl* **2021**, *60* (24), 13542-13547. DOI: 10.1002/anie.202014457.

49.   Hopf, T. A.; Scharfe, C. P.; Rodrigues, J. P.; Green, A. G.; Kohlbacher, O.; Sander, C.; Bonvin, A. M.; Marks, D. S. Sequence co-evolution gives 3D contacts and structures of protein complexes. *Elife* **2014**, *3*. DOI: 10.7554/eLife.03430.

50.   Ovchinnikov, S.; Kinch, L.; Park, H.; Liao, Y. X.; Pei, J. M.; Kim, D. E.; Kamisetty, H.; Grishin, N. V.; Baker, D. Large-scale determination of previously unsolved protein structures using evolutionary information. *Elife* **2015**, *4*. DOI: ARTN e0924810.7554/eLife.09248.

51.   Nicoludis, J. M.; Gaudet, R. Applications of sequence coevolution in membrane protein biochemistry. *Biochim Biophys Acta Biomembr* **2018**, *1860* (4), 895-908. DOI: 10.1016/j.bbamem.2017.10.004.

52.   Senior, A. W.; Evans, R.; Jumper, J.; Kirkpatrick, J.; Sifre, L.; Green, T.; Qin, C.; Zidek, A.; Nelson, A. W. R.; Bridgland, A.; et al. Protein structure prediction using multiple deep neural networks in the 13th Critical Assessment of Protein Structure Prediction (CASP13). *Proteins* **2019**, *87* (12), 1141-1148. DOI: 10.1002/prot.25834.

53.   Jumper, J.; Evans, R.; Pritzel, A.; Green, T.; Figurnov, M.; Ronneberger, O.; Tunyasuvunakool, K.; Bates, R.; Zidek, A.; Potapenko, A.; et al. Highly accurate protein structure prediction with AlphaFold. *Nature* **2021**, *596* (7873), 583-589. DOI: 10.1038/s41586-021-03819-2.

54.   Tunyasuvunakool, K.; Adler, J.; Wu, Z.; Green, T.; Zielinski, M.; Zidek, A.; Bridgland, A.; Cowie, A.; Meyer, C.; Laydon, A.; et al. Highly accurate protein structure prediction for the human proteome. *Nature* **2021**, *596* (7873), 590-596. DOI: 10.1038/s41586-021-03828-1.

55.   Dhiman, A. M.; Wadodkar, K. N.; Patil, S. D. Synthesis and antimicrobial activiy of some bridgehead nitrogen heterocycles. *Indian J Chem B* **2001**, *40* (7), 640-643.

56.   LaPorte, M. G.; Wang, Z.; Colombo, R.; Garzan, A.; Peshkov, V. A.; Liang, M.; Johnston, P. A.; Schurdak, M. E.; Sen, M.; Camarco, D. P.; et al. Optimization of pyrazole-containing 1,2,4-triazolo-[3,4-b]thiadiazines, a new class of STAT3 pathway inhibitors. *Bioorg Med Chem Lett* **2016**, *26* (15), 3581-3585. DOI: 10.1016/j.bmcl.2016.06.017.

57.   Dogruer, D. S.; Fethi Sahin, M.; ünlü, S.; Ito, S. Studies on Some 3(2H)-Pyridazinone Derivatives with Antinociceptive Activity. *Archiv der Pharmazie* **2000**, *333* (4), 79-86. DOI: 10.1002/(sici)1521-4184(20004)333:4<79::aid-ardp79>3.0.co;2-s.

58.   Riddles, P. W. B., R. L.; Zerner, B., . Ellman's reagent: 5,5'-dithiobis(2-nitrobenzoic acid)--a reexamination. *Analytical Biochemistry* **1979**, *94* (1), 75-81.

59.   Anusha P, J. V. R. a. G. K. M. Synthesis, Characterisation and Biological Evaluation of new Bonzoxazole Derivatives as Antibacterial Agents. *International Journal of Pharmacy and Biological Sciences* **2018**, *8* (2), 709-714.

60.   Imaizumi, T.; Kobayashi, A.; Otsubo, S.; Komai, M.; Magara, M.; Otsubo, N. The discovery and optimization of a series of 2-aminobenzoxazole derivatives as ChemR23 inhibitors. *Bioorg Med Chem* **2019**, *27* (21), 115091. DOI: 10.1016/j.bmc.2019.115091.

61.   Iversen, P. W.; Eastwood, B. J.; Sittampalam, G. S.; Cox, K. L. A comparison of assay performance measures in screening assays: signal window, Z' factor, and assay variability ratio. *J Biomol Screen* **2006**, *11* (3), 247-252. DOI: 10.1177/1087057105285610.

62.   Trott, O.; Olson, A. J. AutoDock Vina: improving the speed and accuracy of docking with a new scoring function, efficient optimization, and multithreading. *J Comput Chem* **2010**, *31* (2), 455-461. DOI: 10.1002/jcc.21334.

63.   Kim, S.; Chen, J.; Cheng, T.; Gindulyte, A.; He, J.; He, S.; Li, Q.; Shoemaker, B. A.; Thiessen, P. A.; Yu, B.; et al. PubChem in 2021: new data content and improved web interfaces. *Nucleic Acids Res* **2021**, *49* (D1), D1388-D1395. DOI: 10.1093/nar/gkaa971.

64.   Trott, O.; Olson, A. J. AutoDock Vina: Improving the speed and accuracy of docking with a new scoring function, efficient optimization, and multithreading. *Journal of Computational Chemistry* **2010**, *31* (2), 455-461. DOI: https://doi.org/10.1002/jcc.21334.

65.   Krieger, E.; Vriend, G. YASARA View—molecular graphics for all devices—from smartphones to workstations. *Bioinformatics* **2014**, *30* (20), 2981-2982. DOI: 10.1093/bioinformatics/btu426 (acccessed 11/3/2021).

66.   Jo, S.; Kim, T.; Iyer, V. G.; Im, W. CHARMM-GUI: A web-based graphical user interface for CHARMM. *Journal of Computational Chemistry* **2008**, *29* (11), 1859-1865. DOI: https://doi.org/10.1002/jcc.20945.

67.   Kim, S.; Lee, J.; Jo, S.; Brooks III, C. L.; Lee, H. S.; Im, W. CHARMM-GUI ligand reader and modeler for CHARMM force field generation of small molecules. *Journal of Computational Chemistry* **2017**, *38* (21), 1879-1886. DOI: https://doi.org/10.1002/jcc.24829.

68.   Lee, J.; Cheng, X.; Swails, J. M.; Yeom, M. S.; Eastman, P. K.; Lemkul, J. A.; Wei, S.; Buckner, J.; Jeong, J. C.; Qi, Y.; et al. CHARMM-GUI Input Generator for NAMD, GROMACS, AMBER, OpenMM, and CHARMM/OpenMM Simulations Using the CHARMM36 Additive Force Field. *Journal of Chemical Theory and Computation* **2016**, *12* (1), 405-413. DOI: 10.1021/acs.jctc.5b00935.

69. Lee, J.; Hitzenberger, M.; Rieger, M.; Kern, N. R.; Zacharias, M.; Im, W. CHARMM-GUI supports the Amber force fields. *The Journal of Chemical Physics* **2020**, *153* (3), 035103. DOI: 10.1063/5.0012280.

70. Soteras Gutierrez, I.; Lin, F. Y.; Vanommeslaeghe, K.; Lemkul, J. A.; Armacost, K. A.; Brooks, C. L., 3rd; MacKerell, A. D., Jr. Parametrization of halogen bonds in the CHARMM general force field: Improved treatment of ligand-protein interactions. *Bioorg Med Chem* **2016**, *24* (20), 4812-4825. DOI: 10.1016/j.bmc.2016.06.034.

71. Huang, J.; Rauscher, S.; Nawrocki, G.; Ran, T.; Feig, M.; de Groot, B. L.; Grubmüller, H.; MacKerell, A. D. CHARMM36m: an improved force field for folded and intrinsically disordered proteins. *Nature Methods* **2017**, *14* (1), 71-73. DOI: 10.1038/nmeth.4067.

72. Abraham, M. J.; Murtola, T.; Schulz, R.; Páll, S.; Smith, J. C.; Hess, B.; Lindahl, E. GROMACS: High performance molecular simulations through multi-level parallelism from laptops to supercomputers. *SoftwareX* **2015**, *1-2*, 19-25. DOI: https://doi.org/10.1016/j.softx.2015.06.001.

73. Bussi, G.; Donadio, D.; Parrinello, M. Canonical sampling through velocity rescaling. *The Journal of Chemical Physics* **2007**, *126* (1), 014101. DOI: 10.1063/1.2408420.

74. Berendsen, H. J. C.; Postma, J. P. M.; Gunsteren, W. F. v.; DiNola, A.; Haak, J. R. Molecular dynamics with coupling to an external bath. *The Journal of Chemical Physics* **1984**, *81* (8), 3684-3690. DOI: 10.1063/1.448118.

75. Parrinello, M.; Rahman, A. Polymorphic transitions in single crystals: A new molecular dynamics method. *Journal of Applied Physics* **1981**, *52* (12), 7182-7190. DOI: 10.1063/1.328693.

Chapter 3: Synthesis and testing of cysteine-reactive molecules as GOAT inhibitors

3.1 Introduction

The recent publication of the structures of several members of the membrane-bound O-acyltransferase (MBOAT) family have allowed for direct comparison of the related structures, but have not fully answered how individual acyl transfer reactions occur. Members of the MBOAT family contain a highly conserved asparagine and histidine residue that are required for enzyme functionality, represented in hGOAT as N307 and H338. [1-3] Initially thought to be part of the catalytic mechanism of GOAT, these residues were found to be on opposite sides of the endoplasmic reticulum membrane in topology studies, indicating that these two essential residues may contribute in roles other than catalysis. [4] Comparison of the conserved histidine in the published MBOAT structures reveals that this residue is located within the intermembrane channel common to the family, in contrast to the proposed location from the topology models. [5-10] The central location of histidine reemphasizes the potential of this residue as the general base in an as-yet-unknown mechanism for acyl transfer.

Previous work in the Hougland laboratory identified new small molecule inhibitors of hGOAT through the screening of a library of small molecules that provided a potential insight into essential residues within hGOAT. [11] This study found that a class of synthetic triterpenoids inhibited hGOAT, with further structure-activity relationship studies revealing a less-complex steroid scaffold also capable of inhibition (**Figure 3.1**). The most potent molecules in these two classes both contained an α-cyanoenone warhead on the A-ring of the scaffold, while weaker electron-withdrawing α substituents showed reduced potency, indicating the potential mechanism of inhibition relying on the addition of a nucleophilic residue through a 1,4 Michael addition (**Scheme 3.1**). This inhibition was also shown to be reversible, in contrast to the

3.1: IC$_{50}$ = 8 ± 4 µM   **3.2:** IC$_{50}$ = 8 ± 2 µM
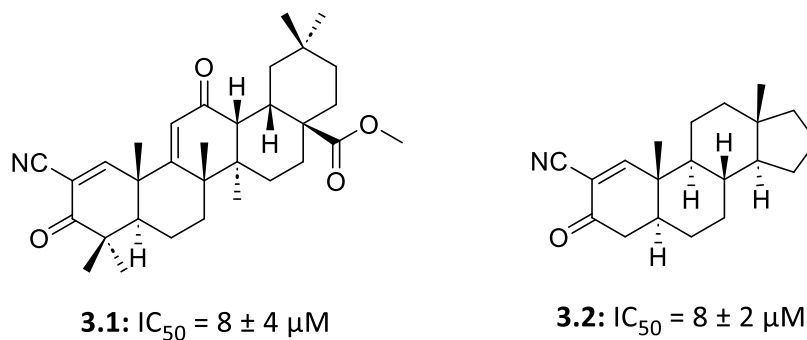
Figure 3.1: Structures of hGOAT inhibitors found from library screening. Triterpenoid **3.1** was found from screening of NIST library. Structure-activity relationship revealed steroid **3.2** as equivalent inhibitory molecule. Both molecules are indicated to reversibly inhibit hGOAT through covalent reversible inhibition. [11]

Scheme 3.1: Proposed catalytic mechanism of hGOAT utilizing functionally essential cysteine. hGOAT utilizes functionally essential cysteine as a nucleophile to initial acyl-enzyme intermediate. Activation of ghrelin by catalytic base, proposed to be H338, allows for transfer of octanoyl group to serine-3.
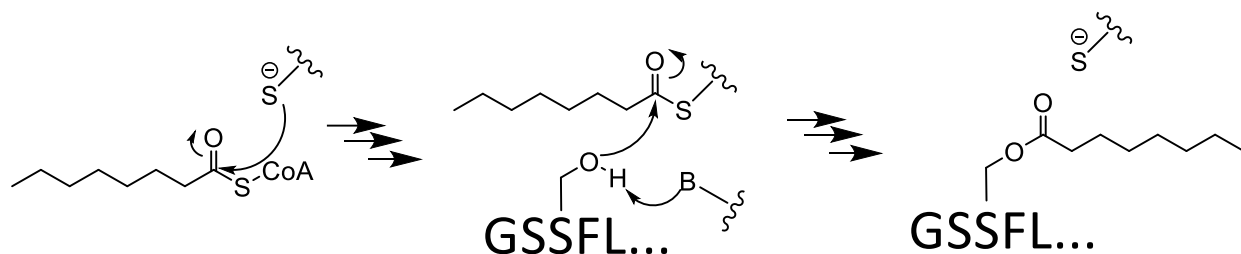
irreversible inhibition by the cysteine-modifying molecule *N*-ethylmaleimide (NEM). Both α-cyanoenones and NEM have been shown to covalently modify nucleophilic thiols, suggesting the covalent modification of a nucleophilic cysteine in hGOAT by both molecules. [12-15] With two cysteine-targeting molecules exhibiting inhibition of hGOAT, the data suggests a functionally essential cysteine in hGOAT. Furthermore, it is possible that hGOAT utilizes this cysteine as the nucleophile necessary for octanoate transfer, similar to the mechanism of the cysteine peptidase papain or DHHC protein acyltransferases. [16, 17] The serendipitous discovery of a distinct inhibitory mechanism of hGOAT through cysteine-reactive molecules raises questions about the role of this essential cysteine in hGOAT, which could be answered through the identification of the residues involved.

One option for probing the potential catalytic cysteine is the methanethiosulfonate (MTS), a class of molecules with a thiol-reactive disulfide bond. The simplest alkane derivative of this warhead is methyl methane thiosulfonate (MMTS), which is a common reagent for trapping thiols as a disulfide, forming dithiomethane. [18, 19] MMTS has been used to identify active sites in enzymes through labeling experiments utilizing mass spectrometry through the detection of mass differences in wild-type and mutant proteins. [20] Other alkane-MTS reagents have been used for similar purposes, including propyl-MTS being used to determine the binding site of the anesthetic propanethiol on glycine receptor and γ-aminobutyric acid type A receptor subunits. [21] MTS reagents have also been used to deliver photocrosslinkers to cysteines of interest to study protein-protein interactions. [22] We proposed to use MTS reagents to label and identify the functionally essential cysteine residue in hGOAT.

3.2 Results

3.2.1 Alkyl methanethiosulfonates as inhibitors of hGOAT

Using an untargeted cysteine-labeling approach to determine the active site cysteine in GOAT is difficult due to the presence of multiple cysteines in the enzyme. In order to specifically label the active site cysteine, we looked to take advantage of GOAT's selectivity towards fatty acids. Previous substrate selectivity studies have shown that GOAT strongly prefers an eight-carbon acyl donor, while also exhibiting tolerance for seven-carbon donors. [23] It was hypothesized that the essential cysteine is likely near the acyl donor site, as if the cysteine is involved in the acyl transfer it must be nearby to facilitate the transfer. Preliminary studies comparing MMTS and hexyl methanethiosulfonate (HMTS) in the Hougland lab indicated a potential chain-length dependence in the inhibition of GOAT by cysteine modifying agents, with HMTS showing increased potency over MMTS (unpublished data obtained by Kayleigh McGovern-Gooch). If GOAT exhibited similar selectivity for alkyl methanethiosulfonates, it might be expected that the S-heptyl methanethiosulfonate would preferentially modify the active site cysteine. To test this hypothesis, a series of cysteine modifying alkyl methanethiosulfonate (alkyl-MTS) reagents were synthesized.

To synthesize a series of alkyl-MTS reagents with varying length alkyl chains, sodium methanethiosulfonate serves as a common starting material for cysteine modifying reagents as can be used to displace leaving groups. In the first step of the synthesis of the alkyl-MTS reagents, distilled mesyl chloride (**3.3**) was reacted with sodium sulfide to generate the sodium salt of methyl thiosulfonate (**3.4**). As shown in **Scheme 3.3**, methyl thiosulfonate (**3.4**) can then be

Scheme 3.2: Alkyl methanethiosulfonate reagents

n = 2-10
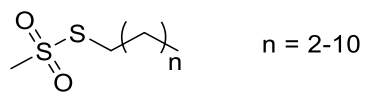
Scheme 3.3: Synthesis of alkyl methanethiosulfonate reagents

3.3   59%   **3.4**

X =
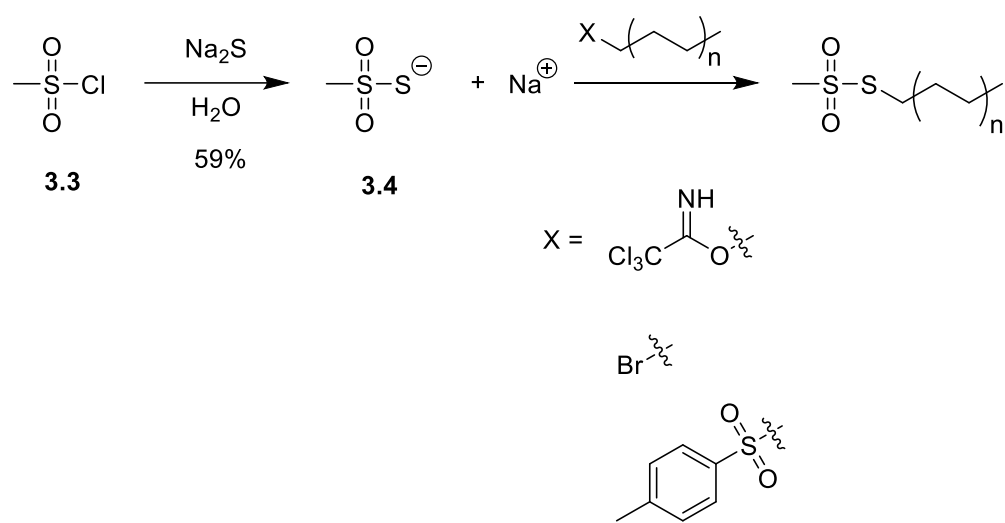
reacted with various alkyl group lengths and leaving groups to provide a panel of alkyl-MTS molecules for GOAT inhibition studies.

The first route explored towards the synthesis of the alkyl-MTS used imidates as the leaving group. Imidates were chosen as a possible synthetic pathway due to their ease of synthesis from alcohols and the precedent of one-pot reactions for creation and displacement of imidates using sulfur as a nucleophile. [24] Initial reactions were prepared by reacting 1 equivalent of butyl imidate, compound **3.5**, with 1.5 equivalents of sodium methanethiosulfonate in refluxing THF for 24 hours (**Scheme 3.4**).

This reaction did not yield a product and the sodium methanethiosulfonate was observed to not be soluble in THF. A phase-transfer reagent, triethylbenzylammonium chloride (TEBAC), was added to increase the solubility of sodium methanethiosulfonate in THF, increasing the yield by NMR to 24% with 0.5 eq TEBAC. Lewis acid catalysts were added to further activate the imidate, with both the addition of p-toluenesulfonic acid (TSA) and boron trifluoride etherate (BF$_3$OEt) increasing the apparent yield by NMR., These acid-catalyzed reactions did not go to completion and a triplet at 4.39 ppm was observed that could not be accounted for in the desired product. Based on these initial findings, it was decided to adjust the synthetic approach in order to more quickly produce the alkyl-MTS series.

Scheme 3.4: **Synthesis of S-butyl methanethiosulfonate (3.6) from butyl imidate (3.5)**
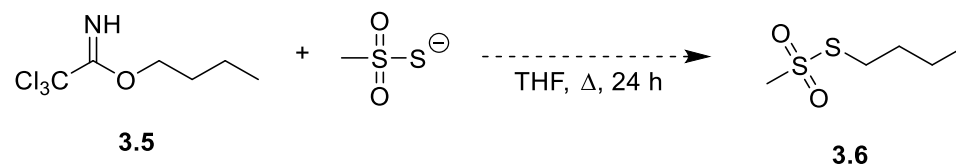
The second approach to the synthesis of the alkyl-MTS series begins with conversion of the appropriate alcohols into tosylates. This was accomplished by reacting the alcohols with tosyl chloride in the presence of triethylamine (TEA) and 4-dimethylaminopyridine (DMAP) as shown in **Scheme 3.5**. This approach yielded the alkyl tosylates (compounds **3.7-3.13**) in yields from 51-83%. These tosylates were then reacted with sodium methanethiosulfonate in the presence of 0.25 equivalents of the phase-transfer reagent tetrabutylammonium bromide (TBAB), giving the alkyl-MTS targets in yields from 27-98% (**Scheme 3.6**, **Table 1**). Octyl-, undecyl-, and dodecyl-MTS were prepared from the reaction of sodium methanethiosulfonate with the corresponding alkyl bromides in ethanol due to the availability of these starting materials. With the combination of these two approaches, compounds **3.6, 3.13-3.19** were synthesized for inhibitor testing against GOAT.

As shown in **Figure 3.2**, all of the alkyl-MTS reagents except for decyl-MTS (**3.18**) exhibit >50% inhibition of GOAT activity at 500 µM and concentration dependence. There is also minor selectivity for the 6- and 7- carbon chain sulfonates, **3.14** and **3.15**, as indicated by increased inhibition at 100 µM inhibitor concentrations. Since heptyl-MTS is anticipated to mimic the natural octanoyl lipid attached to ghrelin, it was chosen for IC_{50} determination (**Figure 3.3**). The IC_{50} of the heptyl methanethiosulfonate (**3.15**) was determined to be 84 ± 22 µM. To determine the capacity of this compound to label cysteines for downstream identification by mass spectrometry, a reversibility experiment was performed on compound **3.15**, with the known inhibitor N-ethyl malemide (NEM) serving as a control for an irreversible inhibitor and known cyano-enone steroid (NSM-48, **3.21**) as a reversible control. Each inhibitor was incubated with the membrane fraction at three times the IC_{50} before being diluted by a factor of ten into a

Scheme 3.5: Synthesis of alkyl tosylates
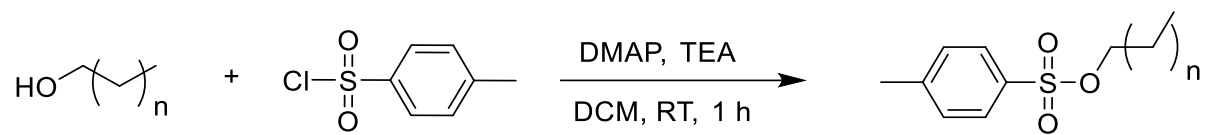
Scheme 3.6: Synthesis of alkyl-methanethiosulfonates
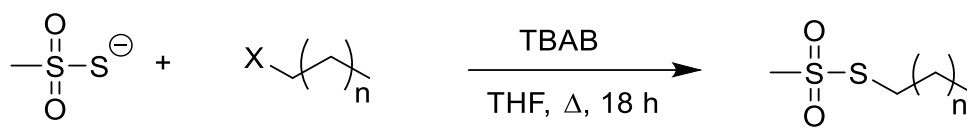
Table 3.1: Compound identification and parent electrophiles of alkyl-methanethiosulfonates

Compound	n	Parent electrophile	Yield
3.6	2	butyl tosylate (**3.7**)	61%
3.13	3	pentyl tosylate (**3.8**)	61%
3.14	4	hexyl tosylate (**3.9**)	98%
3.15	5	heptyl tosylate (**3.10**)	98%
3.16	6	1-bromooctane	99%
3.17	7	nonyl tosylate (**3.11**)	34%
3.18	8	decyl tosylate (**3.12**)	37%
3.19	9	1-bromoundecanol	21%
3.20	10	1-bromododecanol	33%

reaction mixture containing either the same concentration of inhibitor or vehicle (1x or 10x dilution respectively). Unexpectedly, both methyl methane thiosulfonate (MMTS, **3.22**) and the heptyl-MTS both demonstrated inhibition reversibility under these conditions (**Figure 3.4**).

To determine whether the alkyl-MTS reagents are inherently reversible in our system or if the inhibition observed with these compounds was not caused by covalent modification of a cysteine within GOAT as proposed, we acquired ethyl methyl sulfone (EMS, compound **3.22**) which is isosteric for MMTS but cannot react with thiols to form disulfides. EMS was found to not inhibit the enzyme, with >90% normalized activity up to 1000 µM (**Figure 3.6**). These results indicate that the inhibition of GOAT by MMTS is not due to the structure of the compound but rather the reactivity of the molecule. Generalizing this result to other alkyl-MTS inhibitors indicates that the inhibition of hGOAT by alkyl-MTS reagents is dependent on the cysteine-modifying abilities of this class of molecule.
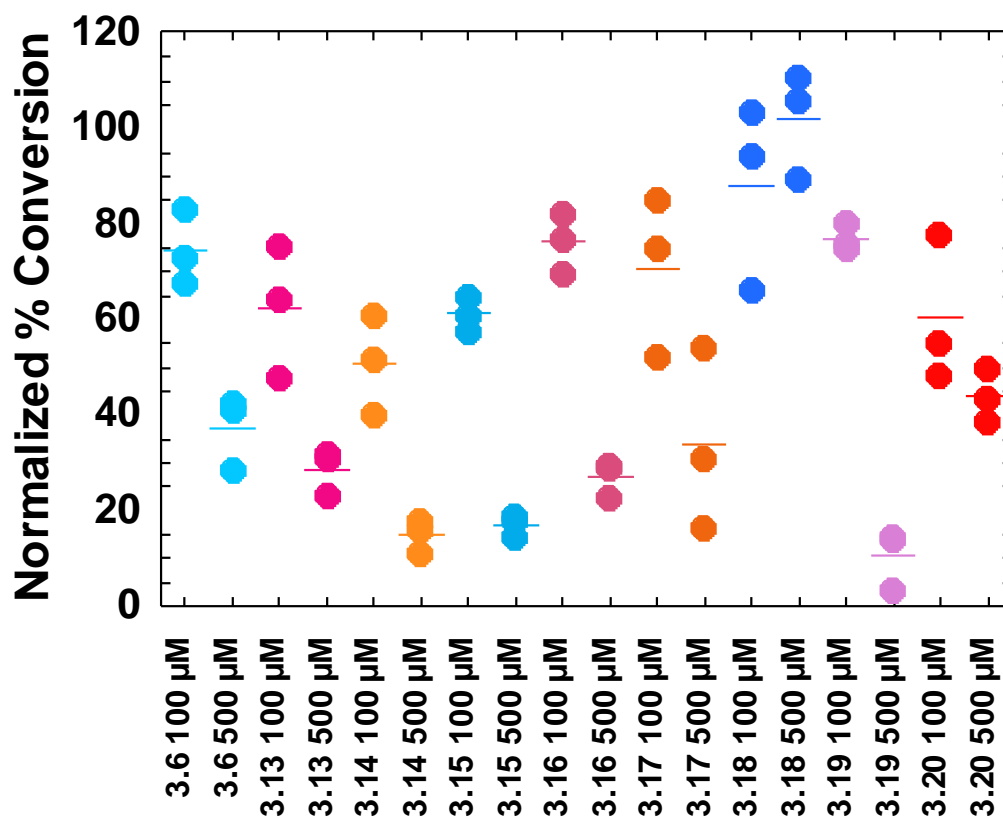
Figure 3.2: Screening of alkyl-methanethiosulfonates against hGOAT. Alkyl-methanethiosulfonates with varying alkyl length were tested at two concentrations (100 µM and 500 µM) for inhibitory activity against hGOAT. Each dot represents an independent trial, and the bar represents the average of the three trials. From left to right: S-butyl (**3.6**), S-pentyl (**3.13**), S-hexyl (**3.14**), S-heptyl (**3.15**), S-octyl (**3.16**), S-nonyl (**3.17**), S-decyl (**3.18),** S-undecyl (**3.19**), S-dodecyl (**3.20**).
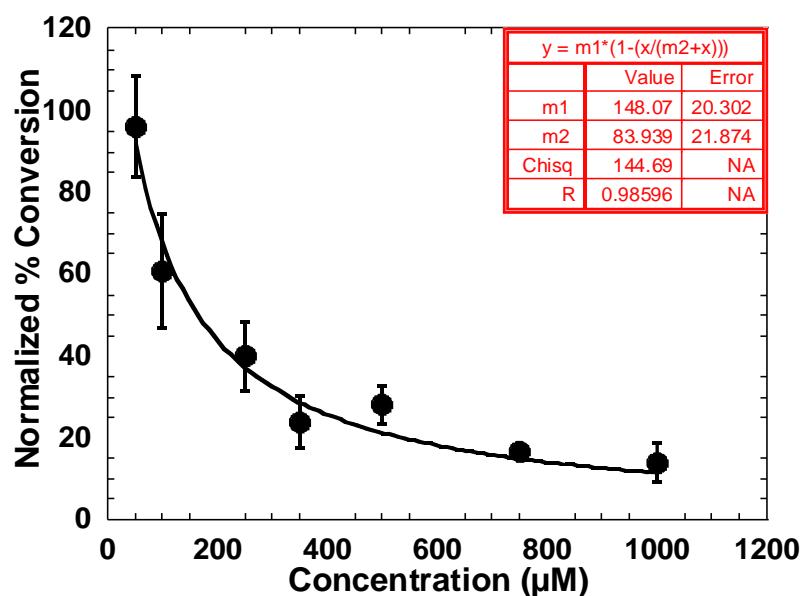
Figure 3.3: Inhibition of hGOAT by heptyl-methanethiosulfonate (3.15). Heptyl-methanethiosulfonate (**3.15**) was selected for IC_{50} determination due to reasonable potency in MTS screening and the availability of alkyne-containing derivative for labeling studies. Compound was incubated for 30 minutes with 100 µg membrane protein before reactions were initiated with 1.5 µM GSSFLC$_{AcDan}$ and 300 µM octanoyl-CoA. Error bars represent the standard deviation of three independent trials.
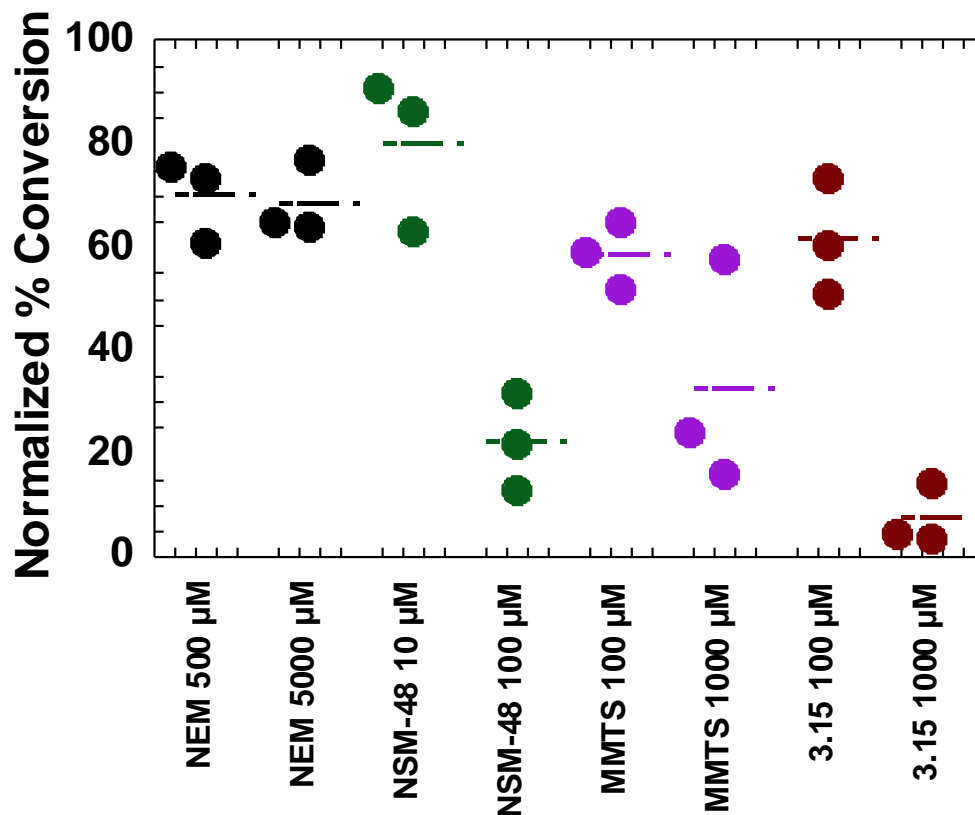
Figure 3.4: Compound 3.15 is a reversible hGOAT inhibitor. Membrane fraction treated with inhibitor was diluted 10X, producing the measured IC_{50}. Restoration of hGOAT activity under diluted condition (1X IC_{50}) indicates reversible inhibition by NSM-48 (**3.2**) and heptyl-MTS (**3.15**). NEM represents N-ethyl maleimide, known covalent irreversible inhibitor of hGOAT. [11] Compounds were tested in reactions containing 100 µg hGOAT-enriched membrane protein, 1.5 µM GSSFLC$_{AcDan}$ and 300 µM octanoyl-CoA in triplicate. Dots represent a single trial, bars represent the average of the trials. 1X IC_{50} concentrations were NEM: 500 µM, **3.2:** 10 µM, and **3.15:** 100 µM. 10X IC_{50} concentrations were NEM: 5.0 mM, **3.2:** 100 µM, and **3.15:** 1.0 mM.
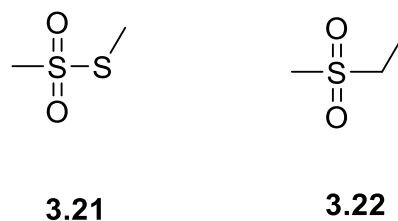
Figure 3.5: The structure of methyl methanethiosulfonate (**3.21**) versus the structure of ethyl methyl sulfone (**3.22**)
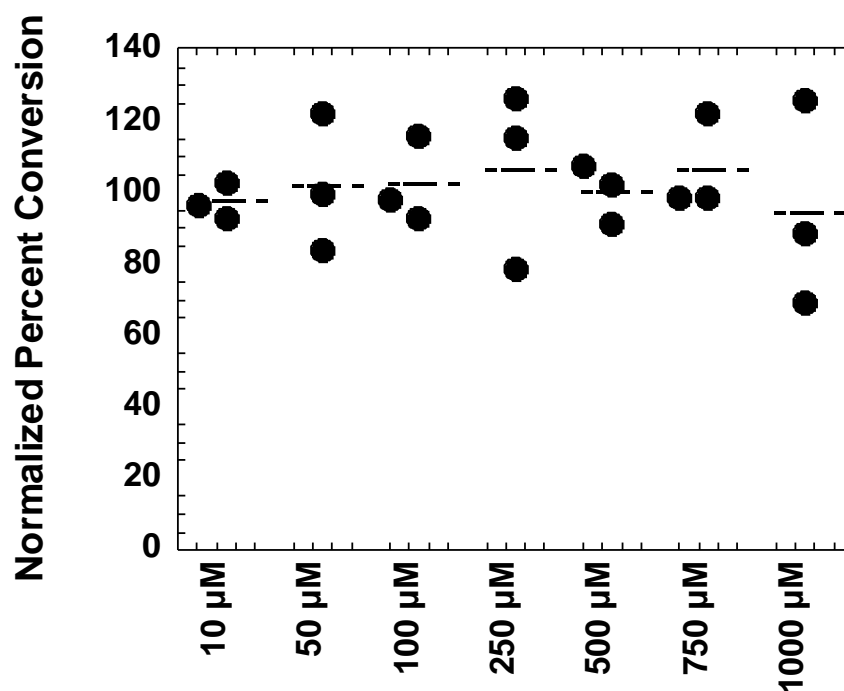
Figure 3.6: Inhibition profile of ethyl methyl sulfone. Ethyl methyl sulfone, compound **3.20,** was tested for inhibitory activity against hGOAT. Compound **3.22** was incubated for 30 minutes with 100 µg hGOAT-enriched membrane protein before reactions were initiated with 1.5 µM GSSFLC$_{AcDan}$, and 300 µM octanoyl-CoA. Dots represent a single trial, bars represent the average of the three independent trials.

3.2.2 Alternate Michael accepting molecules do not inhibit hGOAT

While the studies with EMS indicated that the cysteine-modifying ability of the alkyl-

MTS reagents is necessary for inhibition, it was uncertain whether this class of cysteine-reactive

warhead was essential for inhibition. If alternate cysteine-modifying molecules were capable of

hGOAT inhibition, it would expand the scope of inhibitory molecules dramatically, so

identifying the inhibitory contributions of the electrophilic warhead versus that of the broader

structure was desired. Cysteine-reactive molecules have been used to explore the mechanism of

cysteine-dependent enzymes, such as the cysteine protease cruzain. [25] Small-molecules

containing Michael acceptors were used in this case to target a catalytic cysteine residue. In order

to explore the possibility of a similar active site cysteine in GOAT, we acquired a set of

compounds (**3.23-3.29**) from the Meek lab at Texas A&M containing vinyl heterocycles

designed to form an irreversible Michael adduct upon cysteine addition. Compounds **3.23-3.29**

were determined to not have activity against hGOAT due to their low inhibition potency (>70%

activity at 100 µM) and lack of dose dependence. The compounds supplied by the Meeks lab are

designed building blocks for cysteine protease inhibitors, with the final structures forming

covalent adducts with the enzyme cruzain through addition of Cys_{25} to the alkene of the vinyl-2-

pyridine. [26] As the mechanism for this addition is similar to the putative 1,4 addition between

hGOAT and the α-cyano enone inhibitor NSM-48, the lack of inhibition of the vinyl heterocycles

indicates that the structure of the Michael acceptor is as important as the presence of the

acceptor. [11] This selectivity can be attributed to the difference in substrate between the two

enzymes, as cruzain functions by targeting peptide bonds to degrade proteins. While not proven

to be catalytic, the essential cysteine in hGOAT is hypothesized to interact with the thioester of

octanoyl-CoA, similarly to the acyl-enzyme intermediate in the DHHC mechanism. [17] The

rational differences between these two substrates supports the idea that the non-specific warhead may be less important to targeting the hGOAT essential cysteine than the surrounding substrate providing the contacts to localize the molecules within GOAT.
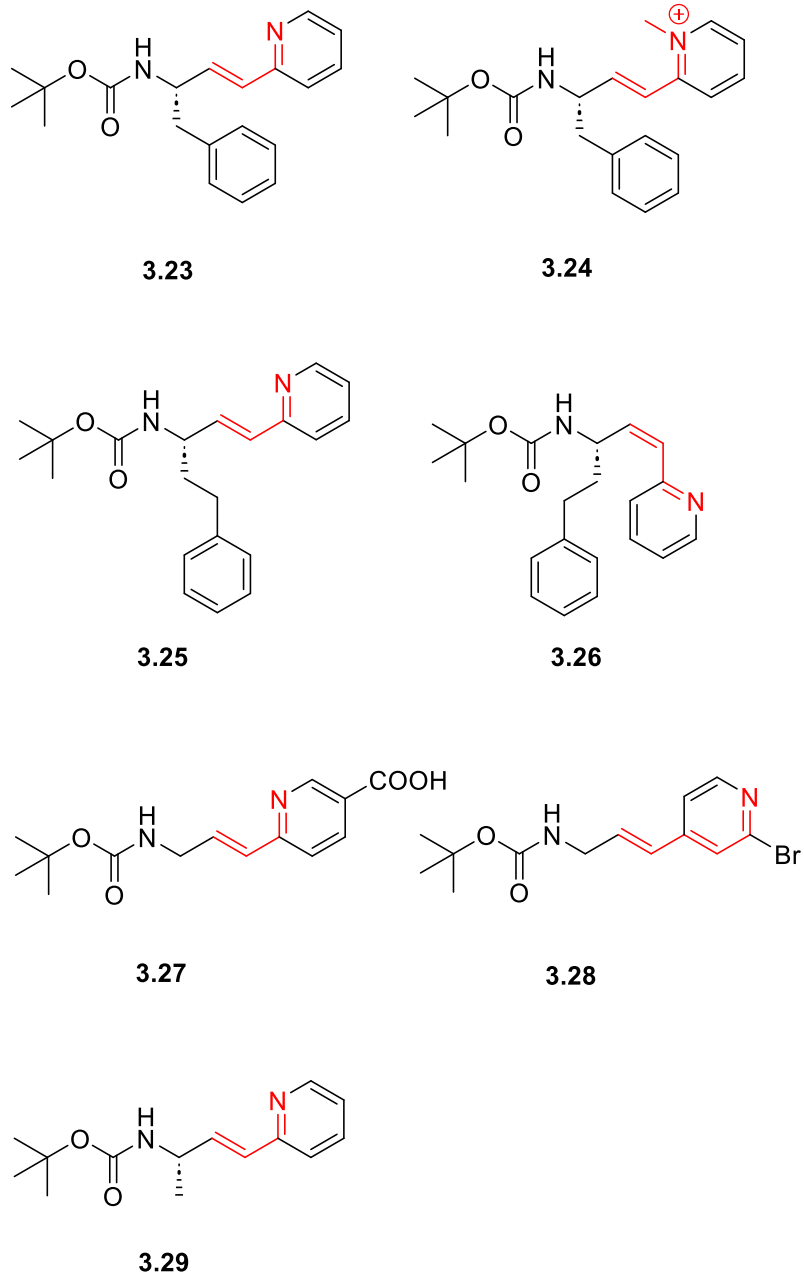
Figure 3.7: Synthetic intermediate compounds acquired from the Meek lab at Texas A&M.
Compounds were part of a synthetic scheme to synthesize inhibitors of the cysteine protease
cruzain through 1,4 addition to the acceptor shown in red. [26]
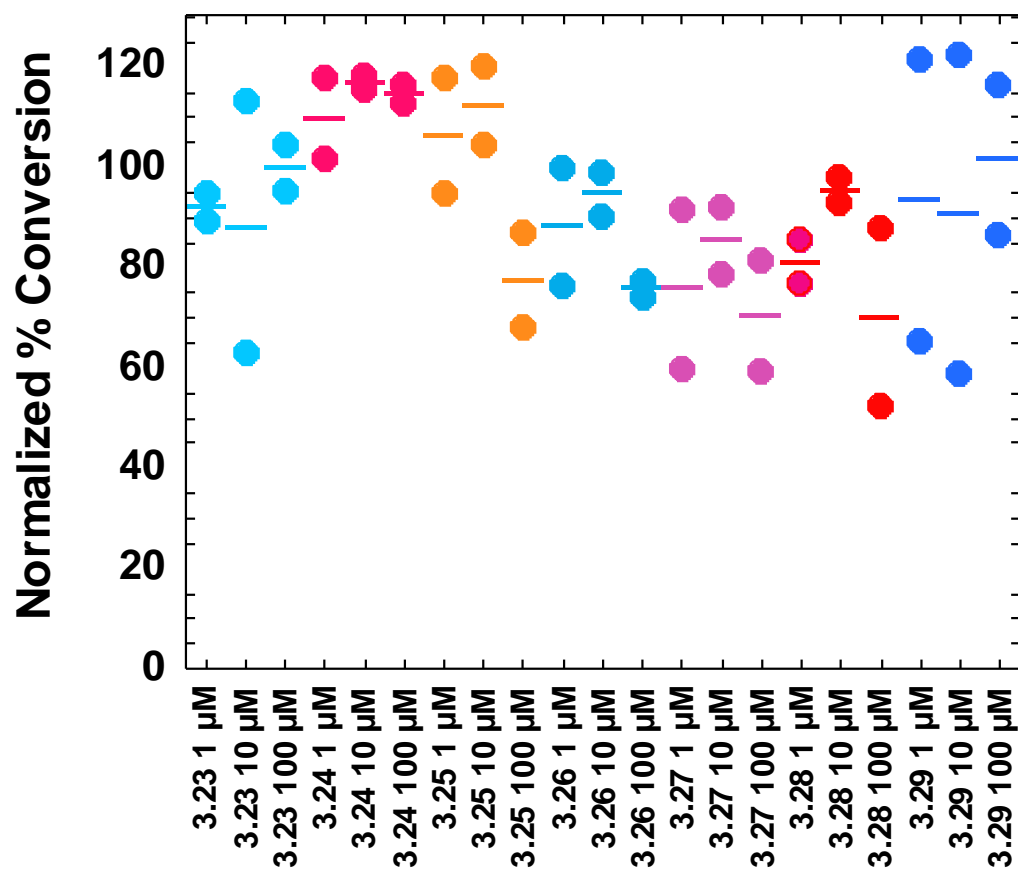
Figure 3.8: Screening of Meek compounds series. Compounds were tested for hGOAT inhibitory activity at 1, 10, and 100 µM. Compounds were incubated for 30 minutes with 100 µg hGOAT-containing membrane protein before reactions were initiated with 1.5 µM GSSFLC$_{AcDan}$, and 300 µM octanoyl-CoA. Dots shown are the results of two independent trials, bars indicate the average of the two trials.

3.2.3 Development of steroidal hGOAT inhibitors

Previous research in the Hougland Lab identified CDDO-Me (**3.1**) as a hGOAT inhibitor with low micromolar potency. [11] Further investigation led to the design and investigation of α-cyanoenone **3.2**, a compound with an IC$_{50}$ of 8 ± 4 µM and a simplified structure (**Figure 3.9**). [11] SAR work done during this initial study did not include investigation of substitution of the D ring. Compounds **3.32-3.37** were obtained from Nilamber Mate from the Chisholm lab at Syracuse University and tested to determine hGOAT tolerance for alkyl chains on C-17, with particular interest in compounds **3.32** and **3.33** due to shared functionality with compounds **3.31** and **3.30** respectively. [11]

Compounds **3.32** and **3.33** contain the same steroidal scaffold identified in previous studies, but contain an alkyl substitution at C-17 that is untested for compatability with hGOAT inhibition. If this modification at C-17 proved to be tolerated by hGOAT, then synthesis of similar steroidal molecules could begin with the easily purchasable cholesterol, where the current route begins with the more expensive epiandrosterone. Compound **3.32** did not inhibit at any concentration but lacked the inhibitory enone moiety previously identified as the Michael acceptor. Compound **3.33** also did not inhibit GOAT, exhibiting >80% normalized activity at 20 µM. While neither compound inhibited at the tested concentrations, the IC$_{50}$ values of compounds **3.30** and **3.31**, analogous compounds missing the alkyl chain at C-17 were both found to have IC$_{50}$ values >100 µM. Compounds **3.32** and **3.33** were tested at low concentrations due to issues with solubility, as both compounds were only soluble up to 1 mM in DMSO or ethanol, whereas the compounds missing the alkyl modifications were soluble up to 50 mM in DMSO.
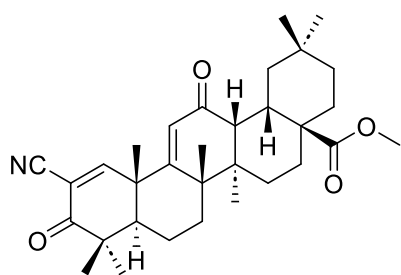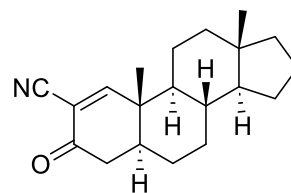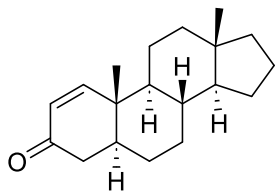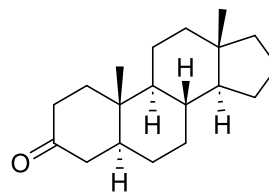
Figure 3.9: Compounds previously tested for inhibition of hGOAT. [11]
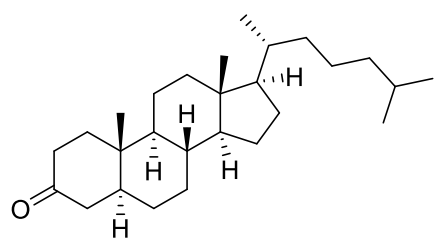
3.32
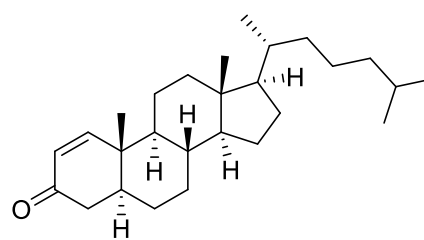
3.33
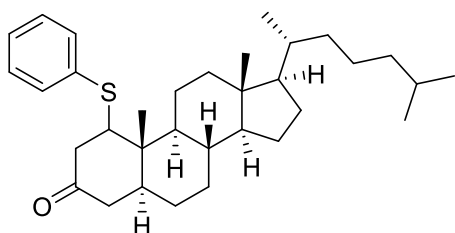
3.34
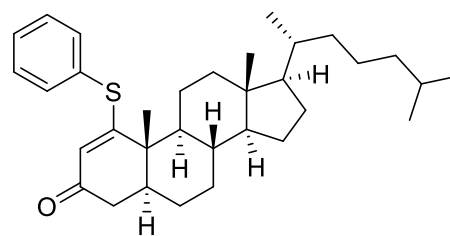
3.35
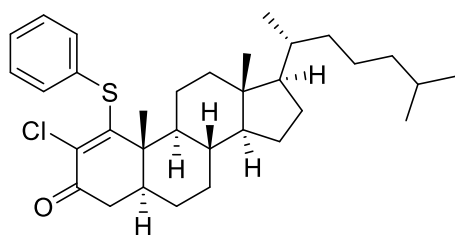
3.36
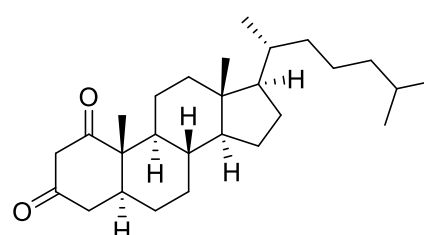
3.37

Figure 3.10: Structures of the NAM series inhibitors. NAM series compounds obtained from Dr. Nilamber Mate (John Chisholm lab, Syracuse University Department of Chemistry) for testing.

Due to the lack of solubility and poor effective potency (**Figure 3.11**), compounds **3.32** and **3.33** were not chosen for further testing.

It was found previously that compound **3.2** displayed reversible inhibition of hGOAT activity, consistent with reversal of covalent inhibition of hGOAT by a retro-Michael elimination reaction involving a hGOAT cysteine residue (**Scheme 3.7**). If this is the case, compounds imitating the inhibitor-enzyme complex could be tested to see if they undergo the same retro-Michael reaction, indicating catalysis by GOAT. A class of inhibitors with varying thiol adducts at the 4-position relative to the ketone would be desired to test this potential mode of reactivity. If the enone-based inhibitors are undergoing a retro-Michael reaction to eliminate the covalent bond formed with the enzyme, it was hypothesized that GOAT must have a general base near the alkylation site to initiate the elimination. Therefore, it would be possible for GOAT to catalyze the elimination reaction of molecules exhibiting structures analogous to the formed Michael adduct (**Scheme 3.8**). Compounds **3.32-3.37** were obtained from the Chisholm lab to examine this hypothesis.

Compounds **3.32-3.37** consist of the previously-identified steroid scaffold and alkyl substitution at C-17, as well as a thiol at C-1. These molecules were screened for activity based on the possibility of catalyzing inhibitor release *in situ* by forming the enone after elimination of the thiophenol. None of the three compounds were found to inhibit (>70% normalized activity) and did not exhibit strong concentration dependence (**Figure 3.11**). In addition, these compounds were found to suffer from the same solubility issues described for Compounds **3.32** and **3.33**, only being soluble to 1 mM in ethanol. Due to the lack of inhibition and insolubility, these molecules were not chosen for further examination.
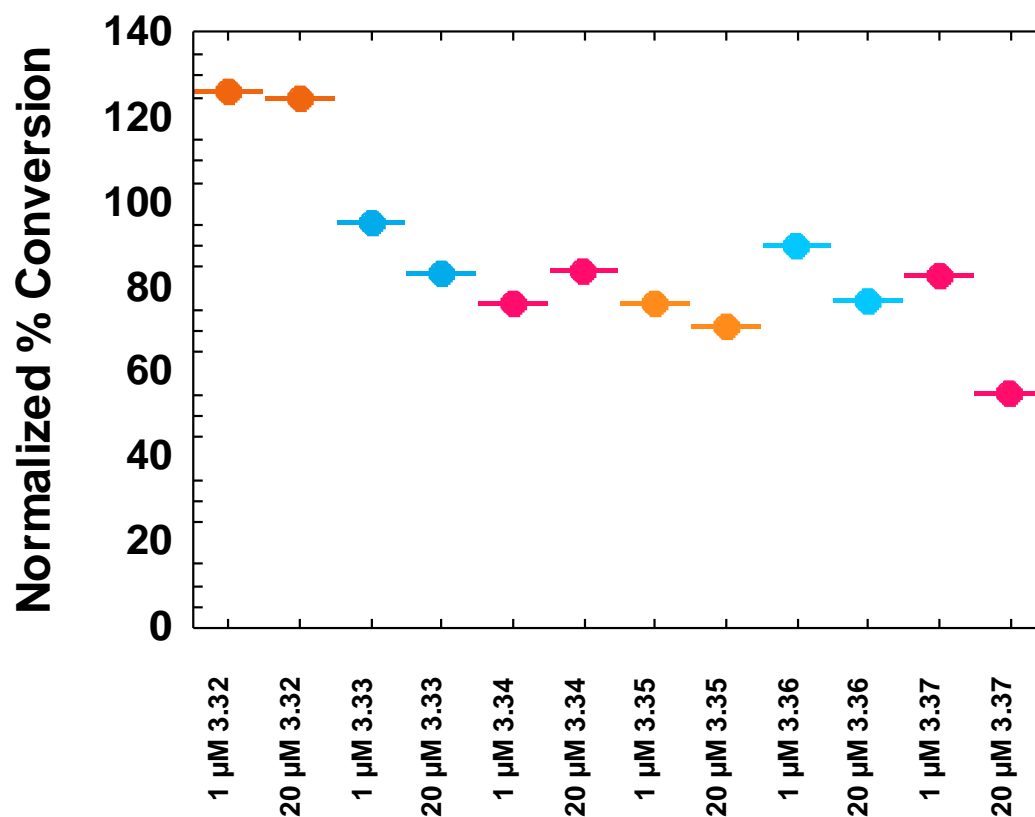
Figure 3.11: Inhibition of hGOAT by the NAM series compounds. Compounds were tested for hGOAT inhibitory activity at 1, and 20 µM due to insolubility. Compounds were incubated for 30 minutes with 100 µg membrane protein before reactions were initiated with 1.5 µM GSSFLC$_{AcDan}$, and 300 µM octanoyl-CoA. Data represents a single trial due to insolubility and lack of indicated inhibition (>50% normalized % conversion) at highest tested concentration.

Scheme 3.7: Proposed mechanism for reversibility of α-cyanoenone hGOAT inhibitors.

Functionally essential cysteine forms the 1,4 adduct with the unsaturated ketone. Tautomerization of the formed enolate allows for nearby general base to catalyze elimination of the thiol.
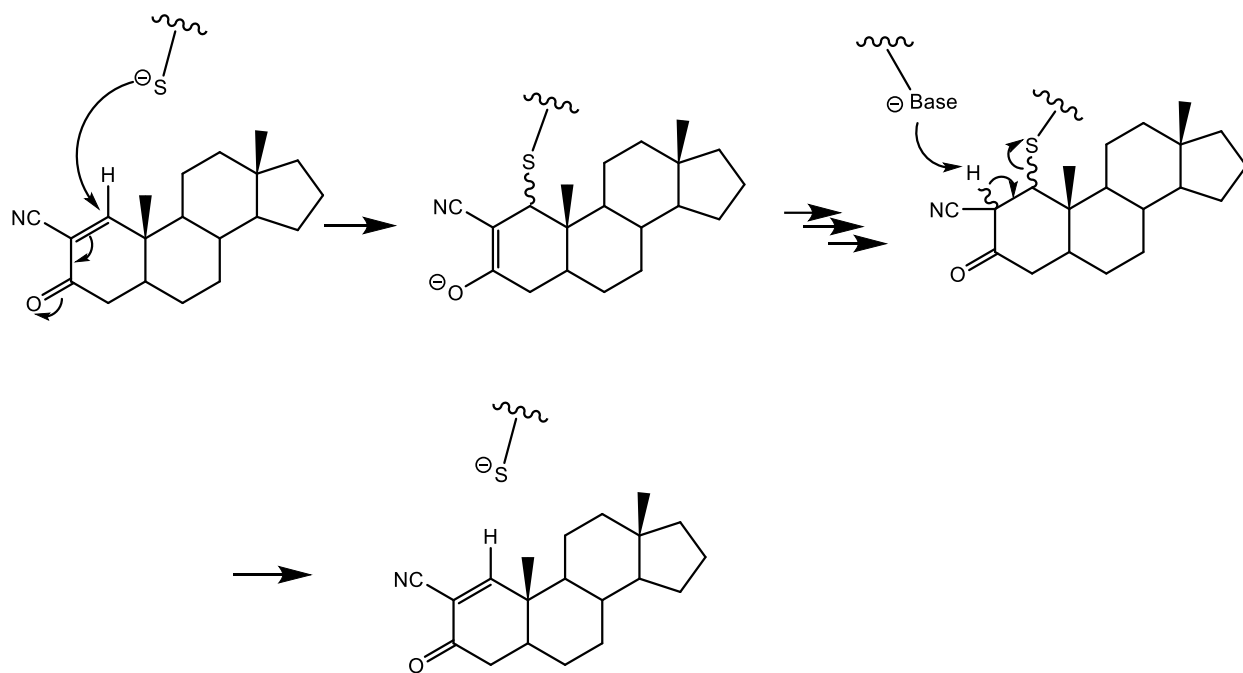
Scheme 3.8: Proposed mechanism for the hGOAT-catalyzed release of α,β unsaturated ketone inhibitor. Proposed general base nearby inhibitory site catalyzes the elimination of the thiophenol to form α,β unsaturated ketone, compound **3.31**.
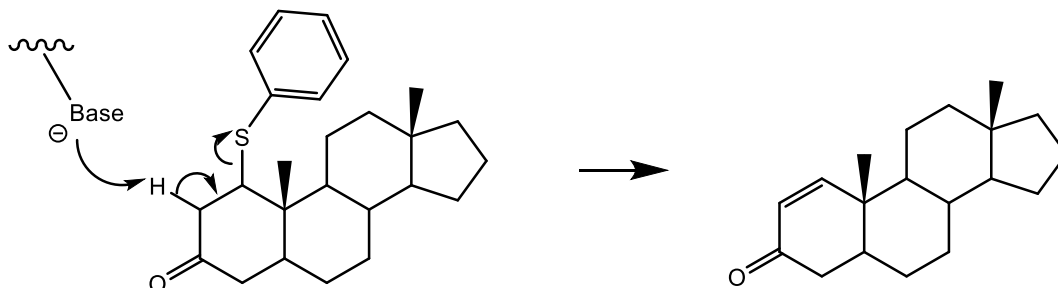
3.2.4 Irreversible steroidal inhibitors for identification of essential cysteine

In order to study the mechanism of GOAT, irreversible inhibitors are desired to be able to probe the active site. One compound chosen for the possibility of irreversible inhibition of GOAT is compound **3.38** (**Figure 3.12**), synthesized by Dr. Nilamber Mate from the Chisholm lab (Department of Chemistry, Syracuse University). This compound should act as an irreversible inhibitor due to the presence of the β-fluorine as a preferential candidate for elimination during the proposed retro-Michael reaction giving rise to the reversibility of the enone-containing molecules (**Scheme 3.9**). Compound **3.38** exhibited an IC_{50} of 68 ± 7 μM (**Figure 3.13**), making it a possible candidate for irreversibility trials. This IC_{50} was obtained within several hours of purification of the compound, and subsequent trials have provided data consistent with compound degradation. As such, further trials and irreversibility studies have been postponed pending compound characterization and determination of compound stability by the Chisholm lab.

3.38
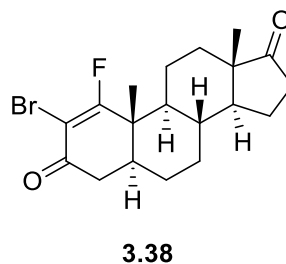
Figure 3.12: Compound 3.38, a potential irreversible inhibitor of hGOAT
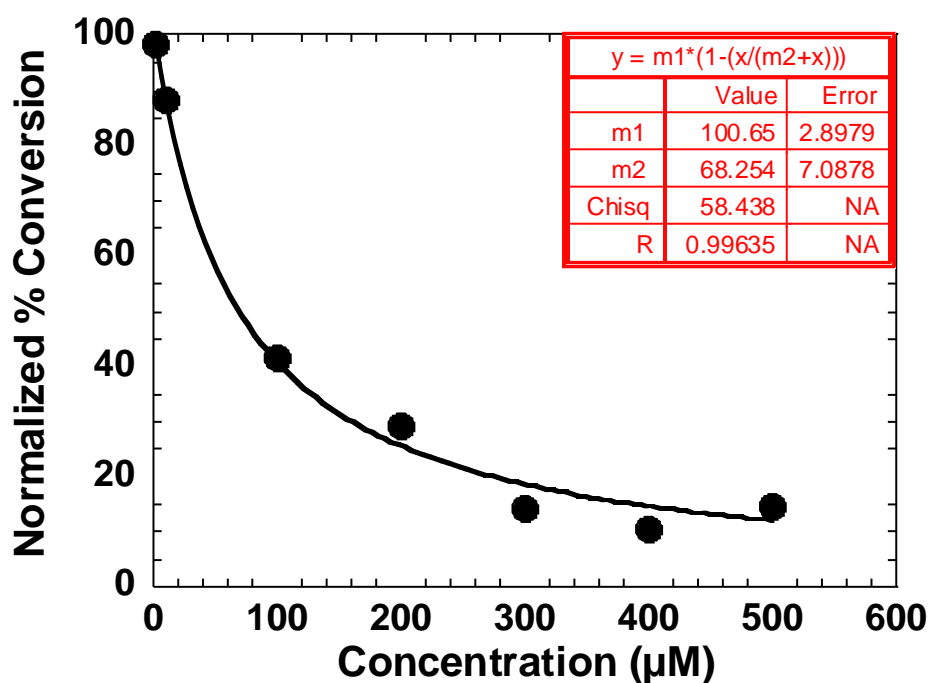
Figure 3.13: IC$_{50}$ of α-bromo, β-fluoro enone, 3.38. . Compound was incubated for 30 minutes with 100 µg hGOAT-containing membrane protein before reaction was initiated with 1.5 µM GSSFLC$_{AcDan}$, and 300 µM octanoyl-CoA. Data is from a single trial due to the instability of the compound, trial was performed immediately following purification and characterization.

Scheme 3.9: Proposed mechanism for covalent irreversible inhibition of GOAT by Compound 3.38. Retro-Michael elimination of fluoride allows for formation of the hGOAT adduct of compound **3.38**.
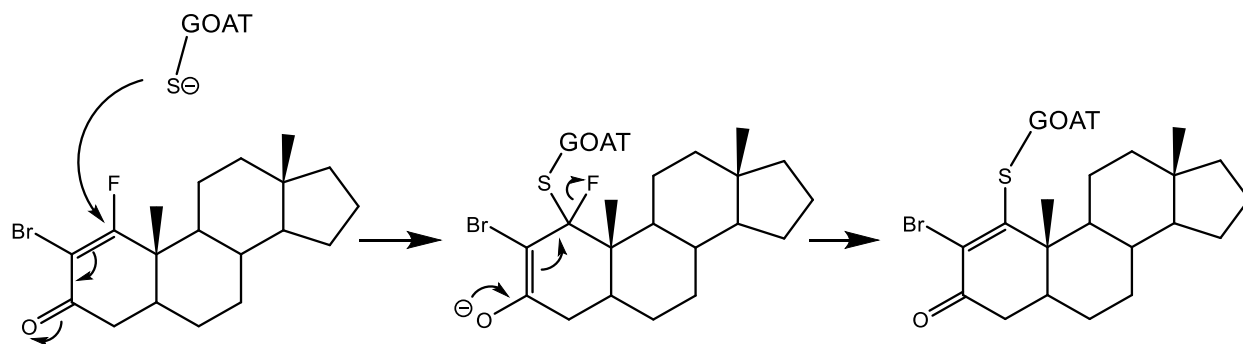
3.2.5 Modification of steroidal scaffold for irreversible inhibition

Considering the ability of the α-cyanoenone **3.**2 to reversibly inhibit hGOAT,

modification of the steroidal scaffold was desired to create an irreversible hGOAT inhibitor.

Epoxide **3.39** was synthesized as a possible irreversible inhibition of GOAT, assteroid epoxides

have been used previously to form irreversible adducts with enzymes. [27] The α-epoxide was

synthesized from the unsaturated ketone with hydrogen peroxide (**Scheme 3.10**). The

stereochemistry shown is based on literature precedent; stereochemistry could be assigned

following the opening of the epoxide and treatment with acetic anhydride but was not performed

due to lack of inhibition. [28, 29] When tested for activity against hGOAT, the α-epoxide was found

to have no activity up to 500 µM. The theorized reason for this is that the nucleophilic cysteine is

restricted to attack from the β-face of the steroid by the enzyme, thus preventing inhibition. The

solution to this is to synthesize the β-epoxide for comparison, which is not as straightforward.

The synthetic route to the epoxide is outlined in **Scheme 3.11**. [27-29]

Treatment of the enone **3.30** with lithium aluminum hydride has been shown to yield the

β-alcohol, which was used to direct mCPBA to form the β-epoxide **3.42**. [28, 29] Treatment of the

enone **3.30** with lithium aluminum hydride has been shown to yield the allylic β-alcohol, and

was used in the synthetic route to allow mCPBA-directed epoxidation to yield β-epoxide **3.39**. [28,

29] Due to the formation of both the allylic β-alcohol **3.40** and known alcohol **3.41** after treatment

with LAH, other methods were explored to reduce the presence of the alcohol. Use of Luche

reduction conditions as a milder alternative also yielded the alcohol mixture. Careful, slow

addition of DIBAL at -78°C was able to minimize the formation of the unwanted alcohol.

Epoxidation of the allylic β-alcohol with mCPBA yielded an impure β-epoxide **3.42**, which was

Scheme 3.10: Synthesis of α-epoxide 3.39

H$_2$O$_2$, NaOH

2:1 DCM/MeOH,
0°C, 4 h

3.30

3.39
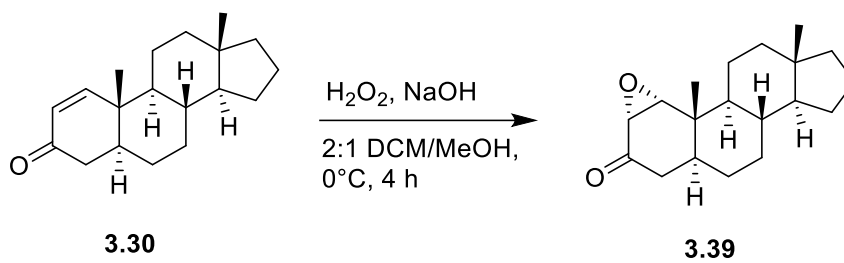
Scheme 3.11: Scheme of the synthesis of β-epoxide 3.43
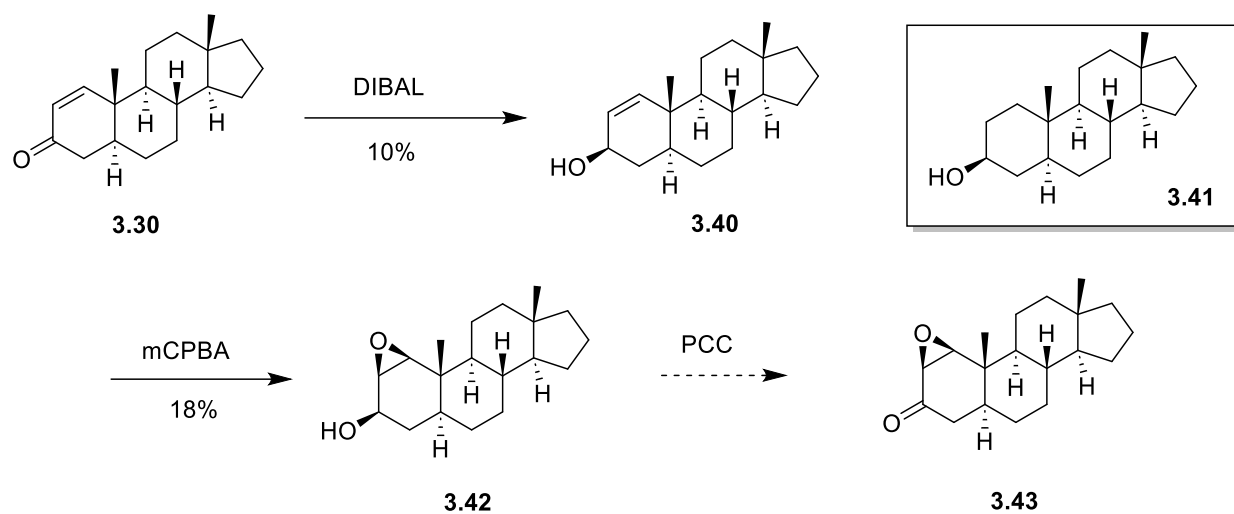
found to have inhibitory activity below 500 μM (**Figure 3.15**), in contrast to the keto α-epoxide

which did not inhibit at the same concentrations (**Figure 3.14**). This difference can be ascribed to

the geometry of the expected nucleophilic attack, with the quaternary carbon adjacent to the

electrophilic site preventing attack from the β face of the steroid. This mixture was also tested for

reversibility, and was found to be reversible (**Figure 3.16**). It is possible that the availability of

an α proton to the site of nucleophilic attack is allowing the elimination of the formed adduct, as

seen in the α-cyanoenone **3.2**. Stereochemistry of compound **3.42** was assigned based on

literature precedent, as the compound was determined to be not of further interest after the

reversibility of the proposed covalent modification of hGOAT. Synthesis and testing of

Compound 3.43 was not attempted due to the reversibility of the intermediate epoxide **3.42**

indicating that this scaffold would be unsuitable for labeling studies without modification. It is

possible that replacing the α-proton in this epoxide would prevent the elimination proposed in

Scheme 3.7, but this was not attempted due to the discovery of privileged electrophiles more

suitable for labeling, as discussed in Chapter 4 of this work.
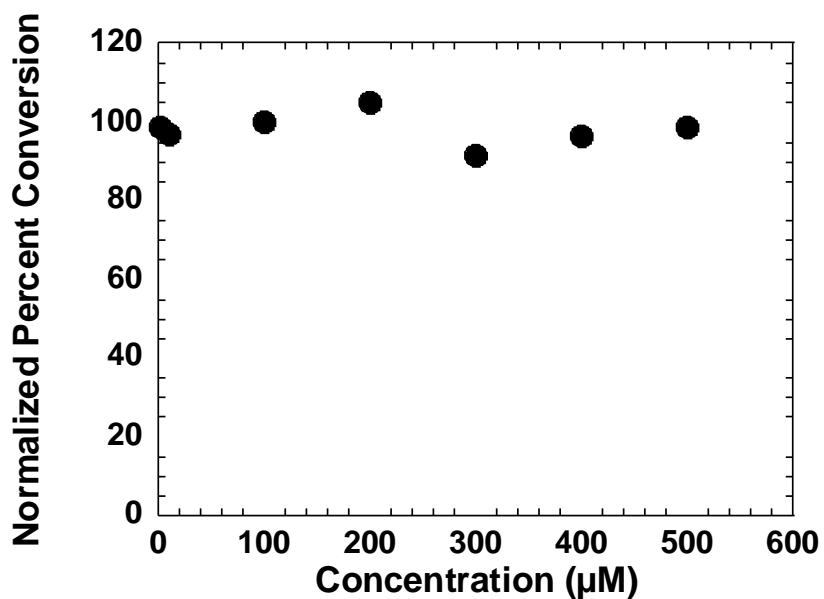
Figure 3.14: Epoxide 3.39 does not inhibit hGOAT . IC_{50} determination of **3.39** reveals that hGOAT is not inhibited by compound **3.39** up to 500 µM. Compound **3.39** was incubated for 30 minutes with 100 µg hGOAT-enriched membrane protein before reactions were initiated with 1.5 µM $GSSFLC_{AcDan}$, and 300 µM octanoyl-CoA. Data represents a single trial.
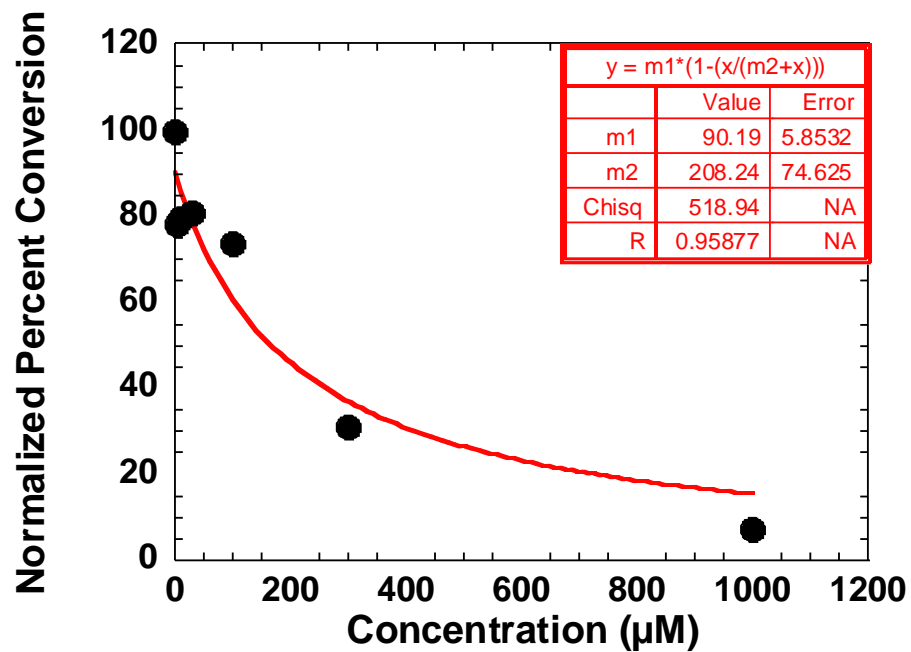
Figure 3.15: **IC$_{50}$ curve for β-epoxide 3.42.** Compound 3.42 inhibits hGOAT with an IC$_{50}$ of 208 µM. Compounds were incubated for 30 minutes with 100 µg membrane protein before reactions were initiated with 1.5 µM GSSFLC$_{AcDan}$, and 300 µM octanoyl-CoA. Data represents a single trial.
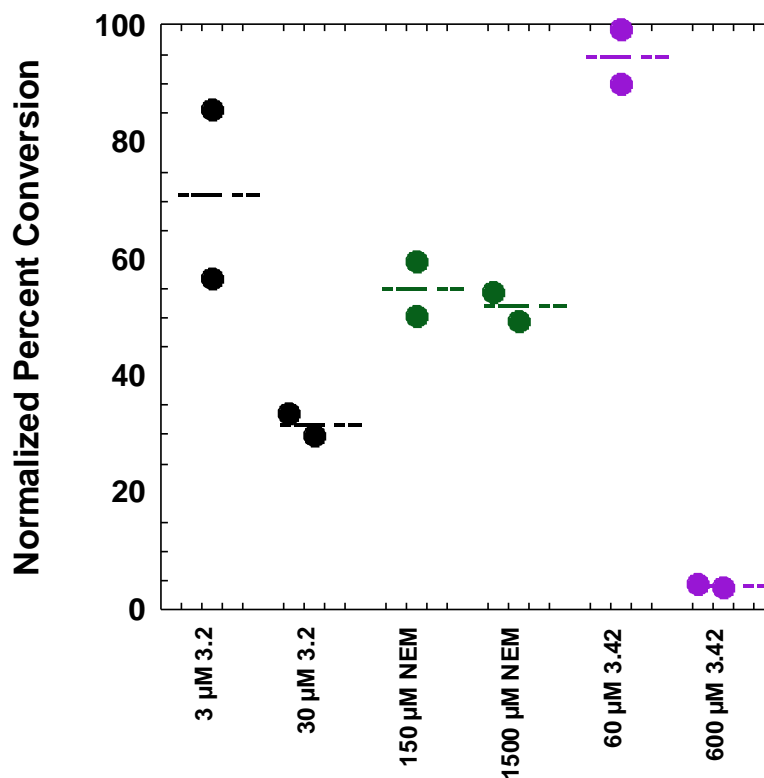
Figure 3.16: β-epoxide 3.42 reversibly inhibits hGOAT. Membrane fraction treated with inhibitor was either diluted 10X or undiluted, producing the indicated concentrations of inhibitor in reaction. Restoration of hGOAT activity under diluted condition (0.3X IC_{50}) indicates reversible inhibition by NSM-48 (**3.2**) and β-epoxide(**3.43**). NEM represents N-ethyl maleimide, known covalent irreversible inhibitor of hGOAT. [11] Compounds were tested in reactions containing 100 µg hGOAT-enriched membrane protein, 1.5 µM $GSSFLC_{AcDan}$ and 300 µM octanoyl-CoA in duplicate. Dots represent a single trial, bars represent the average of the trials. 0.3X IC_{50} concentrations were NEM: 150 µM, **3.2:** 3.0 µM, and **3.43:** 60 µM. 3X IC_{50} concentrations were NEM: 1.5 mM, **3.2:** 30 µM, and **3.43:** 600 µM.

3.3 Discussion and conclusions

In order to identify the functionally essential cysteine in hGOAT, it would be valuable to have irreversible inhibitors that specifically label this residue for chemoproteomic studies. While the cysteine modifying agents such as the alkyl-methanethiosulfonate reagents will label the functionally essential cysteine, they will also react with surface-exposed cysteine residues which limits their usefulness in locating the residues involved. By creating irreversible derivatives of compounds expected to bind into the active site, it would be possible to exclusively label the essential cysteine. The unexpected reversibility of the methanethiosulfonate inhibitors make them a poor choice for further evaluation and development for labeling studies, but also give an insight into the possible mechanism of GOAT acylation of ghrelin. In conjunction with Tasha Davis's studies which have shown that hydrogen peroxide does not inhibit hGOAT (unpublished data), the lack of irreversible inhibition exhibited by the methanethiosulfonates is likely due to the mechanism of GOAT not being dependent on a catalytic cysteine as previously hypothesized.[11]

Further studies into the functionally essential cysteine may be possible by modifying the α-epoxide **3.39** to contain a β nitrile, which may activate the theorized electrophilic site on carbon 1 enough to allow for the adduct to be formed. In addition, the reversibility of the β-epoxide **3.43** may be a result of the α hydrogen and synthesizing compounds that contained halogens or nitriles at this position may be able to trap the covalent modification of hGOAT and label the functionally essential cysteine.

While the summation of this work and work performed by Tasha Davis and Dr. Mariah Pierce (Hougland Lab, Department of Chemistry, Syracuse University) indicate that the functionally essential cysteine is unlikely to be catalytic, identification of this cysteine is still of

importance. As the currently known inhibitors of hGOAT can be classified as either

peptidomimetic or acyl-donor competitive (addressed in Chapter 2 of this work), these molecules

are purported to bind to the GOAT catalytic site. The ability for cysteine-reactive molecules to

inhibit GOAT represent the ability to target a non-catalytic, potentially allosteric site that could

be exploited for alternate therapeutic treatment through GOAT inhibition.

3.4 Materials and Methods

3.4.1 General Experimental Details

Meeks series compounds were obtained as a generous gift from Tom Meek's lab (Texas A&M, College Station, TX) and solubilized in DMSO before testing. Methyl arachidonyl fluorophosphonate (MAFP) was diluted in DMSO from a stock in methyl acetate obtained from Cayman Chemical (Ann Arbor, MI). Octanoyl coenzyme A (octanoyl CoA) was diluted to 5mM in 10 mM Tris-HCL and stored in low adhesion tubes at -80°C until use. The $GSSFLC_{NH2}$ peptide used in fluorescent acrylodan labeling was obtained from Sigma-Genosys (The Woodlands, TX) and synthesized in Pepscreen format. The $GSSFLC_{NH2}$ peptide was solubilized in 1:1 acetonitrile/water solution and stored at -80°C. Peptide concentration was determined spectrophotometrically at 412 nm by reaction of the cysteine thiol with 5,5'dithiobis(2-nitrobenzoic acid) using an ϵ_{412} of 14150 M^{-1} cm^{-1}. [30]

3.4.2 GOAT Inhibition Assay

For inhibition assays, inhibitor samples were first thawed at room temperature and vortexed, followed by dilution in DMSO to working concentrations. Membrane fractions from Sf9 cells expressing GOAT were first thawed on ice, then passed through an 18-gauge needle ten times to homogenize. Assays were performed with approximately 100 µg of membrane protein, determined through a Bradford assay. A master mix was then created with 2.5 µL 50 mM HEPES buffer, 0.1 µL 1 µM MAFP, 5 µL membrane fraction, per reaction, and water to bring the reaction to 50 µL after the addition of sample, octanoyl CoA, and peptide. The master mix was then distributed into low-adhesion microcentrifuge tubes, and the sample was then added and allowed to preincubate for 30 minutes at room temperature while covered. Reactions were started by the addition of 300 uM octanoyl CoA and 1.5 µM acrylodan-labeled peptide, for a

reaction volume of 50 µL. This was incubated for 15 minutes to 1 hour, while covered at room temperature, and then stopped with the addition of 50 µL of 20% acetic acid. Reaction time was determined via timecourse to keep conversion of acyl ghrelin below 50%. Excess membrane fraction was then removed via precipitation with 16.7 µL trichloroacetic acid followed by a 1000 xg centrifugation for 1 minute. The supernatant was then analyzed via reverse-phase HPLC.

3.4.3 Reversibility Assay

Membrane fraction containing hGOAT was incubated with 10 µM MAFP and 10 X IC_{50} or 3X of inhibitor or vehicle (DMSO) for 30 min at room temperature. Inhibitor-treated membrane fraction was then diluted 10-fold into a reaction mixture containing 300 µM octanoyl-CoA, 1.5 µM GSSFLCAcDan, 50 mM HEPES (pH 7.0), and either vehicle or inhibitor (final concentration of 1 X IC_{50} or 0.3X IC_{50}) in a total reaction volume of 50 µL. Reaction mixtures were incubated under foil for 1 h at room temperature, stopped with the addition of 50 µL of 20% acetic acid. Excess membrane fraction was then removed via precipitation with 16.7 µL trichloroacetic acid followed by a 1000 xg centrifugation for 1 minute. The supernatant was then analyzed via reverse-phase HPLC.

3.4.4 HPLC analysis of GOAT Assays

Assays were analyzed on reverse-phase HPLC (Zorbax Eclipse XDB column, 4.6 150 mm) using a solvent gradient from 30% acetonitrile in aqueous 0.05% TFA to 63% acetonitrile in aqueous 0.05% TFA over 14 minutes at a flow rate of 1 mL/min, followed by 100% acetonitrile for 5 minutes. Peptides were detected by the attached acrylodan label with the UV

absorbance at 360 nm and fluorescence (λ_{ex} = 360 nm, λ_{em} = 485 nm). Octanoylated peptide

typically eluted around 12 minutes, with the des-acyl peptide eluting around 6 minutes.

Chemstation for LC (Agilent Technologies) was used for peak integration.

3.4.5 Determination of IC$_{50}$ Values

Peak integrations were used to determine percent activity in the presence of either sample

or vehicle (DMSO). Percent activity was calculated using equations 1 and 2:

$$\% \text{ activity} = \frac{\% \text{ peptide octanoylation in presence of inhibitor}}{\% \text{ peptide octanoylation in absence of inhibitor}} \qquad (1)$$

$$\% \text{ peptide octanoylation} = \frac{\text{fluorescence of octanoylated peptide}}{\text{total peptide fluorescence}} \qquad (2)$$

IC$_{50}$ values were determined by fitting equation 3 to the plot of % activity against

inhibitor concentration.

$$\% \text{ activity} = \% \text{ vehicle activity} \left(1 - \frac{[\text{inhibitor}]}{[\text{inhibitor}]+\text{IC50}}\right) \qquad (3)$$

Plots and data fitting were performed with Kaleidagraph (Synergy Software, Reading,

PA)

3.4.6 Synthetic Methods

General Synthetic Methods

Compounds were used as received from the manufacturer without modification. All

anhydrous reactions were run under a positive pressure of argon. All solvents were dried with the

Grubbs method by passage through an alumina column. [31] Thin-layer chromatography was done

on silica at ambient temperature. Silica gel 60 was used as the stationary phase for flash

chromatography. All ^{1}H NMR were taken using a Bruker Advance 400 MHz Fourier Transform

Nuclear Magnetic Resonance Spectrometer or Bruker Advance 300 MHz Fourier Transform

Nuclear Magnetic Resonance Spectrometer. Abbreviations for spectra: s = singlet, bs = broad

singlet d = doublet, t = triplet, q = quartet, quin = quintet, dd = doublet of doublets, td = triplet of

doublets, m = multiplet.

General Preparation of Alkyl Thiosulfonates

A. *Preparation of alkyl tosylates from primary alcohols*

1.25 equivalents of *p*-toulenesulfonyl chloride were dissolved in dichloromethane,

followed by 0.08 equivalents 4-dimethylaminopyridine. Mixture was stirred at room temperature

for 5 min. 1.7 equivalents of triethylamine were added and the reaction was cooled to 0°C in an

ice bath. To the cooled mixture was added 1 equivalent of the alcohol before stirring at room

temperature for 1 hour. The reaction was quenched with water and allowed to stir overnight.

Layers were separated and the organic layer was washed with saturated ammonium chloride,

water, then brine. Organics were dried over sodium sulfate and filtered. Organics were

evaporated by a stream of air in the hood, leaving the alkyl tosylate which was used without

further purification.

B. *Preparation of alkyl methanethiosulfonates via alkyl tosylate*

1 equivalent of alkyl tosylate was dissolved in tetrahydrofuran. To the reaction mixture

was added 1.2 equivalents of sodium methanethiosulfonate and 0.25 equivalents of

tetrabutylammonium bromide. Reaction was performed at reflux for 18 hours, after which the

reaction was cooled and diluted with hexanes. The reaction was washed twice with water and once with brine, dried with sodium sulfate, and evaporated with a stream of air, yielding the alkyl methanethiosulfonate after column chromatography.

C. Preparation of alkyl methanethiosulfonate from alkyl bromide

1 equivalent of alkyl bromide was dissolved in ethanol and refluxed with 1.2 equivalents of sodium methanethiosulfonate for 18 hours. The reaction was cooled to room temperature and diluted with hexanes. The mixture was washed three times with water and twice with brine. The organic layer was dried with sodium sulfate and subjected to column chromatography to yield the alkyl methanethiosulfonate.

$$\overset{\displaystyle O}{\underset{\displaystyle O}{\overset{\|}{\underset{\|}{-S}}}}-SNa$$

3.4
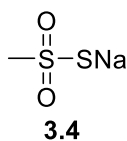
Sodium methanethiosulfonate (3.4): Synthesis of methylthiosulfonate (**3.4**) was derived from a modified literature procedure. [32] 3.33 g (13.9 mmol) of sodium sulfide nonahydrate was dissolved into 15 mL deionized water. To this solution was added 1.07 mL (13.9 mmol) distilled methanesulfonyl chloride. Reaction was run at reflux for 18 hrs. Solvent was removed under vacuum using three 100 mL portions of toluene. Resulting solid was dried under high vacccum overnight before being scraped off sides and crushed into even powder. This ground powder was returned to vacuum for 24 hrs. Powder was suspended in 20 mL of 200 proof ethanol and

filtered. Solid was washed ten times with 20 mL ethanol. Ethanol was removed from filtrate

under vacuum, leaving a pale yellow solid (0.54 g, 29%). ^{1}H NMR (400 MHz, D$_2$O) δ 3.28 (s,

3H). Additional peaks at δ 2.76 and 2.24 represent approximately 2% sodium methanesulfonate

and sodium methanesulfonite impurities.

3.5
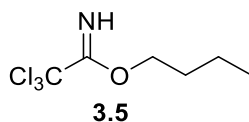
N-butyl 2,2,2-trichloroacetimidate (3.5):Procedure was derived from literature procedure. [24] To

a stirred solution of 0.92 mL (10 mmol) 1-butanol in 50 mL dry THF was added 0.74 mL 1,8-

Diazabicyclo[5.4.0]undec-7-ene (DBU, 5 mmol). This mixture was cooled to 0°C and 2.5 mL

trichloroacetonitrile (TCAN, 25 mmol) was added. The reaction was stirred at room temperature

for 6 hours before being concentrated and subjected to column chromatography (24% acetone,

71% hexanes, 5% triethylamine). Obtained compound was resuspended in DCM and

concentrated three times to yield 2.09 g butyl imidate (**3.6**) (95%) ^{1}H NMR (400 MHz, CDCl$_3$) δ

4.29 (t, J = 6.5, 2H), 1.76 (p, J = 7.0, 6.7, 2H), 1.47 (sex, J = 7.6, 2H), 0.97 (t, J = 7.5, 3H).

3.7
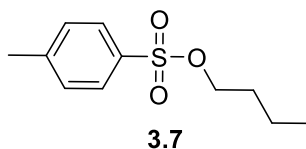
Butyl p-tolyl sulfone (3.7): Following General Procedure **A**, 8.3 mmol 1-butanol was reacted with 10.4 mmol *p*-toluenesulfonic acid in the presence of 0.66 mmol DMAP and 14.3 mmol TEA. Reaction was quenched with 30 mL water and washed with 30 mL each saturated ammonium chloride, water, and brine. Evaporation of DCM under a stream of air yielded butyl tosylate (**3.7**) as a yellow oil in 61% yield. ^{1}H NMR (400 MHz, CDCl$_3$) δ 7.78, (d, J = 8.3, 2H), 7.33, (d, J = 8.1, 2H), 4.02, (t, J = 6.5, 2H), 2.44 (s, 3H), 1.62 (p, J = 7.0, 6.5, 2H), 1.33, (sex, J = 7.5, 2H), 0.85, (t, J = 7.5, 3H).
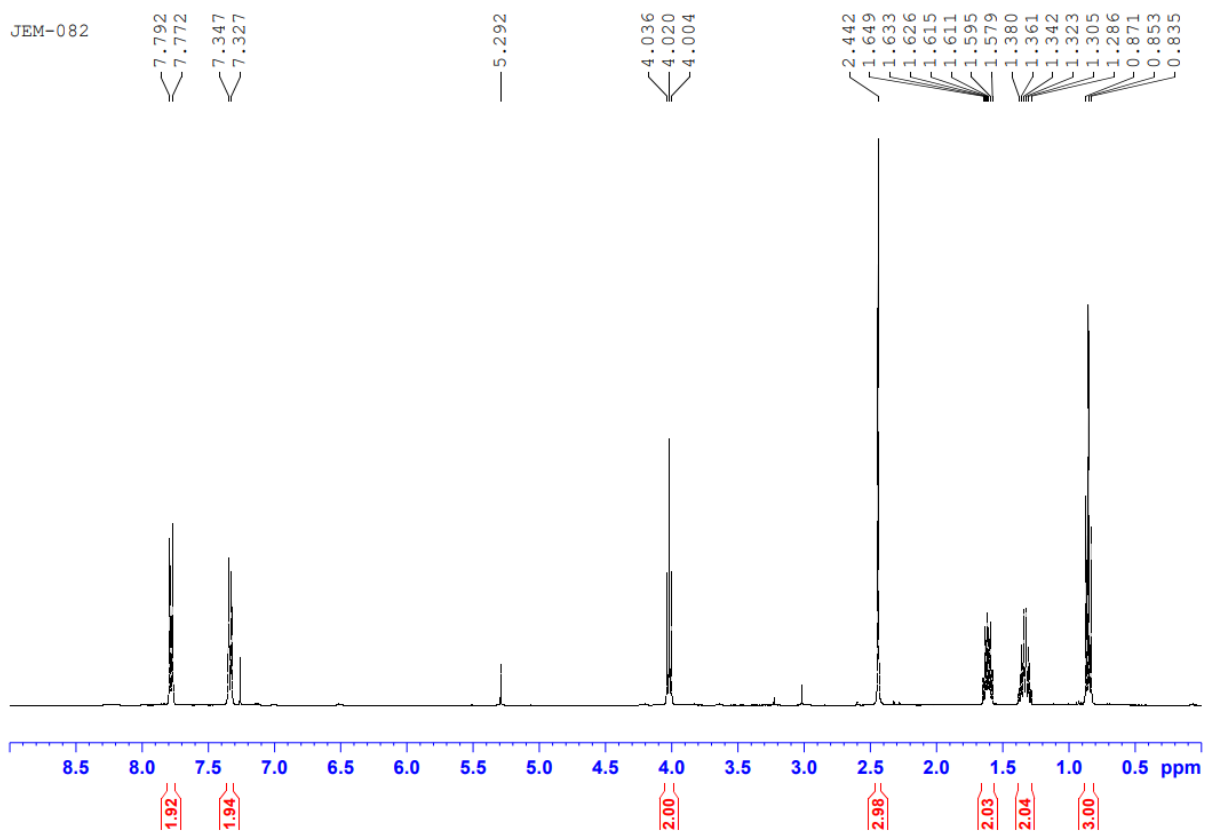
Figure 3.17: ^{1}H NMR of butyl p-tolyl sulfone (3.7)

3.8
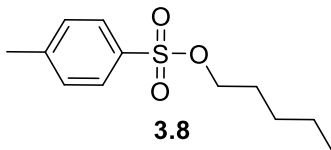
Pentyl p-tolyl sulfone (3.8): Following General Procedure **A**, 8.3 mmol 1-pentanol was reacted with 10.4 mmol *p*-toluenesulfonic acid in the presence of 0.66 mmol DMAP and 14.3 mmol TEA. Reaction was quenched with 30 mL water and washed with 30 mL each saturated ammonium chloride, water, and brine. Evaporation of DCM under a stream of air yielded pentyl tosylate (**3.8**) as a yellow oil in 51% yield. ^{1}H NMR (400 MHz, CDCl$_3$) δ 7.78, (d, J = 8.3, 2H), 7.33, (d, J = 8.1, 2H), 4.02, (t, J = 6.5, 2H), 2.44 (s, 3H), 1.67-1..60 (m, 2H), 1.28-1.23, (m, 4H), 0.84, (t, J = 7.0, 3H)
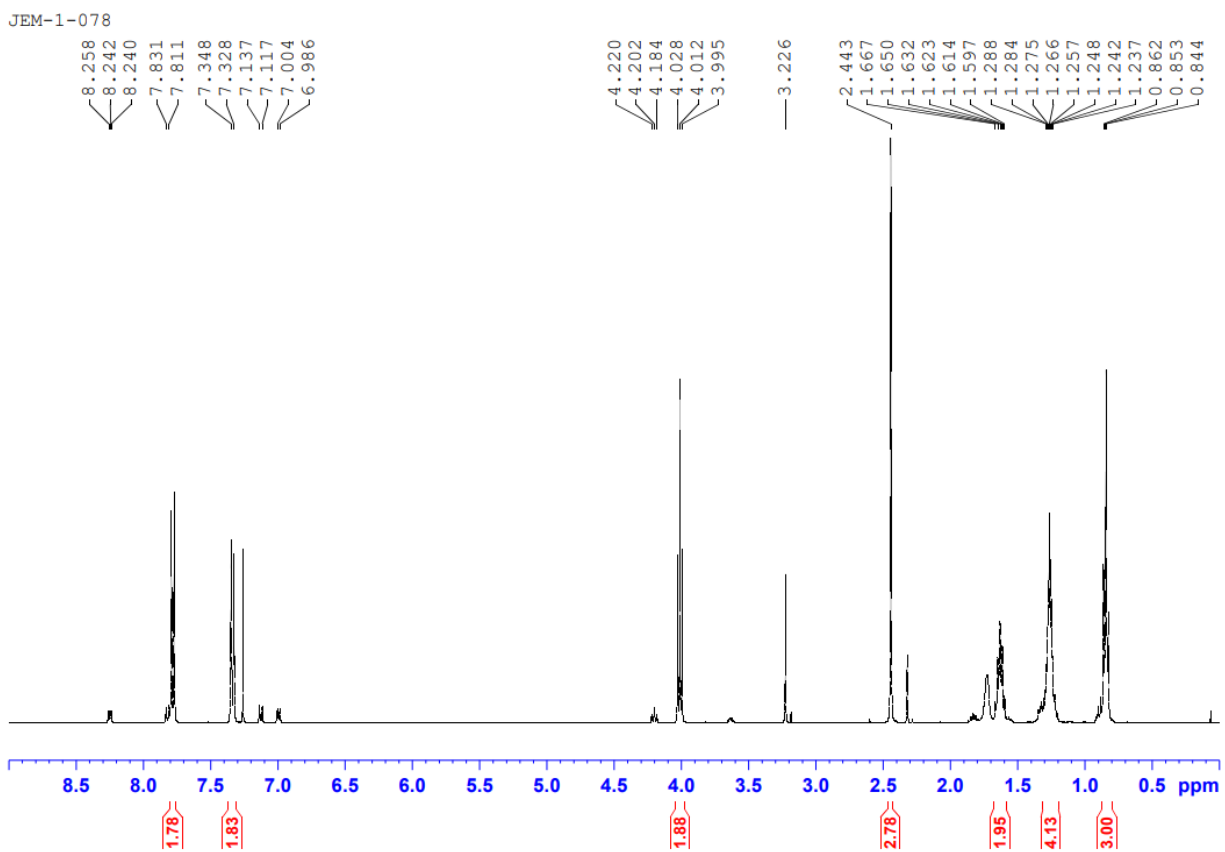
Figure 3.18: ¹H NMR of pentyl p-tolyl sulfone (3.8)

3.9
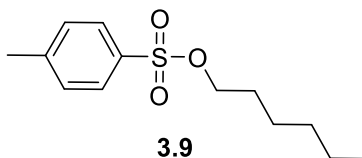
Hexyl p-tolyl sulfone (3.9): Following General Procedure **A**, 8.3 mmol 1-hexanol was reacted

with 10.4 mmol *p*-toluenesulfonic acid in the presence of 0.66 mmol DMAP and 14.3 mmol

TEA. Reaction was quenched with 30 mL water and washed with 30 mL each saturated

ammonium chloride, water, and brine. Evaporation of DCM under a stream of air yielded hexyl

tosylate (**3.9**) as a yellow oil in 83% yield. ^{1}H NMR (400 MHz, CDCl$_3$) δ 7.78, (d, J = 8.1, 2H),

7.33, (d, J = 8.1, 2H), 4.02, (t, J = 6.6, 2H), 2.44 (s, 3H), 1.67-1.54 (m, 2H), 1.31-1.19, (m, 6H),

0.85, (t, J = 6.8, 3H).
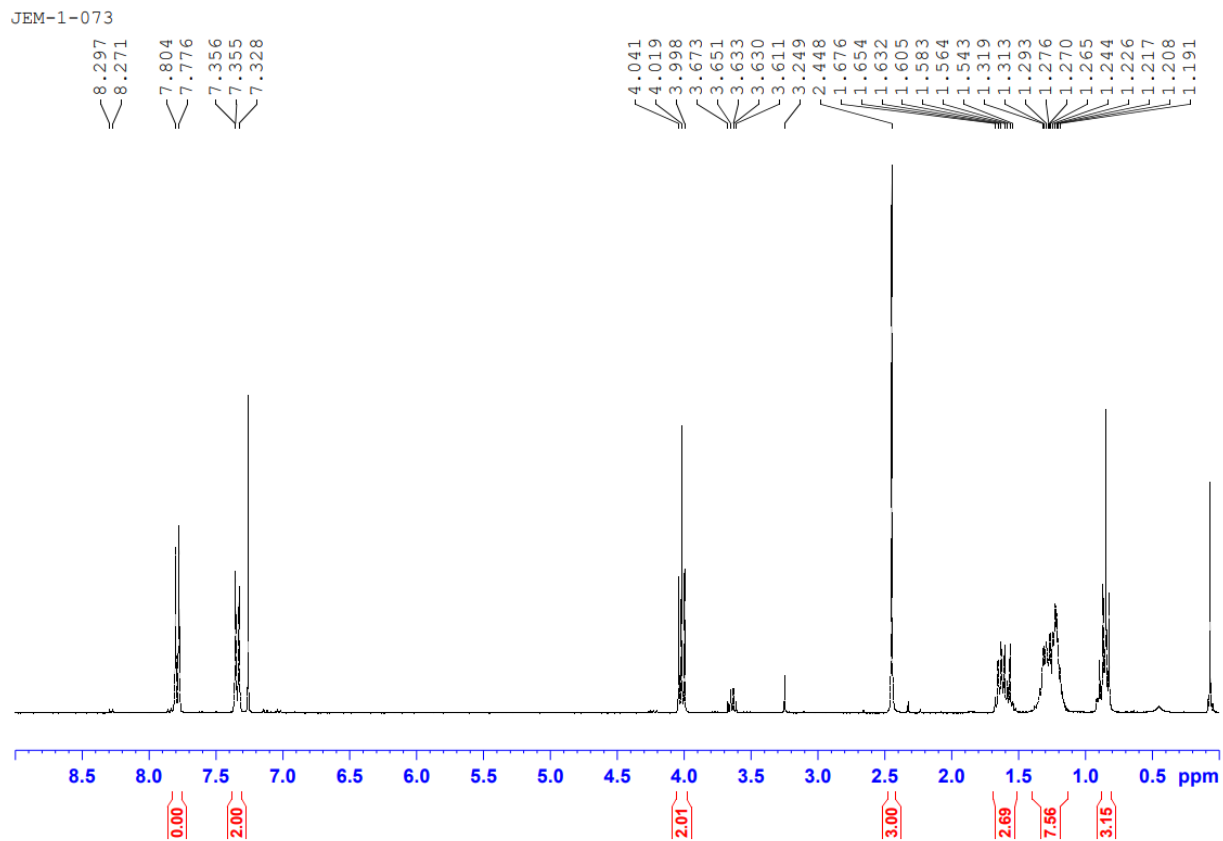
Figure 3.19: ^{1}H NMR of hexyl p-tolyl sulfone (3.9)

3.10
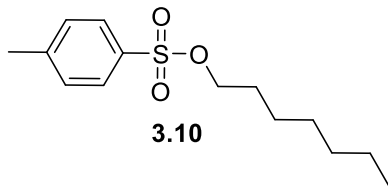
Heptyl p-tolyl sulfone (3.10): Following General Procedure **A**, 8.3 mmol 1-heptanol was reacted with 10.4 mmol *p*-toluenesulfonic acid in the presence of 0.66 mmol DMAP and 14.3 mmol TEA. Reaction was quenched with 30 mL water and washed with 30 mL each saturated ammonium chloride, water, and brine. Evaporation of DCM under a stream of air yielded heptyl tosylate (**3.10**) as a yellow oil in 83% yield. ^{1}H NMR (400 MHz, CDCl$_3$) δ 7.78, (d, J = 8.1, 2H), 7.33, (d, J = 8.1, 2H), 4.01, (t, J = 6.6, 2H), 2.44 (s, 3H), 1.68-1.55 (m, 2H), 1.35-1.16, (m, 8H), 0.85, (t, J = 7.0, 3H)
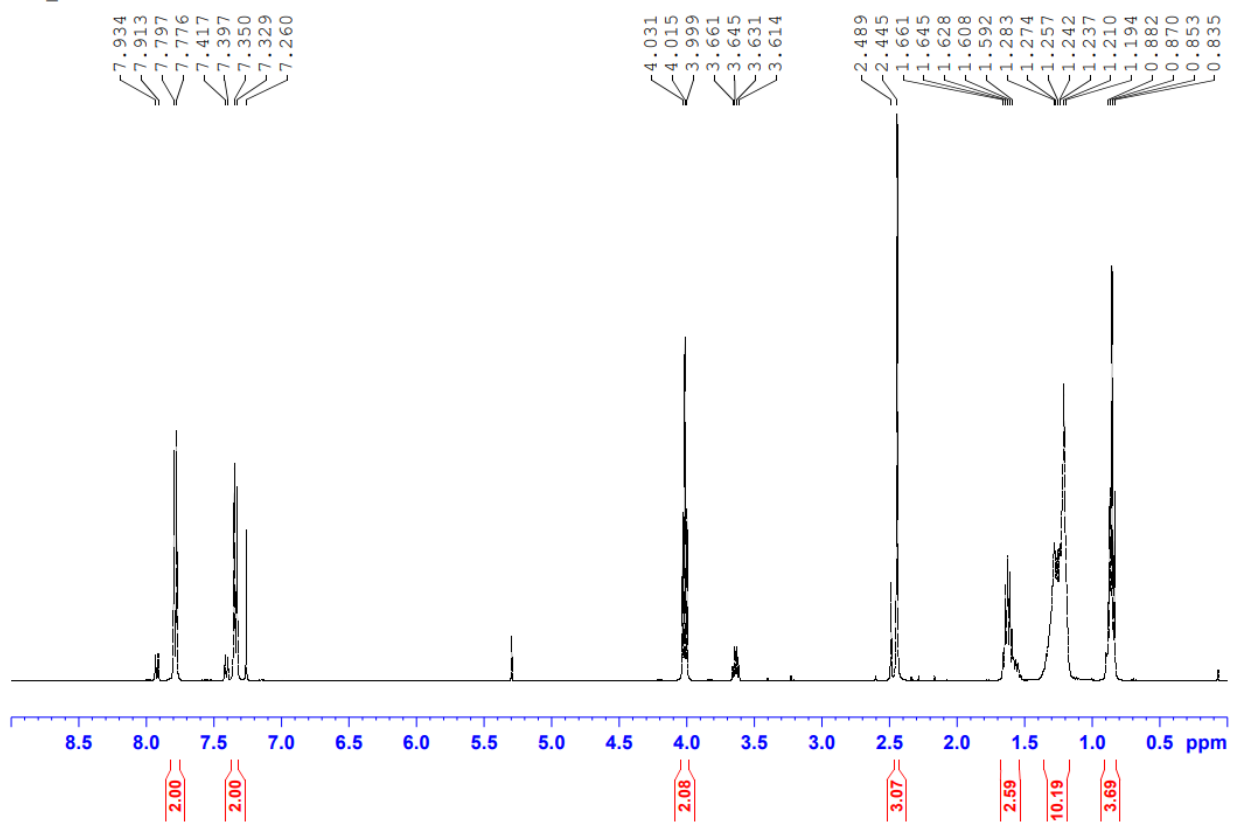
Figure 3.20: ^{1}**H NMR of heptyl p-tolyl sulfone (3.10)**

3.11
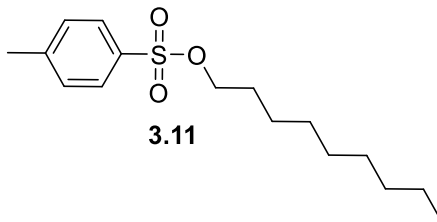
Nonyl p-tolyl sulfone (3.11): Following General Procedure **A**, 8.3 mmol 1-nonanol was reacted with 10.4 mmol *p*-toluenesulfonic acid in the presence of 0.66 mmol DMAP and 14.3 mmol TEA. Reaction was quenched with 30 mL water and washed with 30 mL each saturated ammonium chloride, water, and brine. Evaporation of DCM under a stream of air yielded nonyl tosylate (**3.11**) as a yellow oil in 62% yield. ^{1}H NMR (400 MHz, CDCl$_3$) δ 7.78, (d, J = 8.1, 2H), 7.33, (d, J = 8.1, 2H), 4.01, (t, J = 6.8, 2H), 2.44 (s, 3H), 1.67-1.51 (m, 2H), 1.40-1.14, (m, 12H), 0.85, (t, J = 6.9, 3H)
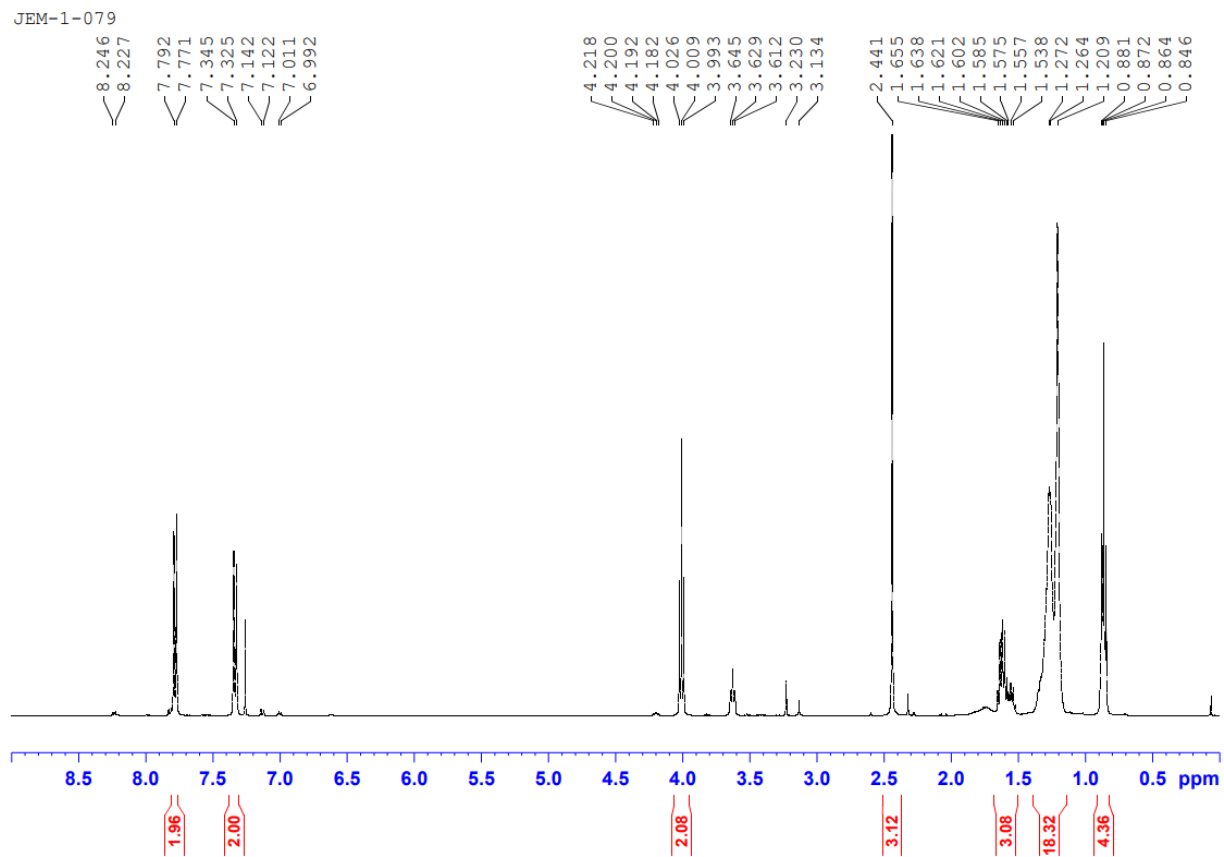
Figure 3.21: ¹H NMR of nonyl p-tolyl sulfone (3.11)

3.12
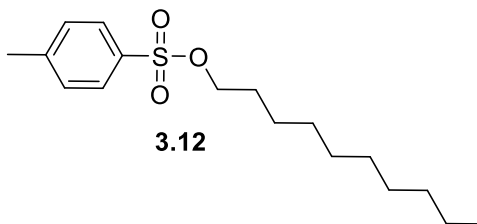
Decyl p-tolyl sulfone (3.12): Following General Procedure **A**, 8.3 mmol 1-decanol was reacted with 10.4 mmol *p*-toluenesulfonic acid in the presence of 0.66 mmol DMAP and 14.3 mmol TEA. Reaction was quenched with 30 mL water and washed with 30 mL each saturated ammonium chloride, water, and brine. Evaporation of DCM under a stream of air yielded decyl tosylate (**3.12**) as a yellow oil in 71% yield. ^{1}H NMR (400 MHz, CDCl$_3$) δ 7.78, (d, J = 8.1, 2H), 7.33, (d, J = 8.1, 2H), 4.01, (t, J = 6.5, 2H), 2.44 (s, 3H), 1.67-1.58 (m, 2H), 1.34-1.16, (m, 14H), 0.85, (t, J = 6.8, 3H)
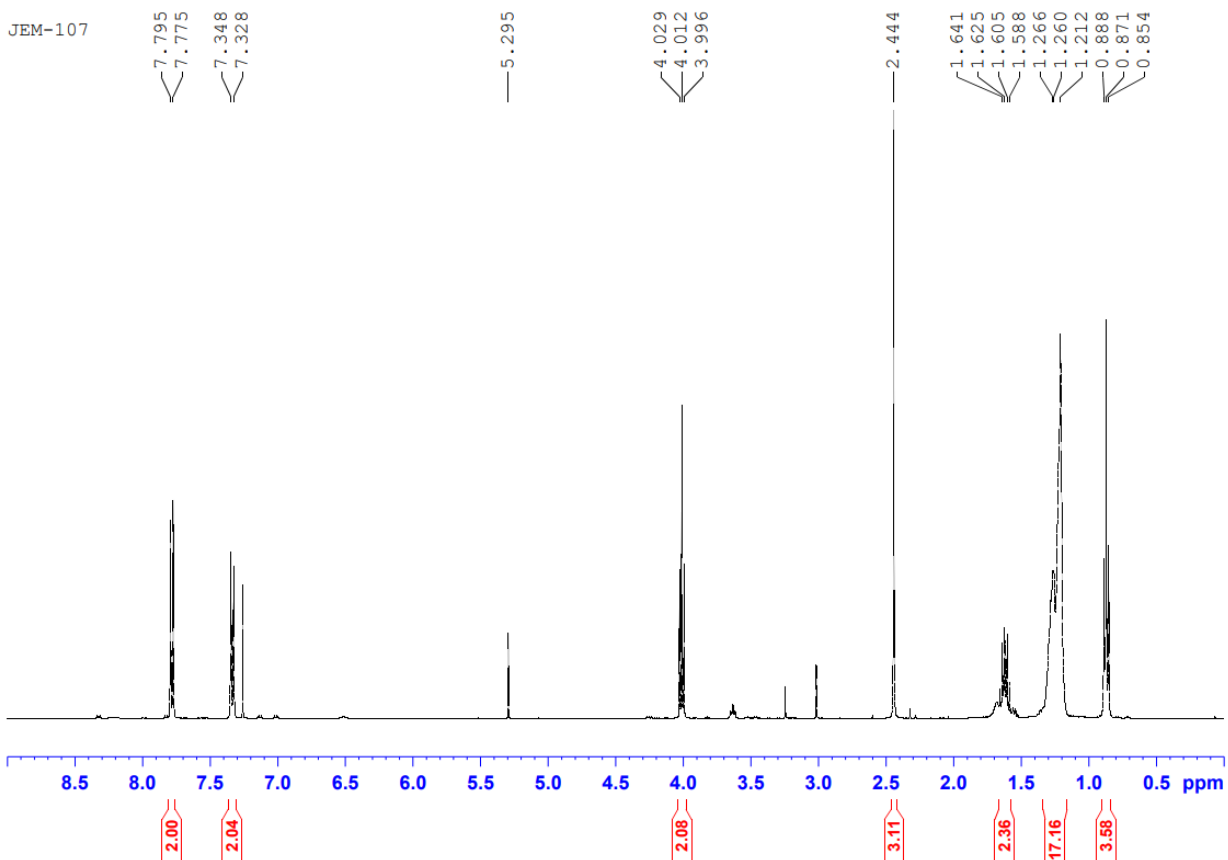
Figure 3.22: ¹H NMR of decyl p-tolyl sulfone (3.12)
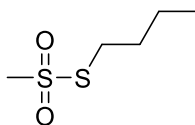
3.6

S-butyl methanethiosulfonate (3.6): Synthesis of S-butyl methanethiosulfonate (**3.6**) was

derived from a literature procedure. [32] Following General Procedure **C**, 130 mg of

methanethiosulfonate (0.97 mmol) was reacted with 0.65 mmol bromobutane in 2.0 mL dry

ethanol. The reaction was heated in an oil bath to 90°C for 20 minutes, then the solvent was

removed by vacuum. The resulting solid was filtered using a silica plug (1:1 Ethyl

acetate/hexanes) and dried under vacuum to yield a white powder. ^{1}H NMR (400 MHz, CDCl$_3$) δ

3.32 (s, 3H), 3.18 (t, J = 7.6, 2H), 1.76 (p, J = 7.2, 2H), 1.47 (m, 2H), 0.96 (t, J = 7.2, 3H).

S-butyl methanethiosulfonate (**3.6**) was also made through the reaction of butyl tosylate

with sodium methane thiosulfonate according to General Procedure **B**. Into 10 mL THF was

added 1.0 mmol butyl tosylate **3.7**, 1.2 mmol sodium methanethiosulfonate, and 0.25 mmol

TBAB. The reaction was refluxed for 18 h, diluted with 20 mL hexanes, and washed 3 X 30 mL

water, 2X 30 mL brine, before organics were dried with magnesium sulfate. Organics were

evaporated under a stream of air after purification on a silica column (5% EtOAc/hexanes),

yielding S-butyl methanethiosulfonate, compound **3.6**, as a yellow oil in 61% yield. ^{1}H NMR

(400 MHz, CDCl$_3$) δ 3.32 (s, 3H), 3.18 (t, J = 7.6, 2H), 1.76 (p, J = 7.2, 2H), 1.47 (m, 2H), 0.96

(t, J = 7.2, 3H)
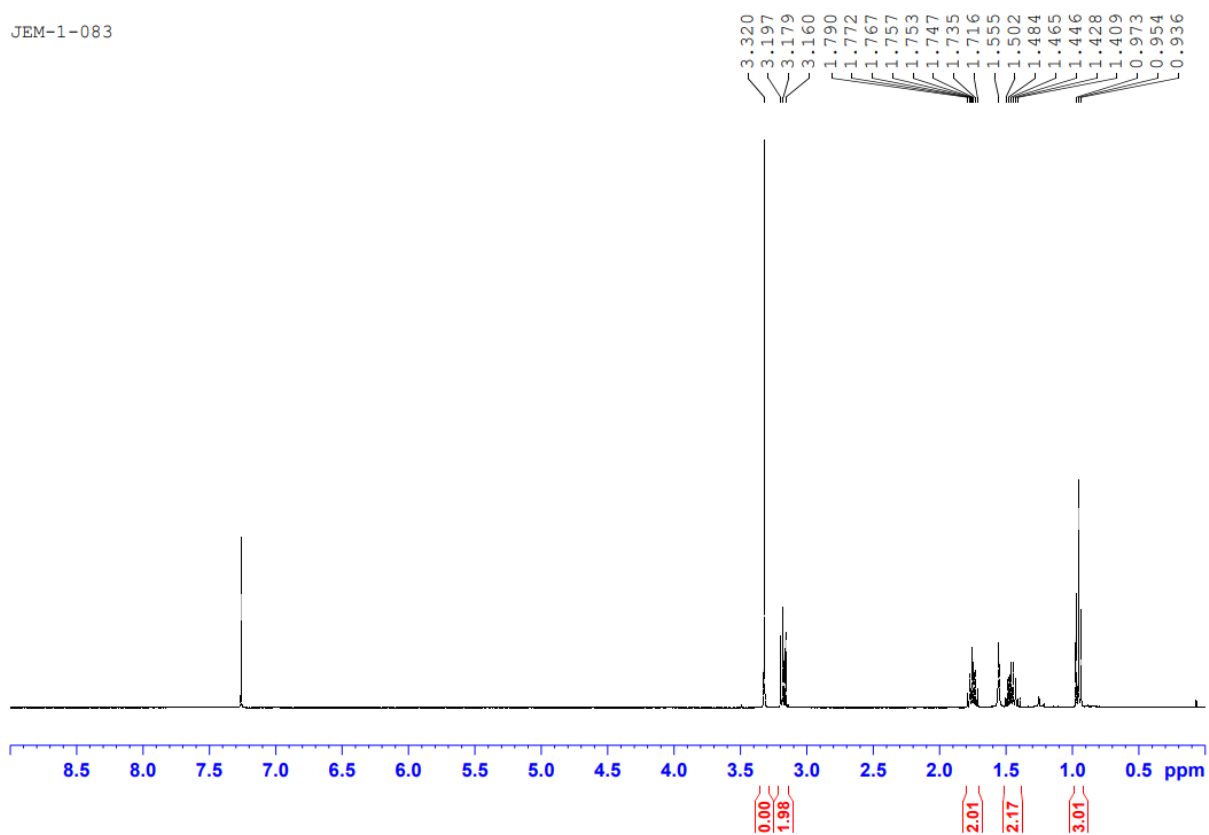
Figure 3.23: ¹H NMR of S-butyl methanethiosulfonate (3.6)

3.13
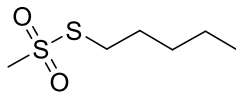
S-pentyl methanethiosulfonate (**3.13**): S-pentyl methanethiosulfonate (3.13) was made according to General Procedure **B**. Into 10 mL THF was added 1.0 mmol pentyl tosylate **3.8**, 1.2 mmol sodium methanethiosulfonate, and 0.25 mmol TBAB. The reaction was refluxed for 18 h, diluted with 20 mL hexanes, and washed 3 X 30 mL water, 2X 30 mL brine, before organics were dried with magnesium sulfate. Organics were evaporated under a stream of air after purification on a silica column (5% EtOAc/hexanes), yielding S-pentyl methanethiosulfonate, compound **3.13**, as a yellow oil in 61% yield. ^{1}H NMR (400 MHz, CDCl3) δ 3.32 (s, 3H), 3.17 (t, $J = 7.6$, 2H), 1.77 (p, $J = 7.2$, 2H), 1.42-1.32 (m, 4H), 0.92 (t, $J = 7.2$, 3H)

JEM-1-081

3.318
3.187
3.169
3.150
1.806
1.787
1.769
1.751
1.732
1.425
1.417
1.408
1.403
1.396
1.391
1.387
1.383
1.379
1.375
1.370
1.362
1.360
1.345
1.342

8.5　8.0　7.5　7.0　6.5　6.0　5.5　5.0　4.5　4.0　3.5　3.0　2.5　2.0　1.5　1.0　0.5　ppm

3.00　1.99　　　　2.00　0.31　4.05　　2.99
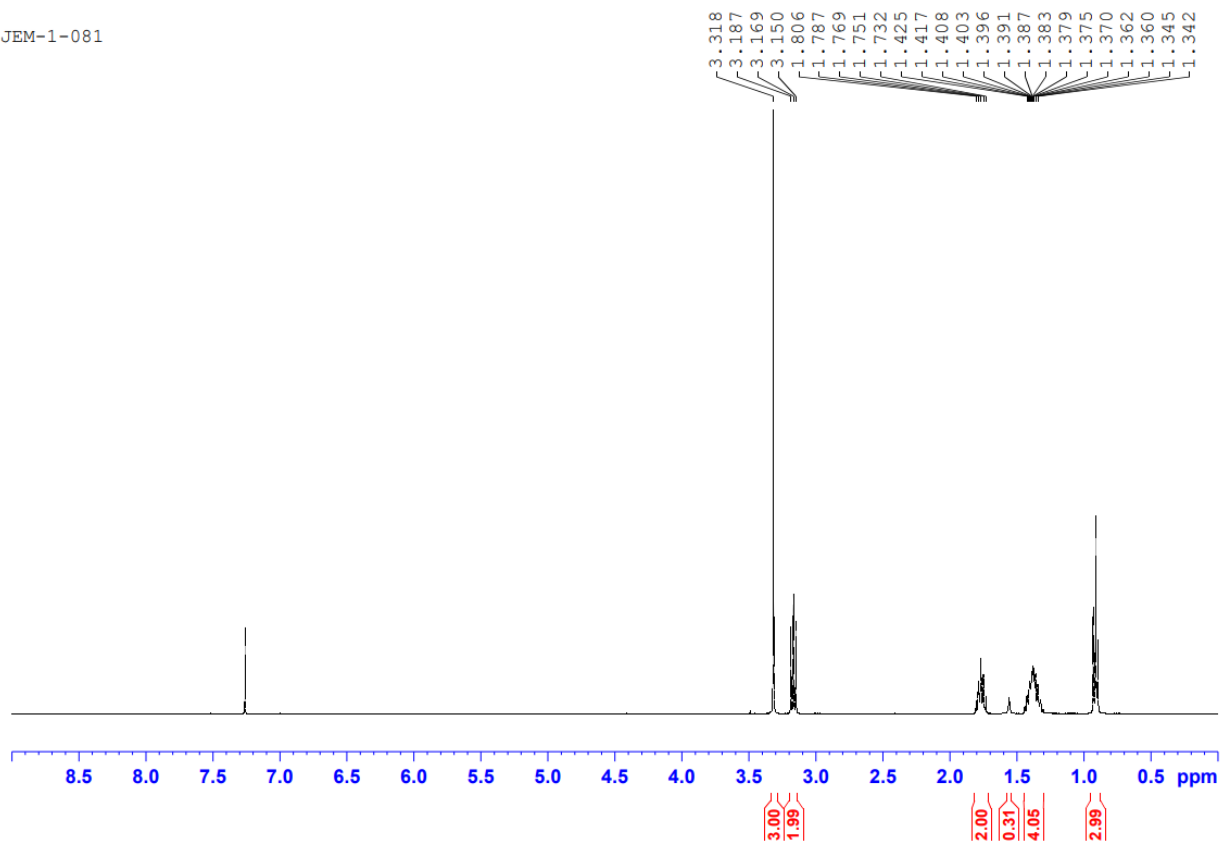
Figure 3.24: ^{1}H NMR of S-pentyl methanethiosulfonate (3.13)

3.14
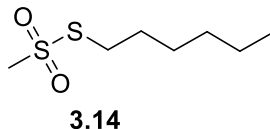
S-hexyl methanethiosulfonate (3.14): S-hexyl methanethiosulfonate (**3.14**) was made according to General Procedure **B**. Into 10 mL THF was added 1.0 mmol hexyl tosylate **3.9**, 1.2 mmol sodium methanethiosulfonate, and 0.25 mmol TBAB. The reaction was refluxed for 18 h, diluted with 20 mL hexanes, and washed 3 X 30 mL water, 2X 30 mL brine, before organics were dried with magnesium sulfate. Organics were evaporated under a stream of air after purification on a silica column (5% EtOAc/hexanes), yielding compound **3.14** as a yellow oil in 98% yield. ^{1}H NMR (400 MHz, CDCl$_3$) δ 3.32 (s, 3H), 3.17 (t, J = 7.6, 2H), 1.77 (p, J = 7.2, 2H), 1.42-1.32 (m, 6H), 0.92 (t, J = 7.2, 3H)
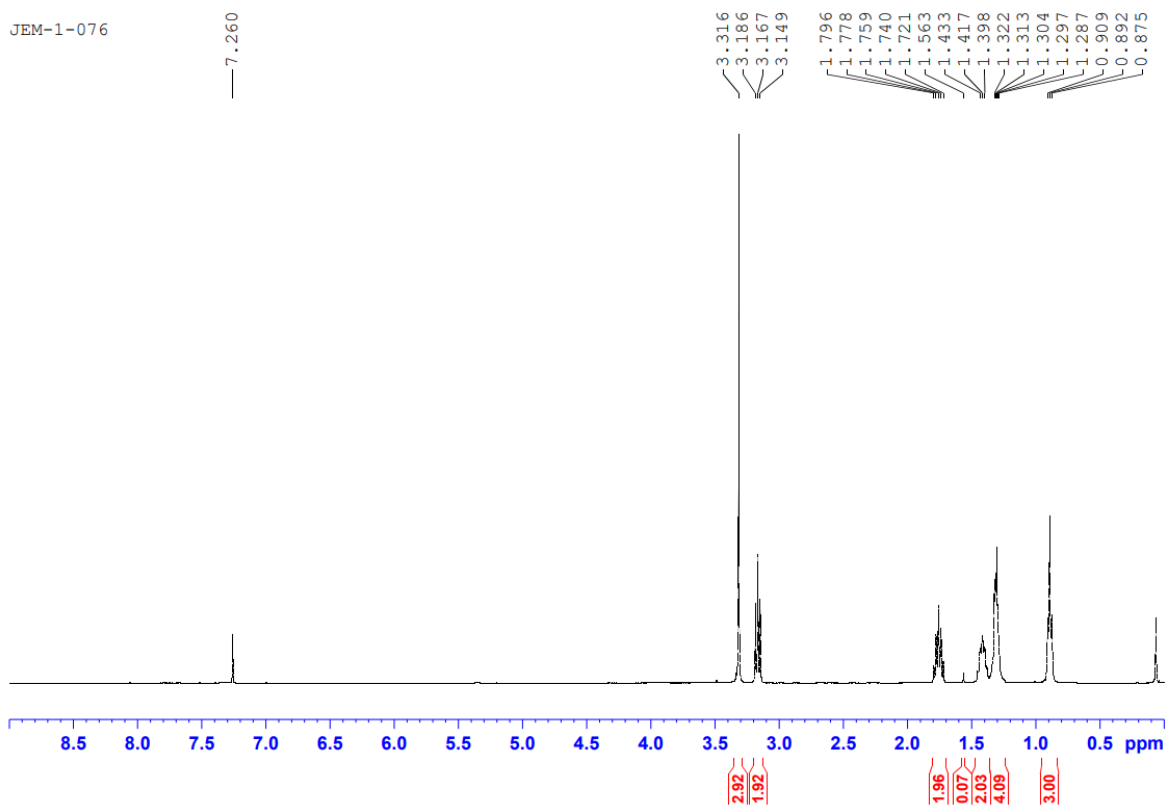
Figure 3.25: ^{1}H NMR of S-hexyl methanethiosulfonate (3.14)

3.15
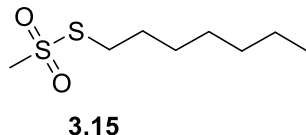
S-heptyl methanethiosulfonate (3.15): S-heptyl methanethiosulfonate (**3.15**) was made

according to General Procedure **B**. Into 10 mL THF was added 1.0 mmol heptyl tosylate **3.10**,

1.2 mmol sodium methanethiosulfonate, and 0.25 mmol TBAB. The reaction was refluxed for 18

h, diluted with 20 mL hexanes, and washed 3 X 30 mL water, 2X 30 mL brine, before organics

were dried with magnesium sulfate. Organics were evaporated under a stream of air after

purification on a silica column (5% EtOAc/hexanes), yielding S-heptyl methanethiosulfonate,

compound **13**, as a yellow oil in 98% yield. ^{1}H NMR (400 MHz, CDCl$_3$) δ 3.32 (s, 3H), 3.17 (t, J

= 7.6, 2H), 1.76 (p, J = 7.2, 2H), 1.47-1.37 (m, 2H), 1.34-1.27 (m, 6H), 0.92 (t, J = 7.2)
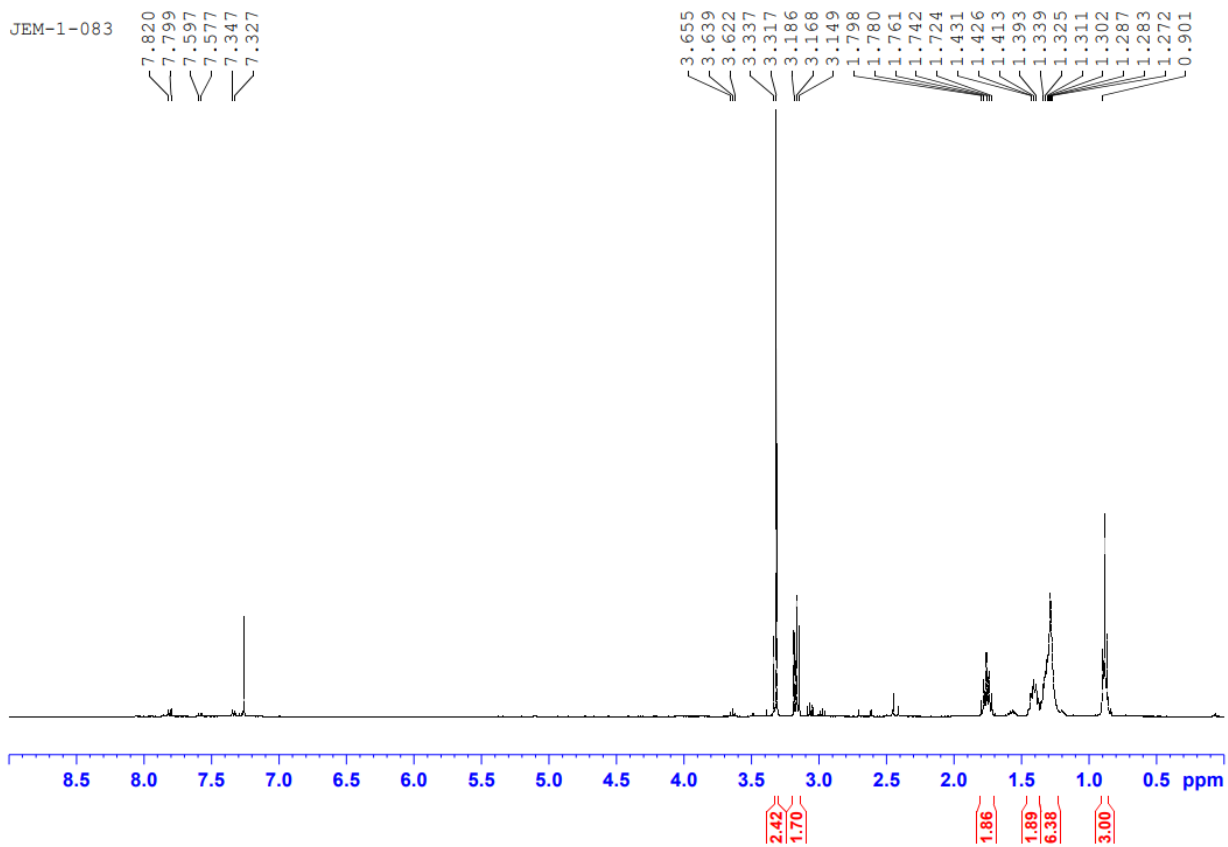
Figure 3.26: ¹H NMR of S-heptyl methanethiosulfonate (3.15)

3.16
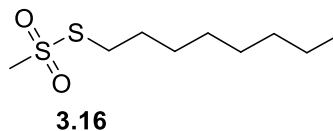
S-octyl methanethiosulfonate (3.16): S-octyl methanethiosulfonate (**3.16**) was made according

to General Procedure **C**. Into 10 mL EtOH was added 1 mmol 1-bromooctane and 1.2 mmol

sodium methanethiosulfonate. The reaction was refluxed for 18 h, diluted with 30 mL hexanes,

and the organic layer was washed with 3 X 30 mL water and 2 X 30 mL brine and dried with

sodium sulfate. Column chromatography (5% EtOAc/hexanes) yielded S-octyl

methanethiosulfonate (**3.16**) in 99% yield after evaporation in the hood under a stream of air. [1]H

NMR (400 MHz, CDCl$_3$) δ 3.32 (s, 3H), 3.17 (t, J = 7.4, 2H), 1.76 (p, J = 7.4, 2H), 1.49-1.36 (m,

2H), 1.36-1.21 (m, 8H), 0.92 (t, J = 6.8)

JEM-1-077
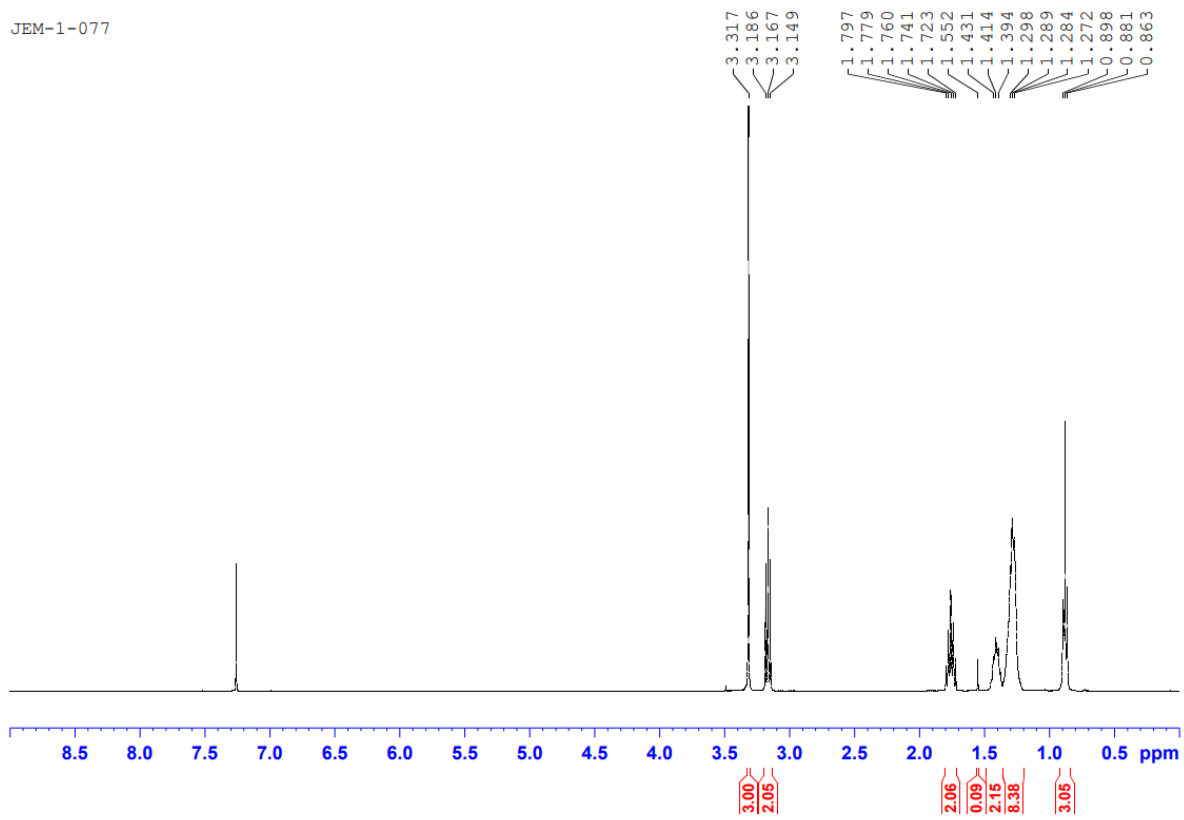
Figure 3.27: ¹H NMR of S-octyl methanethiosulfonate (3.16)

3.17
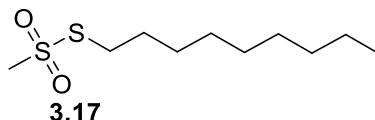
S-nonyl methanethiosulfonate (3.17): S-nonyl methanethiosulfonate (**3.17**) was made

according to General Procedure **B**. Into 10 mL THF was added 1.0 mmol nonyl tosylate **3.11**, 1.2

mmol sodium methanethiosulfonate, and 0.25 mmol TBAB. The reaction was refluxed for 18 h,

diluted with 20 mL hexanes, and washed 3 X 30 mL water, 2X 30 mL brine, before organics

were dried with magnesium sulfate. Organics were evaporated under a stream of air after

purification on a silica column (2% EtOAc/hexanes), yielding S-nonyl methanethiosulfonate,

compound **3.17**, as a yellow oil in 34% yield. ^{1}H NMR (400 MHz, CDCl$_3$) δ 3.32 (s, 3H), 3.16 (t,

J = 7.4, 2H), 1.75 (p, J = 7.2, 2H), 1.46-1.35 (m, 2H), 1.35-1.18 (m, 10H), 0.87 (t, J = 6.8)
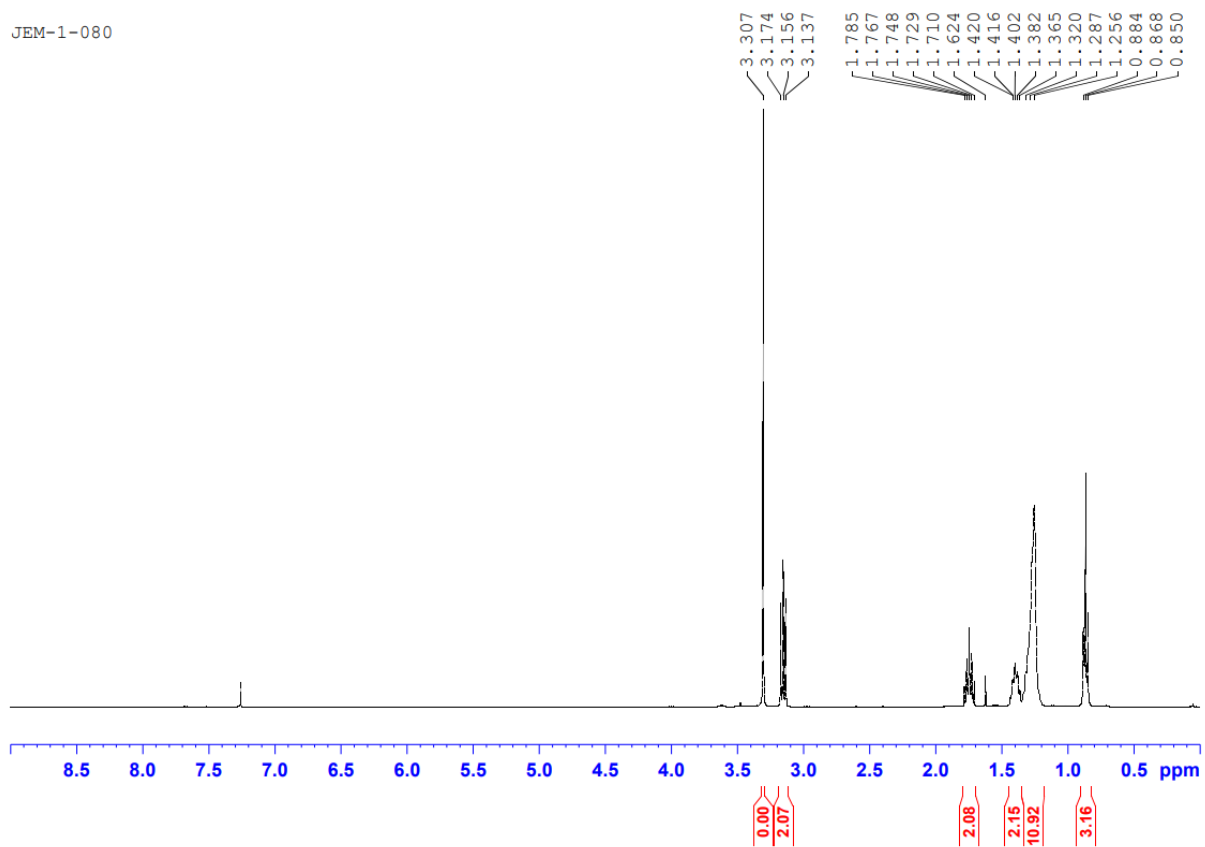
Figure 3.28: ^{1}H NMR of S-nonyl methanethiosulfonate (3.17)

3.18
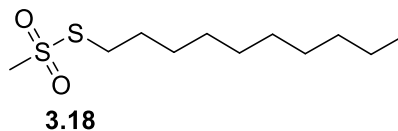
S-decyl methanethiosulfonate (3.18): S-decyl methanethiosulfonate (**3.18**) was made according

to General Procedure **B**. Into 10 mL THF was added 1.0 mmol decyl tosylate (**3.12**), 1.2 mmol

sodium methanethiosulfonate, and 0.25 mmol TBAB. The reaction was refluxed for 18 h, diluted

with 20 mL hexanes, and washed 3 X 30 mL water, 2X 30 mL brine, before organics were dried

with magnesium sulfate. Organics were evaporated under a stream of air after purification on a

silica column (2% EtOAc/hexanes), yielding S-decyl methanethiosulfonate, compound **3.18**, as a

yellow oil in 37% yield. ^{1}H NMR (400 MHz, CDCl$_3$) δ 3.32 (s, 3H), 3.17 (t, J = 7.6, 2H), 1.76

(p, J = 7.4, 2H), 1.46-1.36 (m, 2H), 1.36-1.22 (m, 12H), 0.88 (t, J = 6.7)

JEM-1-109
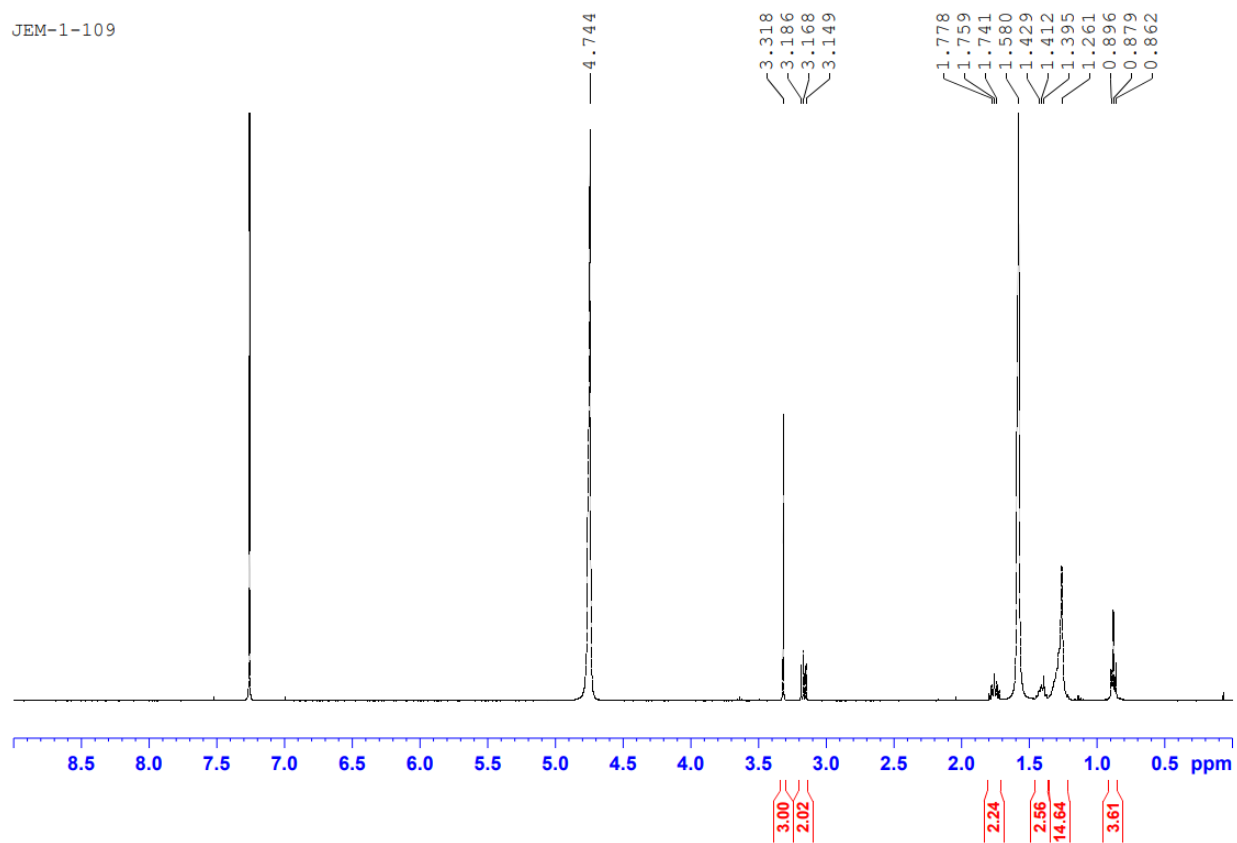
Figure 3.29: ¹H NMR of S-decyl methanethiosulfonate (3.18)

3.19
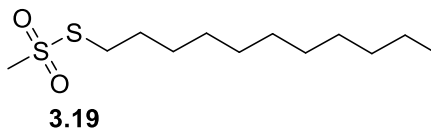
S-undecyl methanethiosulfonate (3.19): S-undecyl methanethiosulfonate (**3.19**) was made according to General Procedure **C**. Into 10 mL EtOH was added 2 mmol 1-bromoundecane and 2.4 mmol sodium methanethiosulfonate. The reaction was refluxed for 18 h, diluted with 30 mL DCM, and the organic layer was washed with 3 X 30 mL water and 2 X 30 mL brine and dried with sodium sulfate. Column chromatography (2% EtOAc/hexanes) yielded S-undecyl methanethiosulfonate, compound **3.19**, as pale yellow needles in 21% yield after evaporation in the hood under a stream of air. ^{1}H NMR (400 MHz, CDCl$_3$) δ 3.32 (s, 3H), 3.17 (t, J = 7.6, 2H), 1.76 (p, J = 7.6, 2H), 1.46-1.36 (m, 2H), 1.36-1.18 (m, 14H), 0.88 (t, J = 6.8)

JEM-117
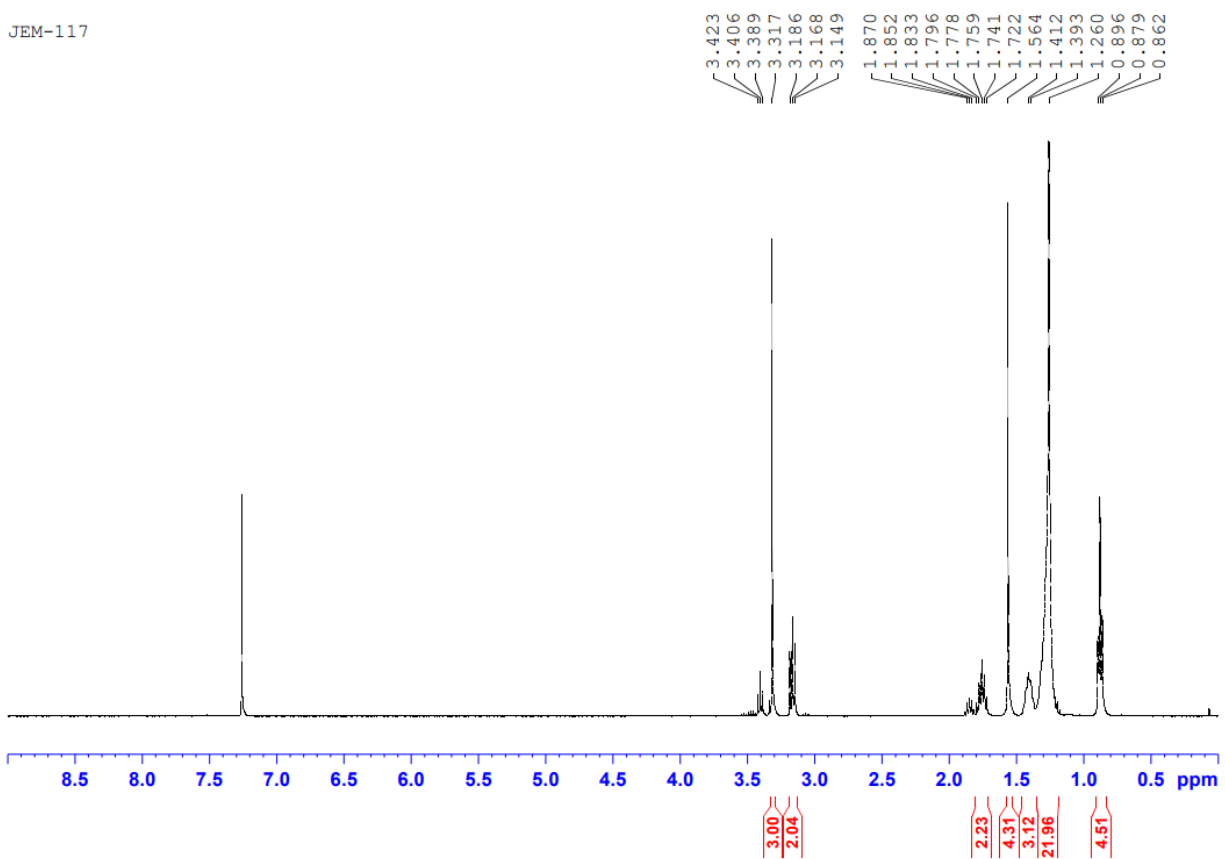
Figure 3.30: ¹H NMR of S-undecyl methanethiosulfonate (3.19)

3.20
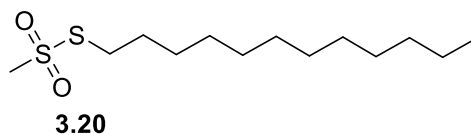
S-dodecyl methanethiosulfonate (3.20): S-dodecyl methanethiosulfonate (**3.20**) was made according to General Procedure **C**. Into 10 mL EtOH was added 2 mmol 1-bromododecane and 2.4 mmol sodium methanethiosulfonate. The reaction was refluxed for 18 h, diluted with 30 mL DCM, and the organic layer was washed with 3 X 30 mL water and 2 X 30 mL brine and dried with sodium sulfate. Column chromatography (2% EtOAc/hexanes) yielded S-dodecyl methanethiosulfonate, compound **3.20**, as pale yellow needles in 33% yield after evaporation in the hood under a stream of air. ^{1}H NMR (400 MHz, CDCl$_3$) δ 3.32 (s, 3H), 3.17 (t, J = 7.4, 2H), 1.76 (p, J = 7.4, 2H), 1.47-1.37 (m, 2H), 1.36-1.21 (m, 16H), 0.88 (t, J = 6.8)

JEM-1-118
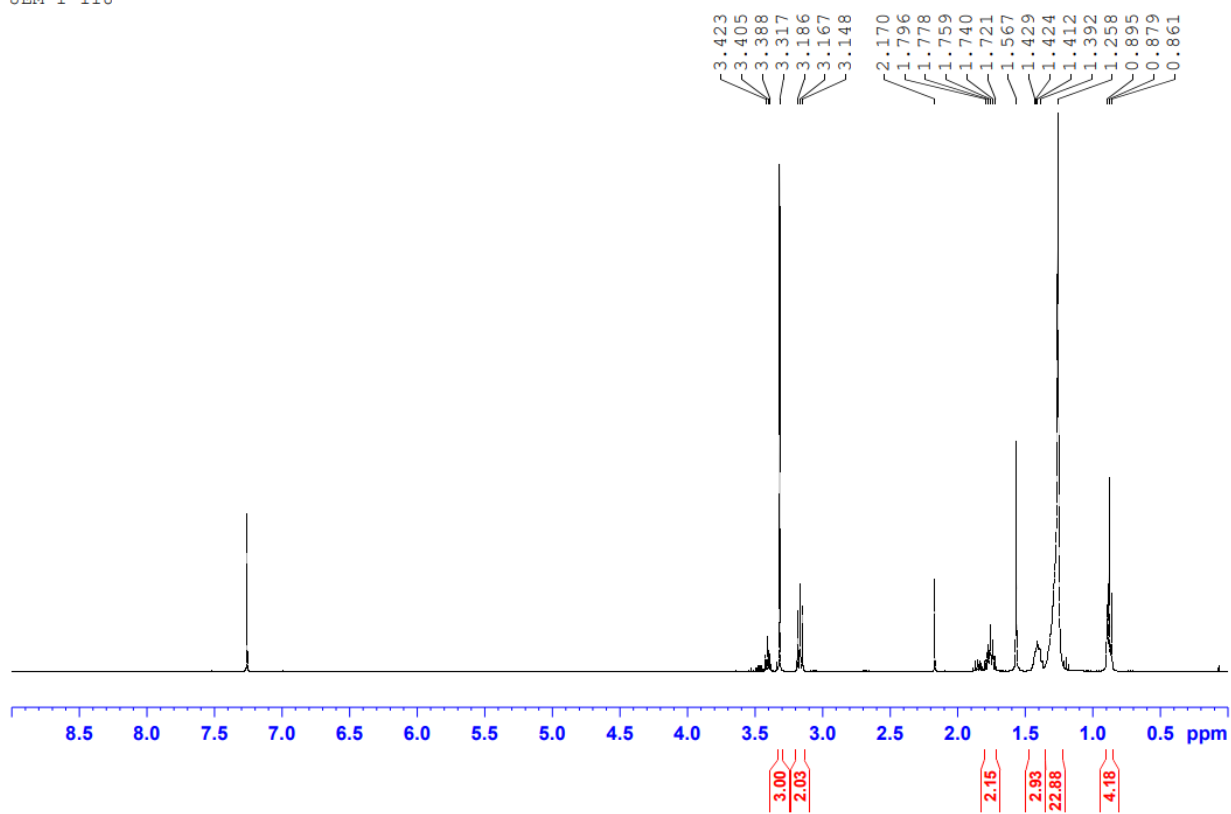
Figure 3.31: ¹H NMR of S-dodecyl methanethiosulfonate (3.20)

3.41
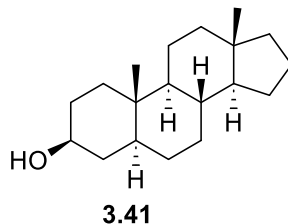
5α-androstan-3β-ol ((3S,10S,13S)–10,13–dimethyl–2,3,4,5,6,7,8,9,10,11,12,13,14,15,16,17–tetradecahydro–1H–cyclopenta[a]phenanthren–3–ol) (3.41): To the mixture of potassium hydroxide (103.3 mmol) in 30 mL of diethylene glycol was added epiandrosterone (20.7 mmol) and hydrazine (82.6 mmol). The reaction mixture was stirred at 245°C for 24 hours, at which point the solution was allowed to cool to room temperature. 150 mL of brine was added, followed by 75 mL of dichloromethane, before transferring the mixture to a separatory funnel. The mixture was worked up by extracting the organic three times with 100 mL of dichloromethane. The organic layer was washed three times with saturated sodium chloride (100 mL) and dried with sodium sulfate and filtered. The organic layer was then removed under vacuum, leaving the compound **3.41** as a white powder with 91% yield. ^{1}H NMR (400 MHz, CDCl$_3$) δ 3.61-3.55 (m, 1H), 1.81 (q, J = 12 Hz, 1H), 1.74-1.50 (m, 8H), 1.41 (td, J = 6 Hz, 2H), 1.34-1.24 (m, 6H), 1.14-1.09 (m, 4H), 0.98-0.88 (m, 3H), 0.81 (s, 3H), 0.69 (s, 3H), 0.69-0.62 (m, 1H).
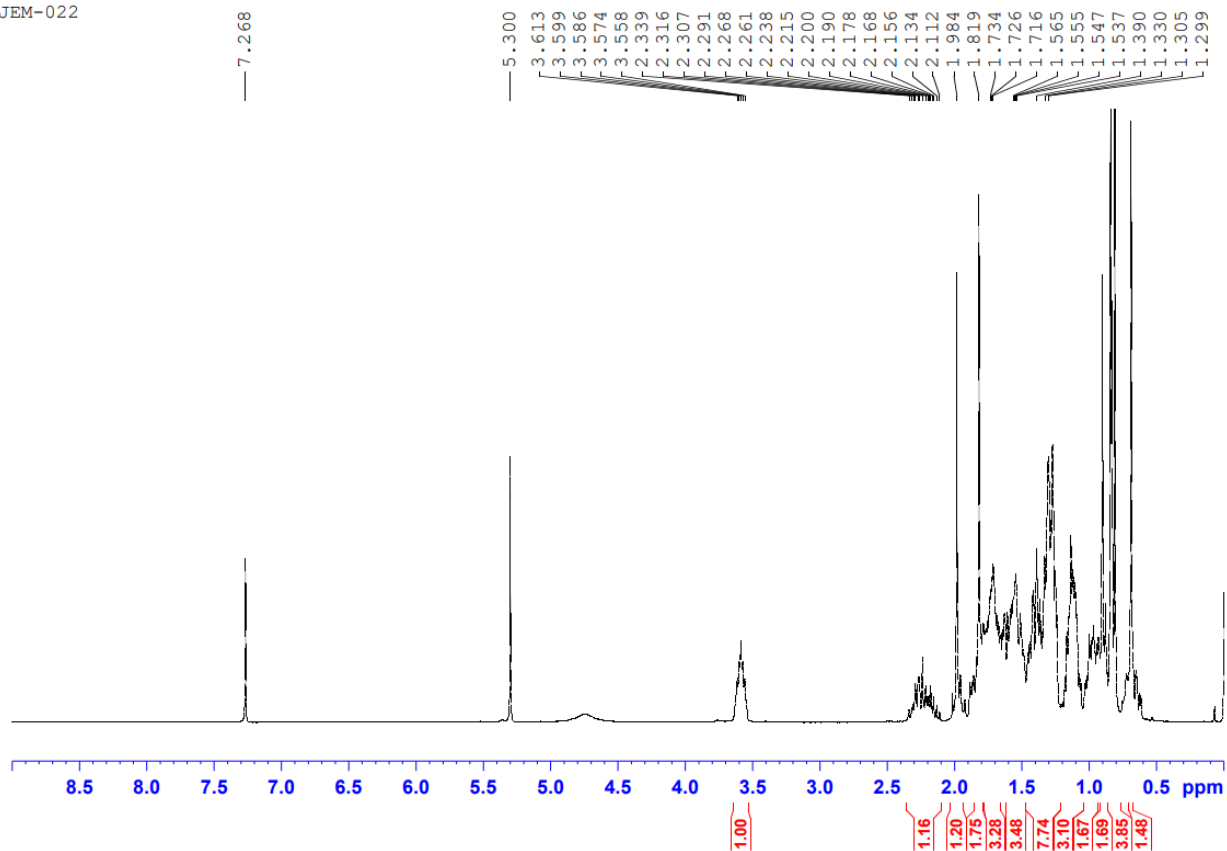
Figure 3.32: ¹H NMR of 5α-androstan-3β-ol (3.41)
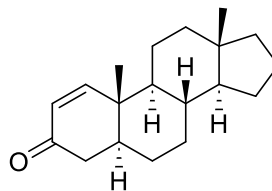
3.30

(2R,5S,8S,9S,10S,13S,14S)–10,13–dimethyl–4,5,6,7,8,9,10,11,12,13,14,15,16,17–

tetradecahydro–3H–cyclopenta[a]phenanthren–3–one (3.30): To the mixture of 3.5 g (12.6

mmol) of 5α-androstan-3β-ol, **3.41**, in 200 mL dimethyl sulfoxide at 90°C was added 10 g (35.7

mmol) 2-iodoxybenzoic acid. The mixture was stirred at 90°C for 6 hrs before being returned to

room temperature. The reaction mixture was transferred to a separatory funnel, to which was

added 200 mL ethyl acetate. The mixture was extracted with 100 mL 5% sodium bicarbonate,

then twice washed with 100 mL saturated sodium chloride. The organic later was concentrated

under vacuum before being purified using silica gel chromatography (10% Ethyl acetate/ 90%

hexanes) to provide the α,β-unsaturated ketone **3.30** (1.67 g, 49%). ^{1}H NMR (400 MHz, CDCl$_3$)

δ 7.16 (d, J = 10, 1H) 5.84 (dd, J = 10 Hz, 0.4 Hz, 1H), 2.41-2.36 (m, 1H), 2.15 (dd, J = 14.4 Hz,

3.5 Hz, 1H) 1.89-1.79 (m 1H), 1.74-1.63 (m, 3H) 1.63-1.47 (m, 3H), 1.45-1.29 (m, 5H), 1.18-

1.05 (m, 4H,) 0.98-.87 (m, 6H), .67 (s, 3H).
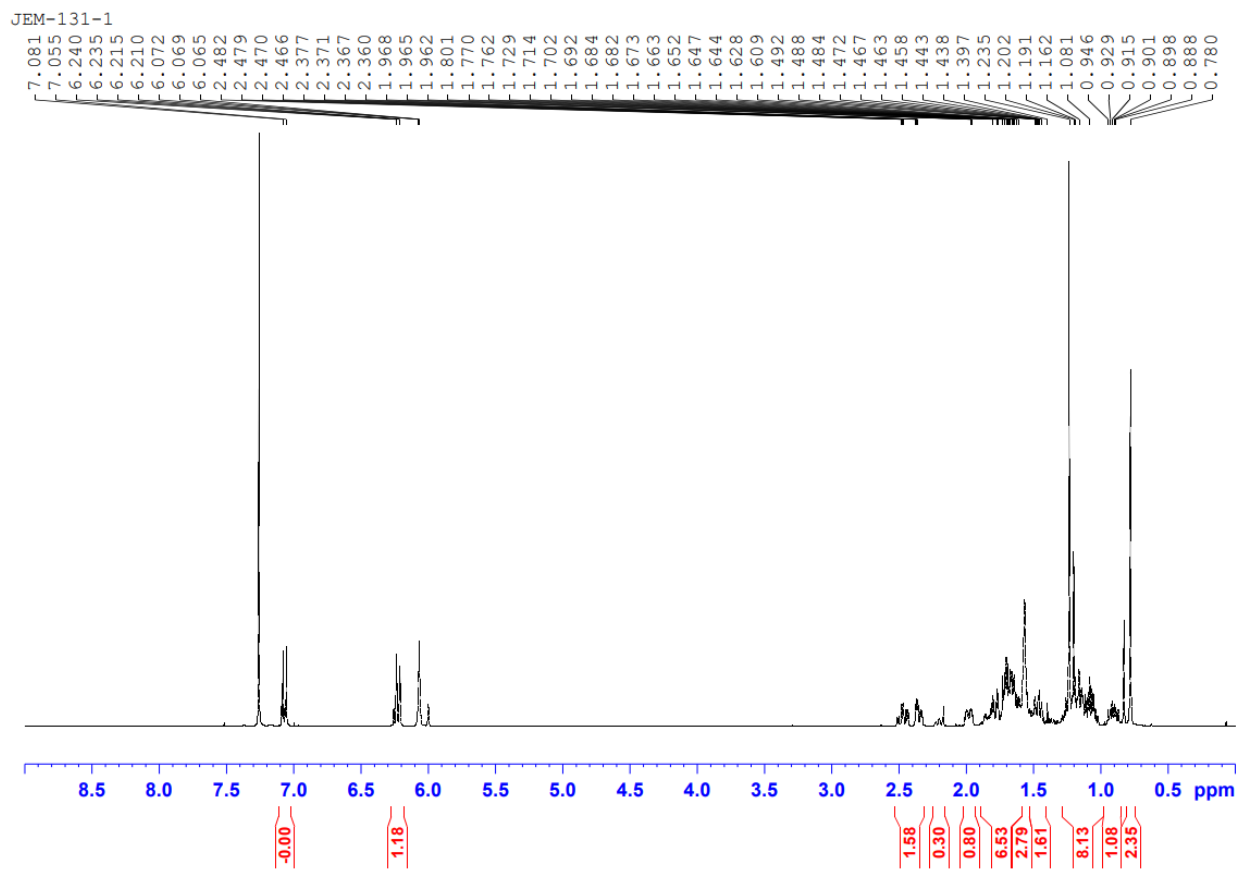
Figure 3.33: ¹H NMR of α,β-unsaturated ketone (3.30)
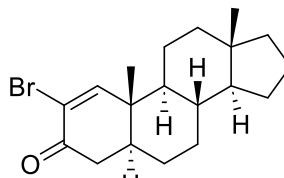
3.44

(5S,8S,9S,10S,13S,14S)-10,13-dimethyl-3-oxo-4,5,6,7,8,9,10,11,12,13,14,15,16,17-

tetradecahydro-3H-cyclopenta[a]phenanthrene-2-bromide (3.44): 400 mg (1.47 mmol) of

α,β-unsaturated ketone **3.30** was dissolved in 4 mL dry dichloromethane (DCM) and cooled in an

ice bath. To the reaction mixture was added dropwise a 0° solution of 75 μL (1.47 mmol) liquid

bromine in 4 mL DCM over 30 minutes. 0.41 mL (2.94 mmol) triethylamine, precooled to 0°C,

was added slowly and the whole reaction was allowed to warm to room temperature and stir for

1.5 hours. The reaction was quenched with 1 M HCl (1 M) and washed with 2 X 8 mL 10%

sodium thiosulfate and 1 X 8 mL brine. The organics were dried with magnesium sulfate before

being removed under reduced pressure. The residue was subjected to column chromatography

(10% EtOAc/hexanes) providing the bromide **3.44** in 63% yield (320 mg). ^{1}H NMR (400 MHz,

CDCl$_3$) δ 7.59 (s, 1H), 2.58-2.43 (m, 2H), 2.03-1.94 (m, 1H), 1.85-1.52 (m, 6H), 1.48-1.34 (m,

5H), 1.22-1.12 (m, 3H), 1.05 (s, 3H), 1.02-0.93 (m, 3H), 0.73 (s, 3H)
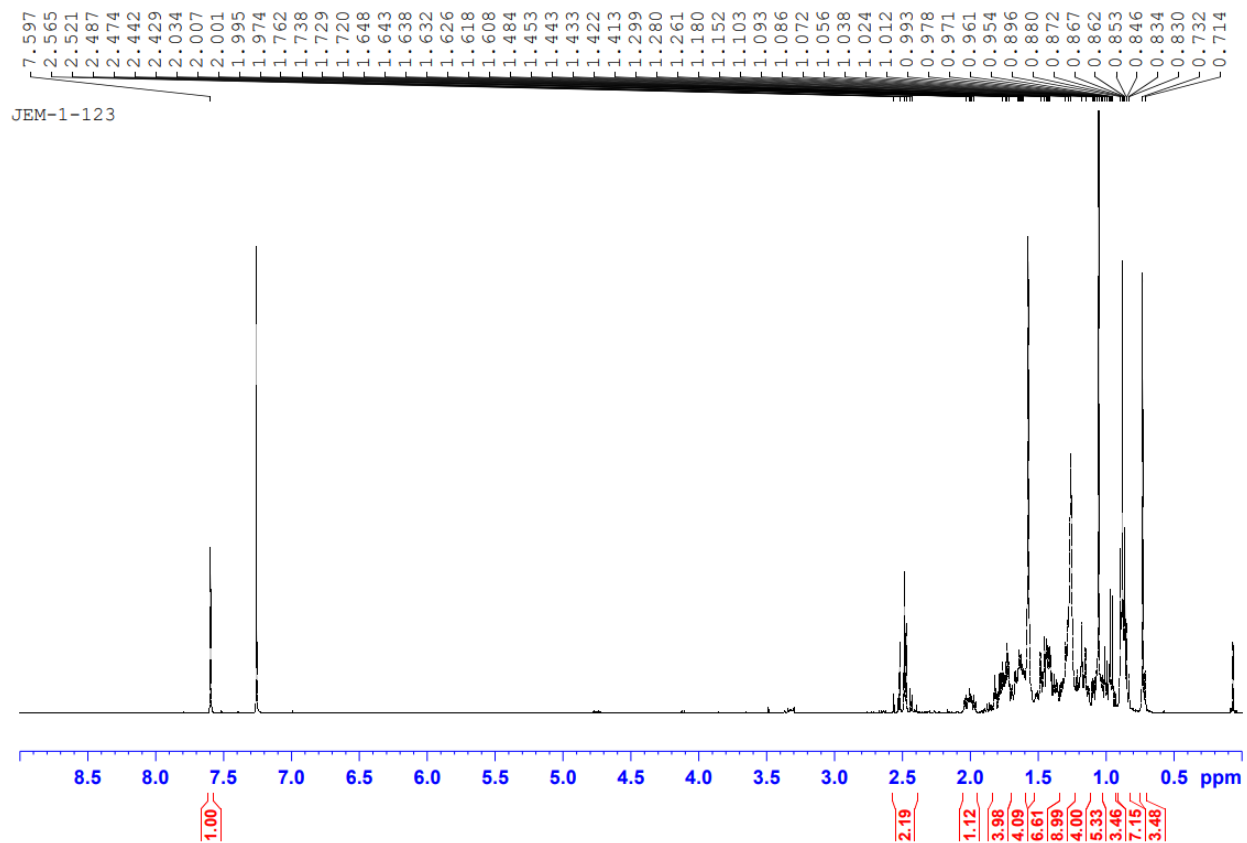
Figure 3.34: ¹H NMR of α-bromo-α,β-unsaturated ketone (3.44)
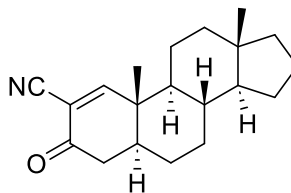
3.2

(5S,8S,9S,10S,13S,14S)-10,13-dimethyl-3-oxo-4,5,6,7,8,9,10,11,12,13,14,15,16,17-tetradecahydro-3H-cyclopenta[a]phenanthrene-2-carbonitrile (3.2): To a solution of 200 mg (0.56 mmol) of bromide **3.44** in 4 mL of dimethylformamide (DMF) was added 9.2 mg (0.056 mmol) of potassium iodide and 56 mg (0.62 mmol) copper (I) cyanide. The reaction mixture was heated to 120°C for 24 hours before being returned to room temperature and quenched with 10 mL water and diluted with 35 mL EtOAc. The layers were separated and the organics were washed with 2 X 10 mL saturated sodium bicarbonate and 1 X 10 mL brine before being dried with magnesium sulfate. Organics were removed under reduced pressure and the residue was purified via column chromatography (30% EtOAc/hexanes), yielding α-cyanoenone **3.2** as a light-yellow powder in 53% yield. ^{1}H NMR (400 MHz, CDCl$_3$) δ 7.88 (s, 1H), 2.48-2.35 (m, 2H), 2.02-1.93 (m, 1H), 1.87-1.57 (m, 7H), 1.50-1.38 (m, 5H), 1.22- 1.12 (m, 3H), 1.09 (s, 3H), 1.05-0.94 (m, 2H), 0.75 (s, 3H)
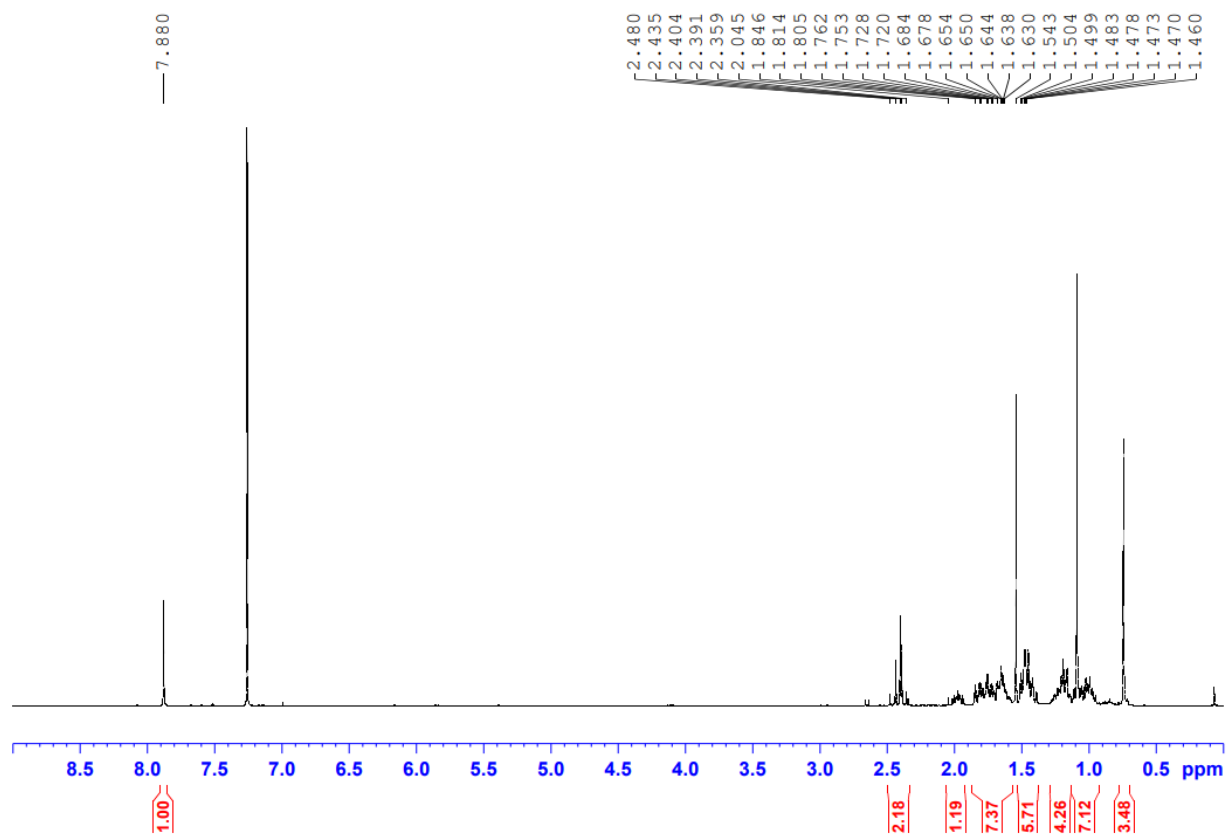
Figure 3.35: ¹H NMR of α-cyano-α,β-unsaturated ketone (3.2)

3.39
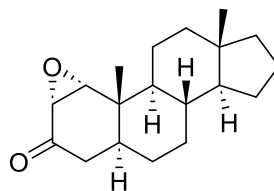
5α-androst-1α,2α -epoxy-3-one (3.39): Procedure was derived from literature procedure. [28, 33]

100 mg (0.367 mmol) α,β-unsaturated ketone **3.30** was dissolved in a mixture 1 mL MeOH and

0.5 mL DCM and cooled to 0°C. To the reaction mixture was added 0.2 mL 30% hydrogen

peroxide and 0.25 mL 4 N sodium hydroxide. The reaction was stirred for 4 hours before the

solvent was removed under reduced pressure. The residue was suspended in 5 mL DCM and

washed with 5 mL brine. The aqueous layer was washed with 2 X 5 mL DCM and the organics

were combined and dried with magnesium sulfate. The organics were removed under reduced

pressure and used without further purification, yielding 104 mg (99%) epoxide 3.**39**. ^{1}H NMR

(400 MHz, CDCl$_3$) δ 3.53 (d, J = 4.3, 1H), 3.24 (d, J = 4.3, 1H), 1.85-1.76 (m, 2H) 1.76-1.56 (m,

4H) 1.56-1.14, (m, 10H) 1.06-0.96 (m, 4H), 0.89 (s, 3H), 0.73 (s, 3H)

3.40
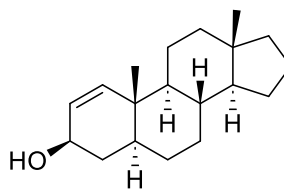
5α-androst-2-ene-3β-ol (3.39): This reaction was modified from a literature procedure. [29] To a -

78°C solution of 200 mg (0.724 mmol) α,β-unsaturated ketone **3.30** in dry THF was slowly

added 0.72 mL of a 1 M solution of DIBAL in THF. This reaction was let stir for 15 min before

quenching with 0.72 mL water, followed by the slow addition of 0.72 mL 4 N NaOH and 2.8 mL

water. This mixture was stirred for 15 minutes before the layer were separated and the aqueous layer was washed with 3 X 10 mL EtOAc. The organic layers were combined and dried with magnesium sulfate before solvent was removed under reduced pressure. The residue was purified by column chromatography (15% EtOAc/hexanes), leaving compound **3.40** as a white powder in 10% yield. ^{1}H NMR (400 MHz, CDCl$_3$) δ 5.92 (dd, J = 10.2, 1.8, 1H), 5.48 (dt, J = 10.2, 1.8, 1H), 4.31 (m, 1H), 1.8-1.5 (m, 6H), 1.5-1.22 (m, 8H), 1.22-1.03 (m, 4H), 1.03-0.76 (m, 6H), .70 (s, 3H)

3.42
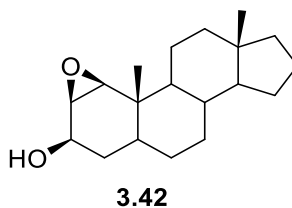
5α-androst-1β,2β -epoxy-3β-ol (3.42): 100 mg (0.367 mmol) α,β-unsaturated ketone **3.30** was dissolved in 1 mL DCM and a small scoop (~10 mg) sodium bicarbonate. To the reaction mixture was added 75 mg (0.44 mmol) mCPBA. The reaction was stirred for 3 hours at room temperature before the reaction was stopped with 1 ml 5% sodium bicarbonate. The layers were separated and the organics were washed with 1 mL saturated sodium thiosulfate. The organics were and dried with magnesium sulfate and filtered. The organics were removed under reduced pressure and the residue was subjected to column chromatography (5% MeOH/DCM) before concentration yielded epoxide **3.42** as a white powder in 18% yield. ^{1}H NMR (400 MHz, CDCl$_3$) δ 4.06-3.96 (m, 1H), 3.25 (t, *J* = 2.9, 1H) 1.81-1.53 (m, 6H), 1.51-1.36 (m, 8H), 1.35-1.06 (m, 4H), 1.03-0.76 (m, 6H), 0.73 (s, 3H)

3.45
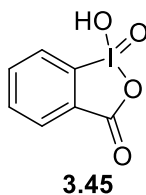
2-iodoxybenzoic acid (**3.45**): **3.45** was synthesized using a modified literature procedure. [34] 75 g (121.9 mmol) oxone was added to 250 mL deionized water, then stirred until dissolved, to which was added 15 g (60.4 mmol) 2-iodobenzoic acid. The mixture was heated to 80°C and stirred for 6 hrs. This was then cooled in an ice bath for 1.5 hours and the resulting solid was filtered. The solid was washed with six 100 mL portions of deionized water, then washed twice with 100 mL acetone. This yielded the product as a white powder (13.62 g, 81%). ^{1}H NMR (400 MHz, CDCl$_3$) δ 8.14 (d, J = 8, 1H), 8.04-7.98 (m, 2H), 7.84 (t, J = 7.2, 1H).

3.5 References

1.   Hofmann, K. A superfamily of membrane-bound O-acyltransferases with implications for wnt signaling. *Trends Biochem Sci* **2000**, *25* (3), 111-112. DOI: 10.1016/s0968-0004(99)01539-x.

2.   Yang, J.; Zhao, T. J.; Goldstein, J. L.; Brown, M. S. Inhibition of ghrelin O-acyltransferase (GOAT) by octanoylated pentapeptides. *Proceedings of the National Academy of Sciences of the United States of America* **2008**, *105* (31), 10750-10755, Article. DOI: 10.1073/pnas.0805353105 Scopus.

3.   Gutierrez, J. A.; Solenberg, P. J.; Perkins, D. R.; Willency, J. A.; Knierman, M. D.; Jin, Z.; Witcher, D. R.; Luo, S.; Onyia, J. E.; Hale, J. E. Ghrelin octanoylation mediated by an orphan lipid transferase. *Proc Natl Acad Sci U S A* **2008**, *105* (17), 6320-6325. DOI: 10.1073/pnas.0800708105.

4.   Taylor, M. S.; Ruch, T. R.; Hsiao, P.-Y.; Hwang, Y.; Zhang, P.; Dai, L.; Ran Lisa Huang, C.; Berndsen, C. E.; Kim, M.-S.; Pandey, A.; et al. Architectural Organization of the Metabolic Regulatory Enzyme Ghrelin O-Acyltransferase. *Journal of Biological Chemistry* **2013**, *288* (45), 32211-32228. DOI: 10.1074/jbc.M113.510313 From American Chemical Society . All Rights Reserved. CAPLUS.

5.   Ma, D.; Wang, Z.; Merrikh, C. N.; Lang, K. S.; Lu, P.; Li, X.; Merrikh, H.; Rao, Z.; Xu, W. Crystal structure of a membrane-bound O-acyltransferase. *Nature (London, U. K.)* **2018**, *562* (7726), 286-290, 10.1038/s41586-018-0568-2. DOI: 10.1038/s41586-018-0568-2.

6.   Qian, H.; Zhao, X.; Yan, R.; Yao, X.; Gao, S.; Sun, X.; Du, X.; Yang, H.; Wong, C. C. L.; Yan, N. Structural basis for catalysis and substrate specificity of human ACAT1. *Nature* **2020**, *581* (7808), 333-338. DOI: 10.1038/s41586-020-2290-0 From NLM Medline.

7.   Long, T.; Liu, Y.; Li, X. Molecular structures of human ACAT2 disclose mechanism for selective inhibition. *Structure* **2021**, *29* (12), 1410-1418 e1414. DOI: 10.1016/j.str.2021.07.009 From NLM Medline.

8.   Wang, L.; Qian, H.; Nian, Y.; Han, Y.; Ren, Z.; Zhang, H.; Hu, L.; Prasad, B. V. V.; Laganowsky, A.; Yan, N.; Zhou, M. Structure and mechanism of human diacylglycerol O-acyltransferase 1. *Nature* **2020**, *581* (7808), 329-332. DOI: 10.1038/s41586-020-2280-2 From NLM Medline.

9.   Liu, Y.; Qi, X.; Donnelly, L.; Elghobashi-Meinhardt, N.; Long, T.; Zhou, R. W.; Sun, Y.; Wang, B.; Li, X. Mechanisms and inhibition of Porcupine-mediated Wnt acylation. *Nature* **2022**, *607* (7920), 816-822. DOI: 10.1038/s41586-022-04952-2.

10.   Campaña, M. B.; Irudayanathan, F. J.; Davis, T. R.; McGovern-Gooch, K. R.; Loftus, R.; Ashkar, M.; Escoffery, N.; Navarro, M.; Sieburg, M. A.; nangia, S.; Hougland, J. L. Molecular architecture of a membrane-spanning hormone acyltransferase required for metabolic regulation. *bioRxiv* **2019**, 556233. DOI: 10.1101/556233.

11.   McGovern-Gooch, K. R.; Mahajani, N. S.; Garagozzo, A.; Schramm, A. J.; Hannah, L. G.; Sieburg, M. A.; Chisholm, J. D.; Hougland, J. L. Synthetic Triterpenoid Inhibition of Human Ghrelin O-Acyltransferase: The Involvement of a Functionally Required Cysteine Provides Mechanistic Insight into Ghrelin Acylation. *Biochemistry* **2017**, *56* (7), 919-931. DOI: 10.1021/acs.biochem.6b01008.

12.   Couch, R. D.; Browning, R. G.; Honda, T.; Gribble, G. W.; Wright, D. L.; Sporn, M. B.; Anderson, A. C. Studies on the reactivity of CDDO, a promising new chemopreventive and chemotherapeutic agent: implications for a molecular mechanism of action. *Bioorg Med Chem Lett* **2005**, *15* (9), 2215-2219. DOI: 10.1016/j.bmcl.2005.03.031.

13. Duplan, V.; Hoshino, M.; Li, W.; Honda, T.; Fujita, M. In Situ Observation of Thiol Michael Addition to a Reversible Covalent Drug in a Crystalline Sponge. *Angew Chem Int Ed Engl* **2016**, *55* (16), 4919-4923. DOI: 10.1002/anie.201509801.

14. Bednar, R. A. Reactivity and pH dependence of thiol conjugation to N-ethylmaleimide: detection of a conformational change in chalcone isomerase. *Biochemistry* **1990**, *29* (15), 3684-3690. DOI: 10.1021/bi00467a014.

15. Kowaltowski, A. J.; Vercesi, A. E.; Castilho, R. F. Mitochondrial membrane protein thiol reactivity with N-ethylmaleimide or mersalyl is modified by Ca2+: correlation with mitochondrial permeability transition. *Biochim Biophys Acta* **1997**, *1318* (3), 395-402. DOI: 10.1016/s0005-2728(96)00111-9.

16. Storer, A. C.; Menard, R. Catalytic mechanism in papain family of cysteine peptidases. *Methods Enzymol* **1994**, *244*, 486-500. DOI: 10.1016/0076-6879(94)44035-2 From NLM Medline.

17. Stix, R.; Lee, C. J.; Faraldo-Gomez, J. D.; Banerjee, A. Structure and Mechanism of DHHC Protein Acyltransferases. *J Mol Biol* **2020**, *432* (18), 4983-4998. DOI: 10.1016/j.jmb.2020.05.023 From NLM Medline.

18. Karala, A. R.; Ruddock, L. W. Does s-methyl methanethiosulfonate trap the thiol-disulfide state of proteins? *Antioxid Redox Signal* **2007**, *9* (4), 527-531. DOI: 10.1089/ars.2006.1473.

19. Makarov, V. A.; Tikhomirova, N. K.; Savvateeva, L. V.; Petushkova, A. I.; Serebryakova, M. V.; Baksheeva, V. E.; Gorokhovets, N. V.; Zernii, E. Y.; Zamyatnin, A. A., Jr. Novel applications of modification of thiol enzymes and redox-regulated proteins using S-methyl methanethiosulfonate (MMTS). *Biochim Biophys Acta Proteins Proteom* **2019**, *1867* (11), 140259. DOI: 10.1016/j.bbapap.2019.07.012.

20.   Lowther, W. T.; Brot, N.; Weissbach, H.; Honek, J. F.; Matthews, B. W. Thiol-disulfide exchange is involved in the catalytic mechanism of peptide methionine sulfoxide reductase. *Proceedings of the National Academy of Sciences* **2000**, *97* (12), 6463-6468. DOI: 10.1073/pnas.97.12.6463.

21.   Mascia, M. P.; Trudell, J. R.; Harris, R. A. Specific binding sites for alcohols and anesthetics on ligand-gated ion channels. *Proc Natl Acad Sci U S A* **2000**, *97* (16), 9305-9310. DOI: 10.1073/pnas.160128797.

22.   Horne, J. E.; Walko, M.; Calabrese, A. N.; Levenstein, M. A.; Brockwell, D. J.; Kapur, N.; Wilson, A. J.; Radford, S. E. Rapid Mapping of Protein Interactions Using Tag-Transfer Photocrosslinkers. *Angew Chem Int Ed Engl* **2018**, *57* (51), 16688-16692. DOI: 10.1002/anie.201809149.

23.   Darling, J. E.; Zhao, F.; Loftus, R. J.; Patton, L. M.; Gibbs, R. A.; Hougland, J. L. Structure-Activity Analysis of Human Ghrelin O-Acyltransferase Reveals Chemical Determinants of Ghrelin Selectivity and Acyl Group Recognition. *Biochemistry* **2015**, *54* (4), 1100-1110. DOI: 10.1021/bi5010359 From American Chemical Society . All Rights Reserved. CAPLUS.

24.   Duffy, B. C.; Howard, K. T.; Chisholm, J. D. Alkylation of thiols with trichloroacetimidates under neutral conditions. *Tetrahedron Letters* **2015**, *56* (23), 3301-3305. DOI: 10.1016/j.tetlet.2014.12.042.

25.   Zhai, X.; Meek, T. D. Catalytic Mechanism of Cruzain from Trypanosoma cruzi As Determined from Solvent Kinetic Isotope Effects of Steady-State and Pre-Steady-State Kinetics. *Biochemistry* **2018**, *57* (22), 3176-3190. DOI: 10.1021/acs.biochem.7b01250.

26.   Chenna, B. C.; Li, L.; Mellott, D. M.; Zhai, X.; Siqueira-Neto, J. L.; Calvet Alvarez, C.; Bernatchez, J. A.; Desormeaux, E.; Alvarez Hernandez, E.; Gomez, J.; et al. Peptidomimetic Vinyl Heterocyclic Inhibitors of Cruzain Effect Antitrypanosomal Activity. *J Med Chem* **2020**, *63* (6), 3298-3316. DOI: 10.1021/acs.jmedchem.9b02078 From NLM Medline.

27.   Wong, M. H.; Bryan, H. K.; Copple, I. M.; Jenkins, R. E.; Chiu, P. H.; Bibby, J.; Berry, N. G.; Kitteringham, N. R.; Goldring, C. E.; O'Neill, P. M.; Park, B. K. Design and Synthesis of Irreversible Analogues of Bardoxolone Methyl for the Identification of Pharmacologically Relevant Targets and Interaction Sites. *J Med Chem* **2016**, *59* (6), 2396-2409. DOI: 10.1021/acs.jmedchem.5b01292.

28.   Cambie, R. C.; Potter, G. J.; Rutledge, P. S.; Woodgate, P. D. The Prévost reaction with 5α-androst-2-ene. *J. Chem. Soc., Perkin Trans. 1* **1977**, (5), 530-537. DOI: 10.1039/p19770000530.

29.   Laing, S. B.; Sykes, P. J. Synthetic steroids. Part IV. The reaction of 3β-hydroxy-5α-cholest-1-ene and 3β-hydroxycholest-4-ene with toluene-p-sulphonyl chloride in pyridine. *J. Chem. Soc. C* **1968**, *0* (0), 421-427. DOI: 10.1039/j39680000421.

30.   Riddles, P. W. B., R. L.; Zerner, B., . Ellman's reagent: 5,5'-dithiobis(2-nitrobenzoic acid)--a reexamination. *Analytical Biochemistry* **1979**, *94* (1), 75-81.

31.   Pangborn, A. B.; Giardello, M. A.; Grubbs, R. H.; Rosen, R. K.; Timmers, F. J. Safe and convenient procedure for solvent purification. *Organometallics* **1996**, *15* (5), 1518-1520. DOI: DOI 10.1021/om9503712.

32.   Grayson, E. J.; Ward, S. J.; Hall, A. L.; Rendle, P. M.; Gamblin, D. P.; Batsanov, A. S.; Davis, B. G. Glycosyl disulfides: novel glycosylating reagents with flexible aglycon alteration. *J Org Chem* **2005**, *70* (24), 9740-9754. DOI: 10.1021/jo051374j.

33.   Quinkert, G.; Englert, H.; Cech, F.; Stegk, A.; Haupt, E.; Leibfritz, D.; Rehm, D.

Lichtinduzierte Reaktionen, XIII. Über das seco-isomere Dienylketen aus 2,4-Androstadien-l-on.

Chemische Berichte **1979**, *112* (1), 310-348. DOI: 10.1002/cber.19791120129.

34.   Frigerio, M.; Santagostino, M.; Sputore, S. A User-Friendly Entry to 2-Iodoxybenzoic

Acid (IBX). *The Journal of Organic Chemistry* **1999**, *64* (12), 4537-4538. DOI:

10.1021/jo9824596.

Chapter 4: Privileged electrophile inhibition of GOAT supports involvement of an activated serine/threonine in GOAT catalysis

4.1 Introduction

As described in Chapter 3, it is unlikely that GOAT is utilizing a catalytic cysteine even through there are functionally essential cysteines within the enzyme implicated by inhibitor studies. An alternate proposed mechanism for GOAT activity would utilize an active site network similar to that of serine hydrolases, utilizing either a direct transfer or acyl-enzyme intermediate mechanism (**Figure 4.1**). [1-3] Previous attempts to determine the site of catalytic activity in serine hydrolases utilized molecules known as "privileged electrophiles," compounds that feature a low-reactivity electrophile. [4, 5] Due to the low reactivity of these privileged electrophiles, the warheads can be tailored to target specific residues with enhanced nucleophilicity, particularly those that are activated by an active site network. [6, 7] As such, many of these privileged electrophiles have been used in activity-based probe (ABP) experiments to identify enzymes utilizing specific residues or the location of catalytic residues in complex systems. [8, 9]

Activated serines are a common target for privileged electrophiles, and a wide array of serine-reactive warheads have been reported. These warheads are shown in **Figure 4.2** and include isocoumarins, [5, 10, 11] aminoalkyl diphenyl phosphonates, [12-15] mixed phenyl phosphonate and phosphinate esters, [16, 17] benzoxazinones, [18] oxolactams, [19, 20] phosphoramidates, [21] sulfonyl fluorides, [6, 22-24] triazole ureas, [25, 26] and fluorophosphonates. [27-29]
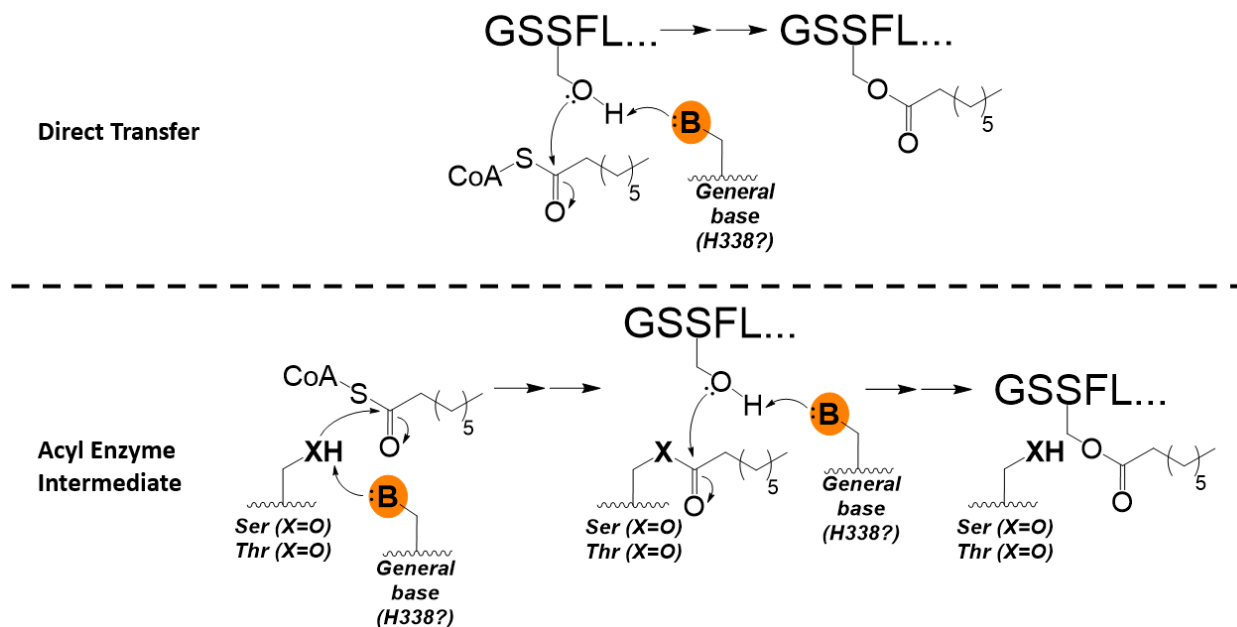
Figure 4.1 Potential mechanisms for GOAT acylation of ghrelin. a.) Proposed direct transfer mechanism, with ghrelin being activated by a general base and directly receiving the octanoylation from octanoyl-CoA. **b.)** Proposed acyl enzyme intermediate mechanism, with an as-yet-unknown activated nucleophile on GOAT accepting the octanoyl moiety before transferring to the ghrelin substrate.
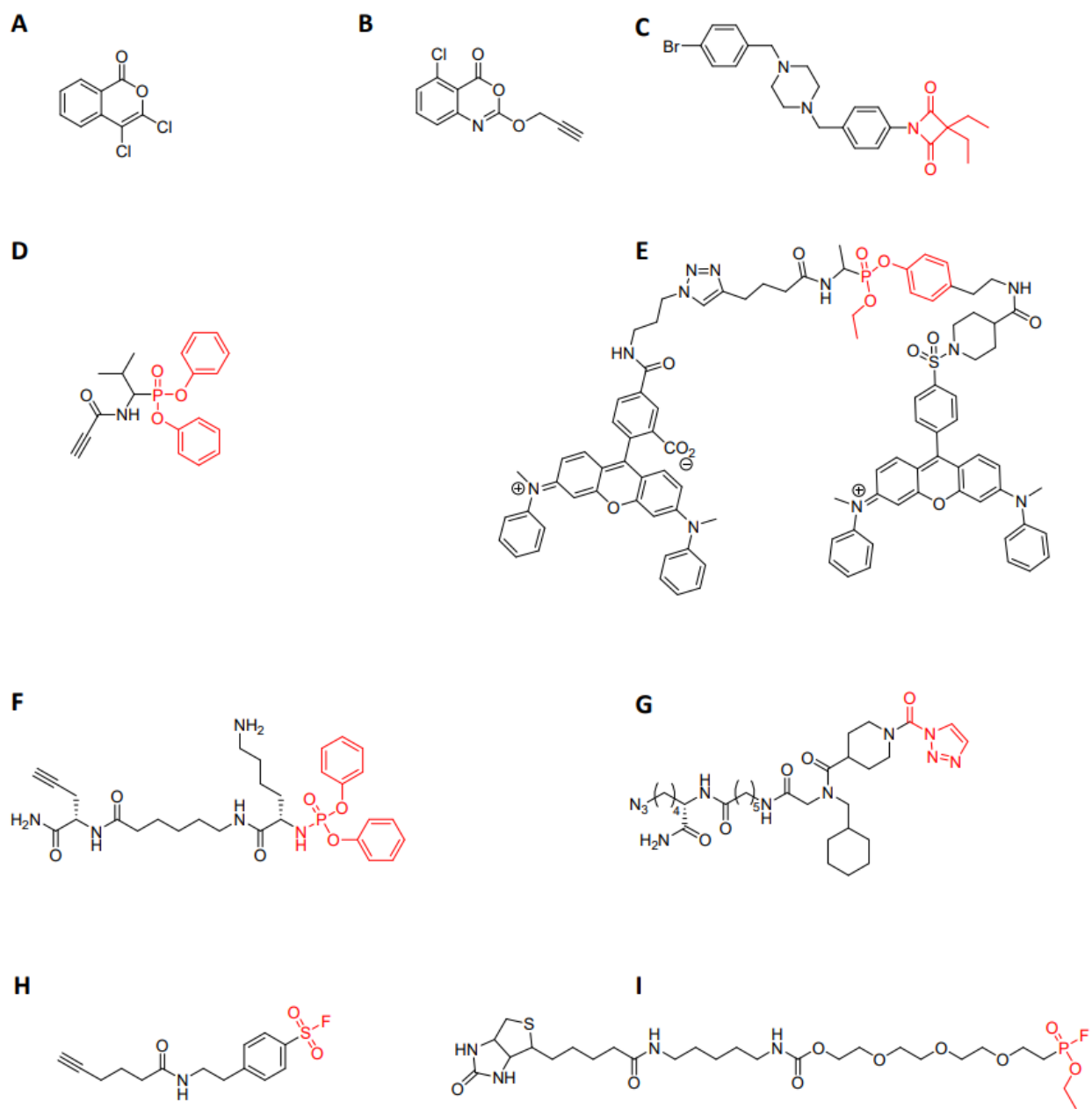
Figure 4.2. Molecules representing privileged electrophiles used for probing activated nucleophiles. For larger scaffolds, electrophilic warhead is represented in red. **a.)** The structure of 3,4-dichloroisocoumarin. **b.)** Benzoxanin-4-one. [18] **c.)** 4-oxo-β-lactam. [20] **d.)** Aminoalkyl diphenyl phosphonate. [15] **e.)** Mixed phenyl phosphonate. [17] **f.)** Phosphoramidate. [21] **g.)** Triazole urea. [25] **h.)** Sulfonyl fluoride. [23] **i.)** Fluorophosphonate. [28]

As threonine and serine share a hydroxyl functionality, molecules that react with serine also have the ability to cross-react with threonine. Radiolabeled DCI has been used to make arguments about the identity of unknown catalytic sites allowing for identification of a threonine residue in the proteasome. [30] Carboxy-terminal vinyl sulfones and α,β epoxyketones have been used to target the catalytic threonine in the β subunit of the proteasome. [31, 32]

Other nucleophilic residues also have the possibility to react with privileged electrophiles. An adapted sulfonyl fluoride probe has been used to label catalytic tyrosine residues of glutathione transferases in plants and mice, further indicating the chemical scope of the sulfonyl fluoride probing capabilities. [33] Sulfonyl fluorides are also capable of reacting with catalytic lysines, having been used to label and detect active kinases in cell lysates and intact cells. [34, 35] DCI does not directly react with histidine, but the generation of an acyl chloride during ring opening by the initial nucleophile allows a secondary reaction with a nearby histidine to occur (**Scheme 4.1**). [36, 37] Due to the minor ambiguity in the targeting of the molecules involved in targeting activated nucleophile, the term "activated serine" could therefore be multiple nucleophilic amino acids for the purposes of this chapter.

Scheme 4.1: Reaction of 3,4 dichloroisocoumarin with activated serine. 3,4-

dichloroisocoumarin (DCI, **Compound 4.1**) reacts with activated nucleophiles to produce a

covalent adduct that can further react with adjacent histidine.[37, 38]
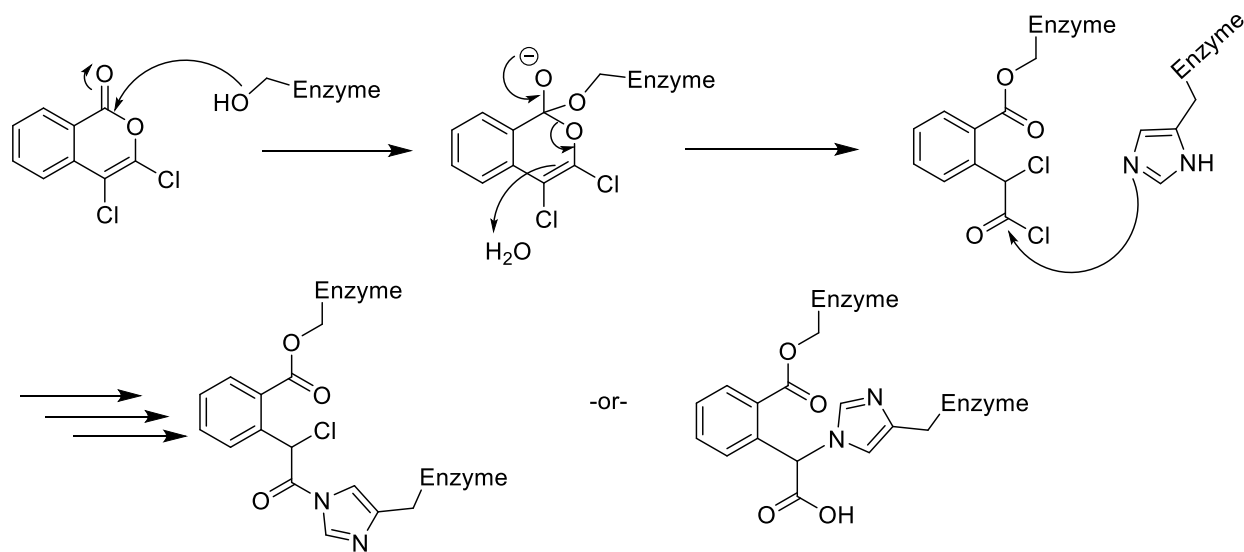
4.1.1 Utilization of privileged electrophiles

3,4-dichloroisocoumarin (DCI, **Compound 4.1**) is an example of a privileged electrophile with a long history of being used to study serine proteases. [37, 39] Isocoumarins react with an activated serine by forming a covalent bond through a ring opening reaction, which can then be further stabilized through a secondary reaction with nearby nucleophilic residues such as histidine (**Scheme 4.1**). [10, 38, 40, 41] DCI has also been shown to be specific for serines, exhibiting little to no activity against cysteine- and metallo-proteases while working as a general serine protease inhibitor. [37] While DCI is a powerful serine protease inhibitor, the short half-life of the compound in common buffers limited the use of the compound and instigated the development of 3- and 7- substituted isocoumarins with significantly increased stability. [37, 39] The expansion of this chemical scaffold also increased the ability of the scaffold to be altered to increase selectivity and potency for studying specific enzymes, including human leukocyte elastase, porcine pancreatic elastase, and GlpG. [5, 41-43]

Another benefit to the addition of side-chains to the DCI scaffold was the introduction of functionality at these positions. Utilization of a biotin-linked isocoumarin derivative allowed the discovery of serine protease PfSUB1 as a key regulator of cell rupture in *Plasmodium falciparum* infected cells through biotin affinity blotting. [44, 45] Isocoumarins have also been modified with 3- or 7-position alkynes allowing for post-inhibition orthogonal reactions through click chemistry, allowing for whole-proteome detection of proteases. [5] The related class of benzoxazinones also can be used in labeling experiments, with alkynyl benzoxazinones functionalized with biotin through click chemistry allowing for isolation of labeled serine proteases. [18]

Diphenyl phosphonates have been used for similar types of labeling experiments, with a recent study using biotin-labeled diphenyl phosphonate probe identifying the proteases

urokinase-type plasminogen activator and tissue plasminogen activator as drivers in ovarian clear cell carcinoma through a streptavidin-biotin pull-down assay. [46] These phosphonates have also been able to be tuned in order to modulate the selectivity of the molecule via extended recognition peptide sequences, allowing for labeling of proteases of different specificities in cell lysate. [15]

The specificity of DCI has been used to support enzyme mechanistic studies, or to identify catalytic residues in enzymes, as shown with the identification of catalytic threonine in the proteasome. [30] DCI was also used in the identification of rhomboids as atypical serine proteases. [47] This insight was then used to crystalize an isocoumarin derivative in the active site of GlpG, which revealed conformational changes in the acyl-enzyme structure, providing insight into the structure of the active site and mechanism of the enzyme. [9, 43]

Alkyne-labeled sulfonyl fluorides have been found capable of enriching and identifying proteases from cell lysate, as well as labeling live cells. [23] Due to the reactivity of this molecule and possibility of off-target reactions with serine, threonine, tyrosine, and lysine, care must be taken to provide specificity for these molecules through their targeting region. Sulfonyl fluorides have also been utilized as mechanistic probes of enzymes. Comparative rate studies performed by Fahrney et al. utilizing a series of sulfonyl fluorides revealed that acetylcholinesterase and chymotrypsin do not undergo an immediate S_N2 reaction with the warhead and instead are governed by the initial binding of the sulfonyl fluorides to the enzyme. [22]

4.2 Results

4.2.1 Screening of 3,4 dichloroisocoumarin reveals new avenue for GOAT inhibition

To probe for the involvement of an activated serine in in the catalysis of hGOAT, DCI (**4.1**) was tested in duplicate at three concentrations (10 µM, 100 µM, and 1000 µM) for potential inhibition (**Figure 4.3**) using our standard HPLC-based fluorescence screen. Under these conditions, DCI inhibited hGOAT, with concentrations of 100 µM reducing hGOAT to approximately 50% activity, indicating DCI had potential for development as a probe for GOAT. To evaluate the potency of DCI, the compound was tested against hGOAT and exhibited modest potency (**Figure 4.4**) of 87 ± 5 µM, consistent with our initial screen, which had indicated an apparent IC_{50} below the 100 µM data point.

The additional step of testing DCI against the mouse isoform of GOAT (mGOAT) was taken due to previous findings from the Hougland lab indicating that cysteine-modifying molecules including N-ethyl malemide (NEM) were unable to maintain potency when tested against mGOAT (**Figure 4.5**) .[48] In contrast to these findings, mGOAT was similarly inhibited when exposed to DCI, indicating that the targeted nucleophilic residue or residues are likely conserved, and more likely to be important to hGOAT catalytic activity due to their conservation.

In order to be effective probes of hGOAT catalytic site residues, the adduct formed from DCI would need to irreversibly label the residues. Inhibitor reversibility was tested by creating a master mix that was subjected to ten times the measured IC_{50} of the inhibitor, then either diluting the mixture to the IC_{50} or maintaining the high concentration before starting the
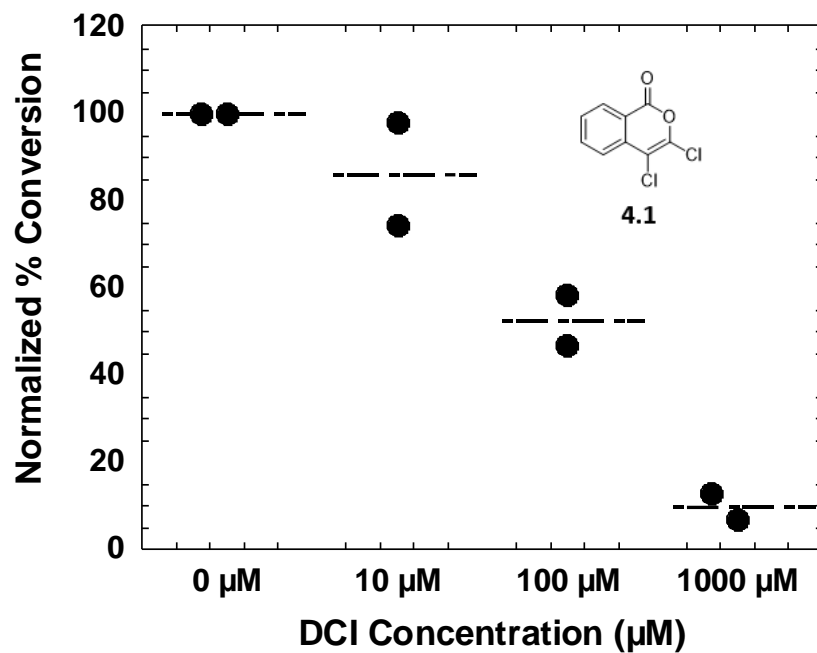
Figure 4.3: Initial screening of DCI indicates hGOAT inhibition. hGOAT was exposed to increasing concentrations of DCI at logarithmic scale. Reactions were run in duplicate and normalized to the vehicle control as described in Materials and Methods.
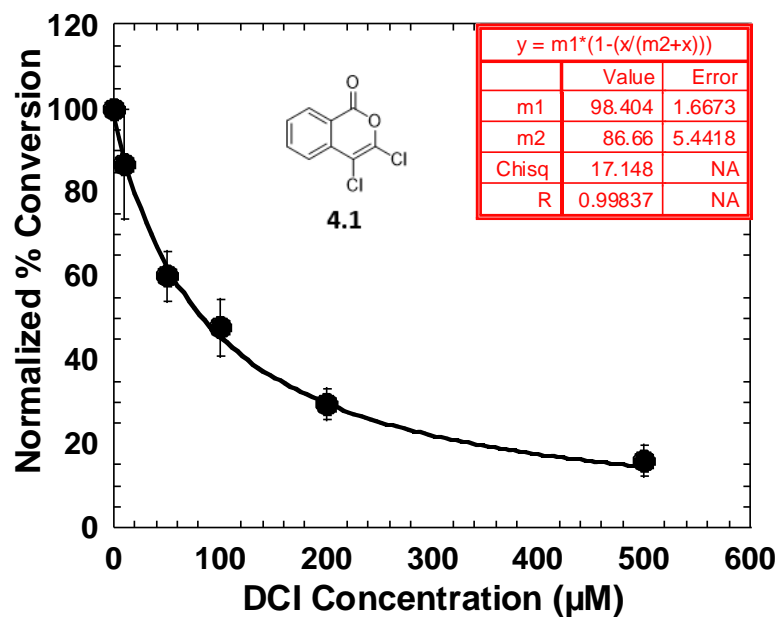
Figure 4.4: DCI effectively inhibits GOAT. Reactions were normalized to vehicle control as described in Materials and Methods. Error bars reflect standard deviation from three independent measurements
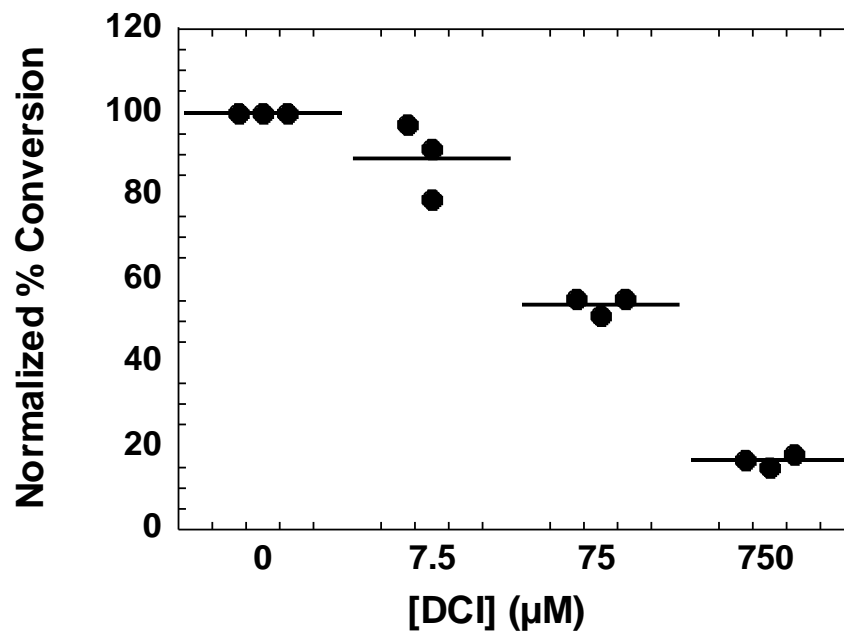
Figure 4.5: mGOAT activity is inhibited by DCI. The mouse isoform of GOAT is inhibited when exposed to concentrations similar to those which inhibit hGOAT. Reactions were normalized to vehicle control as described in Materials and Methods.

reaction (**Figure 4.6**). NSM-48, a previously discovered inhibitor of hGOAT, was used as the reversible control, while NEM was used as an irreversible control. [48] Inhibition with DCI did not reduce after dilution, indicating irreversible inhibition.

4.2.2 Synthesis of sulfonyl fluorides as probes for ghrelin O-acyltransferase

After finding a serine-targeting electrophile capable of inhibiting GOAT, explored other compounds with similar reactivity to determine whether the observed inhibition was specific to the isocoumarin scaffold. Sulfonyl fluorides are another series of privileged electrophiles established to react with activated serines. [4, 49]. Having seen increased potency with increased alkyl chain length in the methanethiosulfonates (Chapter 3), we synthesized *O*-butyl ethanesulfonyl fluoride from ethene sulfonyl fluoride and butanol using an approach that would allow similar diversity in the alkyl chain length (**Scheme 4.2**). This *O*-butyl sulfonyl fluoride exhibited significant inhibition at 10 mM, so we synthesized a series of alkane sulfonyl fluorides to explore the ability of varying chain lengths to increase potency. Consistent with the methanethiosulfonates, the *O*-heptyl and -octyl sulfonyl fluorides exhibit increased potency over mid-length chains (**Figure 4.7b**). By increasing the alkyl chain to 18 carbons with *O*-octadecyl sulfonyl fluoride, potency is lost. This chain-length dependence of the alkyl sulfonyl fluorides resembles the hGOAT chain-length dependence of alkyl-CoA derivatives, with those chain-lengths closest to the canonical eight-carbon octanoyl moiety exhibiting higher potency. [50] This similarity indicates the sulfonyl fluorides may be entering into the catalytic channel inside GOAT near the proposed CoA binding site, which must be near the site of catalysis to assist with the transfer of octanoate to ghrelin. [51]
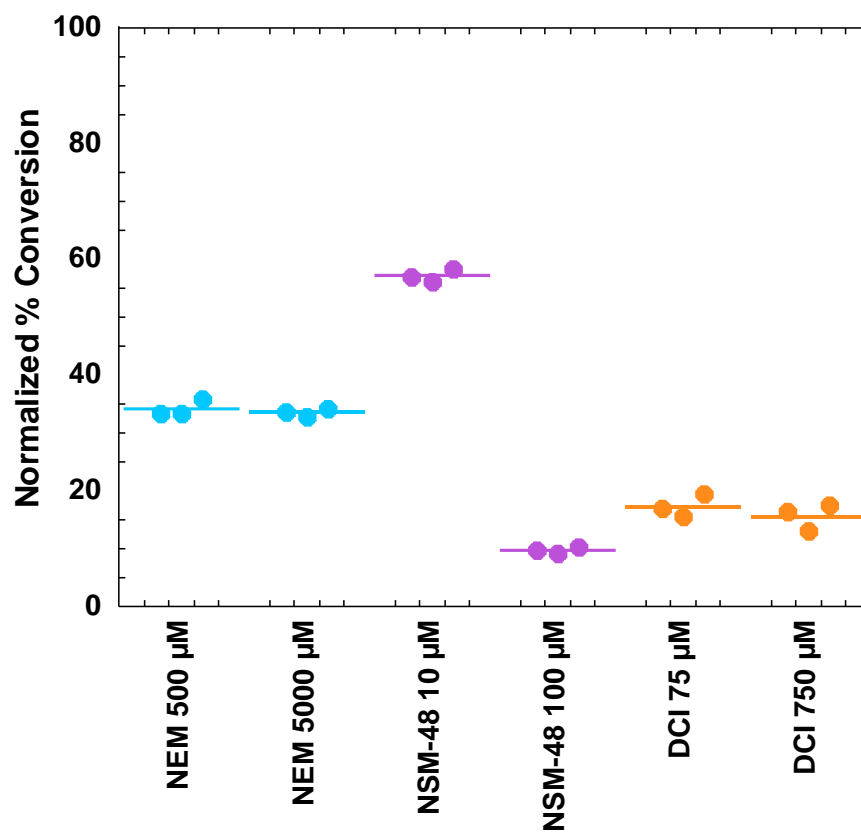
Figure 4.6: DCI irreversibly inhibits hGOAT. DCI compared to NEM (irreversible control) and NSM-48 (reversible control). Reactions were normalized to vehicle control as described in Materials and Methods.

To further explore the reactivity of these molecules, the pentyl (**Compound 4.3**) and

heptyl (**Compound 4.5**) sulfonyl fluorides were selected for reversibility testing. Both

molecules showed preliminary irreversible behavior (**Figure 4.8**) when compared to the NEM

and NSM-48 controls. To probe GOAT and identify the location of the residue modified by these

serine-reactive electrophiles, a class of sulfonyl fluorides containing terminal alkynes were

desired for labeling studies based on the initial alkane sulfonyl fluorides. These compounds were

synthesized in the same manner as the alkane sulfonyl fluorides (**Scheme 4.3**). Two compounds

were created in this way: *O*-pentynyl sulfonyl fluoride (**4.9**) and *O*-heptynyl sulfonyl fluoride

(**4.10**). When tested for reversibility against GOAT, both sulfonyl fluorides exhibited the desired

irreversible behavior (**Figure 4.9b**), further supporting the sulfonyl fluoride warhead as a tool for

probing GOAT. The heptynyl sulfonyl fluoride was also tested against mGOAT and was found

to inhibit mGOAT similarly to hGOAT (**Figure 4.10**), indicating that this molecule may be

targeting a conserved, potentially catalytic residue.

Scheme 4.2 General synthetic path for alkane sulfonyl fluorides.

n = 3-9, 17

(A)

4.2

4.4

4.6

4.3

4.5

4.7

4.8

(B)
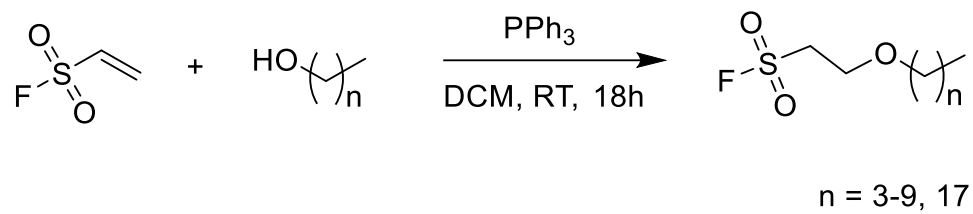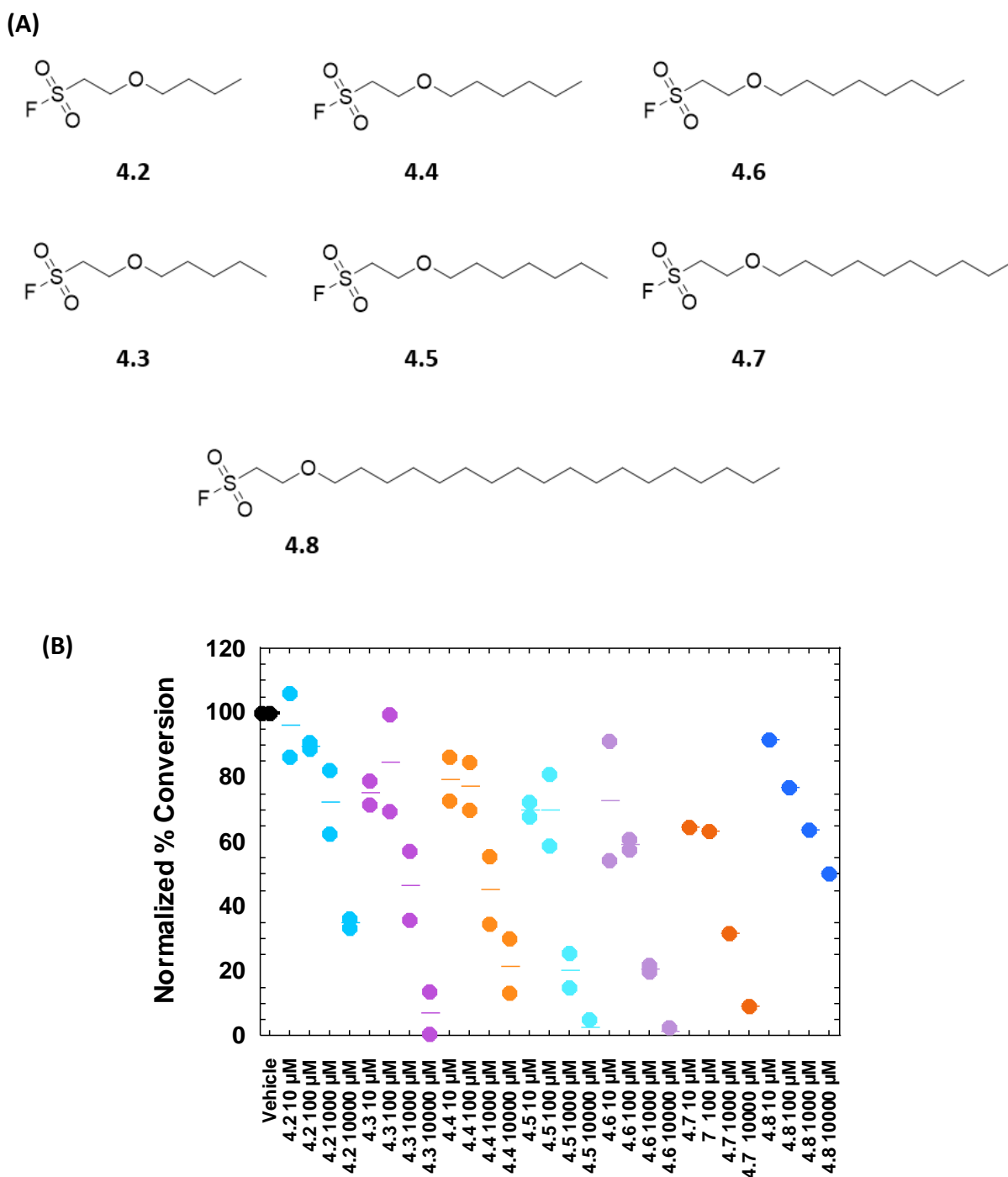
Figure 4.7: Initial screening of alkane sulfonyl fluorides reveals chain length dependence.
a.) Structures of alkane sulfonyl fluorides. **b.)** Alkane sulfonyl fluorides were tested at four logarithmic concentrations for activity against hGOAT. Two independent duplicate reactions were performed for each condition, except for *O*-decyl and O-octadecyl sulfonyl fluoride (**4.7** and **4.8**) which were performed as a single trial.
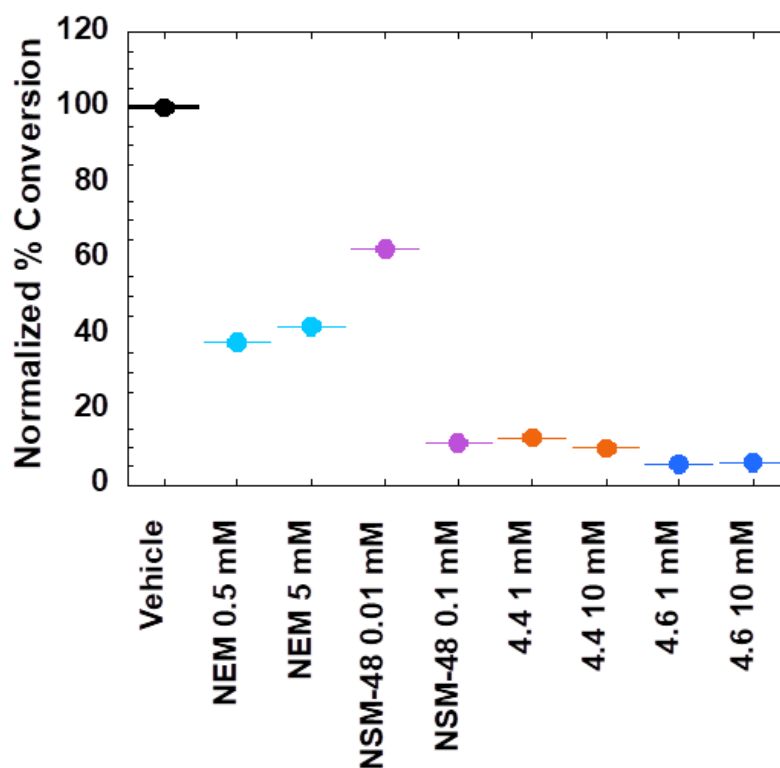
Figure 4.8: Initial reversibility test of sulfonyl fluorides indicate irreversible behavior

Single trial reaction to determine the potential utility of sulfonyl fluoride derivatives for labeling studies. Membrane fraction treated with inhibitor was diluted 10X, producing the measured $IC_{50.}$ Restoration of hGOAT activity under diluted condition (1X IC_{50}) indicates reversible inhibition by NSM-48, known reversible hGOAT inhibitor. NEM represents N-ethyl maleimide, known covalent irreversible inhibitor of hGOAT. [48] Compounds were tested in reactions containing 100 µg hGOAT-enriched membrane protein, 1.5 µM GSSFLC$_{AcDan}$ and 300 µM octanoyl-CoA in triplicate. Dots represent a single trial, bars represent the average of the trials. 1X IC_{50} concentrations were NEM: 500 µM, NSM-48: 10 µM, **4.4:** 1.0 mM, and **4.6**: 1.0 mM. 10X IC_{50} concentrations were NEM: 5.0 mM, NSM-48: 100 µM, **4.4:** 10 mM and **4.6:** 10 mM.

Scheme 4.3 Synthesis of alkynyl sulfonyl fluorides

n = 3,5
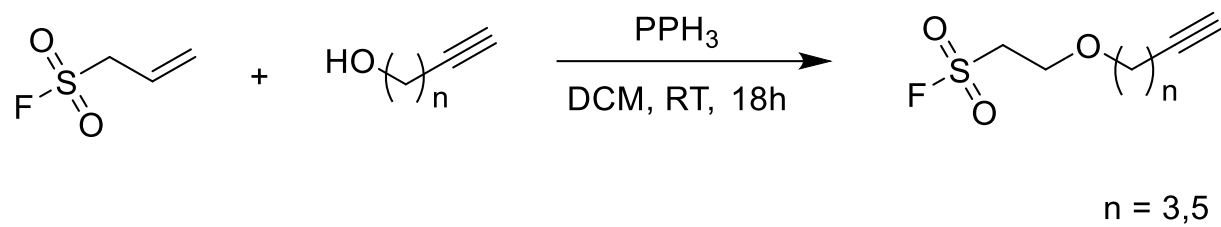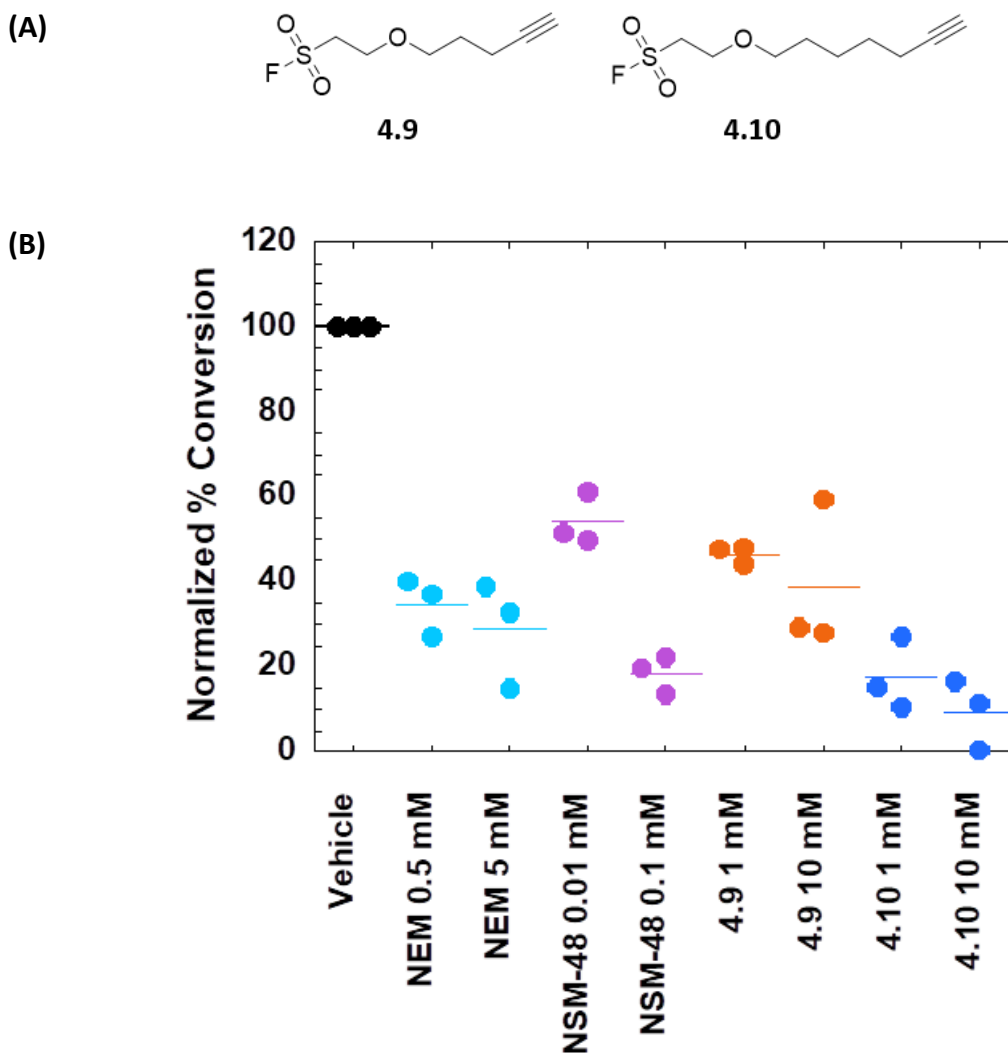
Figure 4.9: Alkynyl sulfonyl fluorides exhibit irreversible inhibition of hGOAT. a.) Structure of *O*-pentynyl and *O*-heptynyl sulfonyl fluoride. **b.)** *O*-pentynyl and *O*-heptynyl sulfonyl fluoride both indicate irreversible behavior when compared to NEM (irreversible control) and NSM-48 (reversible control). Reactions were performed in triplicate and normalized to vehicle control as described in Materials and Methods.
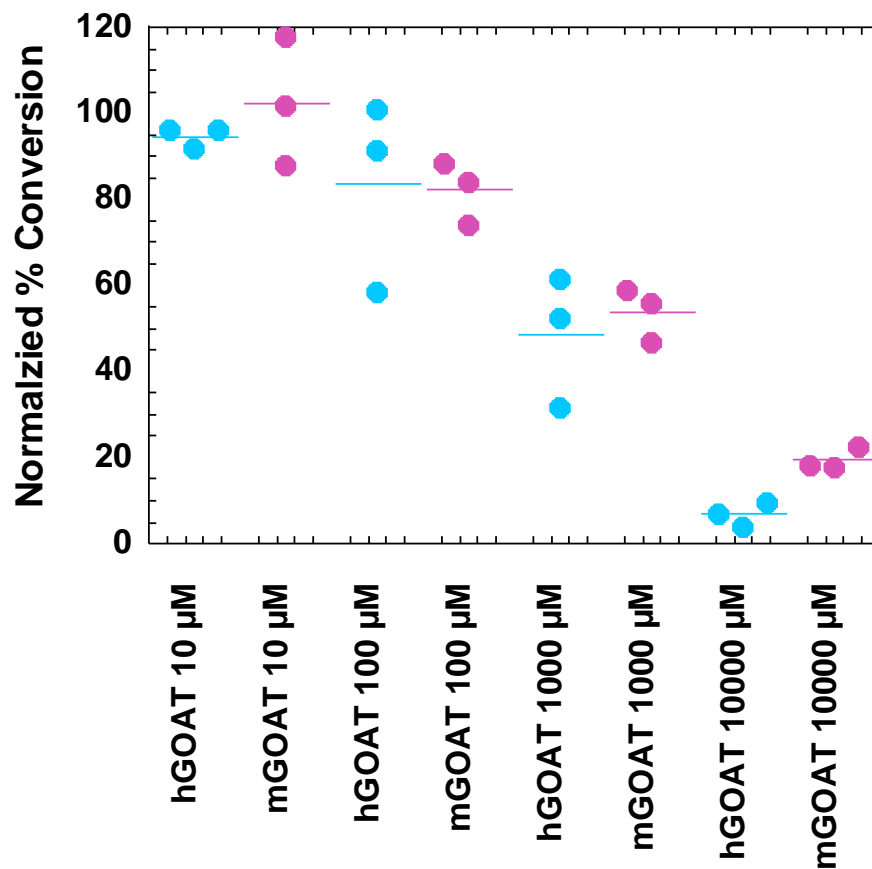
Figure 4.10: *O*-heptynyl sulfonyl fluoride (4.10) inhibits mGOAT. Inhibition with *O*-heptynyl sulfonyl fluoride reduces hGOAT and mGOAT activity to similar levels. Reactions were performed in triplicate and normalized to vehicle control as described in Materials and Methods.

4.2.3 Testing additional classes of privileged electrophiles leads to discovery of new classes of GOAT inhibiting warheads

To complement our studies of isocoumarin and sulfonyl fluoride warheads for targeting GOAT, Dr. Steven Verhelst (University of Leuven) generously provided a series of compounds capable of targeting activated serines. This series included alkyne derivatives of benzoxazinones, isocoumarins, phosphoramidates, diphenyl phosphonates, as well as several triazole urea compounds that contained azides for labeling rather than alkynes. [16-18, 21, 25, 38] This set of compounds was separated into three groups based on warhead type: benzoxazinones with the isocoumarins, the phosphoramidates with diphenyl phosphonates, and the triazole ureas. We utilized DCI as a positive control across theses samples to compare inhibition to a known serine-reactive molecule. The isocoumarin- and benzoxazinone-based inhibitors showed some promise as several compounds showed the ability to reduce ghrelin peptide conversion to product to ~75% at 100 μM inhibitor concentration (**Figure 4.11**), and compounds **4.13, 4.15, 4.16,** and **4.20** approached 60% conversion. Several diphenyl phosphonate inhibitors also were capable of inhibiting hGOAT, including one compound (**4.28**) with similar potency to DCI as well as four other compounds that inhibited to around 75% activity at 100 μM (**4.23, 4.24, 4.25** and **4.26**) (**Figure 4.12**). The triazole ureas tested in the initial screening did not reach the minimum threshold of 25% inhibition (lower than 75% hGOAT activity) at 100 μM to be considered for further testing (**Figure 4.13**). After completion of the initial screen, we selected six compounds that reduced hGOAT activity below the 75% activity threshold at 100 μM and showed concentration dependent inhibition for a verification screen. These six compounds were tested in triplicate with DCI acting as a positive control (**Figure 4.14**). This rescreening of the hit

(A)
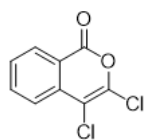
4.1
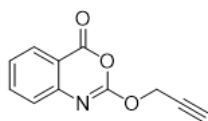
4.11
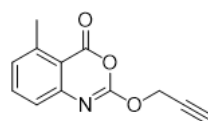
4.12
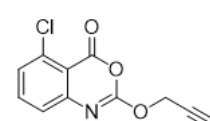
4.13
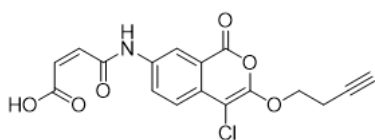
4.14
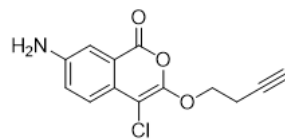
4.15
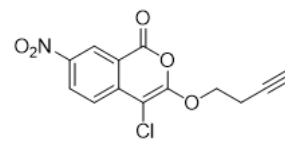
4.16
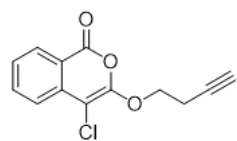
4.17
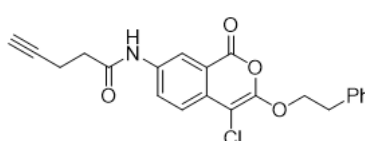
4.18
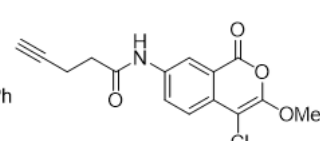
4.19
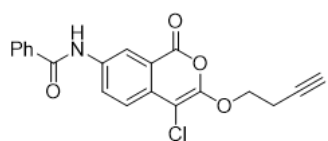
4.20
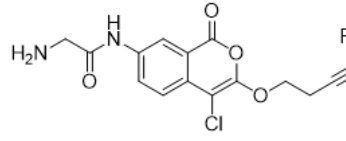
4.21
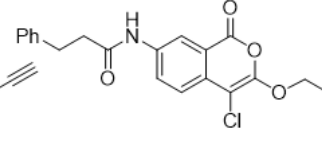
4.22
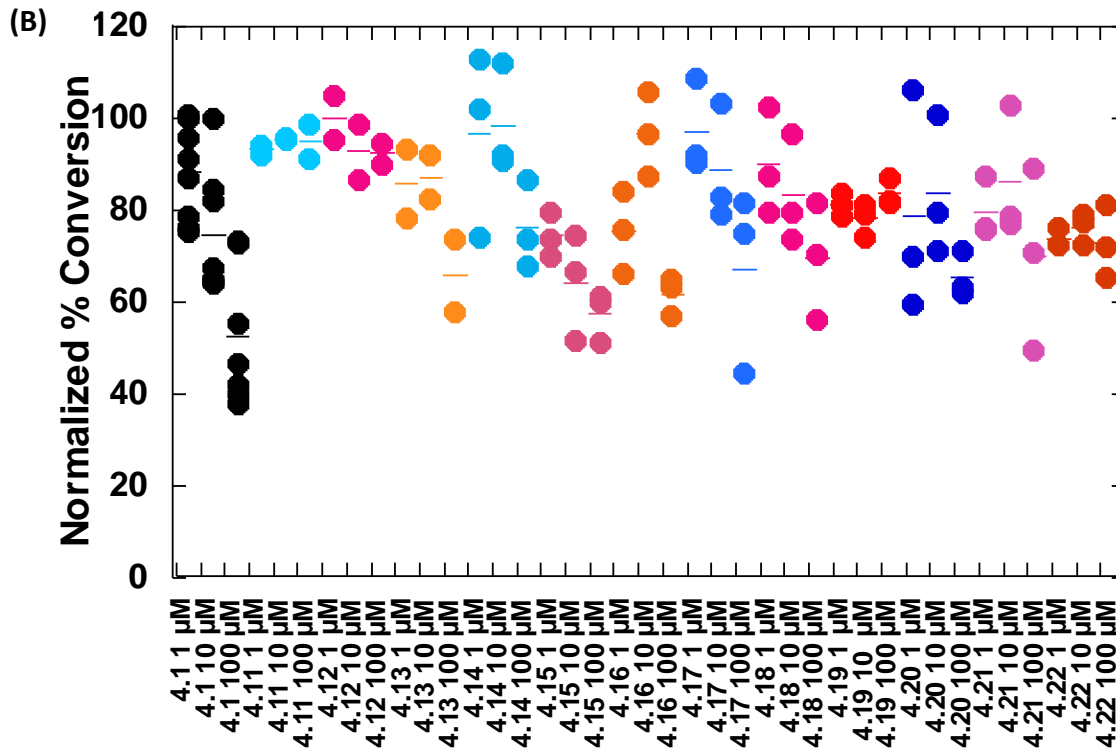
Figure 4.11: Initial screening of isocoumarin and benzoxazinone inhibitors reveals compounds of interest. a.) Structures of tested molecules. **b.)** Compounds were tested in triplicate at 1, 10, and 100 µM for an initial screen, with DCI acting as a positive control for privileged electrophile inhibition of hGOAT. Reactions were performed in at minimum in triplicate and normalized to vehicle control as described in Materials and Methods.
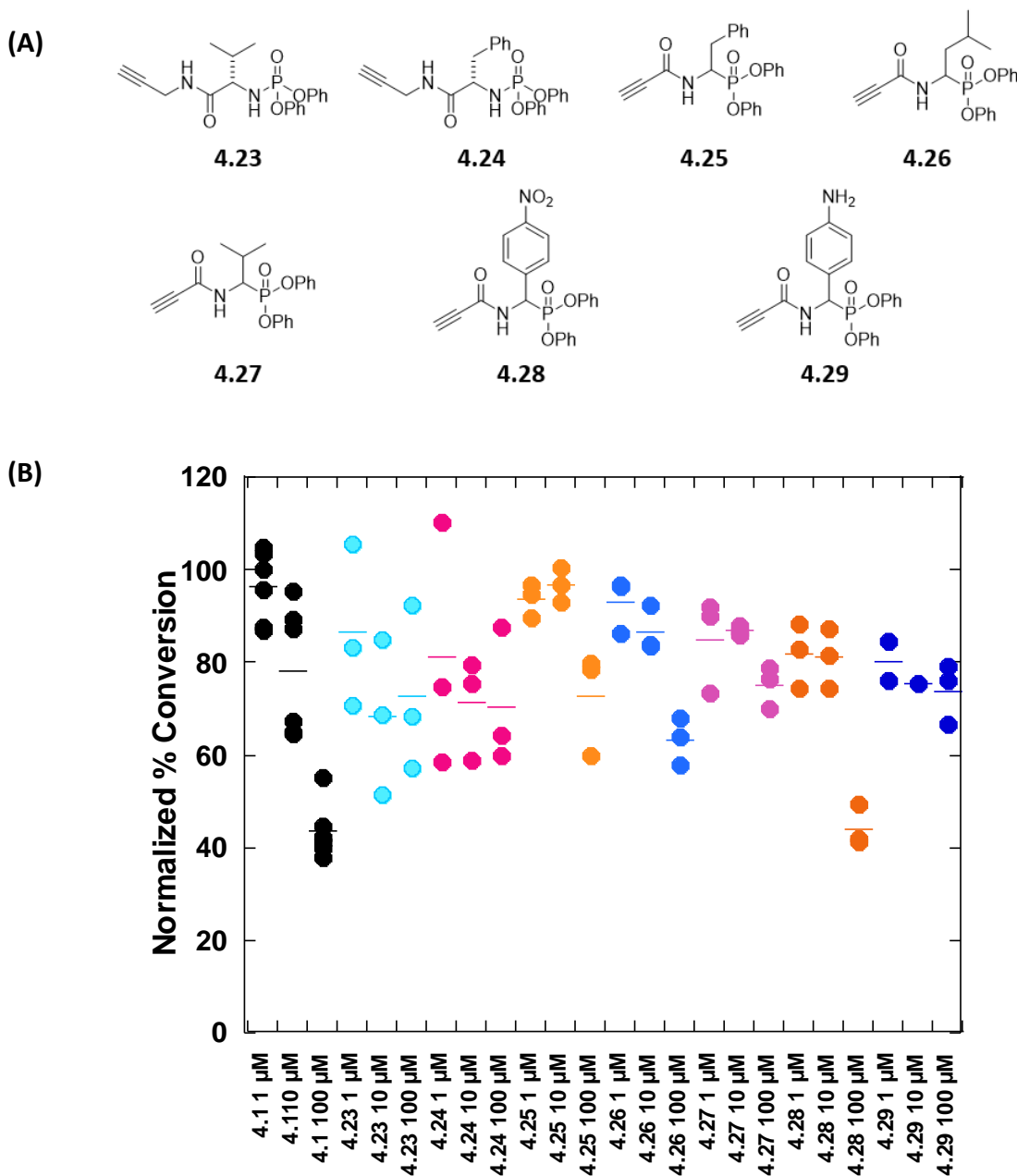
Figure 4.12: Diphenyl phosphonate and phosphoramidate inhibitors reveal new warhead for GOAT inhibition. a.) Structures of compounds tested. **b.)** Compounds were tested in triplicate at 1, 10, and 100 µM for an initial screen, with DCI acting as a positive control for privileged electrophile inhibition of hGOAT. Reactions were performed in at minimum in triplicate and normalized to vehicle control as described in Materials and Methods.

(A)

4.30

4.31

4.32
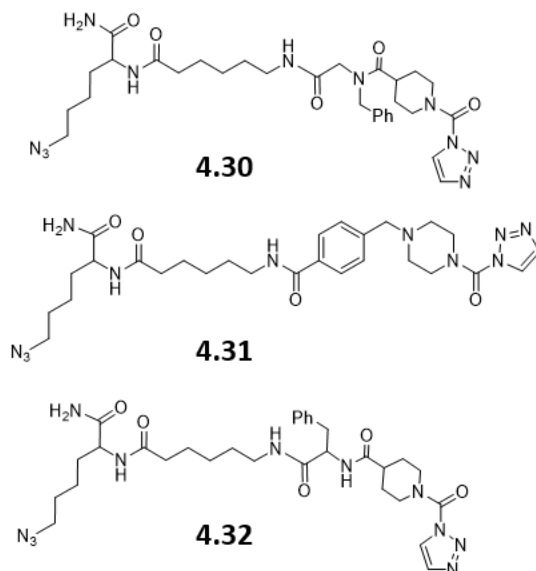
(B)
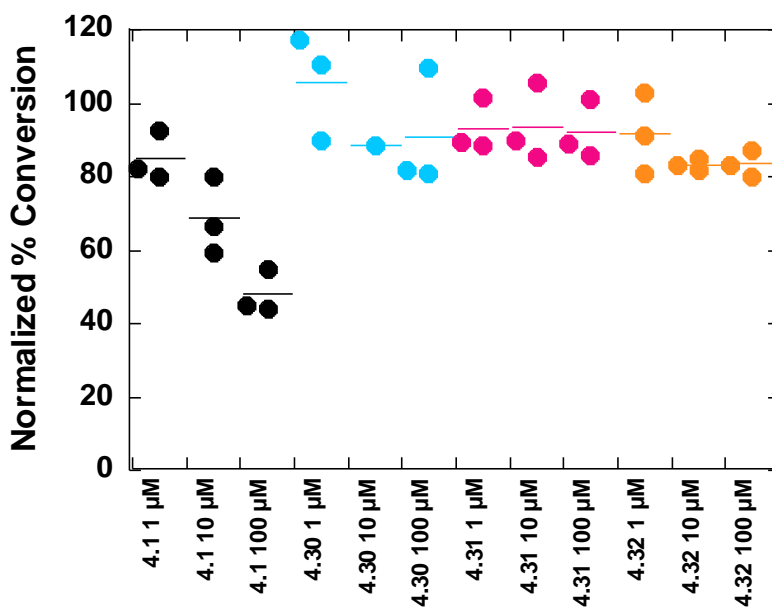
Figure 4.13: Triazole ureas do not inhibit hGOAT. a.) Structure of compounds tested. **b.)**
Compounds were tested in triplicate at 1, 10, and 100 µM for an initial screen, with DCI acting
as a positive control for privileged electrophile inhibition of hGOAT. Reactions were performed
in at minimum in triplicate and normalized to vehicle control as described in Materials and
Methods.

(A)

4.15   **4.16**   **4.17**

4.18   **4.28**   **4.29**
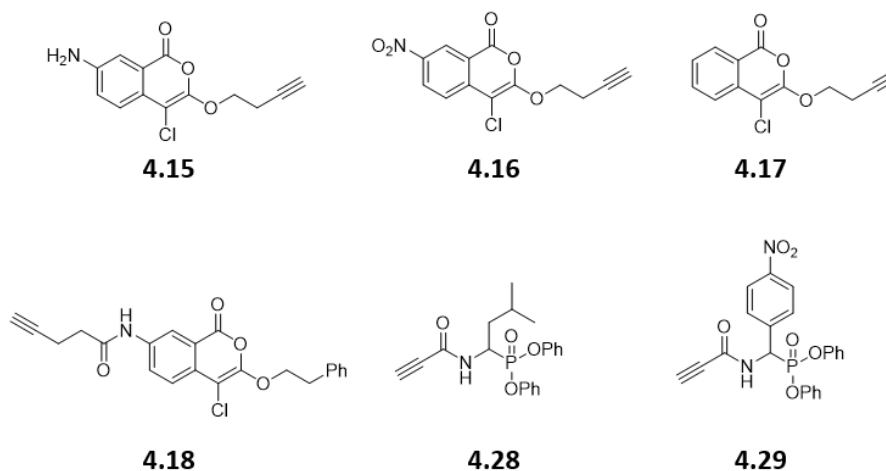
(B)
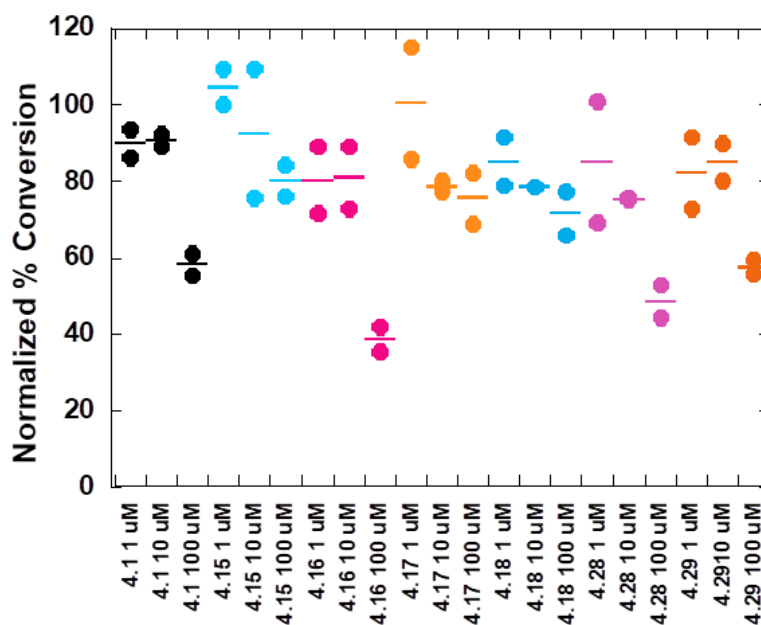
Figure 4.14: Validation testing of hit compounds identifies multiple classes of compounds.
a.) Compounds selected for secondary screening. **b.)** Compounds were tested in triplicate at 1,
10, and 100 µM for an initial screen, with DCI acting as a positive control for privileged
electrophile inhibition of hGOAT. Reactions were performed in at minimum in duplicate and
normalized to vehicle control as described in Materials and Methods. Dots represent a single trial
and bars represent the average of the trials.

compounds revealed that compounds **4.16, 4.26** and **4.28** are the most potent inhibitory

compounds. The potencies of these molecules as reflected by IC_{50} values were determined

(**Figure 4.15**). From this experiment, DCI (**4.1**) had a IC_{50} of 96 ± 11 µM (**Figure 4.15a**), within

error of the previously determined 86 ± 5 µM value. **Compound 4.16** (**Figure 4.15b**) is the most

potent inhibitor in our screen with an IC_{50} of 36 ± 16 µM. Compounds **4.26** and **4.28** are less

potent than DCI (**Figures 4.15c** and **4.15d** respectively), but still exhibit modest potencies of 148

± 35 µM and 107 ± 22 µM and represent a new class of compounds not previously reported to

inhibit GOAT. While these compounds are not as potent as DCI, they do contain alkyne

modifications that would allow for subsequent labeling using Copper-catalyzed Azide-Alkyne

Cycloaddition (CuAAC) with a fluorescent azide. [15, 38] Three of these compounds were selected

for reversibility studies, and all three exhibited irreversible behavior although compound **4.16** did

not inhibit to the level expected (**Figure 4.16**). DCI served as the positive control for irreversible

inhibition in these experiments.
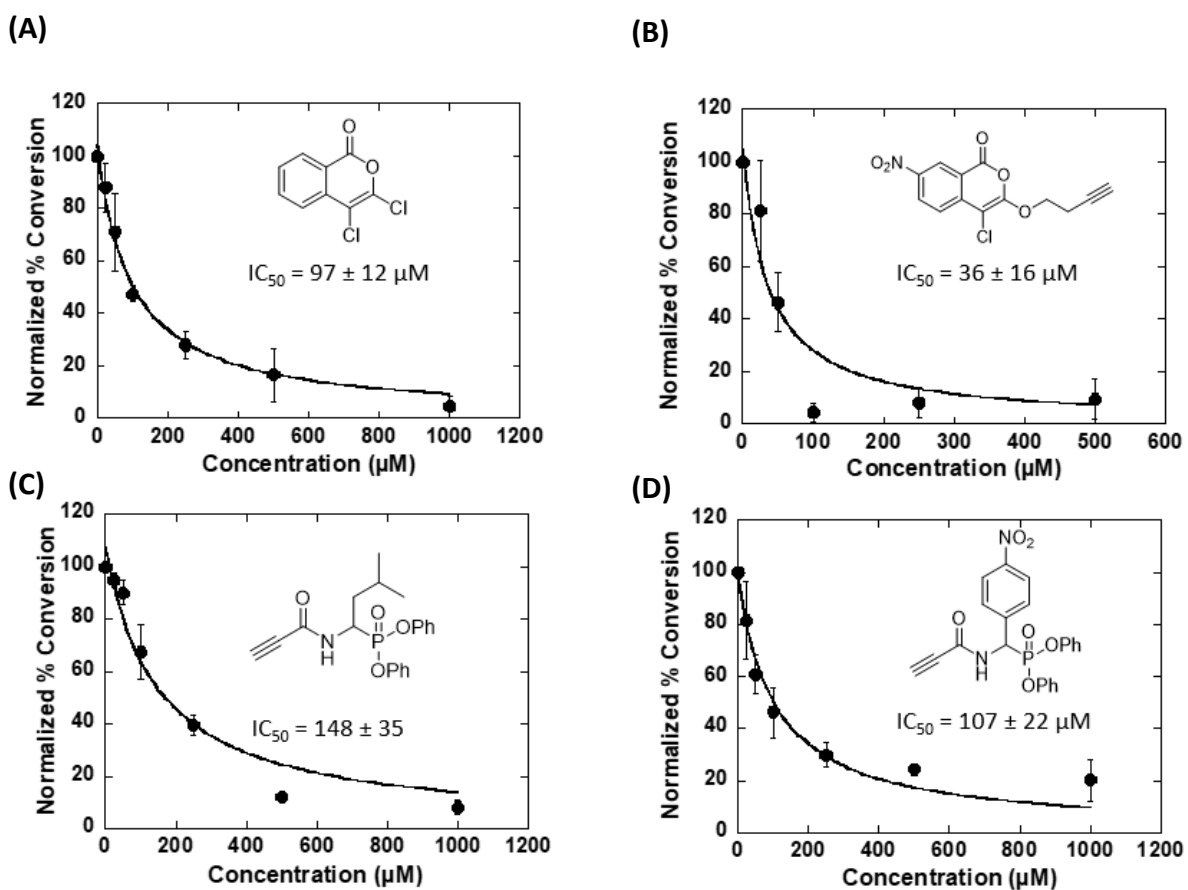
Figure 4.15: Inhibition of hGOAT with hit compounds. a.) IC$_{50}$ determination of DCI (**4.1**). **b.)** IC$_{50}$ determination of **4.16**. **c.)** IC$_{50}$ determination of **4.26**. **d.)** IC$_{50}$ determination of **4.28**. Reactions were performed in at minimum in triplicate and normalized to vehicle control as described in Materials and Methods.
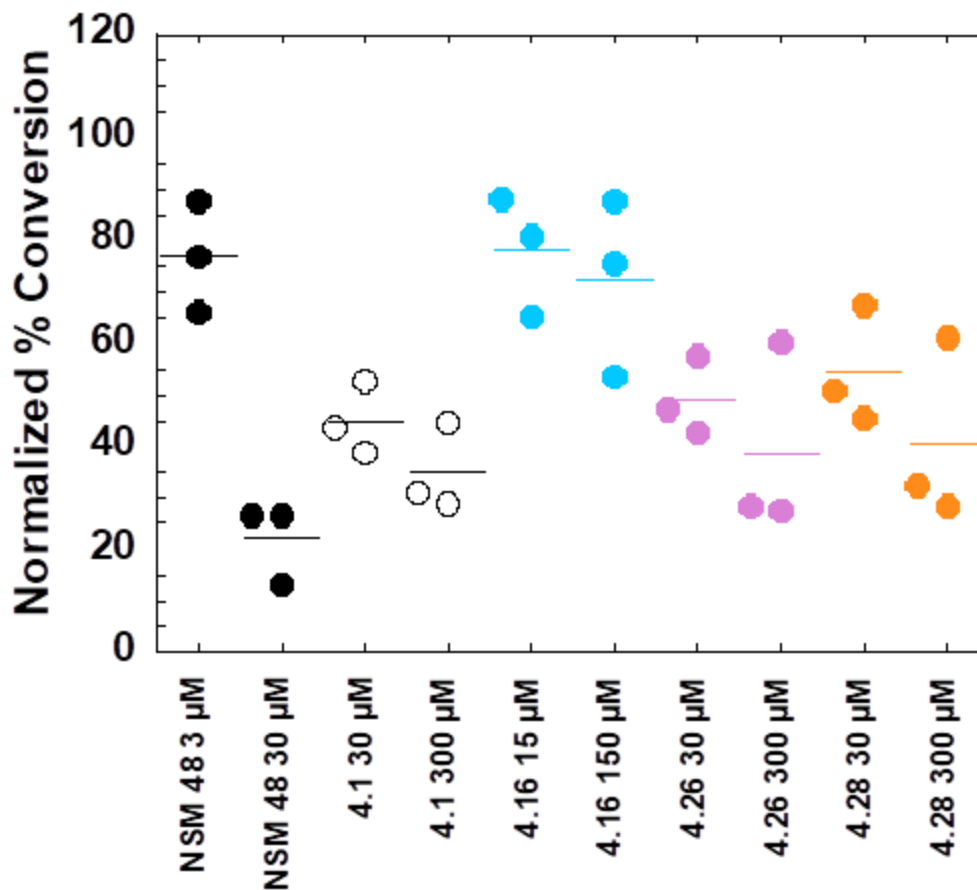
Figure 4.16: Hit compounds exhibit irreversible behavior. Compounds were tested at 0.3 and 3 times their measured IC_{50}. Compounds **4.16, 4.26, and 4.28** all indicate irreversible behavior when compared to DCI (irreversible control) and NSM-48 (reversible control). Reactions were performed in triplicate and normalized to vehicle control as described in Materials and Methods.

4.3 Discussion and Conclusions

As mentioned in Chapter 3, the development of irreversible inhibitors of GOAT allows for valuable insight into the catalytic mechanism of GOAT and the residues involved in catalysis. As the results from studies with cysteine-reactive molecules have supported a functionally essential but non-catalytic role for cysteine within GOAT, the residues capable of catalyzing the acyl transfer are still unknown. The discovery of privileged electrophiles as hGOAT inhibitors has supported an alternative mechanism utilizing an activated serine in catalysis. This mechanism is further supported by the identification of four different privileged electrophilic warheads capable of hGOAT inhibition, with isocoumarins, sulfonyl fluorides benzoxazinones, and diphenyl phosphonates each showing inhibitory activity. The irreversible nature of the isocoumarins and diphenyl phosponates provide a way to label and identify this activated serine present with GOAT.

Sulfonyl fluorides, isocoumarins, benzoaxazinones, and diphenyl phosphonates each represent new classes of hGOAT inhibitors. Considering the literature precedence of these functionalities for specificity in reacting with activated serines, it is likely that GOAT contains an activated serine. The ability for the sulfonyl fluoride and isocoumarin compounds to inhibit both the human and mouse isoforms of GOAT to similar degrees suggests the activated serine is conserved and may play a role in the acyl transfer catalytic mechanism. The highest potency sulfonyl fluoride containing the same chain length as the octanoate substrate indicates that these molecules are likely binding into a catalytic site on GOAT. In particular, the 7-nitro-3,4-dichloroisocoumarin (**Compound 4.16**) represents an exciting new molecule with increased potency over the sulfonyl fluorides.

While the isocoumarin-based molecules tested are more potent than the diphenyl phosphonate inhibitors, the synthetic route to novel diphenyl phosponates is considerably more facile, allowing for rapid synthesis of molecules limited only by available aldehydes. [5, 17] Additionally, the ability of isocoumarins to react with a second nucleophile after the initial ring-opening reaction potentially complicates identification of catalytic residues, while the phosphonates are anticipated to undergo only a single reaction. The GOAT reactions performed in this work are done in an enriched membrane fraction, and it is likely that some amount of the probes are consumed in reactions with proteins contained within the membrane protein fraction that utilize activated hydroxyl nucleophiles, including esterases and proteases. While care was taken to passivate the membrane fraction with the esterase inhibitor MAFP before treatment with the privileged electrophiles, it is unlikely that this will eliminate all non-specific reactions with other proteins in the membrane fraction. Since sulfonyl fluorides are generally more promiscuous than the isocoumarin-based inhibitors, it is possible that the potency of the privileged electrophile inhibitors are not fully reflected by the IC_{50} values obtained. [6, 37, 52] Work is underway in the Hougland lab on the purification of active hGOAT, which would clarify the exact potency of these molecules against hGOAT.

The structures of protein-modifying MBOATs similar to GOAT have been recently determined. The cryo-EM structure of HHAT in complex with palmitoyl-CoA or palmitoyl-CoA analogues revealed the thioester moiety to be near H379 and D339 (analogous to N337 in GOAT). [53, 54] D339 is proposed to activate the substrate amine while H379 stabilizes the thioester on the basis of observed hydrogen bonding between H379 and the amide carbonyl of the palmitoylated product, inverting the roles of the residues compared to DGAT1 and LCAT3. [54] The electron density from a non-hydrolysable palmitoyl-CoA lacking the thioester carbonyl

places H379 close to the site of the missing carbonyl, and molecular dynamics simulations indicate a role for H379 and a hydrogen bond donor, supporting this claim further. [53] PORCN is implicated to have a direct transfer mechanism as well, with cryo-EM structures placing S209 of the WNT3Ap substrate in close proximity to both the palmitoyl-CoA thioester and H336, allowing H336 to deprotonate the serine hydroxyl and initiate nucleophilic attack of the serine on the thioester bond. [55] It is important to note that none of these mechanisms have direct evidence to support the hypotheses, as they are exclusively proposed via crystal structure or cryo-EM. An alternative mechanism would be an acyl-enzyme intermediate like that shown by *S*-acyltransferase human DHHC20, where a catalytic triad of aspartic acid, histidine, and cysteine act to activate the cysteine to induce transfer of the palmitoyl group from palmitoyl-CoA to DHHC20. The role of histidine then shifts to acting as a proton donor, activating the newly-formed thioester bond and allowing transfer of the palmitoyl to the substrate. [56]

Reflecting that the data no longer supports the idea of a catalytic cysteine residue in GOAT, an alternative residue or residues must be involved in hGOAT catalysis. The variety of privileged electrophiles that inhibit GOAT, the history of these electrophiles as serine-reactive molecules, and the evidence for utilization of hydroxyl nucleophiles in other MBOATs indicate that GOAT likely utilizes an activated serine as part of the catalytic mechanism. While it is possible that GOAT utilizes a direct transfer mechanism by activating the serine-3 of ghrelin to act as a nucleophile, no evidence of sulfonyl fluoride- or isocoumarin-labeled peptide has been found in the HPLC traces of reactions including these reagents as would be expected if the ghrelin peptide provided the activated nucleophile.

It is therefore proposed that GOAT utilizes an acyl-enzyme intermediate mechanism, transferring the octanoyl moiety from octanoyl-CoA to a currently undefined activated serine on

the enzyme before the final acylation of ghrelin. In order to identify the serine involved, labeling studies are underway, intending on utilizing the alkyne functionalities present in the privileged electrophile compounds to perform copper-catalyzed [3+2] cycloaddition reactions to visualize the labeling process. [58]

4.4 Materials and Methods

4.4.1 General Experimental Details

Methyl arachidonyl fluorophosphonate (MAFP) was diluted in DMSO from a stock in methyl acetate obtained from Cayman Chemical (Ann Arbor, MI). Octanoyl coenzyme A (octanoyl CoA) was diluted to 5mM in 10 mM Tris-HCl and stored in low adhesion tubes at -80°C until use. The GSSFLC$_{NH2}$ and GSSCLS$_{NH2}$ peptides used in fluorescent acrylodan labeling were obtained from Sigma-Genosys (The Woodlands, TX) and synthesized in Pepscreen format. The peptides were solubilized in 1:1 acetonitrile/water or 50 mM HEPES pH 7.0 solution and stored at -80°C. Peptide concentration was determined spectrophotometrically at 412 nm by reaction of the cysteine thiol with 5,5'dithiobis(2-nitrobenzoic acid) using an ϵ_{412} of 14150 M^{-1} cm^{-1}. [59]

4.4.2 GOAT Inhibition Assay

For inhibition assays, inhibitor samples were first thawed at room temperature and vortexed, followed by dilution in DMSO to working concentrations. Membrane fractions from Sf9 cells expressing GOAT were first thawed on ice, then passed through an 18-gauge needle ten times to homogenize. Assays were performed with approximately 50 µg of membrane protein, determined through a Bradford assay. A master mix was then created with 2.5 µL 1 M HEPES buffer, 0.1 µL 500 µM MAFP, 5 µL membrane fraction, per reaction, and water to bring the reaction to 50 µL after the addition of sample, octanoyl CoA, and peptide. The master mix was then distributed into low-adhesion microcentrifuge tubes, and the sample was then added and allowed to preincubate for 30 minutes at room temperature while covered. Reactions were started

by the addition of 300 µM octanoyl CoA and 1.5 µL acrylodan-labeled peptide, for a reaction volume of 50 µL. This was incubated for 15 minutes to 1 hour, while covered at room temperature, and then stopped with the addition of 50 µL of 20% acetic acid. Reaction time was determined via timecourse to keep conversion of acyl ghrelin below 50%. Excess membrane fraction was then removed via precipitation with 16.7 µL trichloroacetic acid followed by a 1000g centrifugation for 1 minute. The supernatant was then analyzed via reverse-phase HPLC.

4.4.3 Reversibility Assay

Membrane fraction containing hGOAT was incubated with 10 µM MAFP and 10 times or 3 times the approximate IC_{50} of inhibitor or vehicle (DMSO) for 30 min at room temperature. Inhibitor-treated membrane fraction was then diluted 10-fold into a reaction mixture containing 300 µM octanoyl-CoA, 1.5 µM GSSFLCAcDan, 50 mM HEPES (pH 7.0), and either vehicle or inhibitor (final concentration of 1 times or 0.3 times the IC_{50}) in a total reaction volume of 50 µL. Reaction mixtures were incubated under foil for 1 h at room temperature, stopped with the addition of 50 µL of 20% acetic acid. Excess membrane fraction was then removed via precipitation with 16.7 µL trichloroacetic acid followed by a 1000g centrifugation for 1 minute. The supernatant was then analyzed via reverse-phase HPLC.

4.4.4 HPLC analysis of GOAT Assays

Assays were analyzed on reverse-phase HPLC (Zorbax Eclipse XDB column, 4.6 150 mm) using a solvent gradient from 30% acetonitrile in aqueous 0.05% TFA to 63% acetonitrile in aqueous 0.05% TFA over 14 minutes at a flow rate of 1 mL/min, followed by 100%

acetonitrile for 5 minutes. Peptides were detected by the attached acrylodan label with the UV

absorbance at 360 nm and fluorescence (λ_{ex} = 360 nm, λ_{em} = 485 nm). Octanoylated peptide

typically eluted around 12 minutes, with the des-acyl peptide eluting around 6 minutes.

Chemstation for LC (Agilent Technologies) was used for peak integration.

4.4.5 Determination of IC$_{50}$ Values

Peak integrations were used to determine percent activity in the presence of either sample

or vehicle (DMSO). Percent activity was calculated using equations 1 and 2:

$$\% \text{ activity} = \frac{\% \text{ peptide octanoylation in presence of inhibitor}}{\% \text{ peptide octanoylation in absence of inhibitor}} \tag{1}$$

$$\% \text{ peptide octanoylation} = \frac{\text{fluorescence of octanoylated peptide}}{\text{total peptide fluorescence}} \tag{2}$$

IC$_{50}$ values were determined by fitting equation 3 to the plot of % activity against inhibitor

concentration.

$$\% \text{ activity} = \% \text{ vehicle activity} \left(1 - \frac{[\text{inhibitor}]}{[\text{inhibitor}] + \text{IC50}} \right) \tag{3}$$

Plots and data fitting were performed with Kaleidagraph (Synergy Software, Reading, PA)

4.4.6 General Synthetic Methods

Compounds were used as received from the manufacturer without modification. All anhydrous reactions were run under a positive pressure of argon. All solvents were dried with the Grubbs method by passage through an alumina column. [60] Thin-layer Chromatography was done on silica at ambient temperature. Silica gel 60 was used as the stationary phase for flash chromatography. All ^{1}H NMR and ^{13}C NMR were taken using a Bruker Advance 400 MHz Fourier Transform Nuclear Magnetic Resonance Spectrometer. Abbreviations for spectra: s = singlet, bs = broad singlet d = doublet, t = triplet, q = quartet, quin = quintet, dd = doublet of doublets, td = triplet of doublets, m = multiplet.

4.4.7 General Procedure for the Synthesis of Sulfonyl Fluorides

Preparation of O-alkyl Sulfonyl Fluorides from Primary Alcohols

 General Method A. To a mixture of 1 equivalent of primary alcohol (.33 M) in DCM was added 0.1 eq of triphenyl phosphine and 1.1 – 2 eq ethenesulfonyl fluoride. Reaction was stirred for 18-36 hours at room temperature. Reaction was stopped by removal of solvent under reduced pressure by rotary evaporation. Remaining liquid was subjected to column chromatography to yield pure sulfonyl fluoride.
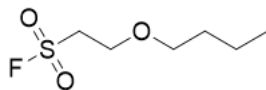
4.2

2-(butyl-1-oxy)ethanesulfonyl fluoride - Compound **4.2** was synthesized using General Method A. 1.35 mmol butanol was reacted with 2.70 mmol ethenesulfonyl fluoride in the presence of 0.135 mmol triphenylphosphine for 18h. Compound was purified using column chromatography (100% DCM) twice before yielding pure **4.2** as a colorless oil. ^{1}H NMR (400 MHz, CDCl$_3$) δ 3.90 (td, J = 1.6, 6 Hz, 2H), 3.62 (m, 2H), 3.49 (t, J = 6.4 Hz, 2H), 1.57 (p, J = 6.4, 8 Hz, 2H), 1.37 (sex, J = 7.6 Hz, 2H), 0.91 (t, J =7.2 Hz, 3H). ^{13}C NMR (100 MHz, CDCl$_3$) δ 71.5, 63.4, 51.2 (d, J = 16.8 Hz), 31.4, 24.7, 19.1, 13.8.
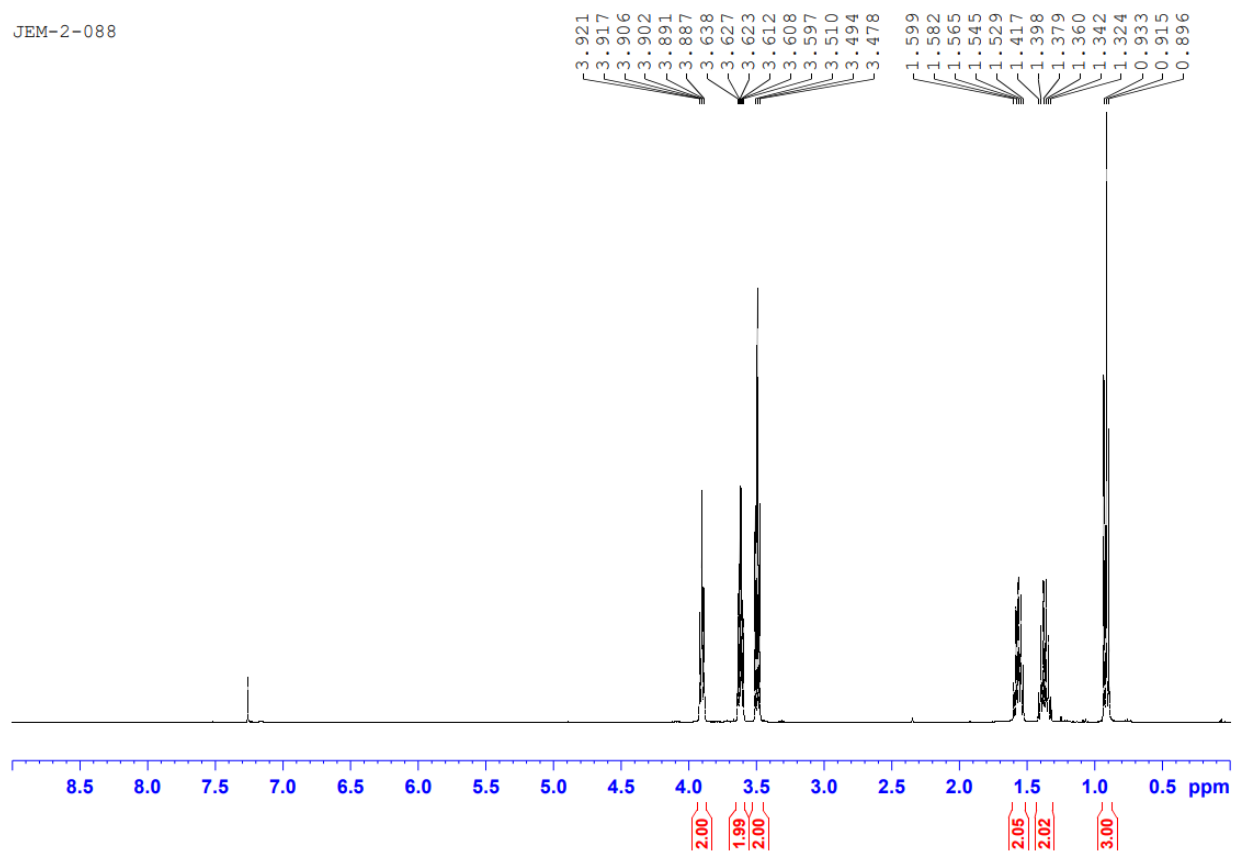
Figure 4.17: ¹H NMR of 2-(butyl-1-oxy)ethanesulfonyl fluoride (4.2)
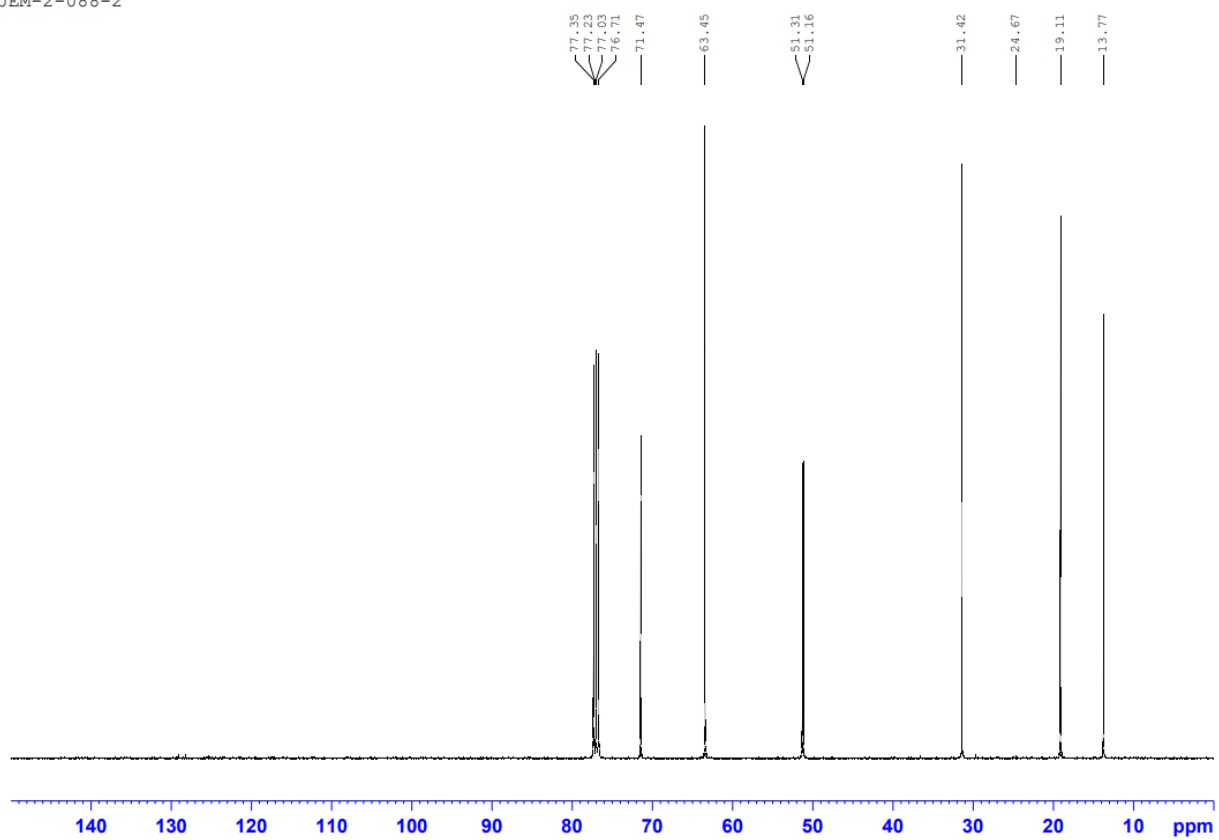
Figure 4.18: ^{13}C NMR of 2-(butyl-1-oxy)ethanesulfonyl fluoride (4.2)
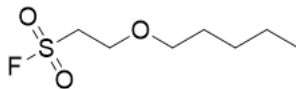
4.3

2-(pentyl-1-oxy)ethanesulfonyl fluoride - Compound **4.3** was synthesized using General

Method A. 1.35 mmol pentanol was reacted with 1.49 mmol ethenesulfonyl fluoride in the

presence of 0.135 mmol triphenylphosphine for 18h. Compound was purified using column

chromatography (100% DCM) twice before yielding pure **4.3** as a colorless oil. ^{1}H NMR (400

MHz, CDCl$_3$) δ 3.91 (td, J = 6, 1.2 Hz, 2H), 3.64-3.60 (m, 2H), 3.49 (t, J = 6.4 Hz, 2H), 1.59 (p,

J = 6.8 Hz, 2H), 1.33-1.29 (m, 4H), 0.89 (t, 6.8 Hz, 3H). ^{13}C NMR (100 MHz, CDCl$_3$) δ 71.8,

63.5, 51.2 (d, 15 Hz), 29.1, 28.1, 22.4, 14.0
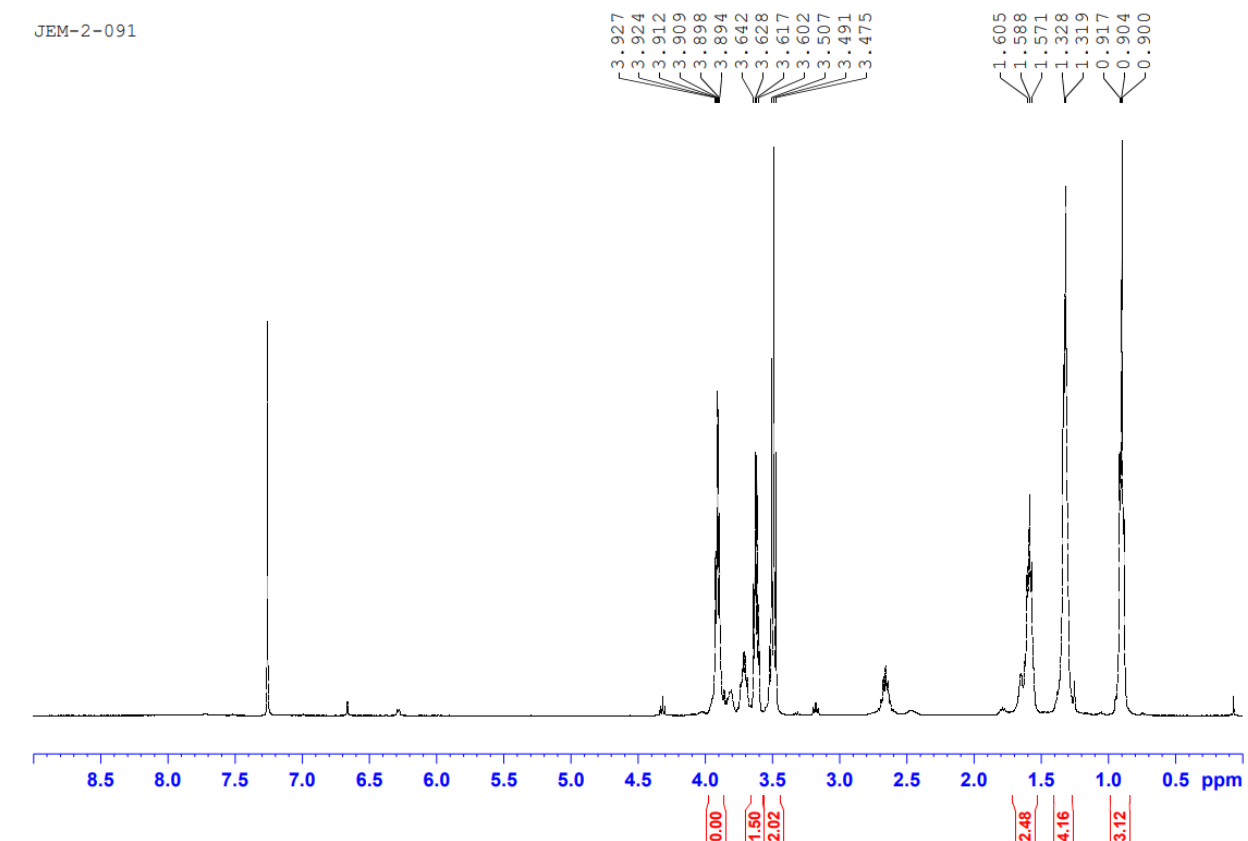
Figure 4.19: ^{1}H NMR of 2-(pentyl-1-oxy)ethanesulfonyl fluoride (4.3)
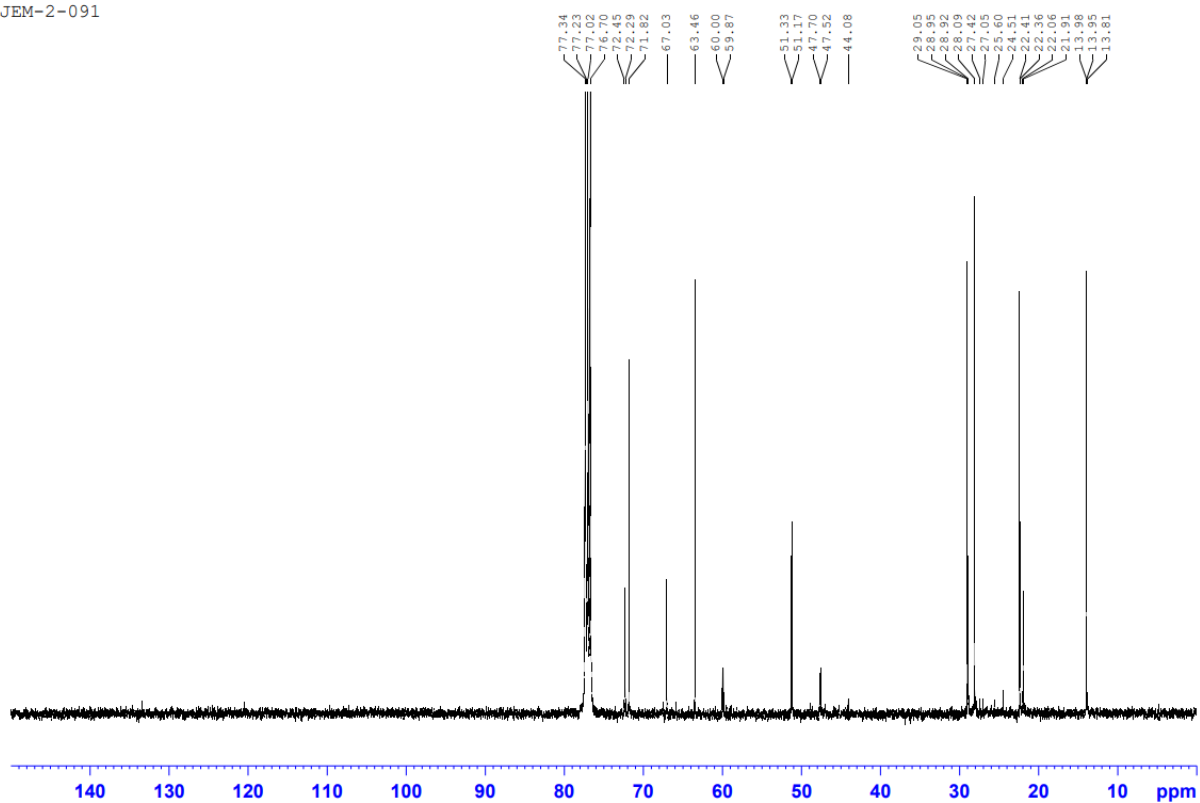
Figure 4.120: **^{13}C NMR of 2-(pentyl-1-oxy)ethanesulfonyl fluoride (4.3)**
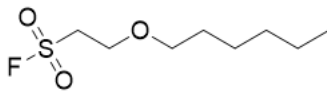
4.4

2-(hexyl-1-oxy)ethanesulfonyl fluoride – Compound **4.4** was synthesized using General Method A. 1.35 mmol hexanol was reacted with 1.49 mmol ethenesulfonyl fluoride in the presence of 0.135 mmol triphenylphosphine for 18h. Compound was purified using column chromatography (100% DCM) twice before yielding pure **4.4** as a colorless oil. ^{1}H NMR (400 MHz, CDCl$_3$) δ 3.90 (td, J = 6, 1.2 Hz, 2H), 3.64-3.60 (m, 2H), 3.49 (t, J = 6.4 Hz, 2H), 1.58 (p, J = 6.8 Hz, 2H), 1.33-1.26 (m, 4H), 0.88 (t, 6.8 Hz, 3H) ^{13}C NMR (100 MHz, CDCl$_3$) δ 71.8, 63.4, 51.2 (d, 15 Hz), 31.5, 29.3, 25.6, 22.5, 14.0
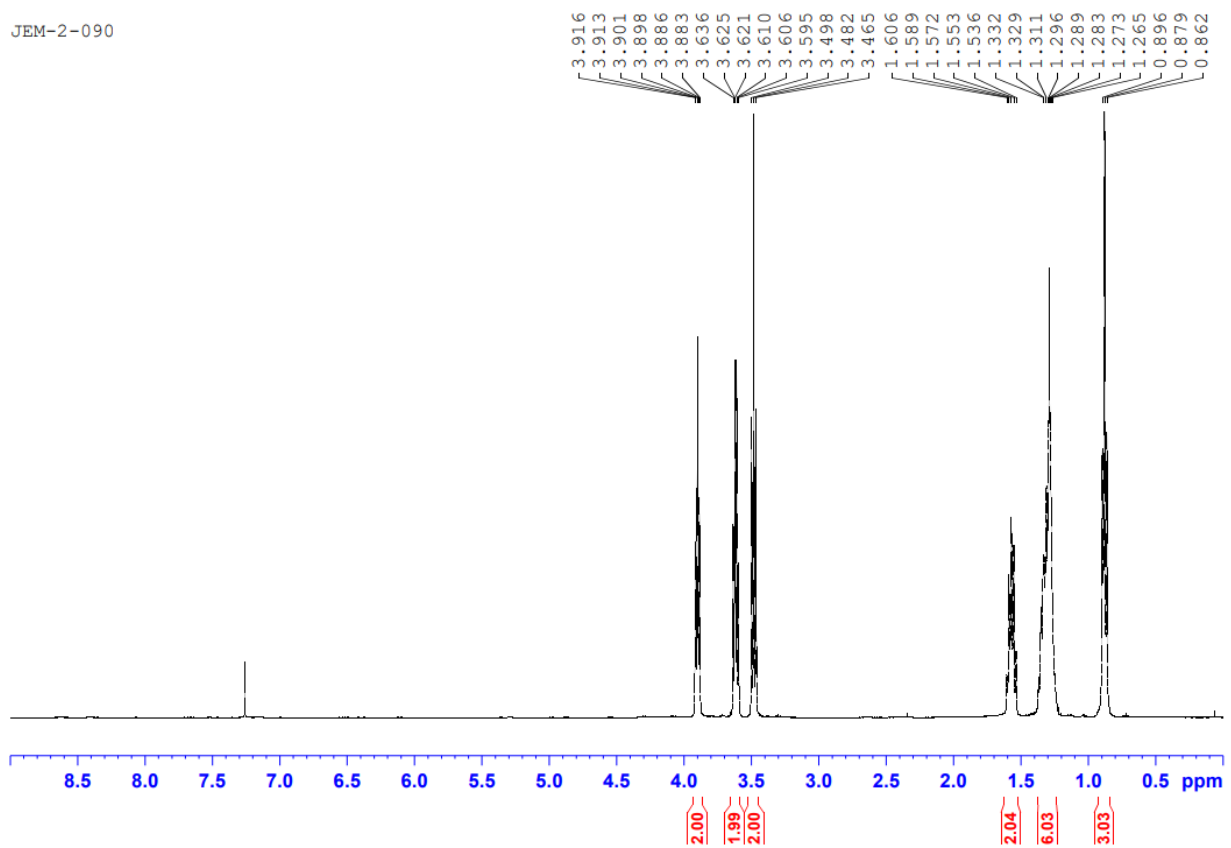
Figure 4.21: ^{1}H NMR of 2-(hexyl-1-oxy)ethanesulfonyl fluoride (4.4)
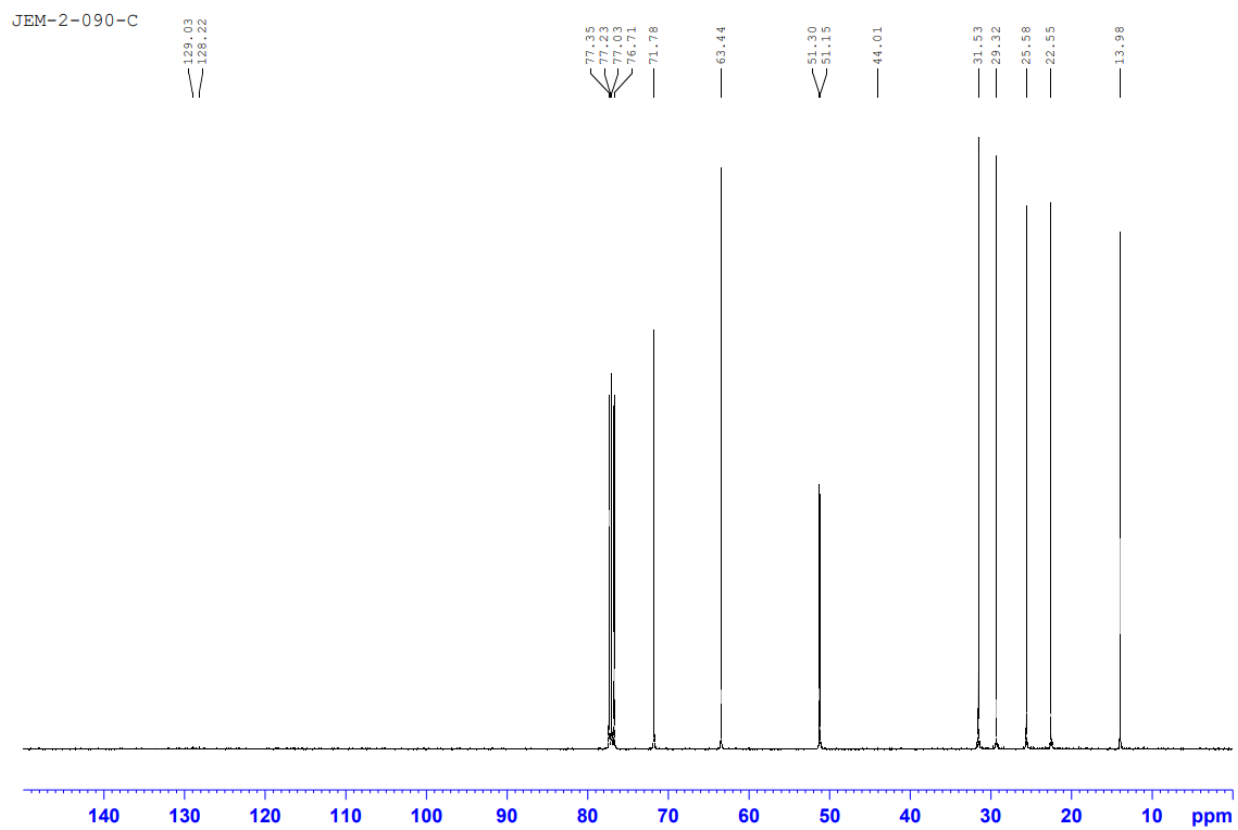
Figure 4.22: ¹³C NMR of 2-(hexyl-1-oxy)ethanesulfonyl fluoride (4.4)
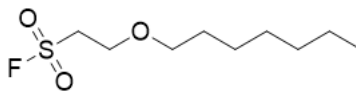
4.5

2-(heptyl-1-oxy)ethanesulfonyl fluoride - Compound **4.5** was synthesized using General

Method A. 1.35 mmol heptanol was reacted with 1.49 mmol ethenesulfonyl fluoride in the

presence of 0.135 mmol triphenylphosphine for 18h. Compound was purified twice using

column chromatography (100% DCM, then 5% EtOAC/hexanes) before yielding pure **4.5** as a

colorless oil. ^{1}H NMR (400 MHz, CDCl$_3$) δ 3.91 (t, J = 6 Hz, 2H), 3.64-3.60 (m, 2H), 3.49 (t, J

= 6.4 Hz, 2H), 1.58 (p, J = 6.8 Hz, 2H), 1.34-1.27 (m, 8 H), 0.88 (t, 6.4 Hz, 3H) ^{13}C NMR (100

MHz, CDCl$_3$) δ 71.8, 63.4, 51.2 (d, 15 Hz), 31.7, 29.4, 29.0, 25.9, 22.6, 14.1.
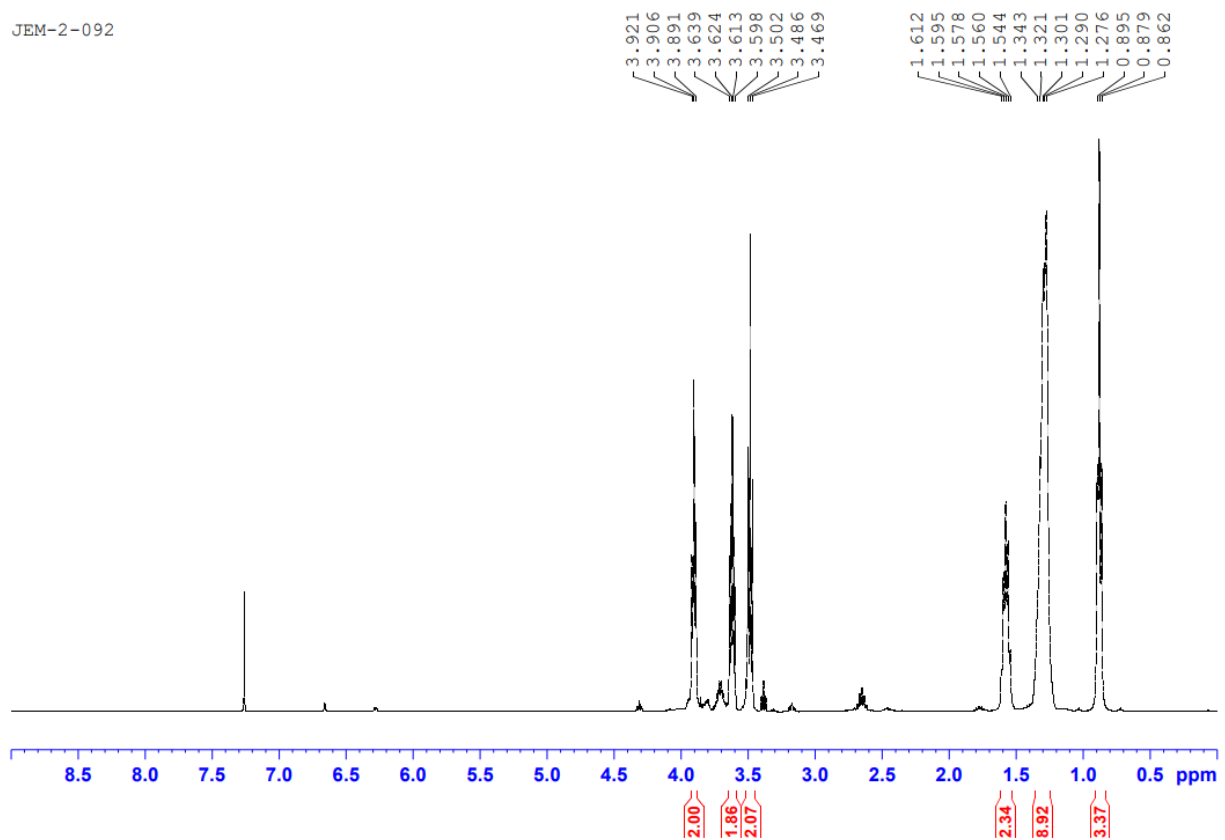
Figure 4.23: ¹H NMR of 2-(heptyl-1-oxy)ethanesulfonyl fluoride (4.5)
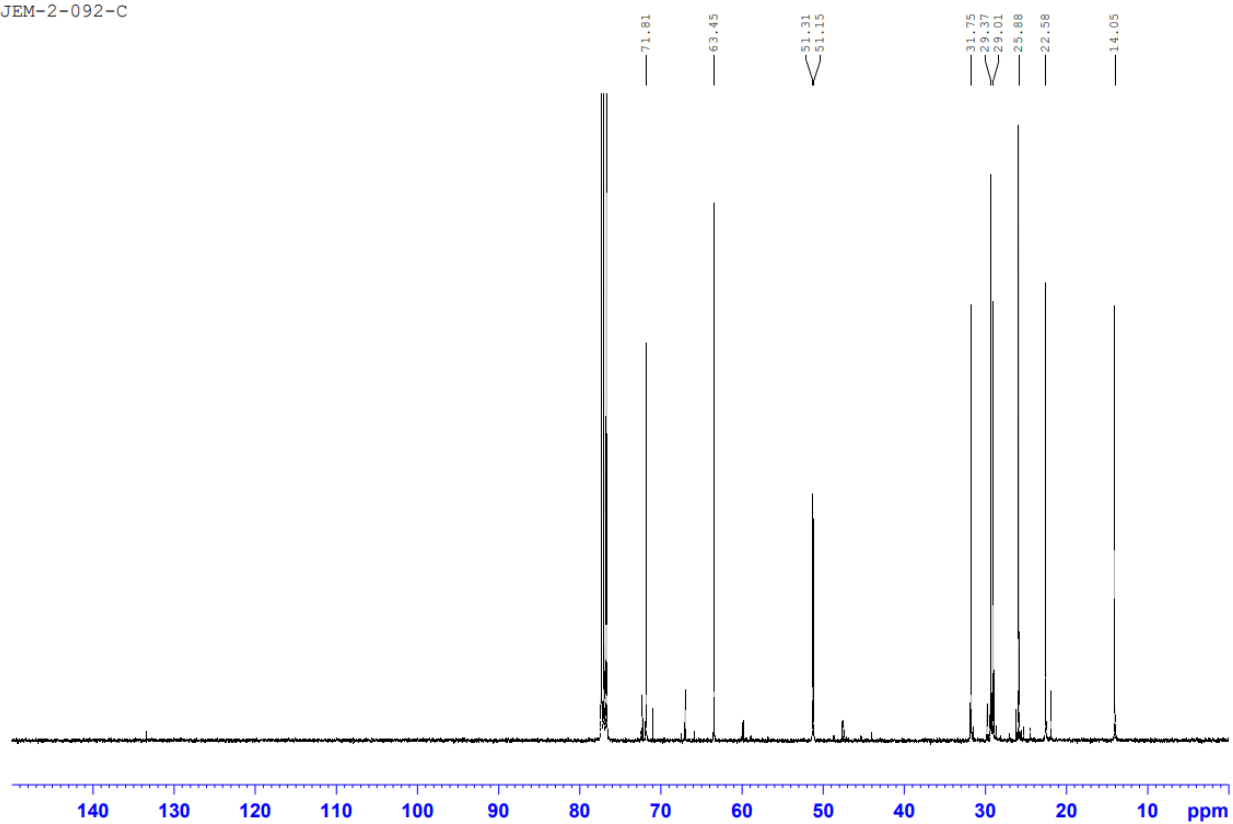
Figure 4.24: ^{13}C NMR of 2-(heptyl-1-oxy)ethanesulfonyl fluoride (4.5)
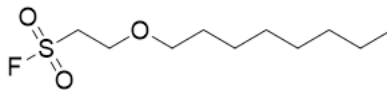
4.6

2-(octyl-1-oxy)ethanesulfonyl fluoride - Compound **4.6** was synthesized using General Method A. 1.35 mmol octanol was reacted with 1.49 mmol ethenesulfonyl fluoride in the presence of 0.135 mmol triphenylphosphine for 18h. Compound was purified twice using column chromatography (100% DCM, then 100% hexanes) before yielding pure **4.6** as a white solid. ^{1}H NMR (400 MHz, CDCl$_3$) δ 3.90 (td, J = 6, 1.5 Hz, 2H), 3.64-3.59 (m, 2H), 3.49 (t, J = 6.6 Hz, 2H), 1.58 (p, J = 6.9 Hz, 2H), 1.37-1.25 (m, 10H), 0.88 (t, J = 6.9 Hz, 3H) ^{13}C NMR (100 MHz, CDCl$_3$) 71.8, 63.5, 51.2 (d, 15 Hz), 44.0, 29.7, 29.5, 29.4,25.9, 22.6, 14.1
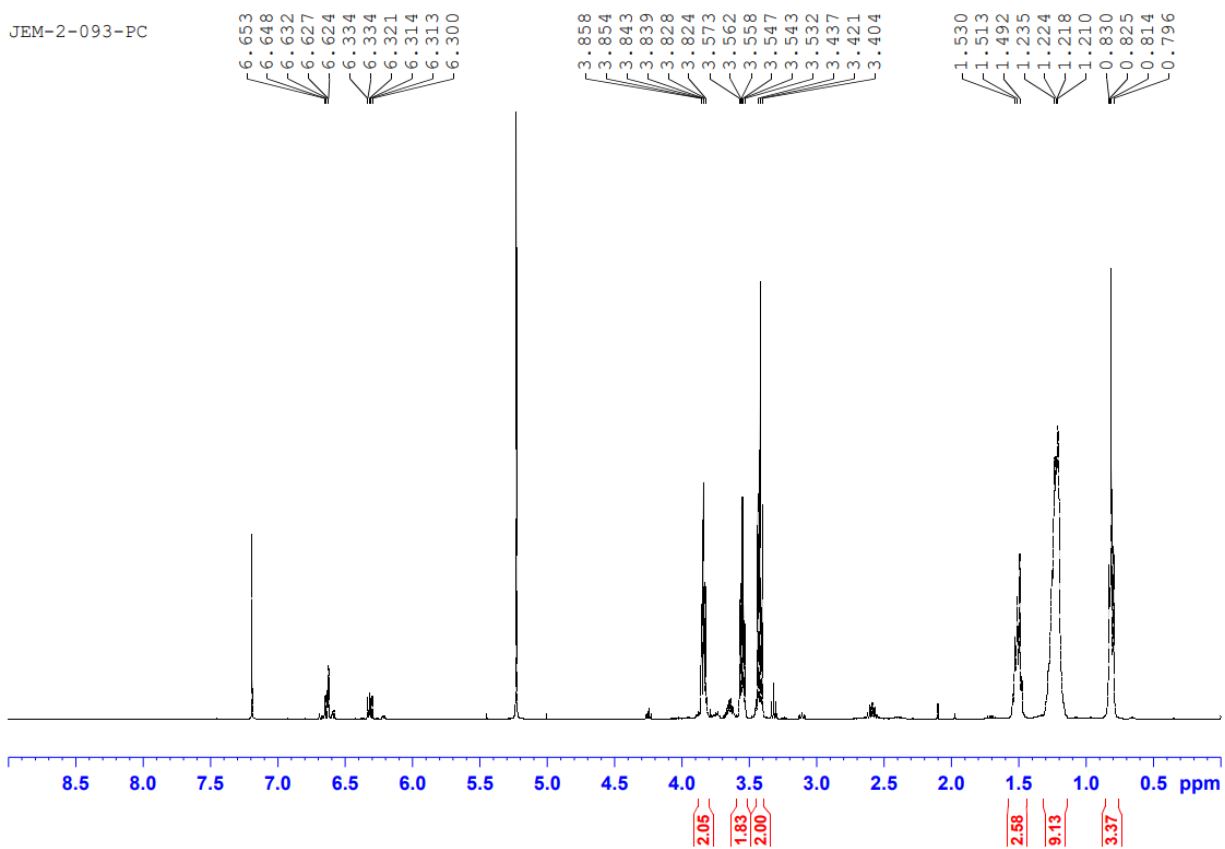
Figure 4.25: ¹H NMR of 2-(octyl-1-oxy)ethanesulfonyl fluoride (4.6)
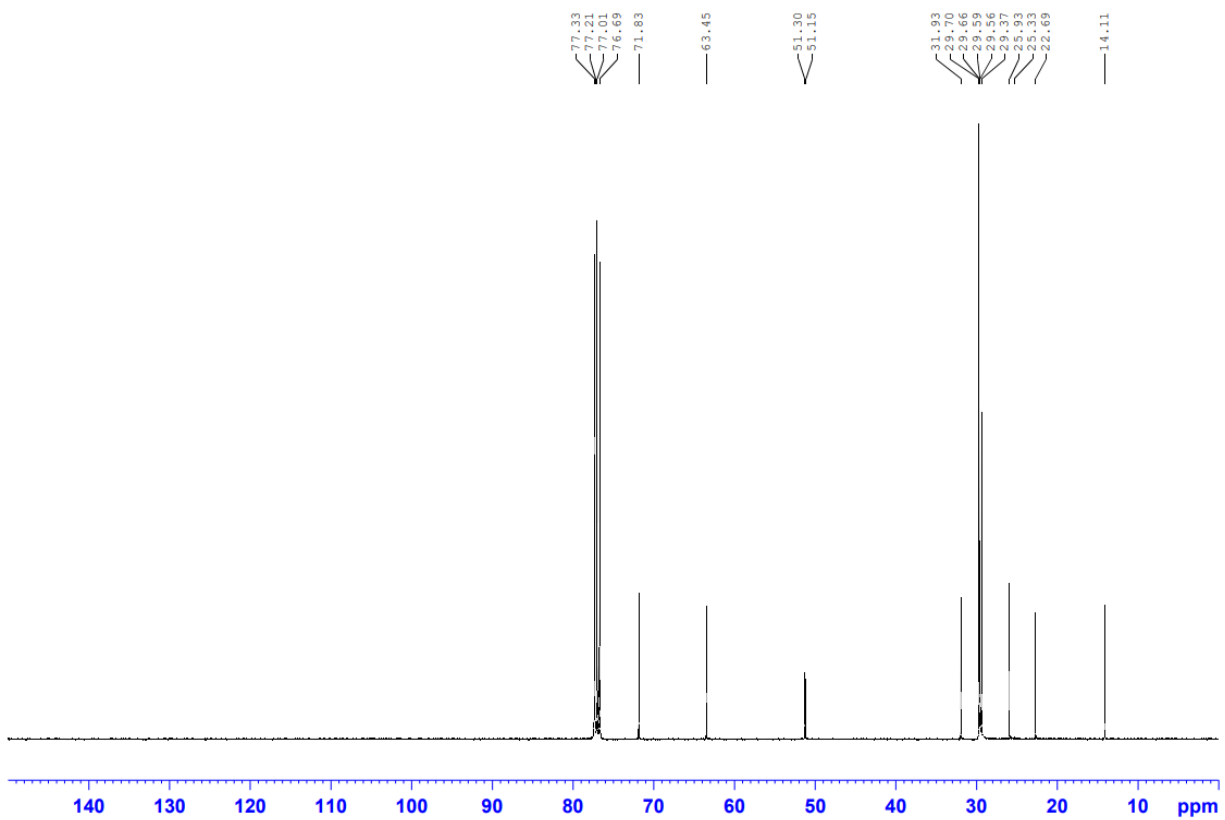
Figure 4.26: ^{13}C NMR of 2-(octyl-1-oxy)ethanesulfonyl fluoride (4.6)
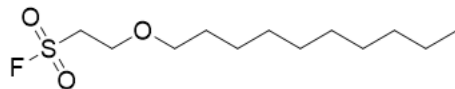
4.7

2-(decyl-1-oxy)ethanesulfonyl fluoride - Compound **4.7** was synthesized using General Method A. 1.35 mmol decanol was reacted with 1.49 mmol ethenesulfonyl fluoride in the presence of 0.135 mmol triphenylphosphine for 18h. Compound was purified twice using column chromatography (100% DCM, then 100% hexanes) before yielding pure **4.7** as a white solid. ^{1}H NMR (400 MHz, CDCl$_3$) δ 3.91 (td, J = 7.8, 1.3 Hz, 2H), 3.65-3.59 (m, 2H), 3.49 (t, J = 8.8 Hz, 2H), 1.58 (p, J = 9.2 Hz), 1.45-1.17 (m, 14H), 0.88 (t, J = 8.8 Hz, 3H) ^{13}C NMR (100 MHz, CDCl$_3$) δ 71.8, 63.5, 51.2 (d, J = 15 Hz), 31.9, 29.5 (2C), 29.4 (2C), 29.3, 25.9, 22.7, 14.1.
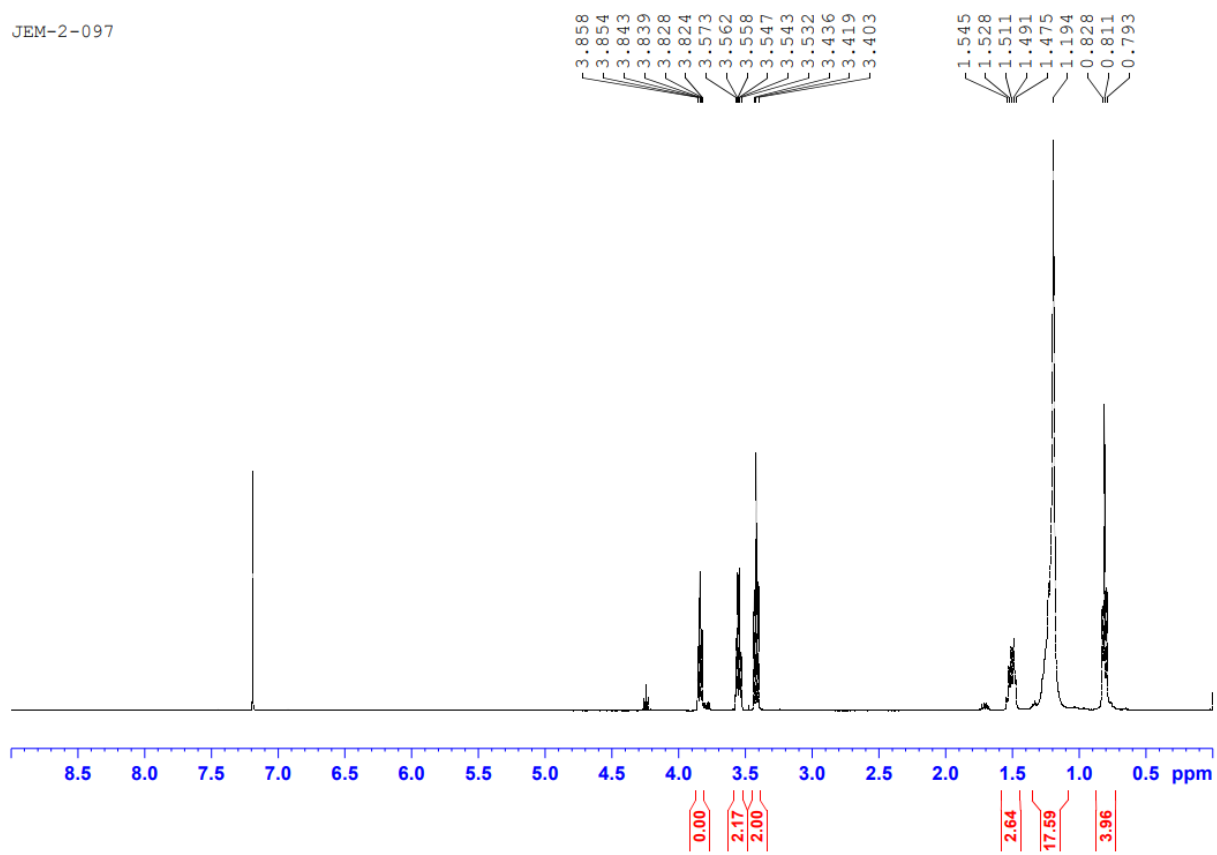
Figure 4.27: ¹H NMR of 2-(decyl-1-oxy)ethanesulfonyl fluoride (4.7)

JEM-2-097-C
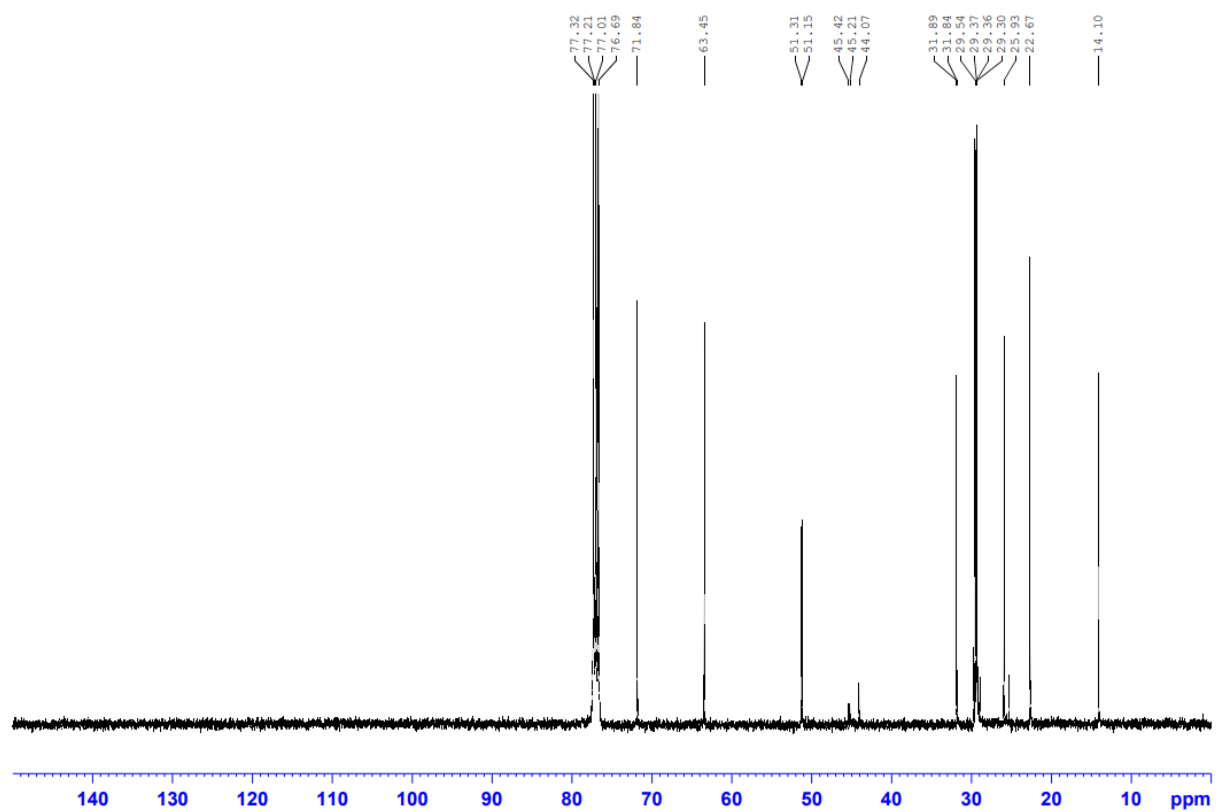
Figure 4.28: ^{13}C NMR of 2-(decyl-1-oxy)ethanesulfonyl fluoride (4.7)

4.8
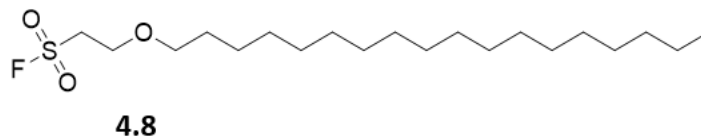
2-(octadecyl-1-oxy)ethanesulfonyl fluoride - Compound **4.8** was synthesized using General

Method A. 1.35 mmol octadecanol was reacted with 1.49 mmol ethenesulfonyl fluoride in the

presence of 0.135 mmol triphenylphosphine for 18h. Compound was purified twice using

column chromatography (100% DCM, then 100% hexanes) before yielding pure **4.7** as a white

solid. ^{1}H NMR (400 MHz, CDCl$_3$) δ 3.91 (td, J = 6, 1.2 Hz, 2H), 3.64-3.60 (m, 2H), 3.49 (t, J =

6.4 Hz, 2H), 1.58 (p, J = 6 Hz, 2H), 1.40-1.25 (m, 30H), 0.88 (t, J = 6.8 Hz, 3H) ^{13}C NMR (100

MHz, CDCl$_3$) δ 71.8, 63.5, 52.2 (d, J = 15 Hz), 31.9, complex spectra between 30-29, assigned

as 13 carbons, 25.9, 22.7, 14.1.

JEM-2-096
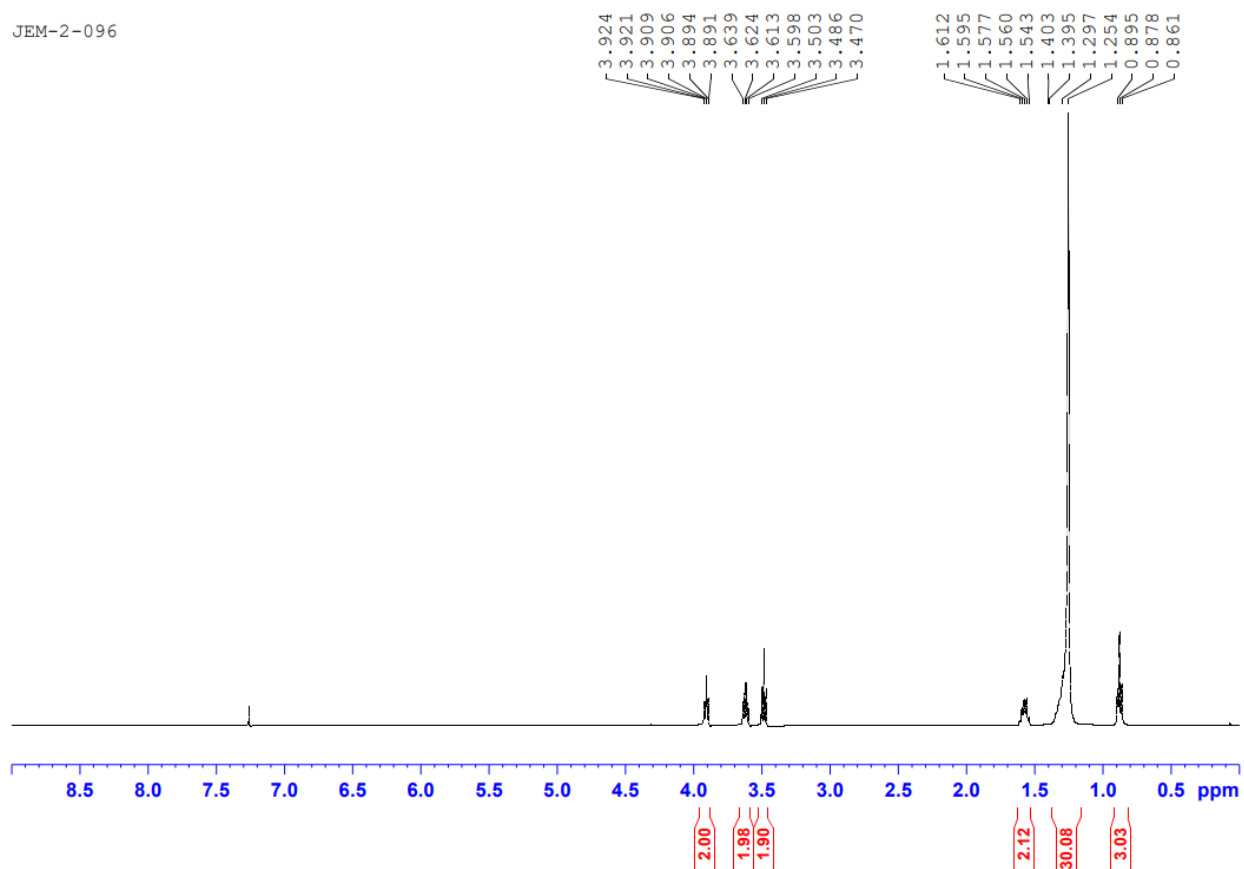
Figure 4.29: ¹H NMR of 2-(octadecyl-1-oxy)ethanesulfonyl fluoride (4.8)
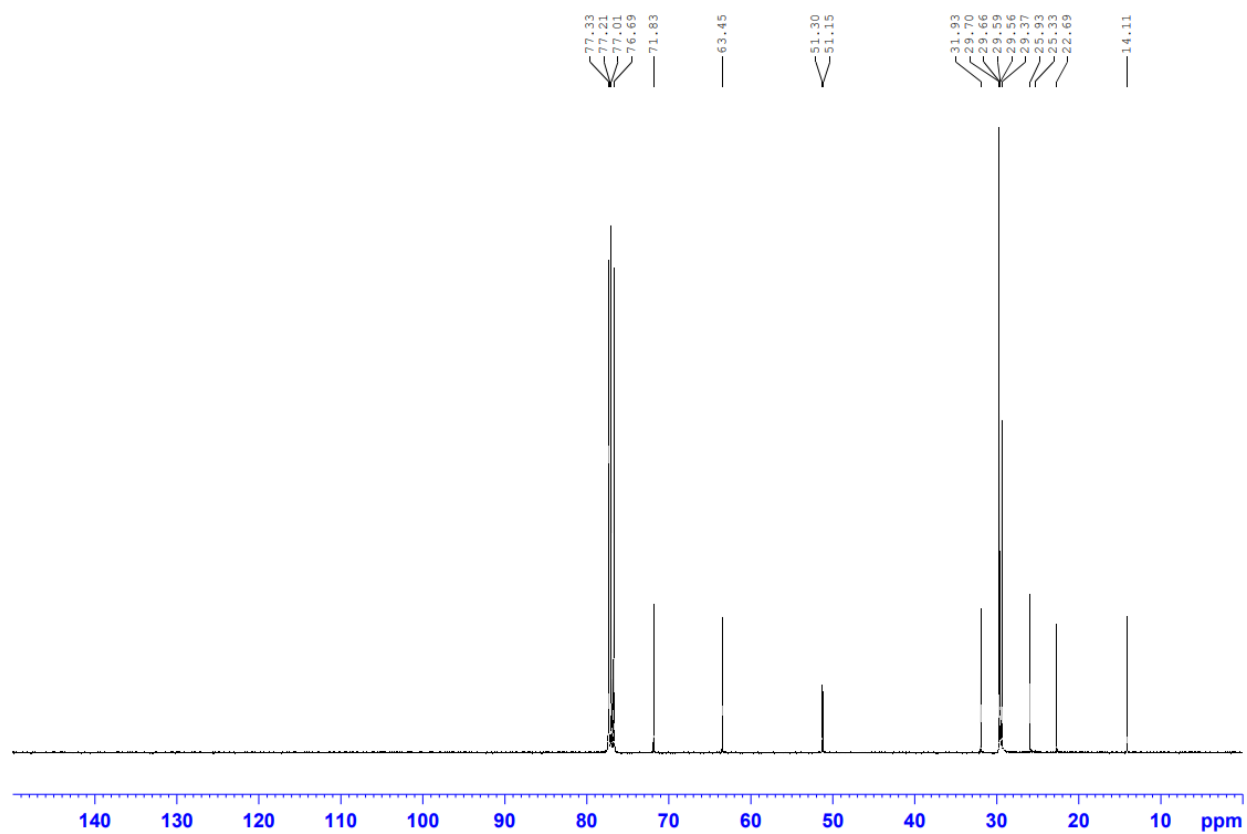
Figure 4.30: **^{13}C NMR of 2-(octadecyl-1-oxy)ethanesulfonyl fluoride (4.8)**
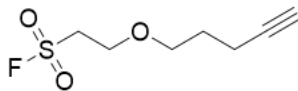
4.9

2-(pent-4-yn-1-yloxy)ethanesulfonyl fluoride - Compound **4.9** was synthesized using General

Method A. 1.35 mmol 4-pentyn-1-ol was reacted with 2.70 mmol ethenesulfonyl fluoride in the

presence of 0.135 mmol triphenylphosphine for 36h. Compound was purified twice using

column chromatography (100% DCM, then 5% EtOAC/hexanes) to yield Compound **4.9** as a

pure colorless oil. ^{1}H NMR (400 MHz, CDCl$_3$) δ 3.96 (td, J = 1.6, 6 Hz, 2H), 3.67-3.61 (m, 4H),

2.32 (td, 2.4, 7.2 Hz, 2H) 1.98 (t, 2.8 Hz, 1H), 1.82 (p, 6, 6.8 Hz, 2H). ^{13}C NMR (100 MHz,

CDCl$_3$) δ 83.5, 69.7, 68.8, 63.6, 51.2 (d, J = 16 Hz), 28.2, 15.0.
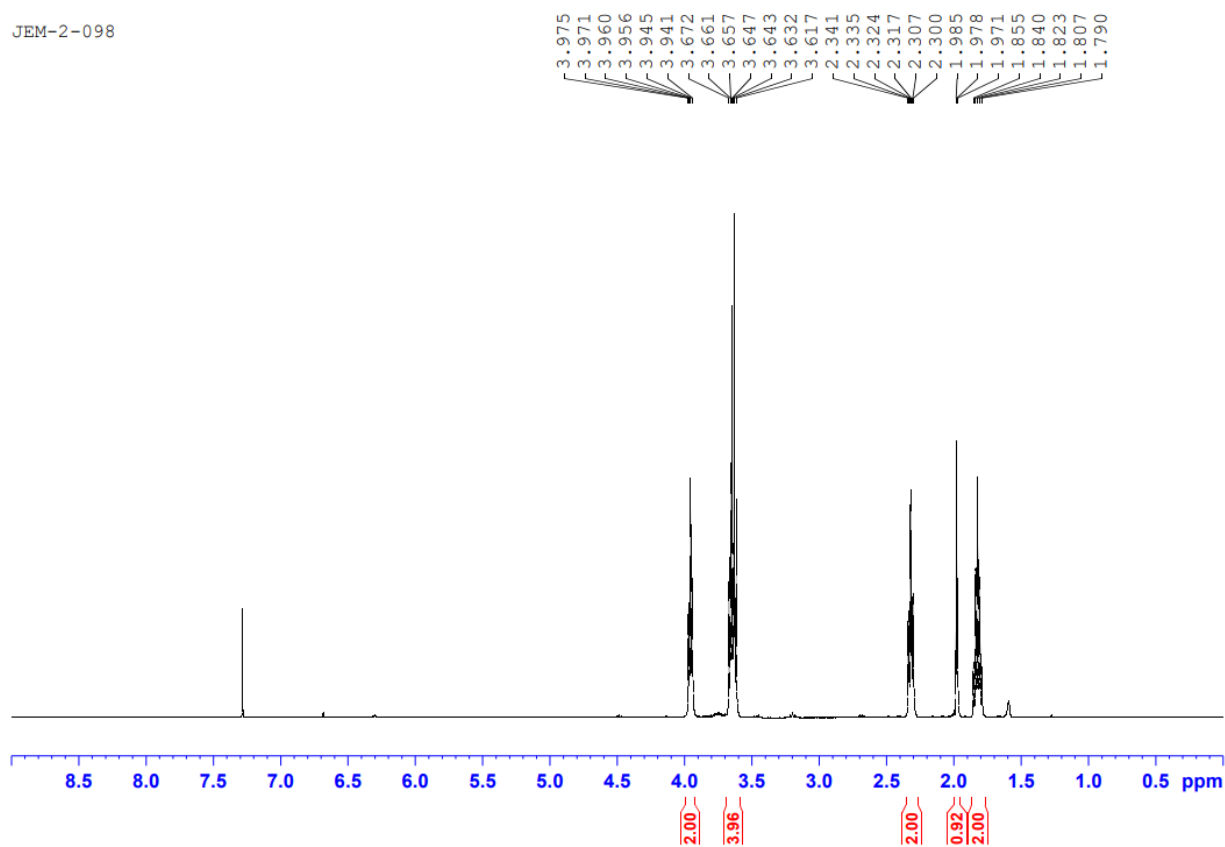
Figure 4.31: ¹H NMR of 2-(pent-4-yn-1-yloxy)ethanesulfonyl fluoride (4.9)
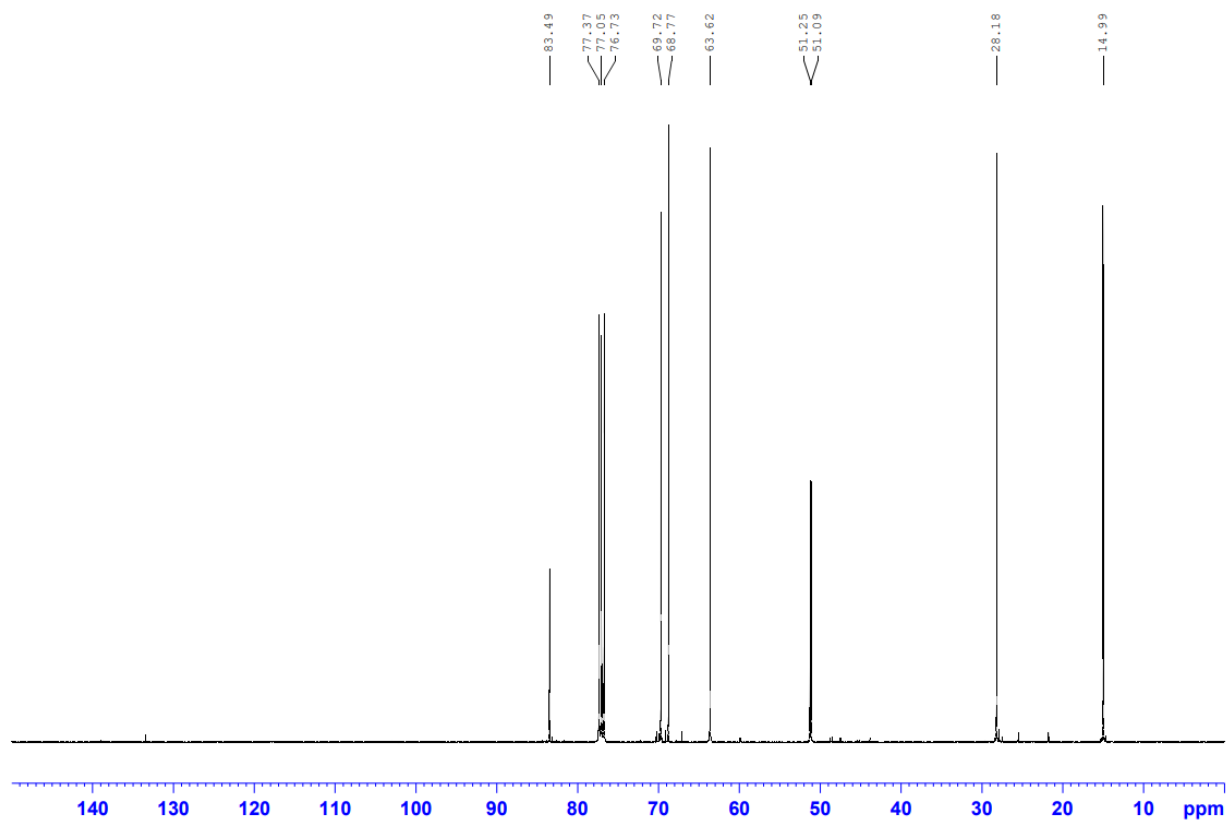
Figure 4.32: ^{13}C NMR of 2-(pent-4-yn-1-yloxy)ethanesulfonyl fluoride (3.9)
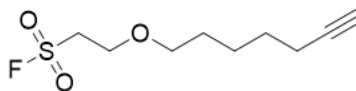
4.10

2-(hept-6-yn-1-yloxy)ethanesulfonyl fluoride - Compound **4.10** was synthesized using General

Method A. 1.35 mmol 6-heptyn-1-ol was reacted with 1.49 mmol ethenesulfonyl fluoride in the

presence of 0.135 mmol triphenylphosphine for 36h. Compound was purified twice using

column chromatography (100% DCM, then 5% EtOAC/hexanes) to yield Compound **4.10** as a

pure colorless oil. ^{1}H NMR (400 MHz, CDCl$_3$) δ 3.91 (td, J = 6, 1.6 Hz, 2H), 3.64-3.60 (m, 2H),

3.50, (t, J = 6.4 Hz, 2 H), 2.20 (td, J = 6.8, 2.6 Hz, 2 H) 1.94, (t, J = 2.7 Hz, 1 H), 1.63-1.42 (m,

6H). ^{13}C NMR (100 MHz, CDCl$_3$) δ 84.4, 71.5, 68.3, 62.5, 51.2 (d, J = 15 Hz), 28.9, 28.3, 25.1,

18.3
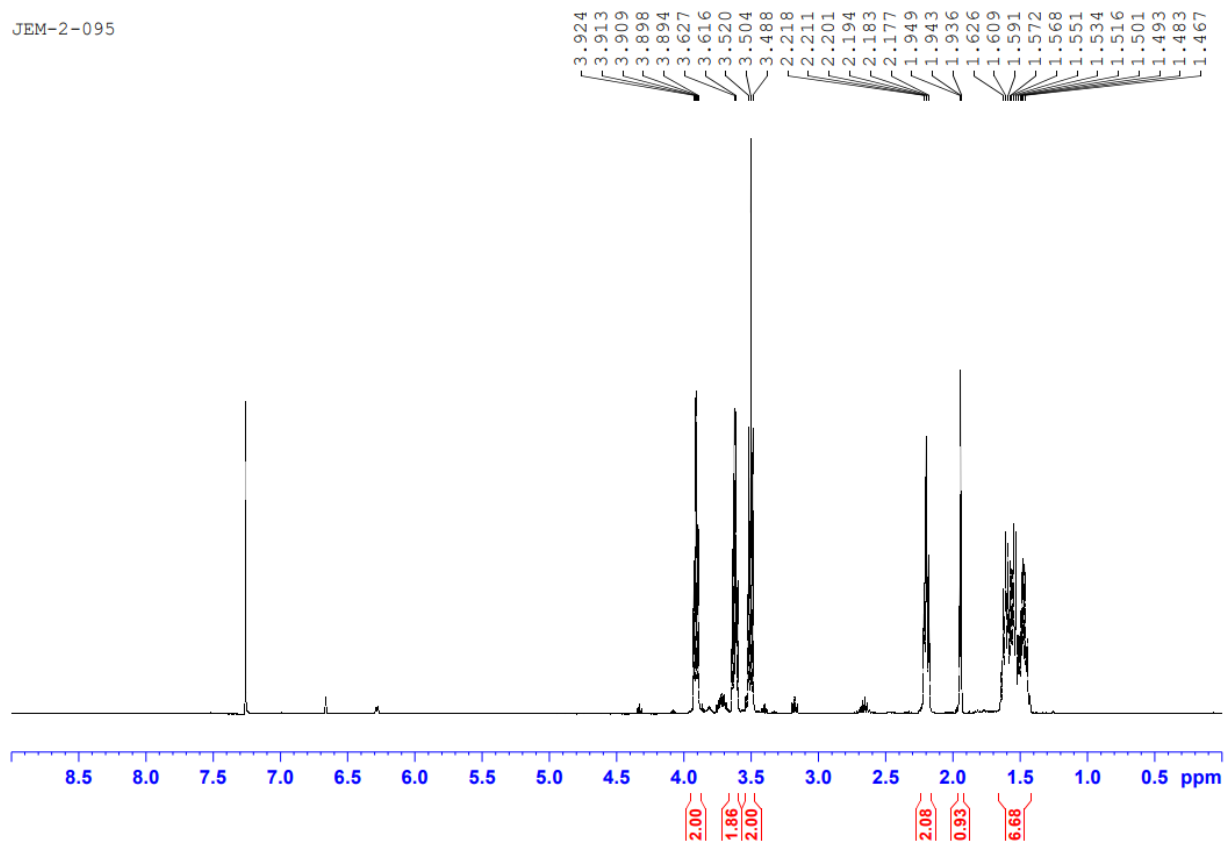
Figure 4.33: ^{1}H NMR of 2-(hept-6-yn-1-yloxy)ethanesulfonyl fluoride (4.10)
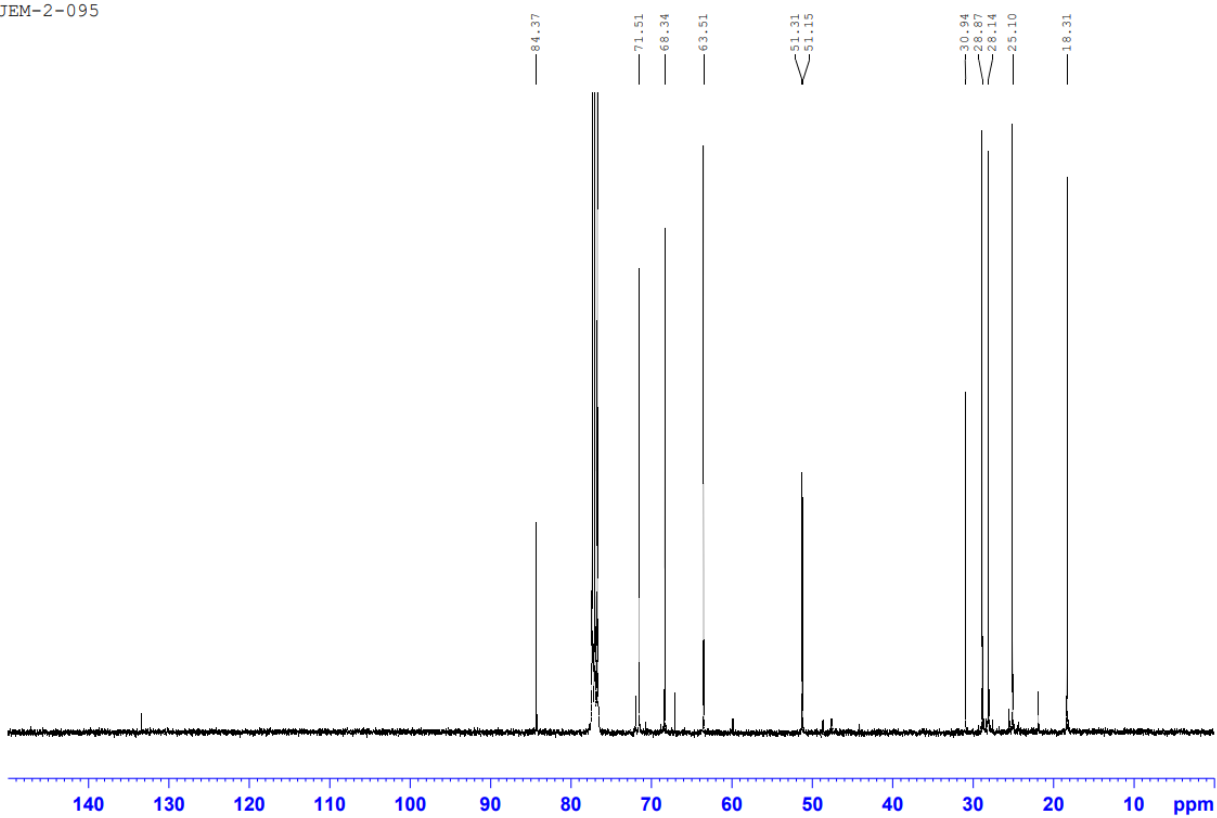
Figure 4.34: ¹³C NMR of 2-(hept-6-yn-1-yloxy)ethanesulfonyl fluoride (4.10)

4.5 References

1.   Simon, G. M.; Cravatt, B. F. Activity-based Proteomics of Enzyme Superfamilies: Serine Hydrolases as a Case Study. *Journal of Biological Chemistry* **2010**, *285* (15), 11051-11055. DOI: 10.1074/jbc.R109.097600.

2.   Holmquist, M. Alpha/Beta-hydrolase fold enzymes: structures, functions and mechanisms. *Curr Protein Pept Sci* **2000**, *1* (2), 209-235. DOI: 10.2174/1389203003381405.

3.   Ekici, O. D.; Paetzel, M.; Dalbey, R. E. Unconventional serine proteases: variations on the catalytic Ser/His/Asp triad configuration. *Protein Sci* **2008**, *17* (12), 2023-2037. DOI: 10.1110/ps.035436.108.

4.   Powers, J. C.; Asgian, J. L.; Ekici, O. D.; James, K. E. Irreversible inhibitors of serine, cysteine, and threonine proteases. *Chem Rev* **2002**, *102* (12), 4639-4750. DOI: 10.1021/cr010182v.

5.   Haedke, U.; Gotz, M.; Baer, P.; Verhelst, S. H. L. Alkyne derivatives of isocoumarins as clickable activity-based probes for serine proteases. *Bioorgan Med Chem* **2012**, *20* (2), 633-640. DOI: 10.1016/j.bmc.2011.03.014.

6.   Narayanan, A.; Jones, L. H. Sulfonyl fluorides as privileged warheads in chemical biology. *Chem Sci* **2015**, *6* (5), 2650-2659. DOI: 10.1039/c5sc00408j.

7.   Faucher, F.; Bennett, J. M.; Bogyo, M.; Lovell, S. Strategies for Tuning the Selectivity of Chemical Probes that Target Serine Hydrolases. *Cell Chem Biol* **2020**, *27* (8), 937-952. DOI: 10.1016/j.chembiol.2020.07.008.

8.   Bottcher, T.; Sieber, S. A. Beta-lactones as privileged structures for the active-site labeling of versatile bacterial enzyme classes. *Angew Chem Int Ed Engl* **2008**, *47* (24), 4600-4603. DOI: 10.1002/anie.200705768.

9.   Xue, Y.; Ha, Y. Catalytic mechanism of rhomboid protease GlpG probed by 3,4-dichloroisocoumarin and diisopropyl fluorophosphonate. *J Biol Chem* **2012**, *287* (5), 3099-3107. DOI: 10.1074/jbc.M111.310482.

10.   Powers, J. C.; Kam, C. M.; Narasimhan, L.; Oleksyszyn, J.; Hernandez, M. A.; Ueda, T. Mechanism-based isocoumarin inhibitors for serine proteases: use of active site structure and substrate specificity in inhibitor design. *J Cell Biochem* **1989**, *39* (1), 33-46. DOI: 10.1002/jcb.240390105.

11.   Babin, B. M.; Keller, L. J.; Pinto, Y.; Li, V. L.; Eneim, A. S.; Vance, S. E.; Terrell, S. M.; Bhatt, A. S.; Long, J. Z.; Bogyo, M. Identification of covalent inhibitors that disrupt M. tuberculosis growth by targeting multiple serine hydrolases involved in lipid metabolism. *Cell Chem Biol* **2022**, *29* (5), 897-909 e897. DOI: 10.1016/j.chembiol.2021.08.013.

12.   Pan, Z.; Jeffery, D. A.; Chehade, K.; Beltman, J.; Clark, J. M.; Grothaus, P.; Bogyo, M.; Baruch, A. Development of activity-based probes for trypsin-family serine proteases. *Bioorg Med Chem Lett* **2006**, *16* (11), 2882-2885. DOI: 10.1016/j.bmcl.2006.03.012.

13.   Oleksyszyn, J.; Powers, J. C. Irreversible inhibition of serine proteases by peptide derivatives of (alpha-aminoalkyl)phosphonate diphenyl esters. *Biochemistry* **1991**, *30* (2), 485-493. DOI: 10.1021/bi00216a026.

14.   Abuelyaman, A. S.; Hudig, D.; Woodard, S. L.; Powers, J. C. Fluorescent derivatives of diphenyl [1-(N-peptidylamino)alkyl]phosphonate esters: synthesis and use in the inhibition and cellular localization of serine proteases. *Bioconjug Chem* **1994**, *5* (5), 400-405. DOI: 10.1021/bc00029a004.

15.   Serim, S.; Mayer, S. V.; Verhelst, S. H. Tuning activity-based probe selectivity for serine proteases by on-resin 'click' construction of peptide diphenyl phosphonates. *Org Biomol Chem* **2013**, *11* (34), 5714-5721. DOI: 10.1039/c3ob40907d.

16.   Kahler, J. P.; Verhelst, S. H. L. Phosphinate esters as novel warheads for activity-based probes targeting serine proteases. *RSC Chem Biol* **2021**, *2* (4), 1285-1290. DOI: 10.1039/d1cb00117e.

17.   Serim, S.; Baer, P.; Verhelst, S. H. Mixed alkyl aryl phosphonate esters as quenched fluorescent activity-based probes for serine proteases. *Org Biomol Chem* **2015**, *13* (8), 2293-2299. DOI: 10.1039/c4ob02444c.

18.   Yang, J.; Mendowicz, R. J.; Verhelst, S. H. L. Tagged Benzoxazin-4-Ones as Novel Activity-Based Probes for Serine Proteases. *Chembiochem* **2021**, *22* (9), 1578-1581. DOI: 10.1002/cbic.202000848.

19.   Ruivo, E. F.; Goncalves, L. M.; Carvalho, L. A.; Guedes, R. C.; Hofbauer, S.; Brito, J. A.; Archer, M.; Moreira, R.; Lucas, S. D. Clickable 4-Oxo-beta-lactam-Based Selective Probing for Human Neutrophil Elastase Related Proteomes. *ChemMedChem* **2016**, *11* (18), 2037-2042. DOI: 10.1002/cmdc.201600258.

20.   Carvalho, L. A. R.; Ross, B.; Fehr, L.; Bolgi, O.; Wohrle, S.; Lum, K. M.; Podlesainski, D.; Vieira, A. C.; Kiefersauer, R.; Felix, R.; et al. Chemoproteomics-Enabled Identification of 4-Oxo-beta-Lactams as Inhibitors of Dipeptidyl Peptidases 8 and 9. *Angew Chem Int Ed Engl* **2022**, *61* (47), e202210498. DOI: 10.1002/anie.202210498.

21.   Haedke, U. R.; Frommel, S. C.; Hansen, F.; Hahne, H.; Kuster, B.; Bogyo, M.; Verhelst, S. H. Phosphoramidates as novel activity-based probes for serine proteases. *Chembiochem* **2014**, *15* (8), 1106-1110. DOI: 10.1002/cbic.201400013.

22.   Fahrney, D., Gold, Allen. Sulfonyl Fluorides as Inhibitors of Esterases. I. Rates of Reaction with Acetylcholinesterase, α-Chymotrypsin, and Trypsin. *JACS* **1963**, *85*, 997-1000.

23.   Shannon, D. A.; Gu, C.; McLaughlin, C. J.; Kaiser, M.; van der Hoorn, R. A.; Weerapana, E. Sulfonyl fluoride analogues as activity-based probes for serine proteases. *Chembiochem* **2012**, *13* (16), 2327-2330. DOI: 10.1002/cbic.201200531.

24.   Lively, M. O.; Powers, J. C. Specificity and reactivity of human granulocyte elastase and cathepsin G, porcine pancreatic elastase, bovine chymotrypsin and trypsin toward inhibition with sulfonyl fluorides. *Biochim Biophys Acta* **1978**, *525* (1), 171-179. DOI: 10.1016/0005-2744(78)90211-5.

25.   Vanhoutte, R.; Verhelst, S. H. L. Combinatorial Optimization of Activity-Based Probes for Acyl Protein Thioesterases 1 and 2. *ACS Med Chem Lett* **2022**, *13* (7), 1144-1150. DOI: 10.1021/acsmedchemlett.2c00174.

26.   Ferguson, T. E. G.; Reihill, J. A.; Martin, S. L.; Walker, B. Novel Inhibitors and Activity-Based Probes Targeting Trypsin-Like Serine Proteases. *Front Chem* **2022**, *10*, 782608. DOI: 10.3389/fchem.2022.782608.

27.   Liu, Y.; Patricelli, M. P.; Cravatt, B. F. Activity-based protein profiling: the serine hydrolases. *Proc Natl Acad Sci U S A* **1999**, *96* (26), 14694-14699. DOI: 10.1073/pnas.96.26.14694.

28.   Kidd, D.; Liu, Y.; Cravatt, B. F. Profiling serine hydrolase activities in complex proteomes. *Biochemistry* **2001**, *40* (13), 4005-4015. DOI: 10.1021/bi002579j.

29.   Patricelli, M. P.; Giang, D. K.; Stamp, L. M.; Burbaum, J. J. Direct visualization of serine hydrolase activities in complex proteomes using fluorescent active site-directed probes.

Proteomics **2001**, *1* (8), 1067-1071. DOI: 10.1002/1615-9861(200109)1:9<1067::aid-prot1067>3.0.co;2-4.

30.   Orlowski, M.; Cardozo, C.; Eleuteri, A. M.; Kohanski, R.; Kam, C. M.; Powers, J. C. Reactions of [14C]-3,4-dichloroisocoumarin with subunits of pituitary and spleen multicatalytic proteinase complexes (proteasomes). *Biochemistry* **1997**, *36* (45), 13946-13953. DOI: 10.1021/bi970666e.

31.   Bogyo, M.; Shin, S.; McMaster, J. S.; Ploegh, H. L. Substrate binding and sequence preference of the proteasome revealed by active-site-directed affinity probes. *Chem Biol* **1998**, *5* (6), 307-320. DOI: 10.1016/s1074-5521(98)90169-7.

32.   Ovaa, H.; van Swieten, P. F.; Kessler, B. M.; Leeuwenburgh, M. A.; Fiebiger, E.; van den Nieuwendijk, A. M.; Galardy, P. J.; van der Marel, G. A.; Ploegh, H. L.; Overkleeft, H. S. Chemistry in living cells: detection of active proteasomes by a two-step labeling strategy. *Angew Chem Int Ed Engl* **2003**, *42* (31), 3626-3629. DOI: 10.1002/anie.200351314.

33.   Gu, C.; Shannon, D. A.; Colby, T.; Wang, Z.; Shabab, M.; Kumari, S.; Villamor, J. G.; McLaughlin, C. J.; Weerapana, E.; Kaiser, M.; et al. Chemical proteomics with sulfonyl fluoride probes reveals selective labeling of functional tyrosines in glutathione transferases. *Chem Biol* **2013**, *20* (4), 541-548. DOI: 10.1016/j.chembiol.2013.01.016.

34.   Gushwa, N. N.; Kang, S.; Chen, J.; Taunton, J. Selective targeting of distinct active site nucleophiles by irreversible SRC-family kinase inhibitors. *J Am Chem Soc* **2012**, *134* (50), 20214-20217. DOI: 10.1021/ja310659j.

35.   Khandekar, S. S.; Feng, B.; Yi, T.; Chen, S.; Laping, N.; Bramson, N. A liquid chromatography/mass spectrometry-based method for the selection of ATP competitive kinase inhibitors. *J Biomol Screen* **2005**, *10* (5), 447-455. DOI: 10.1177/1087057105274846.

36.   Pereira, M. E.; Nguyen, T.; Wagner, B. J.; Margolis, J. W.; Yu, B.; Wilk, S. 3,4-dichloroisocoumarin-induced activation of the degradation of beta-casein by the bovine pituitary multicatalytic proteinase complex. *Journal of Biological Chemistry* **1992**, *267* (11), 7949-7955. DOI: 10.1016/s0021-9258(18)42604-x.

37.   Harper, J. W.; Hemmi, K.; Powers, J. C. Reaction of serine proteases with substituted isocoumarins: discovery of 3,4-dichloroisocoumarin, a new general mechanism based serine protease inhibitor. *Biochemistry* **1985**, *24* (8), 1831-1841. DOI: 10.1021/bi00329a005.

38.   Haedke, U.; Gotz, M.; Baer, P.; Verhelst, S. H. Alkyne derivatives of isocoumarins as clickable activity-based probes for serine proteases. *Bioorg Med Chem* **2012**, *20* (2), 633-640. DOI: 10.1016/j.bmc.2011.03.014.

39.   Kam, C. M.; Fujikawa, K.; Powers, J. C. Mechanism-based isocoumarin inhibitors for trypsin and blood coagulation serine proteases: new anticoagulants. *Biochemistry* **1988**, *27* (7), 2547-2557. DOI: 10.1021/bi00407a042.

40.   Powers, J. C.; Oleksyszyn, J.; Narasimhan, S. L.; Kam, C. M. Reaction of porcine pancreatic elastase with 7-substituted 3-alkoxy-4-chloroisocoumarins: design of potent inhibitors using the crystal structure of the complex formed with 4-chloro-3-ethoxy-7-guanidinoisocoumarin. *Biochemistry* **1990**, *29* (12), 3108-3118. DOI: 10.1021/bi00464a030.

41.   Vijayalakshmi, J.; Meyer, E. F., Jr.; Kam, C. M.; Powers, J. C. Structural study of porcine pancreatic elastase complexed with 7-amino-3-(2-bromoethoxy)-4-chloroisocoumarin as a nonreactivatable doubly covalent enzyme-inhibitor complex. *Biochemistry* **1991**, *30* (8), 2175-2183. DOI: 10.1021/bi00222a022.

42.   Kerrigan, J. E.; Oleksyszyn, J.; Kam, C. M.; Selzler, J.; Powers, J. C. Mechanism-based isocoumarin inhibitors for human leukocyte elastase. Effect of the 7-amino substituent and 3-

alkoxy group in 3-alkoxy-7-amino-4-chloroisocoumarins on inhibitory potency. *J Med Chem* **1995**, *38* (3), 544-552. DOI: 10.1021/jm00003a017.

43.   Vinothkumar, K. R.; Strisovsky, K.; Andreeva, A.; Christova, Y.; Verhelst, S.; Freeman, M. The structural basis for catalysis and substrate specificity of a rhomboid protease. *EMBO J* **2010**, *29* (22), 3797-3809. DOI: 10.1038/emboj.2010.243.

44.   Arastu-Kapur, S.; Ponder, E. L.; Fonovic, U. P.; Yeoh, S.; Yuan, F.; Fonovic, M.; Grainger, M.; Phillips, C. I.; Powers, J. C.; Bogyo, M. Identification of proteases that regulate erythrocyte rupture by the malaria parasite Plasmodium falciparum. *Nat Chem Biol* **2008**, *4* (3), 203-213. DOI: 10.1038/nchembio.70.

45.   Kam, C. M.; Abuelyaman, A. S.; Li, Z.; Hudig, D.; Powers, J. C. Biotinylated isocoumarins, new inhibitors and reagents for detection, localization, and isolation of serine proteases. *Bioconjug Chem* **1993**, *4* (6), 560-567. DOI: 10.1021/bc00024a021.

46.   Mehner, C.; Hockla, A.; Coban, M.; Madden, B.; Estrada, R.; Radisky, D. C.; Radisky, E. S. Activity-based protein profiling reveals active serine proteases that drive malignancy of human ovarian clear cell carcinoma. *J Biol Chem* **2022**, *298* (8), 102146. DOI: 10.1016/j.jbc.2022.102146.

47.   Urban, S.; Lee, J. R.; Freeman, M. Drosophila rhomboid-1 defines a family of putative intramembrane serine proteases. *Cell* **2001**, *107* (2), 173-182. DOI: 10.1016/s0092-8674(01)00525-6.

48.   McGovern-Gooch, K. R.; Mahajani, N. S.; Garagozzo, A.; Schramm, A. J.; Hannah, L. G.; Sieburg, M. A.; Chisholm, J. D.; Hougland, J. L. Synthetic Triterpenoid Inhibition of Human Ghrelin O-Acyltransferase: The Involvement of a Functionally Required Cysteine Provides

Mechanistic Insight into Ghrelin Acylation. *Biochemistry* **2017**, *56* (7), 919-931. DOI:

10.1021/acs.biochem.6b01008

49.   Narayanan, A.; Jones, L. H. Sulfonyl fluorides as privileged warheads in chemical biology.

Chem Sci **2015**, *6* (5), 2650-2659. DOI: 10.1039/c5sc00408j.

50.   Darling, J. E.; Zhao, F.; Loftus, R. J.; Patton, L. M.; Gibbs, R. A.; Hougland, J. L.

Structure-Activity Analysis of Human Ghrelin O-Acyltransferase Reveals Chemical

Determinants of Ghrelin Selectivity and Acyl Group Recognition. *Biochemistry* **2015**, *54* (4),

1100-1110. DOI: 10.1021/bi5010359

51.   Campana, M. B.; Irudayanathan, F. J.; Davis, T. R.; McGovern-Gooch, K. R.; Loftus, R.;

Ashkar, M.; Escoffery, N.; Navarro, M.; Sieburg, M. A.; Nangia, S.; Hougland, J. L. The ghrelin

O-acyltransferase structure reveals a catalytic channel for transmembrane hormone acylation. *J

Biol Chem* **2019**, *294* (39), 14166-14174. DOI: 10.1074/jbc.AC119.009749.

52.   Petri, L.; Abranyi-Balogh, P.; Csorba, N.; Keeley, A.; Simon, J.; Randelovic, I.; Tovari, J.;

Schlosser, G.; Szabo, D.; Drahos, L.; Keseru, G. M. Activation-Free Sulfonyl Fluoride Probes

for Fragment Screening. *Molecules* **2023**, *28* (7). DOI: 10.3390/molecules28073042

53.   Coupland, C. E.; Andrei, S. A.; Ansell, T. B.; Carrique, L.; Kumar, P.; Sefer, L.; Schwab,

R. A.; Byrne, E. F. X.; Pardon, E.; Steyaert, J.; et al. Structure, mechanism, and inhibition of

Hedgehog acyltransferase. *Mol Cell* **2021**, *81* (24), 5025-5038 e5010. DOI:

10.1016/j.molcel.2021.11.018.

54.   Jiang, Y.; Benz, T. L.; Long, S. B. Substrate and product complexes reveal mechanisms of

Hedgehog acylation by HHAT. *Science* **2021**, *372* (6547), 1215-1219. DOI:

10.1126/science.abg4998.

55.   Liu, Y.; Qi, X.; Donnelly, L.; Elghobashi-Meinhardt, N.; Long, T.; Zhou, R. W.; Sun, Y.; Wang, B.; Li, X. Mechanisms and inhibition of Porcupine-mediated Wnt acylation. *Nature* **2022**, *607* (7920), 816-822. DOI: 10.1038/s41586-022-04952-2.

56.   Rana, M. S.; Kumar, P.; Lee, C. J.; Verardi, R.; Rajashankar, K. R.; Banerjee, A. Fatty acyl recognition and transfer by an integral membrane S-acyltransferase. *Science* **2018**, *359* (6372). DOI: 10.1126/science.aao6326

57.   Zhang, Q.; Yao, D.; Rao, B.; Jian, L.; Chen, Y.; Hu, K.; Xia, Y.; Li, S.; Shen, Y.; Qin, A.; et al. The structural basis for the phospholipid remodeling by lysophosphatidylcholine acyltransferase 3. *Nat Commun* **2021**, *12* (1), 6869. DOI: 10.1038/s41467-021-27244-1.

58.   Haedke, U.; Gotz, M.; Baer, P.; Verhelst, S. H. Alkyne derivatives of isocoumarins as clickable activity-based probes for serine proteases. *Bioorg Med Chem* **2012**, *20* (2), 633-640. DOI: 10.1016/j.bmc.2011.03.014.

59.   Riddles, P. W. B., R. L.; Zerner, B., . Ellman's reagent: 5,5'-dithiobis(2-nitrobenzoic acid)--a reexamination. *Analytical Biochemistry* **1979**, *94* (1), 75-81.

60.   Pangborn, A. B.; Giardello, M. A.; Grubbs, R. H.; Rosen, R. K.; Timmers, F. J. Safe and convenient procedure for solvent purification. *Organometallics* **1996**, *15* (5), 1518-1520. DOI: DOI 10.1021/om9503712.

Chapter 5: Investigation of the impact of ethanol and small-molecule GHSR inverse agonist on ghrelin acylation: The intersection of ghrelin signaling and addictive behavior.

The work performed herein is a part of a multi-lab collaborative team that investigated ghrelin production and signaling from enzyme to cell to organism to patient, and has been published in two papers: "Initial Pharmacological Characterization of a Major Hydroxy Metabolite of PF-5190457: Inverse Agonist Activity of PF-6870961 at the Ghrelin Receptor", [1] and "A closer look at alcohol-induced changes in the ghrelin system: novel insights from preclinical and clinical data." [2]

I performed the testing of ethanol and inverse agonist and inverse agonist metabolites for GOAT inhibition in these publications.

5.1 Introduction

5.1.1 Ethanol administration alters the ghrelin axis

Recent studies have indicated that ghrelin signaling is linked to the neuropharmacology of addiction in addition to its canonical orexigenic effect. [3-7] Stimulation of the mesolimbic dopaminergic system results in dopamine release in local neurons. Located in the ventral tegmental area (VTA) of the brain, release of dopamine in this area is associated with the reward pathways triggered through pleasurable behaviors like feeding or drugs of abuse, including alcohol. [8-12] Ghrelin injections into the VTA have been shown to release dopamine in a manner consistent with the activation of this reward pathway. [13] This ability for ghrelin to alter the brain response to pleasurable stimuli led to the examination of ghrelin in the context of altered seeking behaviors, including drug addiction. Other studies have positively correlated ghrelin levels to alcohol cravings. [14-17] Furthermore, recent fMRI studies have indicated that increased ghrelin levels are significantly associated with alcohol cue-induced brain response, while an increase in total ghrelin level does not induce the same response. [18, 19] Ghrelin has been shown to modulate alcohol cravings and alcohol seeking behavior through GHSR, as rats treated with GHSR antagonists or GSHR knockout rats exhibit lowered alcohol preference. [20]

Administration of ethanol in rats has been shown to decrease the levels of both ghrelin and total ghrelin, which is reflected in a reduction of plasma ghrelin in humans upon exposure to ethanol. [21-25] This further extends to patients with alcohol use disorder (AUD), who exhibit reduced levels of ghrelin compared to non-AUD controls. [17] Patients with AUD who actively consume alcohol exhibit lower levels of ghrelin than patients who abstain. [17] A study performed with patients in hospital treatment for alcohol addiction reported that ghrelin levels were significantly increased in this cohort, even when corrected for BMI. [26, 27] Over the course of

patient withdrawal, plasma ghrelin levels continued to increase but could not be correlated to craving experienced by the subjects. [26] In humans, intravenous (IV) administration of ghrelin increases self-reported alcohol craving, alcohol self-administration, and functional magnetic resonance imaging (fMRI) response to alcohol in the amygdala. [28, 29] The contrast between the effects of ghrelin on the ability to stimulate alcohol cravings under acute treatment with the evidence of lowered ghrelin upon administration of ethanol indicate a relationship between ethanol and ghrelin that is not yet fully characterized. Exploration of the effects of GOAT inhibition on alcohol use disorder (AUD) and other substances is desired due to the potential therapeutic value of ghrelin inhibition in treating these conditions[6, 30]

5.1.2 PF-6870961 and PF-5190457 are potential GOAT inhibitors

PF-5190457, is a recently discovered spiro-azetidino-piperidine compound developed by Pfizer with the ability to modulate Type II Diabetes (T2D) through the modulation of GHSR. [31] PF-5190457 was shown to have *in vitro* and *ex vivo* activity against GHSR, acting as an inverse agonist by decreasing the normal constitutive activity of the receptor. [31-33] In humans, PF-5190457 at was shown to decrease ghrelin-induced GH secretion by 77% and gastric emptying time by 20%, indicating modulation of GH levels through inverse agonism of GHSR. [34] Studies at the NIH have identified that PF-5190457 had no effects on alcohol metabolism in rats, combined with behavior modification consistent with reduced alcohol and food craving. [35] Continued studies identified a novel major human metabolite of PF-5190457 which was characterized as a hydroxy addition on the piperidine group of PF-5190457 to produce the metabolite deemed PF-6870961 (**Figure 5.1**). The potential effects of these molecules on GOAT

activity needed to be understood to understand the physiological effects of these molecules and fully characterize their pharmacological profiles.
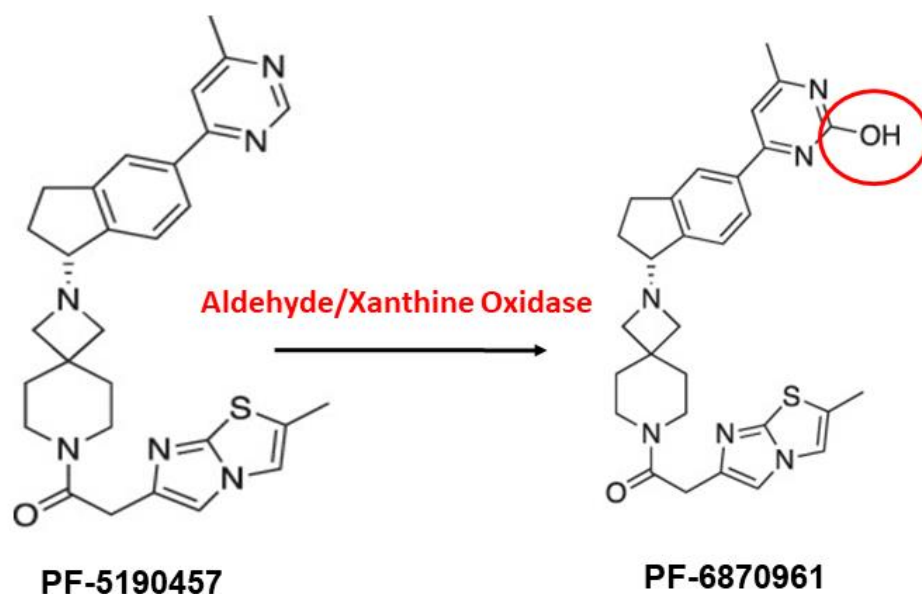
Figure 5.1: Structure and metabolism of PF-5190457, inverse agonist of GHSR. PF-5190457 is oxidized in humans, giving rise to PF-6870961, novel metabolite of PF-5190457. Figure taken with permission from Deschaine et. al, 2023. [1] © 2023 American Society for Pharmacology and Experimental Therapeutics.

5.2 Results

5.2.1 GOAT is not affected by physiological levels of ethanol

Since the levels of ghrelin are indicated to decrease under administration of ethanol in both rodents and humans, it was desired to test the possibility that direct ethanol inhibition of hGOAT-catalyzed ghrelin acylation is responsible for a decrease in acylated ghrelin production. [21-24, 29, 36] Therefore, we assayed GOAT acylation activity *in vitro* in increasing concentrations of ethanol using membrane protein from Sf9 cells expressing hGOAT. Ethanol was tested at concentrations representing intracellular ethanol levels ranging from sub-intoxicating (1 mM) to grossly (lethal) intoxicating (87 mM) doses. [37, 38] We found that ghrelin acylation by GOAT was not dose-dependently inhibited by ethanol over this physiologically relevant concentration range, with less than 20% inhibition observed at the highest concentration tested (**Figure 5.2**).

Complementary studies were performed by our collaborations to elucidate the mechanism of ghrelin suppression by consumed alcohol for potential treatment of AUD. Analysis of ghrelin and total grelin levels performed by Mehdi Farokhnia (Johns Hopkins Bloomberg School of Public Health), Sara L. Deschaine (National Institute of Health), and Lorenzo Leggio (National Institute of Health) found that both acyl- and total ghrelin levels are decreased after alcohol intake, regardless of administration route. The effects of alcohol were found to be independent of GHSR, as GHSR rat knockouts still exhibit a reduced ghrelin level upon treatment with alcohol (Adriana Gregory-Flores, Lia J. Zallar, Renata C. N. Marchette, Brendan J. Tunstall, Leandro F. Vendruscolo; National Institute of Health). Furthermore, the reduction in baseline ghrelin levels in AUD patients is not a result of altered GHSR, GHRL, or MBOAT4 (GOAT) gene expression in the brain, as mRNA expression of these proteins was not found to be significantly altered patients with AUD. Epithelial cells grown in the presence of alcohol exhibit no significant
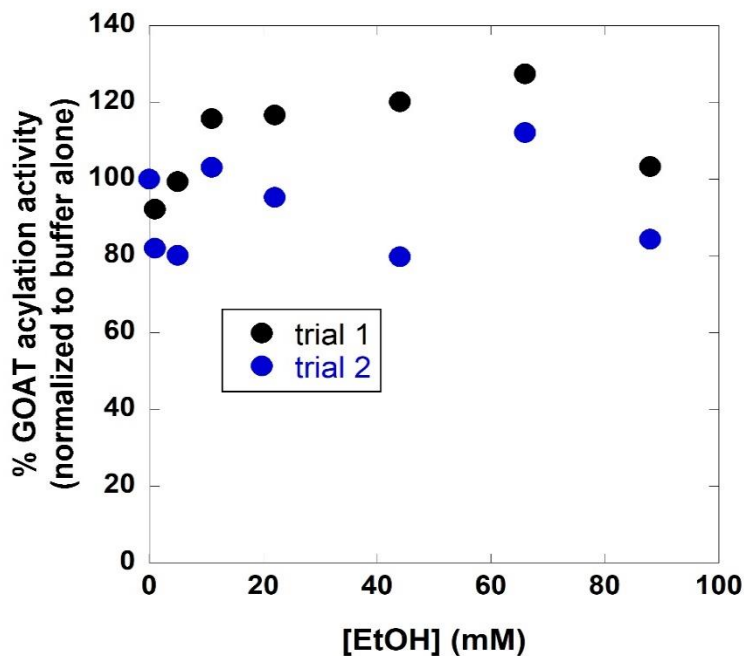
Figure 5.2: Inhibition profile of ethanol against hGOAT. Effects of increasing ethanol concentration on hGOAT activity. Physiologically relevant concentrations (1 mm – 88 mM) of ethanol were added to reaction mixtures containing 70 µg membrane protein, 1.5 µM GSSFLC$_{AcDan}$, and 300 µM octanoyl-CoA and allowed to react for 30 minutes. Trial 1 and Trial 2 are independent replications of the same experiment. Figure reused with permission from Deschaine et Al (2022). [2] © 2022 Society for the Study of Addiction

decrease in ghrelin secretion, indicating that ghrelin secretion is unaffected by physiological levels of alcohol (Barath K. Mani and Jeffrey M. Zigman; UT Southwestern Medical Center). Finally, rats treated with a calorically equivalent amount of alcohol or sucrose were found to have exhibited a decrease in ghrelin levels when treated with alcohol, while no such decrease was exhibited in those treated with sucrose in the same timeframe (Mehdi Farokhnia, Sara L. Deschaine, Adriana Gregory-Flores, Lia J. Zallar, Renata C. N. Marchette, Brendan J. Tunstall, George F. Koob, Leandro F. Vendruscolo, Lorenzo Leggio). [2]

5.2.2   GOAT is not affected by either PF-6870961 and PF-5190457

To determine whether the GHSR inverse agonist PF-5190457 and its metabolite PF-6870961 could interfere with ghrelin acylation activity of GOAT, PF-5190457 and PF-6870961 were tested for hGOAT inhibitory activity. PF-5190457 was limited in testing due to poor solubility and did not appreciably inhibit hGOAT at the highest tested concentration (~30% inhibition at 195 μM), exhibiting no evidence for concentration-dependent inhibition. PF-6870961 also did not inhibit hGOAT, with less than 20% inhibition at 1000 μM. (**Figure 5.3**). PF-5190457 and PF-6870961 did not inhibit GOAT enzymatic activity, indicating that neither the parent nor the metabolite compounds suppress ghrelin acylation through direct inhibition of GOAT.
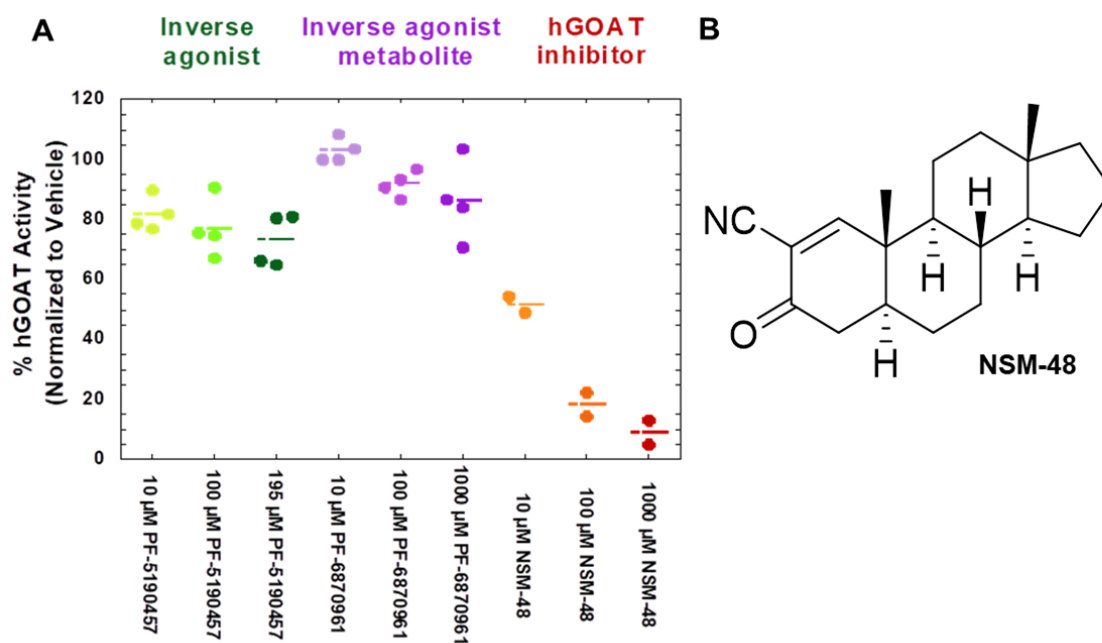
Figure 5.3: Inhibition of hGOAT by GSHR inverse agonist PF-5190457, metabolite PF-6870961, and known hGOAT inhibitor NSM-48. a.) Effect of PF-5190457 at 10-195 µM and PF-6870961 at 10-1000 µM in comparison to known GOAT inhibitor, NSM-48, at 10–1000 µM. %hGOAT activity = octanoylation of ghrelin mimetic $GSSFLC_{NH2}$ peptide in presence of inhibitor expressed as a percentage of that in the absence of inhibitor and is normalized to vehicle condition. **b.)** Structure of NSM-48 provided for reference. Data represents mean and individual values from independent experiments. n = 2-4. hGOAT = human ghrelin O-acyltransferase. Data has been published in Deschaine et. Al (2023) and is reused with permission. [1] © 2023 American Society for Pharmacology and Experimental Therapeutics.

5.3   Discussion

5.3.1 Ethanol, PF-6870961 and PF-5190457 do not affect AUD through inhibition of ghrelin octanoylation

We found that ghrelin acylation by GOAT was not dose-dependently inhibited by ethanol over a physiologically relevant concentration range. While GOAT may not be affected by ethanol, collaborators in this study did find that alcohol administration led to a reduction in ghrelin levels. Gene expression of *GHRL*, *GHSR,* and *MBOAT4* was not appreciably changed in AUD when compared to control groups.[2] Further experiments indicated that no direct interaction between ethanol and ghrelin modulation could be observed, suggesting that ghrelin reduction is likely a result of indirect effects, possibly a result of caloric load. While plausible, previous experiments indicate that ghrelin levels do not correlate to caloric intake from ethanol.[39]

PF-5190457 has been found to lower self-reported food craving following food cue exposure, possibly by interacting with the ghrelin axis through modulation of GOAT activity.[35, 40-44] Both PF-5190457 and PF-6870961 did not inhibit GOAT enzymatic activity, indicating that both the parent and metabolite compounds do not suppress ghrelin acylation, even with both compounds suppressing food intake in rats, suggesting modulation of the hunger response through an unknown alternative mechanism.[1]

5.3.2   Insights on methods of action of PF-6870961 and PF-5190457

Initial clinical work had not analyzed the effects of treatment with PF-05190457 on ghrelin levels directly, instead focusing on GH release and interaction of the molecule with GHSR to cause inverse agonism.[45] Recent studies analyzed levels of both ghrelin and total

ghrelin both upon treatment with PF-5190457, and subsequent alcohol dosing post-treatment, finding a significant decrease in the ghrelin/total ghrelin ratio as an effect of drug dosage. [35] This finding indicated that the effects of PF-5190457 on GH secretion may be in part due to this reduction in the ghrelin/total ghrelin ratio, and the potential for the novel hydroxymetabolite PF-6870961 to contribute to the alteration of the ghrelin/total ghrelin ration is currently unknown. The modulation of this axis by both molecules could be the result of preventing acylation of ghrelin through direct inhibition of GOAT, decreasing the ghrelin concentration in serum. The lack of inhibition of GOAT by PF-5190457 and the metabolite PF-6870961 in our study precludes this possibility, indicating the lowered ghrelin/total ghrelin axis is a result of an as-yet-unknown alternative pathway.

Injections of PF-6870961 into rats fed *ab libitum* reduced food intake in both fed and fasting populations. These effects were eliminated when repeated on GHSR knockout rats, indicating that the effects of PF-6870961 are modulated through GHSR. Computational analysis of PF-5190457 and PF-6870961 with GHSR indicates the differentially hydroxylated moiety interacts with the majorly hydrophobic cleft between TMD2 and TMD3, potentially giving reason for the 25-fold lower affinity of PF-6870961 due to the unfavorable polarity increase in this contact. [46] Accordingly, PF-6870961 is not as efficient an inverse agonist of GHSR, being around 25 times less potent than PF-5190457, and alanine substitution of polar residues that interact with the hydroxylated moiety of the metabolite reduce inhibition of GHSR. [46] Contrary to this finding, comparison of effective inhibitory concentrations of PF-5190457 and PF-6870961 revealed that PF-6870961 had the highest potency for the GHSR recruitment of β-arrestin, chosen to indicate the effect on downstream signaling. [1, 47] This may be an indication of higher receptor reserves for the metabolite than the parent compounds, although further studies

will be needed in this area. This does provide an exciting insight into the structure-activity relationship of this interaction, due to the compounds differing by only a hydroxyl group.

GHSR inverse agonist PF-5190457 and its hydroxylated metabolite PF-6870961 each bind GHSR, with the hydroxylation resulting in distinct differences in the binding and inverse agonist abilities of these compounds. Human studies of PF-5190457 and PF-6870961 in the plasma in humans indicate that the metabolite circulates at approximately 25% of the concentration of the parent compound. [1] The presence of these two compounds with distinct activities indicate that the observed effects of treatment with PF-5190457 are likely a combination of the parent compound and the metabolite. The contribution of PF-6870961 in humans is currently unknown, and *in vivo* work supporting the ability of the metabolite to cause a reduction in food intake was performed at concentrations exceeding the potential circulating metabolite concentrations in humans, limiting the potential impact of this compound.

5.4 Conclusion

While exposure to ethanol reduces ghrelin and total ghrelin levels, the mechanism of the interaction with the ghrelin axis is currently unknown. [21-25] One potential solution to this interaction would be the direct inhibition of GOAT by ethanol. We have shown that hGOAT is not inhibited by ethanol. This data was used in support of further investigation of the ghrelin axis in alcohol use disorder, finding that neither GHSR nor GOAT are required for the modulation of the ghrelin system. In addition, ghrelin secretion from gastric mucosal cells is not inhibited by ethanol, and the variation of ghrelin cannot be attributed to caloric intake. [2] In conclusion, ethanol suppresses ghrelin without direct interaction with the ghrelin system, and further study is needed to elucidate the physiological basis for this effect.

Continuing the investigation of the GHSR inverse agonist PF-5190457, we determined that PF-5190457 and the metabolite PF-6870961 do not exert their anorexic effects through inhibition of GOAT. This data was used to support findings improving insights into the mechanism of action of these two compounds and their effects on the modulation of hunger cues through GHSR. These findings suggest that PF-5190457 should consider additional activity due to formation of the active hydroxymetabolite, PF-6870961, while providing insight into future GHSR antagonists.

There are a growing number of GHSR modulators in the literature, and few of these molecules have been characterized for their effects on the other canonical ghrelin-binding protein: GOAT. [48-55] As GHSR modulators have been shown to impact the ghrelin levels in plasma and bind both GHSR and GOAT, it is imperative that molecules that impact the ghrelin signaling pathway are evaluated for their potential effects on GOAT. [35, 56]

5.5 Materials and Methods

5.5.1 General Methods

Methyl arachidonyl fluorophosphonate (MAFP, Cayman Chemical, Ann Arbor, MI) was diluted in DMSO from a stock in methyl acetate. Absolute ethanol was purchased from Pharmco (Brookfield, CT). Octanoyl-coenzyme A (Octanoyl-CoA, CoALA Biosciences, Austin, TX) was diluted to 5 mM in 10 mM Tris-HCl pH 7.0 and stored in low adhesion tubes at -80°C until use. The ghrelin-mimetic GSSFLC$_{NH2}$ peptide substrate was commercially synthesized by Sigma-Genosys (The Woodlands, TX) in Pepscreen format. The GSSFLC$_{NH2}$ peptide was solubilized in 1:1 acetonitrile/water solution and stored at -80°C. The peptide concentration was determined spectrophotometrically at 412 nm by reaction of the cysteine thiol with 5,5'dithiobis (2-nitrobenzoic acid) using an ϵ_{412} of 14,150 M^{-1} cm^{-1} [57]. Peptide substrates were fluorescently labeled with acrylodan and purified via reverse phase HPLC as previously reported. hGOAT was expressed and enriched in insect (Sf9) membrane protein fractions using a previously published procedure [58, 59].

Membrane proteins fractions from Sf9 cells expressing hGOAT were thawed on ice and then homogenized by passage through an 18-gauge needle ten times. Ethanol working stocks (5.44 mM, 10.87 mM, 21.74 mM, 43.48 mM, 65.22 mM, and 86.96 mM) were prepared by serial dilution. Assays were performed with 70 µg of membrane protein as determined by Bradford assay. For each set of eleven assays, a master mix (495 µL) was prepared containing 2.5 mM HEPES, 10 µM methyl arachidonyl fluorophosphonate (MAFP), and 770 µg membrane protein. The master mix was aliquoted (44 µL) into each low-adhesion microcentrifuge tube, followed by addition of 1 µL of the appropriate ethanol stock. The reaction mixture was then pre-incubated for 30 min at room temperature in a sealed microcentrifuge tube. Reactions were initiated by the

addition of octanoyl-CoA (300 µM final concentration) and GSSFLC$_{AcDan}$ peptide (1.5 µM final

concentration) to yield a final reaction volume of 50 µL. Reactions were incubated for 1 h at

room temperature while sealed, and then stopped by addition of 50 µL of 20% acetic acid in

isopropanol. Membrane proteins were then removed via precipitation with 16.7 µL of 20%

trichloroacetic acid followed by centrifugation (1000 x g, 1 min). The supernatant was then

analyzed via reverse-phase HPLC as described previously [60, 61]. GOAT acylation activity was

determined by substrate and product peak integration in the presence of either ethanol or water

(vehicle). Percent activity for each reaction was calculated using equations 5.1 and 5.2 [58].

$$\text{(5.1)} \quad \text{\% peptide octanoylation} = \frac{\text{fluorescence of octanoylated peptide}}{\text{total peptide fluorescence (substrate and product)}}$$

$$\text{(5.2)} \quad \text{\% activity} = \frac{\text{\% peptide octanoylation in presence of inhibitor}}{\text{\% peptide octanoylation in absence of inhibitor}}$$

5.5.2 Ghrelin O-acyltransferase (GOAT) Activity Assay with PF-5190457 and PF-6870961

PF-6870961 and PF-5190457 were received as a gift from the Leggio laboratory (NIH).

Methyl arachidonyl fluorophosphonate (MAFP, Cayman Chemical, Ann Arbor, MI) was diluted

in DMSO from a stock in methyl acetate. Octanoyl coenzyme A (octanoyl CoA, CoALA, Austin,

TX USA) was diluted to 5 mM in 10 mM Tris-HCl pH 7.0 and stored in low adhesion tubes at -

80°C until use. The ghrelin-mimetic GSSFLC$_{NH2}$ peptide substrate was commercially

synthesized by Sigma-Genosys (The Woodlands, TX USA) in Pepscreen format. The

GSSFLC$_{NH2}$ peptide was solubilized in 1:1 acetonitrile/water solution and stored at -80°C.

Peptide concentration was determined spectrophotometrically at 412 nm by reaction of the

cysteine thiol with 5,5'dithiobis(2-nitrobenzoic acid) using an ϵ_{412} of 14,150 M^{-1} cm^{-1}[57]. Peptide

substrates were fluorescently labeled with acrylodan and purified via reverse phase high-performance liquid chromatography (HPLC), as previously reported [58, 61]. Human GOAT (hGOAT) was expressed and enriched in insect (Sf9) membrane protein fractions using a previously published procedure [58, 61, 62]. Membrane proteins fractions from Sf9 cells expressing hGOAT were thawed on ice, then homogenized by passage through an 18-gauge needle ten times. Assays were performed with 10 µg of membrane protein as determined by Bradford assay. For each set of ten samples, a 440 µL master mix was prepared containing 2.5 mM N-2-hydroxyethylpiperazine-N-2-ethane sulfonic acid (HEPES), 10 µM methyl-arachidonyl fluorophosphate (MAFP), and 110 µg membrane protein. 40 µL of the master mix was aliquoted into each low-adhesion microcentrifuge tube. Compounds PF-6870961 and the previously reported GOAT inhibitor NSM-48 were diluted in DMSO to concentrations of 0.5 mM, 5.0 mM, and 50 mM prior to addition to the reaction mixture [62]. Due to solubility limitations, compound PF-5190457 was solubilized in DMSO to concentrations of 0.1 mM, 1.0 mM, 1.95 mM prior to addition to the reaction mixture. 1 µL of inhibitor stock and 4 µL DMSO (5 µL of PF-5190457 stocks) were added to each reaction and allowed to preincubate for 30 min at room temperature. Reactions were initiated by the addition of octanoyl CoA (300 µM final concentration) and GSSFLC$_{AcDan}$ peptide (1.5 µM final concentration) to yield a final reaction volume of 50 µL. Reactions were incubated for 30 min at room temperature while sealed and then stopped by addition of 50 µL of 20% acetic acid in isopropanol. Membrane proteins were then removed via precipitation with 16.7 µL of 20% trichloroacetic acid followed by centrifugation (1000 x g, 1 min). The supernatant was analyzed via reverse-phase HPLC, as previously described [61]. GOAT acylation activity was determined by substrate and product peak integration in the presence of

either sample or vehicle (DMSO). Percent activity was calculated using the Equations 5.1 and

5.2, as above.

Order Date	29-Apr-2024	Type of Use	Republish in a thesis/dissertation
Order License ID	1478451-1	Publisher	AMERICAN SOCIETY FOR PHARMACOLOGY AND EXPERIMENTAL THERAPEUTICS
ISSN	1521-0103	Portion	Image/photo/illustration

LICENSED CONTENT

Publication Title	The journal of pharmacology and experimental therapeutics	Country	United States of America
Author/Editor	American Society for Pharmacology and Experimental Therapeutics.	Rightsholder	Am Soc for Pharmacology & Experimental Therapeutics
Date	01/01/1909	Publication Type	e-Journal
Language	English	URL	http://jpet.aspetjournals.org/

REQUEST DETAILS

Portion Type	Image/photo/illustration	Distribution	United States
Number of Images / Photos / Illustrations	2	Translation	Original language of publication
Format (select all that apply)	Print, Electronic	Copies for the Disabled?	No
Who Will Republish the Content?	Academic institution	Minor Editing Privileges?	No
Duration of Use	Life of current edition	Incidental Promotional Use?	No
Lifetime Unit Quantity	Up to 999	Currency	USD
Rights Requested	Main product		

NEW WORK DETAILS

Title	Development and application of small-molecule probes targeting ghrelin O-acyltransferase	Institution Name	Syracuse University
		Expected Presentation Date	2024-05-15
Instructor Name	James Hougland		

ADDITIONAL DETAILS

The Requesting Person / Organization to Appear on the License	Jacob E. Moose

REQUESTED CONTENT DETAILS

Title, Description or Numeric Reference of the Portion(s)	Figure 1, Figure 2	Title of the Article / Chapter the Portion Is From	Initial pharmacological characterization of a major hydroxy metabolite of PF-5190457: inverse agonist activity of PF-6870961 at the ghrelin receptor
Editor of Portion(s)	N/A		
Volume / Edition	386	Author of Portion(s)	Sara Deschaine, Jacob Moose
Page or Page Range of Portion	117-128	Publication Date of Portion	2023-08-01

Appendix III: Reprint permission for Reference 1, Chapter 5

CCC | RightsLink

A closer look at alcohol-induced changes in the ghrelin system: novel insights from preclinical and clinical data
Author: Lorenzo Leggio, Leandro F. Vendruscolo, George F. Koob, et al
Publication: Addiction Biology
Publisher: John Wiley and Sons
Date: Apr 27, 2021

Published 2021. This article is a U.S. Government work and is in the public domain in the USA.

Order Completed

Thank you for your order.

This Agreement between Jacob Moose ("You") and John Wiley and Sons ("John Wiley and Sons") consists of your license details and the terms and conditions provided by John Wiley and Sons and Copyright Clearance Center.

Your confirmation email will contain your order number for future reference.

License Number   5778891501860

License date   Apr 30, 2024

Licensed Content

Licensed Content Publisher	John Wiley and Sons
Licensed Content Publication	Addiction Biology
Licensed Content Title	A closer look at alcohol-induced changes in the ghrelin system: novel insights from preclinical and clinical data
Licensed Content Author	Lorenzo Leggio, Leandro F. Vendruscolo, George F. Koob, et al
Licensed Content Date	Apr 27, 2021
Licensed Content Volume	27
Licensed Content Issue	1
Licensed Content Pages	18

Order Details

Type of use	Dissertation/Thesis
Requestor type	Author of this Wiley article
Format	Print and electronic
Portion	Figure/table
Number of figures/tables	1
Will you be translating?	No

About Your Work

Title of new work	Development and application of small-molecule probes targeting ghrelin O-acyltransferase
Institution name	Syracuse University
Expected presentation date	May 2024

Additional Data

Order reference number	19676
Portions	Figure 03

Requestor Location

Jacob Moose
206 Mackay Ave

Requestor Location   Syracuse, NY 13219
United States
Attn: Jacob Moose

Tax Details

Publisher Tax ID	EU826007151

Would you like to purchase the full text of this article? If so, please continue on to the content ordering system located here: Purchase PDF
If you click on the buttons below or close this window, you will not be able to return to the content ordering system.

Total: 0.00 USD

CLOSE WINDOW   ORDER MORE

Appendix IV: Reprint Permission for Reference 2, Chapter 5

5.6 References

1. Deschaine, S. L.; Hedegaard, M. A.; Pince, C. L.; Farokhnia, M.; Moose, J. E.; Stock, I. A.; Adusumalli, S.; Akhlaghi, F.; Hougland, J. L.; Sulima, A.; et al. Initial Pharmacological Characterization of a Major Hydroxy Metabolite of PF-5190457: Inverse Agonist Activity of PF-6870961 at the Ghrelin Receptor. *Journal of Pharmacology and Experimental Therapeutics* **2023**, *386* (2), 117-128. DOI: 10.1124/jpet.122.001393.

2. Deschaine, S. L.; Farokhnia, M.; Gregory-Flores, A.; Zallar, L. J.; You, Z. B.; Sun, H.; Harvey, D. M.; Marchette, R. C. N.; Tunstall, B. J.; Mani, B. K.; et al. A closer look at alcohol-induced changes in the ghrelin system: novel insights from preclinical and clinical data. *Addict Biol* **2022**, *27* (1), e13033. DOI: 10.1111/adb.13033.

3. Kojima, M.; Hosoda, H.; Date, Y.; Nakazato, M.; Matsuo, H.; Kangawa, K. Ghrelin is a growth-hormone-releasing acylated peptide from stomach. *Nature* **1999**, *402* (6762), 656-660. DOI: Doi 10.1038/45230.

4. Hewson, A. K.; Dickson, S. L. Systemic administration of ghrelin induces Fos and Egr-1 proteins in the hypothalamic arcuate nucleus of fasted and fed rats. *J Neuroendocrinol* **2000**, *12* (11), 1047-1049. DOI: 10.1046/j.1365-2826.2000.00584.x

5. Nakazato, M.; Murakami, N.; Date, Y.; Kojima, M.; Matsuo, H.; Kangawa, K.; Matsukura, S. A role for ghrelin in the central regulation of feeding. *Nature* **2001**, *409* (6817), 194-198. DOI: 10.1038/35051587.

6. Zallar, L. J.; Farokhnia, M.; Tunstall, B. J.; Vendruscolo, L. F.; Leggio, L. The Role of the Ghrelin System in Drug Addiction. *Int Rev Neurobiol* **2017**, *136*, 89-119. DOI: 10.1016/bs.irn.2017.08.002.

7.   Panagopoulos, V. N.; Ralevski, E. The role of ghrelin in addiction: a review. *Psychopharmacology (Berl)* **2014**, *231* (14), 2725-2740. DOI: 10.1007/s00213-014-3640-0.

8.   Wise, R. A. Brain reward circuitry: insights from unsensed incentives. *Neuron* **2002**, *36* (2), 229-240. DOI: 10.1016/s0896-6273(02)00965-0.

9.   Martel, P.; Fantino, M. Mesolimbic dopaminergic system activity as a function of food reward: A microdialysis study. *Pharmacol Biochem Be* **1996**, *53* (1), 221-226. DOI: Doi 10.1016/0091-3057(95)00187-5.

10.   Volkow, N. D.; Wang, G. J.; Maynard, L.; Jayne, M.; Fowler, J. S.; Zhu, W.; Logan, J.; Gatley, S. J.; Ding, Y. S.; Wong, C.; Pappas, N. Brain dopamine is associated with eating behaviors in humans. *Int J Eat Disord* **2003**, *33* (2), 136-142. DOI: 10.1002/eat.10118.

11.   Wise, R. A. The role of reward pathways in the development of drug dependence. *Pharmacol Ther* **1987**, *35* (1-2), 227-263. DOI: 10.1016/0163-7258(87)90108-2.

12.   Nestler, E. J. Is there a common molecular pathway for addiction? *Nat Neurosci* **2005**, *8* (11), 1445-1449. DOI: 10.1038/nn1578.

13.   Jerlhag, E.; Egecioglu, E.; Dickson, S. L.; Douhan, A.; Svensson, L.; Engel, J. A. Ghrelin administration into tegmental areas stimulates locomotor activity and increases extracellular concentration of dopamine in the nucleus accumbens. *Addict Biol* **2007**, *12* (1), 6-16. DOI: 10.1111/j.1369-1600.2006.00041.x.

14.   Leggio, L.; Ferrulli, A.; Cardone, S.; Nesci, A.; Miceli, A.; Malandrino, N.; Capristo, E.; Canestrelli, B.; Monteleone, P.; Kenna, G. A.; et al. Ghrelin system in alcohol-dependent subjects: role of plasma ghrelin levels in alcohol drinking and craving. *Addict Biol* **2012**, *17* (2), 452-464. DOI: 10.1111/j.1369-1600.2010.00308.x.

15.   Akkisi Kumsar, N.; Dilbaz, N. Relationship between craving and ghrelin, adiponectin, and resistin levels in patients with alcoholism. *Alcohol Clin Exp Res* **2015**, *39* (4), 702-709. DOI: 10.1111/acer.12689.

16.   Hillemacher, T.; Kraus, T.; Rauh, J.; Weiss, J.; Schanze, A.; Frieling, H.; Wilhelm, J.; Heberlein, A.; Groschl, M.; Sperling, W.; et al. Role of appetite-regulating peptides in alcohol craving: an analysis in respect to subtypes and different consumption patterns in alcoholism. *Alcohol Clin Exp Res* **2007**, *31* (6), 950-954. DOI: 10.1111/j.1530-0277.2007.00388.x.

17.   Addolorato, G.; Capristo, E.; Leggio, L.; Ferrulli, A.; Abenavoli, L.; Malandrino, N.; Farnetti, S.; Domenicali, M.; D'Angelo, C.; Vonghia, L.; et al. Relationship between ghrelin levels, alcohol craving, and nutritional status in current alcoholic patients. *Alcohol Clin Exp Res* **2006**, *30* (11), 1933-1937. DOI: 10.1111/j.1530-0277.2006.00238.x.

18.   Koopmann, A.; Bach, P.; Schuster, R.; Bumb, J. M.; Vollstadt-Klein, S.; Reinhard, I.; Rietschel, M.; Witt, S. H.; Wiedemann, K.; Kiefer, F. Ghrelin modulates mesolimbic reactivity to alcohol cues in alcohol-addicted subjects: a functional imaging study. *Addict Biol* **2019**, *24* (5), 1066-1076. DOI: 10.1111/adb.12651.

19.   Bach, P.; Bumb, J. M.; Schuster, R.; Vollstadt-Klein, S.; Reinhard, I.; Rietschel, M.; Witt, S. H.; Wiedemann, K.; Kiefer, F.; Koopmann, A. Effects of leptin and ghrelin on neural cue-reactivity in alcohol addiction: Two streams merge to one river? *Psychoneuroendocrinology* **2019**, *100*, 1-9. DOI: 10.1016/j.psyneuen.2018.09.026.

20.   Jerlhag, E.; Egecioglu, E.; Landgren, S.; Salome, N.; Heilig, M.; Moechars, D.; Datta, R.; Perrissoud, D.; Dickson, S. L.; Engel, J. A. Requirement of central ghrelin signaling for alcohol reward. *Proc Natl Acad Sci U S A* **2009**, *106* (27), 11318-11323. DOI: 10.1073/pnas.0812809106.

21.   Szulc, M.; Mikolajczak, P. L.; Geppert, B.; Wachowiak, R.; Dyr, W.; Bobkiewicz-Kozlowska, T. Ethanol affects acylated and total ghrelin levels in peripheral blood of alcohol-dependent rats. *Addict Biol* **2013**, *18* (4), 689-701. DOI: 10.1111/adb.12025.

22.   Calissendorff, J.; Danielsson, O.; Brismar, K.; Rojdmark, S. Alcohol ingestion does not affect serum levels of peptide YY but decreases both total and octanoylated ghrelin levels in healthy subjects. *Metabolism* **2006**, *55* (12), 1625-1629. DOI: 10.1016/j.metabol.2006.08.003.

23.   Calissendorff, J.; Gustafsson, T.; Holst, J. J.; Brismar, K.; Rojdmark, S. Alcohol intake and its effect on some appetite-regulating hormones in man: influence of gastroprotection with sucralfate. *Endocr Res* **2012**, *37* (3), 154-162. DOI: 10.3109/07435800.2012.662662.

24.   Calissendorff, J.; Danielsson, O.; Brismar, K.; Rojdmark, S. Inhibitory effect of alcohol on ghrelin secretion in normal man. *Eur J Endocrinol* **2005**, *152* (5), 743-747. DOI: 10.1530/eje.1.01905.

25.   Zimmermann, U. S.; Buchmann, A.; Steffin, B.; Dieterle, C.; Uhr, M. Alcohol administration acutely inhibits ghrelin secretion in an experiment involving psychosocial stress. *Addict Biol* **2007**, *12* (1), 17-21. DOI: 10.1111/j.1369-1600.2006.00026.x.

26.   Kraus, T.; Schanze, A.; Groschl, M.; Bayerlein, K.; Hillemacher, T.; Reulbach, U.; Kornhuber, J.; Bleich, S. Ghrelin levels are increased in alcoholism. *Alcohol Clin Exp Res* **2005**, *29* (12), 2154-2157. DOI: 10.1097/01.alc.0000191753.82554.7e.

27.   Kim, D. J.; Yoon, S. J.; Choi, B.; Kim, T. S.; Woo, Y. S.; Kim, W.; Myrick, H.; Peterson, B. S.; Choi, Y. B.; Kim, Y. K.; Jeong, J. Increased fasting plasma ghrelin levels during alcohol abstinence. *Alcohol* **2005**, *40* (1), 76-79. DOI: 10.1093/alcalc/agh108.

28.   Leggio, L.; Zywiak, W. H.; Fricchione, S. R.; Edwards, S. M.; de la Monte, S. M.; Swift, R. M.; Kenna, G. A. Intravenous ghrelin administration increases alcohol craving in alcohol-

dependent heavy drinkers: a preliminary investigation. *Biol Psychiatry* **2014**, *76* (9), 734-741.
DOI: 10.1016/j.biopsych.2014.03.019.

29.   Farokhnia, M.; Grodin, E. N.; Lee, M. R.; Oot, E. N.; Blackburn, A. N.; Stangl, B. L.;
Schwandt, M. L.; Farinelli, L. A.; Momenan, R.; Ramchandani, V. A.; Leggio, L. Exogenous
ghrelin administration increases alcohol self-administration and modulates brain functional
activity in heavy-drinking alcohol-dependent individuals. *Mol Psychiatry* **2018**, *23* (10), 2029-
2038. DOI: 10.1038/mp.2017.226.

30.   You, Z. B.; Gardner, E. L.; Galaj, E.; Moore, A. R.; Buck, T.; Jordan, C. J.; Humburg, B.
A.; Bi, G. H.; Xi, Z. X.; Leggio, L. Involvement of the ghrelin system in the maintenance of
oxycodone self-administration: converging evidence from endocrine, pharmacologic and
transgenic approaches. *Mol Psychiatry* **2022**. DOI: 10.1038/s41380-022-01438-5.

31.   Kung, D. W.; Coffey, S. B.; Jones, R. M.; Cabral, S.; Jiao, W.; Fichtner, M.; Carpino, P.
A.; Rose, C. R.; Hank, R. F.; Lopaze, M. G.; et al. Identification of spirocyclic piperidine-
azetidine inverse agonists of the ghrelin receptor. *Bioorg Med Chem Lett* **2012**, *22* (13), 4281-
4287. DOI: 10.1016/j.bmcl.2012.05.024.

32.   Bhattacharya, S. K.; Andrews, K.; Beveridge, R.; Cameron, K. O.; Chen, C.; Dunn, M.;
Fernando, D.; Gao, H.; Hepworth, D.; Jackson, V. M.; et al. Discovery of PF-5190457, a Potent,
Selective, and Orally Bioavailable Ghrelin Receptor Inverse Agonist Clinical Candidate. *ACS
Med Chem Lett* **2014**, *5* (5), 474-479. DOI: 10.1021/ml400473x.

33.   Kong, J.; Chuddy, J.; Stock, I. A.; Loria, P. M.; Straub, S. V.; Vage, C.; Cameron, K. O.;
Bhattacharya, S. K.; Lapham, K.; McClure, K. F.; et al. Pharmacological characterization of the
first in class clinical candidate PF-05190457: a selective ghrelin receptor competitive antagonist

with inverse agonism that increases vagal afferent firing and glucose-dependent insulin secretion ex vivo. *Br J Pharmacol* **2016**, *173* (9), 1452-1464. DOI: 10.1111/bph.13439.

34.   Denney, W. S.; Sonnenberg, G. E.; Carvajal-Gonzalez, S.; Tuthill, T.; Jackson, V. M. Pharmacokinetics and pharmacodynamics of PF-05190457: The first oral ghrelin receptor inverse agonist to be profiled in healthy subjects. *Br J Clin Pharmacol* **2017**, *83* (2), 326-338. DOI: 10.1111/bcp.13127.

35.   Lee, M. R.; Tapocik, J. D.; Ghareeb, M.; Schwandt, M. L.; Dias, A. A.; Le, A. N.; Cobbina, E.; Farinelli, L. A.; Bouhlal, S.; Farokhnia, M.; et al. The novel ghrelin receptor inverse agonist PF-5190457 administered with alcohol: preclinical safety experiments and a phase 1b human laboratory study. *Mol Psychiatry* **2020**, *25* (2), 461-475. DOI: 10.1038/s41380-018-0064-y.

36.   Leggio, L.; Schwandt, M. L.; Oot, E. N.; Dias, A. A.; Ramchandani, V. A. Fasting-induced increase in plasma ghrelin is blunted by intravenous alcohol administration: a within-subject placebo-controlled study. *Psychoneuroendocrinology* **2013**, *38* (12), 3085-3091. DOI: 10.1016/j.psyneuen.2013.09.005

37.   Harrison, N. L.; Skelly, M. J.; Grosserode, E. K.; Lowes, D. C.; Zeric, T.; Phister, S.; Salling, M. C. Effects of acute alcohol on excitability in the CNS. *Neuropharmacology* **2017**, *122*, 36-45. DOI: 10.1016/j.neuropharm.2017.04.007.

38.   Roberto, M.; Madamba, S. G.; Moore, S. D.; Tallent, M. K.; Siggins, G. R. Ethanol increases GABAergic transmission at both pre- and postsynaptic sites in rat central amygdala neurons. *Proc Natl Acad Sci U S A* **2003**, *100* (4), 2053-2058. DOI: 10.1073/pnas.0437926100.

39.   Cummings, D. E. Ghrelin and the short- and long-term regulation of appetite and body weight. *Physiol Behav* **2006**, *89* (1), 71-84. DOI: 10.1016/j.physbeh.2006.05.022.

40.	Farokhnia, M.; Portelli, J.; Lee, M. R.; McDiarmid, G. R.; Munjal, V.; Abshire, K. M.; Battista, J. T.; Browning, B. D.; Deschaine, S. L.; Akhlaghi, F.; Leggio, L. Effects of exogenous ghrelin administration and ghrelin receptor blockade, in combination with alcohol, on peripheral inflammatory markers in heavy-drinking individuals: Results from two human laboratory studies. *Brain Res* **2020**, *1740*, 146851. DOI: 10.1016/j.brainres.2020.146851.

41.	Lee, M. R.; Farokhnia, M.; Cobbina, E.; Saravanakumar, A.; Li, X.; Battista, J. T.; Farinelli, L. A.; Akhlaghi, F.; Leggio, L. Endocrine effects of the novel ghrelin receptor inverse agonist PF-5190457: Results from a placebo-controlled human laboratory alcohol co-administration study in heavy drinkers. *Neuropharmacology* **2020**, *170*, 107788. DOI: 10.1016/j.neuropharm.2019.107788.

42.	Sulima, A.; Akhlaghi, F.; Leggio, L.; Rice, K. C. Synthesis of PF-6870961, a major hydroxy metabolite of the novel ghrelin receptor inverse agonist PF-5190457. *Bioorg Med Chem* **2021**, *50*, 116465. DOI: 10.1016/j.bmc.2021.116465.

43.	Adusumalli, S.; Jamwal, R.; Leggio, L.; Akhlaghi, F. Development and validation of an assay for a novel ghrelin receptor inverse agonist PF-5190457 and its major hydroxy metabolite (PF-6870961) by LC-MS/MS in human plasma. *J Chromatogr B Analyt Technol Biomed Life Sci* **2019a**, *1130-1131*, 121820. DOI: 10.1016/j.jchromb.2019.121820.

44.	Adusumalli, S.; Jamwal, R.; Obach, R. S.; Ryder, T. F.; Leggio, L.; Akhlaghi, F. Role of Molybdenum-Containing Enzymes in the Biotransformation of the Novel Ghrelin Receptor Inverse Agonist PF-5190457: A Reverse Translational Bed-to-Bench Approach. *Drug Metab Dispos* **2019b**, *47* (8), 874-882. DOI: 10.1124/dmd.119.087015.

45.	Denney, W. S.; Sonnenberg, G. E.; Carvajal-Gonzalez, S.; Tuthill, T.; Jackson, V. M. Pharmacokinetics and pharmacodynamics of PF-05190457: The first oral ghrelin receptor

inverse agonist to be profiled in healthy subjects. *British Journal of Clinical Pharmacology* **2017**, *83* (2), 326-338, Article. DOI: 10.1111/bcp.13127 Scopus.

46.   Qin, J.; Cai, Y.; Xu, Z.; Ming, Q.; Ji, S. Y.; Wu, C.; Zhang, H.; Mao, C.; Shen, D. D.; Hirata, K.; et al. Molecular mechanism of agonism and inverse agonism in ghrelin receptor. *Nat Commun* **2022**, *13* (1), 300. DOI: 10.1038/s41467-022-27975-9.

47.   Hedegaard, M. A.; Holst, B. The Complex Signaling Pathways of the Ghrelin Receptor. *Endocrinology* **2020**, *161* (4). DOI: 10.1210/endocr/bqaa020

48.   Zhao, J.; Du, X.; Chen, M.; Zhu, S. Growth Hormone Secretagogue Receptor 1A Antagonist JMV2959 Effectively Prevents Morphine Memory Reconsolidation and Relapse. *Front Pharmacol* **2021**, *12*, 718615. DOI: 10.3389/fphar.2021.718615

49.   Engel, J. A.; Nylander, I.; Jerlhag, E. A ghrelin receptor (GHS-R1A) antagonist attenuates the rewarding properties of morphine and increases opioid peptide levels in reward areas in mice. *Eur Neuropsychopharmacol* **2015**, *25* (12), 2364-2371. DOI: 10.1016/j.euroneuro.2015.10.004

50.   Hassouna, R.; Labarthe, A.; Zizzari, P.; Videau, C.; Culler, M.; Epelbaum, J.; Tolle, V. Actions of agonists and antagonists of the ghrelin/GHS-R pathway on GH secretion, appetite, and cFos activity. *Frontiers in Endocrinology* **2013**, *4* (MAR), Article. DOI: 10.3389/fendo.2013.00025

51.   Gross, J. D.; Kim, D. W.; Zhou, Y.; Jansen, D.; Slosky, L. M.; Clark, N. B.; Ray, C. R.; Hu, X.; Southall, N.; Wang, A.; et al. Discovery of a functionally selective ghrelin receptor (GHSR(1a)) ligand for modulating brain dopamine. *Proc Natl Acad Sci U S A* **2022**, *119* (10), e2112397119. DOI: 10.1073/pnas.2112397119

52.   Jerlhag, E. Animal studies reveal that the ghrelin pathway regulates alcohol-mediated responses. *Front Psychiatry* **2023**, *14*, 1050973. DOI: 10.3389/fpsyt.2023.1050973

53.   Yin, Y.; Li, Y.; Zhang, W. The growth hormone secretagogue receptor: its intracellular signaling and regulation. *Int J Mol Sci* **2014**, *15* (3), 4837-4855. DOI: 10.3390/ijms15034837 From NLM Medline.

54.   Pastor-Cavada, E.; Pardo, L. M.; Kandil, D.; Torres-Fuentes, C.; Clarke, S. L.; Shaban, H.; McGlacken, G. P.; Schellekens, H. A Novel Non-Peptidic Agonist of the Ghrelin Receptor with Orexigenic Activity In vivo. *Sci Rep* **2016**, *6*, 36456. DOI: 10.1038/srep36456

55.   Giorgioni, G.; Del Bello, F.; Quaglia, W.; Botticelli, L.; Cifani, C.; Micioni Di Bonaventura, E.; Micioni Di Bonaventura, M. V.; Piergentili, A. Advances in the Development of Nonpeptide Small Molecules Targeting Ghrelin Receptor. *J Med Chem* **2022**, *65* (4), 3098-3118. DOI: 10.1021/acs.jmedchem.1c02191

56.   Campana, M. B.; Davis, T. R.; Novak, S. X.; Cleverdon, E. R.; Bates, M.; Krishnan, N.; Curtis, E. R.; Childs, M. D.; Pierce, M. R.; Morales-Rodriguez, Y.; et al. Cellular Uptake of a Fluorescent Ligand Reveals Ghrelin O-Acyltransferase Interacts with Extracellular Peptides and Exhibits Unexpected Localization for a Secretory Pathway Enzyme. *ACS Chem Biol* **2023**, *18* (8), 1880-1890. DOI: 10.1021/acschembio.3c00334.

57.   Riddles, P. W. B., R. L.; Zerner, B., . Ellman's reagent: 5,5'-dithiobis(2-nitrobenzoic acid)--a reexamination. *Analytical Biochemistry* **1979**, *94* (1), 75-81.

58.   Darling, J. E.; Zhao, F.; Loftus, R. J.; Patton, L. M.; Gibbs, R. A.; Hougland, J. L. Structure-activity analysis of human ghrelin O-acyltransferase reveals chemical determinants of ghrelin selectivity and acyl group recognition. *Biochemistry* **2015**, *54* (4), 1100-1110. DOI: 10.1021/bi5010359.

59.   McGovern-Gooch, K. R.; Rodrigues, T.; Darling, J. E.; Sieburg, M. A.; Abizaid, A.; Hougland, J. L. Ghrelin Octanoylation Is Completely Stabilized in Biological Samples by Alkyl Fluorophosphonates. *Endocrinology* **2016**, *157* (11), 4330-4338. DOI: 10.1210/en.2016-1657.

60.   Darling, J. E.; Prybolsky, E. P.; Sieburg, M.; Hougland, J. L. A fluorescent peptide substrate facilitates investigation of ghrelin recognition and acylation by ghrelin O-acyltransferase. *Anal Biochem* **2013**, *437* (1), 68-76. DOI: 10.1016/j.ab.2013.02.013.

61.   Sieburg, M. A.; Cleverdon, E. R.; Hougland, J. L. Biochemical Assays for Ghrelin Acylation and Inhibition of Ghrelin O-Acyltransferase. *Methods Mol Biol* **2019**, *2009*, 227-241. DOI: 10.1007/978-1-4939-9532-5_18.

62.   McGovern-Gooch, K. R.; Mahajani, N. S.; Garagozzo, A.; Schramm, A. J.; Hannah, L. G.; Sieburg, M. A.; Chisholm, J. D.; Hougland, J. L. Synthetic Triterpenoid Inhibition of Human Ghrelin O-Acyltransferase: The Involvement of a Functionally Required Cysteine Provides Mechanistic Insight into Ghrelin Acylation. *Biochemistry* **2017**, *56* (7), 919-931. DOI: 10.1021/acs.biochem.6b01008.

Chapter 6: Conclusions and Future Directions

6.1 Introduction

Ghrelin is a unique peptide hormone both for its activation through the posttranslational addition of an octanoyl moiety, and for its primary role in the stimulation of hunger.[1-5] With expression detected in the stomach, heart, pituitary, hypothalamus, duodenum, jejunum, ileum, colon, lung, pancreas, and kidneys, the role of ghrelin in physiology is widespread and still under investigation.[6-12] The overall lack of consensus on the effects of ghrelin is in part due to the availability of two forms of ghrelin – the acylated form (called ghrelin) and the des-acyl ghrelin, which have differing physiological effects. While ghrelin must be acylated for the activation of the endogenous GHSR, des-acyl ghrelin has been shown to act as an insulin secretagogue while also increasing insulin sensitivity.[6, 13] In contrast, the acylated form of ghrelin reduces insulin sensitivity.[13, 14] As the ratio of acyl to des-acyl ghrelin appears to play a role in insulin sensitivity, modulation of ghrelin acylation opens potential avenues to addressing insulin signaling insufficiency in Type II diabetes. Since ghrelin has been shown to interact with other physiological pathways, including obesity and addiction, controlling the ghrelin to des-acyl ghrelin ratio is of interest in treating pathophysiologies related to these conditions.[15-19]

Membrane-bound *O*-acyltransferases (MBOATs) are a class of enzymes characterized by their shared role in acyl transfer reactions.[20] Beyond the function, MBOATs share a conserved histidine and asparagine/arginine shown to be essential in catalysis.[21-24] The location of these proposed catalytic residues has only recently been identified in several MBOAT structures, including DltB, ACAT1, ACAT2, DGAT1, and PORCN.[25-29] The publication of these structures has finally allowed a comparison of the structures of the MBOATs, revealing the family utilizes a catalytic core containing the conserved histidine, which resides with a transmembrane channel. Comparison of the protein-modifying MBOATs GOAT, PORCN, and HHAT reveals the

transmembrane channel extends to the cytosolic and luminal faces of the enzymes, consistent with their role in bringing together the acyl donor with the ER-synthesized substrate protein.[29-31] While the structures of these enzymes and the location of the conserved residues within are an exciting step forward in the understanding of these proteins, the mechanism by which GOAT and other MBOATs catalyze the acylation of their substrates is not yet proven. Insights into MBOAT mechanisms would allow for the development of molecules capable of a treating a broad range of conditions, including cancer (DGAT1, HHAT, PORCN), Alzheimer's Disease (ACAT1), and Type II Diabetes (GOAT).[32-35]

GOAT is a therapeutic target of interest due to its unique role as the only known octanoyl acyl transferase and preproghrelin being the only predicted substrate for GOAT.[36, 37] These idiosyncrasies limit the potential unintended effects of inhibiting GOAT, making targeting GOAT with inhibitors a reasonable strategy in controlling obesity, type II diabetes, and addiction. Contributing to the limited number of small-molecule inhibitors available for therapeutic trials is a lack of understanding of the GOAT acylation mechanism and limited insight into the binding site or sites for current small-molecule inhibitors. With the studies described in this thesis, we achieved progress on all of these issues: putting in place a foundation for further differentiation of the mechanism of GOAT, as well as developing a high-throughput assay while using this assay to discover several new lead molecules capable of inhibiting GOAT.

6.2 Mechanism-based inhibitors of GOAT

Efforts towards the understanding the mechanisms of several MBOATs have suggested a catalytic role for the conserved asparagine and histidine residues found in MBOAT family members. A study on chicken lysophophatidylcholine acyltransferase 3 (cLPCAT3) revealed the H388 residue lines up with the arachidonoyl-CoA substrate, with the authors suggesting a one-step acyl-transfer reaction catalyzed by the activation of the thioether and the nucleophilic acyl acceptor.[38] A similar result was also obtained in the mechanistic study of human hedgehog acyltransferase (hHHAT), which also placed the palmitoyl-CoA substrate close to the H379 and N339 residues, activating the nucleophilic Hedgehog substrate to attack the CoA thioether bond.[30, 31] The structure of human diacylglycerol *O*-acyltransferase 1 (hDGAT1) takes this further, with the catalytic H415 located and positioned such that the it may be partially deprotonated by the nearby E416, leading to the activation of the diacylglycerol substrate as a nucleophile in a direct transfer reaction.[28] The ability for multiple classes of privileged electrophiles to inhibit GOAT supports activation of a nucleophile by general base, likely the conserved H338. The inhibition profile of the isocoumarins, sulfonyl fluorides, and diphenyl phosphonates leads to a serine or threonine acting as the activated nucleophile due to the reactivity profile of these molecules. Whether the GOAT mechanism proceeds through a direct transfer mechanism or an acyl-enzyme intermediate, as well as the location and identity of the nucleophilic residues involved are under investigation.

6.3 Development of a high-throughput screen for GOAT inhibitors

The high-throughput screen developed in this work allowed for the rapid detection and characterization of three novel hGOAT inhibitors. While the assay is not a replacement for the HPLC-based assay currently used by the Hougland lab for the detection of GOAT activity, it supplements and complements the HPLC assay. The swift generation of a positive or negative indication of the inhibitory potential of molecules represents a jump forward in the ability of the lab to screen and generate molecules of interest without relying on expensive acyl-ghrelin detecting ELISA kits. The three molecules found in the validation of the screen share similar characteristics, as all bind in the transmembrane channel indicated in the structural model of GOAT and are octanoyl-CoA competitive regardless of specific binding contacts. In addition, all three molecules share a highly planar, heterocyclic-containing structure comparable to the structures of similarly acyl-competitive compounds from Takeda Pharmaceutical.[39] While none of the identified molecules exhibit potencies below mid-micromolar, SAR studies and rational design of inhibitors to maximize binding contacts based on the initial findings of these scaffolds are underway. These studies aim to increase the potency of similar compounds to generate molecules of pharmaceutically relevant potency. The development of new scaffolds in the hunt for small-molecule modulators of GOAT activity represent novel avenues of research in developing treatments for obesity, type II diabetes, and addiction.

6.4 Identification of novel GOAT inhibitors reveals insight into consensus inhibitor binding domain

Due to the previously undetermined structure of GOAT, the nature of the binding interactions of literature inhibitors such as those discovered at Eli Lily and Takeda were unknown other than their octanoyl-CoA competitive behavior.[39, 40] The recent development of a computational model of GOAT allowed binding studies to be performed, which indicate that these literature inhibitors share a consensus binding domain consisting of three sub-regions in the transmembrane channel. These regions were designated as the obligate binding domain (O), and two supplemental domains (S_1 and S_2). The obligate binding domain can be represented as the area around W351, the residue that acts as the cap at the end of the octanoyl-CoA binding pocket of GOAT. Alanine mutation of W351 has been shown to allow GOAT to catalyze the transfer of longer-chain acyl groups to labeled ghrelin peptide truncations, consistent with the findings that compounds interacting with this residue are octanoyl-CoA competitive.[41] While mutation of residues in the obligate binding domain did not lead to lowered potency of Takeda A, studies are under way to determine whether this behavior is consistent in Takeda B, which is similarly octanoyl-CoA competitive. Understanding how these literature inhibitors bind GOAT could allow for rational development of new therapeutics using the previously-identified inhibitors as the starting point for new molecules.

6.5 Future developments in the understanding of GOAT

As part of the studies presented here, mechanistic inhibitors of GOAT were developed that implicated an activated serine or threonine as a potential nucleophile in an acyl-enzyme intermediate acylation of ghrelin. The ability of these molecules to form covalent interactions only with activated nucleophiles has the ability to lead to the determination of the GOAT active site. Molecules that contain an alkyne could allow for the conjugation of a tag to the active site through a [3+2] cycloaddition.[42-44] Due to the covalent nature of the bonds formed, this tag would allow identification of the activated residue. Work is currently underway with the goal of using an alkyne-containing mechanistic probe to attach a TAMRA-azide fluorophore to the labeled nucleophile. Loss of TAMRA labeling upon mutation of the potential nucleophile as evaluated through in-gel fluorescence and colocalization with a positive anti-GOAT Western blot will allow for identification of the active site.

While GOAT was originally canonically localized to the endoplasmic reticulum, recent reports of localized ghrelin acylation in the hippocampus and marrow adipocytes has challenged the notion that the ER is the sole site of ghrelin acylation.[16, 45, 46] The extent and physiological relevance of GOAT localization to the cell surface and acting on extracellular ghrelin is currently under investigation, but may give rise to the ability to have localized areas of high ghrelin to alter the ghrelin/desacyl-ghrelin axis. GOAT being exposed to extracellular circulation opens potential uses for GOAT to be used as a biomarker in disease. GOAT has been shown to be overexpressed in prostate cancer, and the recent development of fluorescent ligands that specifically bind to surface-exposed GOAT may allow for early detection of prostate cancers through non-invasive imaging methods.[47, 48] This approach may be further developed for other cancers that overproduce GOAT, including certain breast and endocrine cancers.[49-51] The

identification of the GOAT active site would allow for rational design of molecules capable of

binding GOAT, increasing the availability of the enzyme as a biomarker in these conditions. As

such, the discovery of potential mechanism-based inhibitors of GOAT provides an avenue to

elucidate the active site, and develop new therapeutic and diagnostic probes for GOAT.

6.6 References

1.   Levin, F.; Edholm, T.; Schmidt, P. T.; Gryback, P.; Jacobsson, H.; Degerblad, M.; Hoybye, C.; Holst, J. J.; Rehfeld, J. F.; Hellstrom, P. M.; Naslund, E. Ghrelin stimulates gastric emptying and hunger in normal-weight humans. *J Clin Endocrinol Metab* **2006**, *91* (9), 3296-3302. DOI: 10.1210/jc.2005-2638.

2.   Kojima, M.; Kangawa, K. Ghrelin: structure and function. *Physiol Rev* **2005**, *85* (2), 495-522. DOI: 10.1152/physrev.00012.2004.

3.   Tschop, M.; Smiley, D. L.; Heiman, M. L. Ghrelin induces adiposity in rodents. *Nature* **2000**, *407* (6806), 908-913. DOI: 10.1038/35038090.

4.   Wren, A. M.; Seal, L. J.; Cohen, M. A.; Brynes, A. E.; Frost, G. S.; Murphy, K. G.; Dhillo, W. S.; Ghatei, M. A.; Bloom, S. R. Ghrelin enhances appetite and increases food intake in humans. *Journal of Clinical Endocrinology and Metabolism* **2001**, *86* (12), 5992-5995, Article. DOI: 10.1210/jc.86.12.5992

5.   Wren, A. M.; Small, C. J.; Abbott, C. R.; Dhillo, W. S.; Seal, L. J.; Cohen, M. A.; Batterham, R. L.; Taheri, S.; Stanley, S. A.; Ghatei, M. A.; Bloom, S. R. Ghrelin causes hyperphagia and obesity in rats. *Diabetes* **2001**, *50* (11), 2540-2547. DOI: 10.2337/diabetes.50.11.2540.

6.   Kojima, M.; Hosoda, H.; Date, Y.; Nakazato, M.; Matsuo, H.; Kangawa, K. Ghrelin is a growth-hormone-releasing acylated peptide from stomach. *Nature* **1999**, *402* (6762), 656-660. DOI: Doi 10.1038/45230.

7.   Date, Y.; Kojima, M.; Hosoda, H.; Sawaguchi, A.; Mondal, M. S.; Suganuma, T.; Matsukura, S.; Kangawa, K.; Nakazato, M. Ghrelin, a novel growth hormone-releasing acylated

peptide, is synthesized in a distinct endocrine cell type in the gastrointestinal tracts of rats and humans. *Endocrinology* **2000**, *141* (11), 4255-4261. DOI: DOI 10.1210/en.141.11.4255.

8.   Takaya, K.; Ariyasu, H.; Kanamoto, N.; Iwakura, H.; Yoshimoto, A.; Harada, M.; Mori, K.; Komatsu, Y.; Usui, T.; Shimatsu, A.; et al. Ghrelin strongly stimulates growth hormone release in humans. *J Clin Endocrinol Metab* **2000**, *85* (12), 4908-4911. DOI: 10.1210/jcem.85.12.7167.

9.   Sakata, I.; Nakamura, K.; Yamazaki, M.; Matsubara, M.; Hayashi, Y.; Kangawa, K.; Sakai, T. Ghrelin-producing cells exist as two types of cells, closed- and opened-type cells, in the rat gastrointestinal tract. *Peptides* **2002**, *23* (3), 531-536. DOI: Pii S0196-9781(01)00633-7

10.   Korbonits, M.; Bustin, S. A.; Kojima, M.; Jordan, S.; Adams, E. F.; Lowe, D. G.; Kangawa, K.; Grossman, A. B. The expression of the growth hormone secretagogue receptor ligand ghrelin in normal and abnormal human pituitary and other neuroendocrine tumors. *J Clin Endocrinol Metab* **2001**, *86* (2), 881-887. DOI: 10.1210/jcem.86.2.7190.

11.   Ghelardoni, S.; Carnicelli, V.; Frascarelli, S.; Ronca-Testoni, S.; Zucchi, R. Ghrelin tissue distribution: Comparison between gene and protein expression. *J Endocrinol Invest* **2006**, *29* (2), 115-121. DOI: 10.1007/Bf03344083.

12.   Gnanapavan, S.; Kola, B.; Bustin, S. A.; Morris, D. G.; McGee, P.; Fairclough, P.; Bhattacharya, S.; Carpenter, R.; Grossman, A. B.; Korbonits, M. The tissue distribution of the mRNA of ghrelin and subtypes of its receptor, GHS-R, in humans. *J Clin Endocrinol Metab* **2002**, *87* (6), 2988. DOI: 10.1210/jcem.87.6.8739.

13.   Gauna, C.; Kiewiet, R. M.; Janssen, J. A. M. J. L.; De Zande, B. V.; Delhanty, P. J. D.; Ghigo, E.; Hofland, L. J.; Themmen, A. P. N.; Van der Lely, A. J. Unacylated ghrelin acts as a potent insulin secretagogue in glucose-stimulated conditions. *Am J Physiol-Endoc M* **2007**, *293* (3), E697-E704. DOI 10.1152/ajpendo.00219.2007.

14.   Gauna, C.; Meyler, F. M.; Janssen, J. A.; Delhanty, P. J.; Abribat, T.; van Koetsveld, P.; Hofland, L. J.; Broglio, F.; Ghigo, E.; van der Lely, A. J. Administration of acylated ghrelin reduces insulin sensitivity, whereas the combination of acylated plus unacylated ghrelin strongly improves insulin sensitivity. *J Clin Endocrinol Metab* **2004**, *89* (10), 5035-5042. DOI: 10.1210/jc.2004-0363.

15.   Perez-Tilve, D.; Heppner, K.; Kirchner, H.; Lockie, S. H.; Woods, S. C.; Smiley, D. L.; Tschop, M.; Pfluger, P. Ghrelin-induced adiposity is independent of orexigenic effects. *FASEB J* **2011**, *25* (8), 2814-2822. DOI: 10.1096/fj.11-183632.

16.   Hopkins, A. L.; Nelson, T. A.; Guschina, I. A.; Parsons, L. C.; Lewis, C. L.; Brown, R. C.; Christian, H. C.; Davies, J. S.; Wells, T. Unacylated ghrelin promotes adipogenesis in rodent bone marrow via ghrelin O-acyl transferase and GHS-R(1a) activity: evidence for target cell-induced acylation. *Sci Rep* **2017**, *7*, 45541. DOI: 10.1038/srep45541.

17.   Tessari, M.; Catalano, A.; Pellitteri, M.; Di Francesco, C.; Marini, F.; Gerrard, P. A.; Heidbreder, C. A.; Melotto, S. Correlation between serum ghrelin levels and cocaine-seeking behaviour triggered by cocaine-associated conditioned stimuli in rats. *Addict Biol* **2007**, *12* (1), 22-29. DOI: 10.1111/j.1369-1600.2007.00052.x.

18.   Leggio, L.; Ferrulli, A.; Cardone, S.; Nesci, A.; Miceli, A.; Malandrino, N.; Capristo, E.; Canestrelli, B.; Monteleone, P.; Kenna, G. A.; et al. Ghrelin system in alcohol-dependent subjects: role of plasma ghrelin levels in alcohol drinking and craving. *Addict Biol* **2012**, *17* (2), 452-464. DOI: 10.1111/j.1369-1600.2010.00308.x.

19.   Leggio, L. Ghrelin Signaling Via GOAT Inhibition in Alcohol Use Disorder. National Institute on Alcohol Abuse and Alcoholism (NIAAA): ClinicalTrials.gov Identifier: NCT03896516, 2019-2020.

20.   Hofmann, K. A superfamily of membrane-bound O-acyltransferases with implications for wnt signaling. *Trends Biochem Sci* **2000**, *25* (3), 111-112. DOI: 10.1016/s0968-0004(99)01539-x.

21.   Buglino, J. A.; Resh, M. D. Identification of conserved regions and residues within Hedgehog acyltransferase critical for palmitoylation of Sonic Hedgehog. *PLoS One* **2010**, *5* (6), e11195. DOI: 10.1371/journal.pone.0011195.

22.   Rios-Esteves, J.; Haugen, B.; Resh, M. D. Identification of key residues and regions important for porcupine-mediated Wnt acylation. *J Biol Chem* **2014**, *289* (24), 17009-17019. DOI: 10.1074/jbc.M114.561209.

23.   Das, A.; Davis, M. A.; Rudel, L. L. Identification of putative active site residues of ACAT enzymes. *J Lipid Res* **2008**, *49* (8), 1770-1781. DOI: 10.1194/jlr.M800131-JLR200 From NLM Medline.

24.   Yang, J.; Zhao, T.-J.; Goldstein, J. L.; Brown, M. S. Inhibition of ghrelin O-acyltransferase (GOAT) by octanoylated pentapeptides. *Proc. Natl. Acad. Sci. U. S. A.* **2008**, *105* (31), 10750-10755, 10.1073/pnas.0805353105. DOI: 10.1073/pnas.0805353105.

25.   Ma, D.; Wang, Z.; Merrikh, C. N.; Lang, K. S.; Lu, P.; Li, X.; Merrikh, H.; Rao, Z.; Xu, W. Crystal structure of a membrane-bound O-acyltransferase. *Nature (London, U. K.)* **2018**, *562* (7726), 286-290, 10.1038/s41586-018-0568-2. DOI: 10.1038/s41586-018-0568-2.

26.   Qian, H.; Zhao, X.; Yan, R.; Yao, X.; Gao, S.; Sun, X.; Du, X.; Yang, H.; Wong, C. C. L.; Yan, N. Structural basis for catalysis and substrate specificity of human ACAT1. *Nature* **2020**, *581* (7808), 333-338. DOI: 10.1038/s41586-020-2290-0

27.   Long, T.; Liu, Y.; Li, X. Molecular structures of human ACAT2 disclose mechanism for selective inhibition. *Structure* **2021**, *29* (12), 1410-1418 e1414. DOI: 10.1016/j.str.2021.07.009

28.   Wang, L.; Qian, H.; Nian, Y.; Han, Y.; Ren, Z.; Zhang, H.; Hu, L.; Prasad, B. V. V.; Laganowsky, A.; Yan, N.; Zhou, M. Structure and mechanism of human diacylglycerol O-acyltransferase 1. *Nature* **2020**, *581* (7808), 329-332. DOI: 10.1038/s41586-020-2280-2

29.   Liu, Y.; Qi, X.; Donnelly, L.; Elghobashi-Meinhardt, N.; Long, T.; Zhou, R. W.; Sun, Y.; Wang, B.; Li, X. Mechanisms and inhibition of Porcupine-mediated Wnt acylation. *Nature* **2022**, *607* (7920), 816-822. DOI: 10.1038/s41586-022-04952-2.

30.   Coupland, C. E.; Andrei, S. A.; Ansell, T. B.; Carrique, L.; Kumar, P.; Sefer, L.; Schwab, R. A.; Byrne, E. F. X.; Pardon, E.; Steyaert, J.; et al. Structure, mechanism, and inhibition of Hedgehog acyltransferase. *Mol Cell* **2021**, *81* (24), 5025-5038 e5010. DOI: 10.1016/j.molcel.2021.11.018.

31.   Jiang, Y.; Benz, T. L.; Long, S. B. Substrate and product complexes reveal mechanisms of Hedgehog acylation by HHAT. *Science* **2021**, *372* (6547), 1215-1219. DOI: 10.1126/science.abg4998.

32.   Nardi, F.; Franco, O. E.; Fitchev, P.; Morales, A.; Vickman, R. E.; Hayward, S. W.; Crawford, S. E. DGAT1 Inhibitor Suppresses Prostate Tumor Growth and Migration by Regulating Intracellular Lipids and Non-Centrosomal MTOC Protein GM130. *Sci Rep* **2019**, *9* (1), 3035. DOI: 10.1038/s41598-019-39537-z

33.   Chahal, K. K.; Parle, M.; Abagyan, R. Hedgehog pathway and smoothened inhibitors in cancer therapies. *Anticancer Drugs* **2018**, *29* (5), 387-401. DOI: 10.1097/CAD.0000000000000609

34.   Zhong, Z.; Sepramaniam, S.; Chew, X. H.; Wood, K.; Lee, M. A.; Madan, B.; Virshup, D. M. PORCN inhibition synergizes with PI3K/mTOR inhibition in Wnt-addicted cancers. *Oncogene* **2019**, *38* (40), 6662-6677. DOI: 10.1038/s41388-019-0908-1

35.   Alavez-Rubio, J. S.; Juarez-Cedillo, T. ACAT1 as a Therapeutic Target and its Genetic

Relationship with Alzheimer's Disease. *Curr Alzheimer Res* **2019**, *16* (8), 699-709. DOI:

10.2174/1567205016666190823125245

36.   Yang, J.; Brown, M. S.; Liang, G.; Grishin, N. V.; Goldstein, J. L. Identification of the

acyltransferase that octanoylates ghrelin, an appetite-stimulating peptide hormone. *Cell* **2008**,

132 (3), 387-396. DOI: 10.1016/j.cell.2008.01.017.

37.   Darling, J. E.; Zhao, F.; Loftus, R. J.; Patton, L. M.; Gibbs, R. A.; Hougland, J. L.

Structure-Activity Analysis of Human Ghrelin O-Acyltransferase Reveals Chemical

Determinants of Ghrelin Selectivity and Acyl Group Recognition. *Biochemistry* **2015**, *54* (4),

1100-1110. DOI: 10.1021/bi5010359

38.   Zhang, Q.; Yao, D.; Rao, B.; Jian, L.; Chen, Y.; Hu, K.; Xia, Y.; Li, S.; Shen, Y.; Qin, A.;

et al. The structural basis for the phospholipid remodeling by lysophosphatidylcholine

acyltransferase 3. *Nat Commun* **2021**, *12* (1), 6869. DOI: 10.1038/s41467-021-27244-1.

39.   Yoneyama-Hirozane, M.; Deguchi, K.; Hirakawa, T.; Ishii, T.; Odani, T.; Matsui, J.;

Nakano, Y.; Imahashi, K.; Takakura, N.; Chisaki, I.; et al. Identification and Characterization of

a New Series of Ghrelin O-Acyl Transferase Inhibitors. *SLAS Discovery* **2018**, *23* (2), 154-163,

DOI: 10.1177/2472555217727097.

40.   Galka, C. S.; Hembre, E. J.; Honigschmidt, N. A.; Keding, S. J.; Martinez-Grau, M. A.;

Plaza, G. R.; Rubio, A.; Smith, D. L. Preparation of N-acylamino acid derivatives as ghrelin o-

acyl transferase inhibitors. WO2016168225A1, 2016.

41.   Campaña, M. B.; Irudayanathan, F. J.; Davis, T. R.; McGovern-Gooch, K. R.; Loftus, R.;

Ashkar, M.; Escoffery, N.; Navarro, M.; Sieburg, M. A.; nangia, S.; Hougland, J. L. Molecular

architecture of a membrane-spanning hormone acyltransferase required for metabolic regulation. *bioRxiv* **2019**, 556233. DOI: 10.1101/556233.

42.   Garner, A. L.; Janda, K. D. A small molecule antagonist of ghrelin O-acyltransferase (GOAT). *Chem. Commun.* **2011**, *47* (26), 7512-7514, 10.1039/c1cc11817j. DOI: 10.1039/c1cc11817j.

43.   Lang, K.; Chin, J. W. Cellular incorporation of unnatural amino acids and bioorthogonal labeling of proteins. *Chem Rev* **2014**, *114* (9), 4764-4806. DOI: 10.1021/cr400355w

44.   Speers, A. E.; Adam, G. C.; Cravatt, B. F. Activity-based protein profiling in vivo using a copper(i)-catalyzed azide-alkyne [3 + 2] cycloaddition. *J Am Chem Soc* **2003**, *125* (16), 4686-4687. DOI: 10.1021/ja034490h

45.   Taylor, M. S.; Ruch, T. R.; Hsiao, P. Y.; Hwang, Y.; Zhang, P.; Dai, L.; Huang, C. R.; Berndsen, C. E.; Kim, M. S.; Pandey, A.; et al. Architectural organization of the metabolic regulatory enzyme ghrelin O-acyltransferase. *J Biol Chem* **2013**, *288* (45), 32211-32228. DOI: 10.1074/jbc.M113.510313.

46.   Murtuza, M. I.; Isokawa, M. Endogenous ghrelin-O-acyltransferase (GOAT) acylates local ghrelin in the hippocampus. *J. Neurochem.* **2018**, *144* (1), 58-67, 10.1111/jnc.14244. DOI: 10.1111/jnc.14244.

47.   Hormaechea-Agulla, D.; Gomez-Gomez, E.; Ibanez-Costa, A.; Carrasco-Valiente, J.; Rivero-Cortes, E.; F, L. L.; Pedraza-Arevalo, S.; Valero-Rosa, J.; Sanchez-Sanchez, R.; Ortega-Salas, R.; et al. Ghrelin O-acyltransferase (GOAT) enzyme is overexpressed in prostate cancer, and its levels are associated with patient's metabolic status: Potential value as a non-invasive biomarker. *Cancer Lett* **2016**, *383* (1), 125-134. DOI: 10.1016/j.canlet.2016.09.022.

48.   Campana, M. B.; Davis, T. R.; Novak, S. X.; Cleverdon, E. R.; Bates, M.; Krishnan, N.; Curtis, E. R.; Childs, M. D.; Pierce, M. R.; Morales-Rodriguez, Y.; et al. Cellular Uptake of a Fluorescent Ligand Reveals Ghrelin O-Acyltransferase Interacts with Extracellular Peptides and Exhibits Unexpected Localization for a Secretory Pathway Enzyme. *ACS Chem Biol* **2023**, *18* (8), 1880-1890. DOI: 10.1021/acschembio.3c00334.

49.   Gahete, M. D.; Cordoba-Chacon, J.; Hergueta-Redondo, M.; Martinez-Fuentes, A. J.; Kineman, R. D.; Moreno-Bueno, G.; Luque, R. M.; Castano, J. P. A novel human ghrelin variant (In1-ghrelin) and ghrelin-O-acyltransferase are overexpressed in breast cancer: potential pathophysiological relevance. *PLoS One* **2011**, *6* (8), e23302. DOI: 10.1371/journal.pone.0023302.

50.   Ibanez-Costa, A.; Gahete, M. D.; Rivero-Cortes, E.; Rincon-Fernandez, D.; Nelson, R.; Beltran, M.; de la Riva, A.; Japon, M. A.; Venegas-Moreno, E.; Galvez, M. A.; et al. In1-ghrelin splicing variant is overexpressed in pituitary adenomas and increases their aggressive features. *Sci Rep* **2015**, *5*, 8714. DOI: 10.1038/srep08714.

51.   Luque, R. M.; Sampedro-Nunez, M.; Gahete, M. D.; Ramos-Levi, A.; Ibanez-Costa, A.; Rivero-Cortes, E.; Serrano-Somavilla, A.; Adrados, M.; Culler, M. D.; Castano, J. P.; Marazuela, M. In1-ghrelin, a splice variant of ghrelin gene, is associated with the evolution and aggressiveness of human neuroendocrine tumors: Evidence from clinical, cellular and molecular parameters. *Oncotarget* **2015**, *6* (23), 19619-19633. DOI: 10.18632/oncotarget.4316.

Jacob E. Moose

315-244-4434 | jcbmoose@yahoo.com

Visiting Instructor of Chemistry, Colgate University

Academic History

August 2016- Present	**Syracuse University**	Syracuse, New York

Ph.D. in Chemistry

ABD - Expected Summer 2024

M.Phil. in Chemistry

Awarded December 2018

August 2016- May 2020 — **Nazareth College** | Rochester, New York

B.S. in Biochemistry

Awarded May 2016

Teaching Experience

Visiting Instructor — **Colgate University** | July 2023 – Current

CHEM 102 – General Chemistry II Lecture and Laboratory

- Teaching semester two of General Chemistry in a two-semester sequence. Course utilizes an atoms-first approach to study reaction behavior, including chemical kinetics, thermodynamics, and equilibria.
- Continued support of peer-led learning through mentoring workshop leaders and study groups.

CHEM 264L – Organic Chemistry II Laboratory

- Supporting student learning in Organic II through hands-on application of small-scale synthetic chemical principles, including instrumentation use and spectral analysis.

CHEM 101/101L – General Chemistry I Lecture and Laboratory

- Taught semester one of General Chemistry in a two-semester sequence. Course utilized an atoms-first approach to introduce atomic principles, gas laws, and thermochemistry.
- Facilitated learning goals through mentoring peer-led workshop leaders and formation of peer study groups.

Visiting Instructor   **Hamilton College** | July 2022 – June 2023

CHEM 270/270L – Biological Chemistry

- Taught Biochemistry and associated laboratory with a focus on catalysis and bioenergetics. Course introduces principles of experimental biochemistry, isolation methods and techniques for analyzing structure and function of biomacromolecules.
- Supervised several laboratory Teaching Assistants to assist with laboratory operations and grading.

CHEM 190L – Organic Chemistry I Lab

- Worked Organic Chemistry laboratory, focusing on introduction to organic spectroscopy and synthetic laboratory principles alongside an undergraduate Teaching Assistant.

CHEM 120 – Principles of Chemistry

- Lectured on basic chemical theory with an emphasis on molecular structure, bonding theories, and electronic properties.
- Utilized Universal Design concepts to offer multiple opportunities for students to demonstrate mastery of core concepts.

CHEM 371W – Research Methods in Chemistry

- Led students in self-guided research experience centered around porphyrin chemistry, developing relevant synthetic and spectroscopic laboratory skills.
- Writing intensive class stressed literature research as well as oral and written communication skills.

Visiting Assistant Professor   **Nazareth College** | January 2022 – May 2022

BCH 422/423L – Biochemistry II

- Taught upper-level Biochemistry and associated laboratory sections, focusing on preparing students to be successful in biochemical and medical fields

- Utilized Problem-Based Learning (PBL) opportunities to facilitate student learning objectives and reinforce core class concepts

CHM 140/140L – General Chemistry

- Introduced a mixture of majors and non-majors to foundational chemical concepts
- Facilitated student learning objectives and safe laboratory practices through experiential learning of concepts

SCI 120 – Introduction to Scientific Communication

- Incorporated peer-learning and review processes to reinforce scientific communication skills, including reading, writing, and presenting literature.
- Guided students along the development of a term paper on a scientific and ethical question.

Adjunct Professor   **Nazareth College** | August 2021 – December 2022

SCI 120 – Introduction to Scientific Communication

Teaching Mentor   **Syracuse University** | May 2019 – August 2021

Teaching Assistant Orientation Program

- Led new graduate student teaching assistants in large- and small-group discussions pertaining to their new roles as instructors, including introduction to remote learning.

Teaching Assistant   **Syracuse University** | August 2016 – December 2021

Medicinal Chemistry - Spring 2018, Spring 2021

- Writing, designing, and grading test and homework questions for a combined undergraduate/graduate course revolving around providing students tools to succeed in graduate school or pharmaceutical research. Led hybrid-remote lectures for several weeks in April 2021.

Organic Chemistry Laboratory – Fall 2017 – Fall 2021

- Facilitated student laboratory experience using leading questions to allow students to arrive at their own conclusion as part of a TA

pair responsible for day-to-day laboratory operations. Experience with both classic and hybrid-remote teaching.

General Chemistry Laboratory – Fall 2016 – Spring 2017

- Taught laboratory skills and scientific reasoning to a mixture of chemistry majors and non-majors.

Tutor and Workshop Leader **Nazareth College** | September 2013 – April 2016

Fundamentals of Organic and Biochemistry

- Led workshops designed for Physical Therapy students to become familiar with chemical behavior before undertaking Anatomy and Physiology.

Organic Chemistry

- Worked as part of an active-learning community of peers expected to facilitate understanding of critical organic chemistry concepts.

Research Experience

January 2017- Present **Syracuse University** | Syracuse, New York

Advisor: Dr. James Hougland

Project: Synthesis and Development of Small-Molecule Probes of Ghrelin *O*-acyl Transferase

September 2013- May 2016 **Nazareth College** | Rochester, NY

Advisor: Dr. Stephen Tajc

Project: Characterization of Metal Cation Binding to Pyridine-based Compounds in Aqueous Solution

Publications

ORCID: 0000-0002-8659-1918

Primary author:

Jacob E. Moose, Katelyn A. Leets, Nilamber A. Mate, John D. Chisholm, and James L. Hougland. (2020) An overview of ghrelin *O*-acyltransferase inhibitors: a literature and patent

review for 2010-2019, Expert Opinion on Therapeutic Patents, 30:8, 581-593, DOI: [10.1080/13543776.2020.1776263](10.1080/13543776.2020.1776263)

(In preparation) *Jacob E. Moose,* Katelyn A. Leets, Jingjing Ji, Kayleigh McGovern-Gooch, Jackson Calhoun, Zachary Spada, Cassie L. Grossman, John D. Chisholm, Shikha Nangia, and James L. Hougland. Inhibitor binding sites within ghrelin *O*-acyltransferase revealed by structural modeling and high-throughput screening.

(In preparation) *Jacob E. Moose,* Mariah Pierce, Robert Anderson, Alexandra C. Olanescu, Nicholas Burgado, Jackson Calhoun, John D. Chisholm, and James L. Hougland. Electrophilic small molecule probes enable identification of activated residue within ghrelin O-acyltransferase

Posters/Presentations:

Jacob E. Moose, Kayleigh R. McGovern-Gooch, Jackson Calhoun, Zachary Spada, John D. Chisholm, and James L. Hougland. (2021) Virtual screening and a continuous acylation assay enables discovery of new GOAT inhibitors. Presented at Federation of American Societies for Experimental Biologies.

Jacob Moose, Stephen Tajc. (2015) Characterization of metal cation binding to pyridine-based compounds in aqueous solution. Presented at 249th American Chemical Society National Meeting.

Shane Fuentes, Matthew Leverich, *Jacob Moose*, Stephen Tajc. (2016) Binding group II cations with DPA-amino acid complexes. Presented at 251st American Chemical Society National Meeting.

Contributed to:

Sara L. Deschaine, Mehdi Farokhnia, Adriana Gregory-Flores, Lia J. Zallar, Zhi-Bing You, Hui Sun, Deon M. Harvey, Renata C. N. Marchette, Brendan J. Tunstall, Bharath K. Mani, *Jacob E. Moose*, Mary R. Lee, Eliot Gardner, Fatemeh Akhlaghi, Marisa Roberto, James L. Hougland, Jeffrey M. Zigman, George F. Koob, Leandro F. Vendruscolo, and Lorenzo Leggio. (2021) A closer look at alcohol-induced changes in the ghrelin system: novel insights from preclinical and clinical data. Addiction Biology, e13033, DOI: [10.1111/adb.13033](10.1111/adb.13033)

Sara L. Deschaine, Morten A. Hedegaard, Claire L. Pince, Mehdi Farokhnia, *Jacob E Moose*, Ingrid A Stock, Sravani Adusumalli, Fatemeh Akhlaghi, James L. Hougland, Agnieszka Sulima, Kenner C. Rice, George F. Koob, Leandro Vendruscolo, Birgitte Holst and Lorenzo Leggio. (2023) Initial pharmacological characterization of a major hydroxy metabolite of PF-5190457: inverse agonist activity of PF-6870961 at the ghrelin receptor. The Journal of Pharmacology and Experimental Therapeutics. DOI: 10.1124/jpet.122.001393

Training and Mentoring

As Principal Investigator

| Summer 2024 (upcoming) | Sydney Arlin |
| | Samuel Epstein |

As Graduate Student Mentor

Summer 2022	Nicholas Burgado (REU, Rochester Institute of Technology)
Summer 2021	Daniera Gomez-Sotomayor (REU)
Spring 2020	Zachary Spada
	Subsequent position: Lead Technical Report Writer, SGS, Rockaway NJ
Summer 2019 - Spring 2021	Jackson Calhoun (Renee Crown Honors student, graduated with Honors and Distinction in Biochemistry)
	Subsequent position: Doctoral program in Medicinal Chemistry, University of Connecticut
Fall 2018 – Spring 2019	Rebecca Walker
	Subsequent position: Doctoral program in Clinical Psychology, William James College

Awards and Honors

Syracuse University Outstanding TA Award - 2020

Awarded to TAs nominated by their department for demonstrating excellence in undergraduate instruction, recognizing approximately the top 4% of all campus TAs.

FASEB Short Talk Finalist - 2021

Selected from submitted abstracts for a short talk at the Federation of American Societies for Experimental Biology Protein Lipidation Conference, June 2021 on research topic titled "Virtual screening and a continuous acylation assay enables discovery of new GOAT inhibitors".

ACS Biological Chemistry Division Travel Award - Spring 2020

Received travel award based on abstract and application (conference cancelled due to pandemic).

Teaching Mentor – 2019-2021

Selected by a panel of peers to serve as an orientation leader and mentor for the Syracuse TA Orientation.

Teaching Mentor Selection Committee – 2020-2021

Served as part of a committee to review portfolios and interview applicants for Syracuse TA Orientation.

Faculty Appreciation 2022/2023 – Selected for recognition by students in General Chemistry at both Colgate University (2023) and Hamilton College (2022) in acknowledgement of instructional ability and efforts.